frontiers | Research Topics

Women in veterinary neurology and neurosurgery: 2021

Edited by
Luisa De Risio

Published in
Frontiers in Veterinary Science

ISSN 1664-8714
ISBN 978-2-83251-752-9
DOI 10.3389/978-2-83251-752-9

About Frontiers

Frontiers is more than just an open access publisher of scholarly articles: it is a pioneering approach to the world of academia, radically improving the way scholarly research is managed. The grand vision of Frontiers is a world where all people have an equal opportunity to seek, share and generate knowledge. Frontiers provides immediate and permanent online open access to all its publications, but this alone is not enough to realize our grand goals.

Frontiers journal series

The Frontiers journal series is a multi-tier and interdisciplinary set of open-access, online journals, promising a paradigm shift from the current review, selection and dissemination processes in academic publishing. All Frontiers journals are driven by researchers for researchers; therefore, they constitute a service to the scholarly community. At the same time, the *Frontiers journal series* operates on a revolutionary invention, the tiered publishing system, initially addressing specific communities of scholars, and gradually climbing up to broader public understanding, thus serving the interests of the lay society, too.

Dedication to quality

Each Frontiers article is a landmark of the highest quality, thanks to genuinely collaborative interactions between authors and review editors, who include some of the world's best academicians. Research must be certified by peers before entering a stream of knowledge that may eventually reach the public - and shape society; therefore, Frontiers only applies the most rigorous and unbiased reviews. Frontiers revolutionizes research publishing by freely delivering the most outstanding research, evaluated with no bias from both the academic and social point of view. By applying the most advanced information technologies, Frontiers is catapulting scholarly publishing into a new generation.

What are Frontiers Research Topics?

Frontiers Research Topics are very popular trademarks of the *Frontiers journals series*: they are collections of at least ten articles, all centered on a particular subject. With their unique mix of varied contributions from Original Research to Review Articles, Frontiers Research Topics unify the most influential researchers, the latest key findings and historical advances in a hot research area.

Find out more on how to host your own Frontiers Research Topic or contribute to one as an author by contacting the Frontiers editorial office: frontiersin.org/about/contact

Women in veterinary neurology and neurosurgery: 2021

Topic editor
Luisa De Risio — Linnaeus Veterinary Limited, United Kingdom

Citation
De Risio, L., ed. (2023). *Women in veterinary neurology and neurosurgery: 2021.* Lausanne: Frontiers Media SA. doi: 10.3389/978-2-83251-752-9

Table of contents

frontiers | Frontiers in Veterinary Science

TYPE Editorial
PUBLISHED 10 February 2023
DOI 10.3389/fvets.2023.1147908

OPEN ACCESS

EDITED AND REVIEWED BY
Andrea Tipold,
University of Veterinary Medicine
Hannover, Germany

*CORRESPONDENCE
Luisa De Risio
luisa.derisio@linnaeusgroup.co.uk

SPECIALTY SECTION
This article was submitted to
Veterinary Neurology and Neurosurgery,
a section of the journal
Frontiers in Veterinary Science

RECEIVED 19 January 2023
ACCEPTED 26 January 2023
PUBLISHED 10 February 2023

CITATION
De Risio L (2023) Editorial: Women in veterinary
neurology and neurosurgery: 2021.
Front. Vet. Sci. 10:1147908.
doi: 10.3389/fvets.2023.1147908

Editorial: Women in veterinary neurology and neurosurgery: 2021

Luisa De Risio*

Linnaeus Veterinary Limited, Shirley, United Kingdom

KEYWORDS

dog, cat, neurology—clinical, neurosurgical procedures, editorial

Editorial on the Research Topic
Women in veterinary neurology and neurosurgery: 2021

This Frontiers in Veterinary Science Women in Veterinary Neurology and Neurosurgery collection of scientific articles presents the innovative work of female neurologists working in the UK, Europe, and North America. The series comprises 13 articles showcasing original research and case reports in various fields of Veterinary Neurology and Neurosurgery, including advances in diagnostic imaging techniques and novel neurosurgical procedures.

Diffusion MRI is a specific sequence that detects and quantifies water diffusivity, which is the molecular motion (Brownian movement) of water and represents an intrinsic feature of tissues. Diffusion-weighted imaging (DWI) and apparent diffusion coefficient (ADC) are MRI sequences routinely used in the diagnostic investigation of suspected cerebrovascular accidents (CVA) in people (1). There is limited information on diffusion-weighted characteristics of naturally occurring CVA in dogs. Extrapolation from other species has limitations due to differences in how CVA appears on DWI over time (i.e., from the onset of CVA to the time of MRI) (2). The retrospective study by Boudreau et al. describes DWI MRI findings of spontaneous canine CVA in relation to the time of clinical onset, the DWI type (EPI vs. non-EPI), and the presence or absence of a haemorrhagic component of the lesion. The results of this study help to inform the appropriate clinical interpretation of these sequences by veterinary neurologists and neuroradiologists.

Steroid-responsive meningitis-arteritis (SRMA) is an inflammatory disorder of probable immune mediated origin, commonly recognized in dogs (3). It typically affects young, medium to large breed dogs and can present as an acute or chronic condition (3). The acute form of SRMA is characterized by cervical hyperalgesia, pyrexia, and cerebrospinal fluid (CSF) neutrophilic pleocytosis (4). Some biomarkers have been used to understand the pathogenesis of SRMA and support its diagnosis (5, 6). Clinical and laboratory findings in dogs with a chronic form of SRMA are less specific than those observed in the acute form, making the diagnosis more challenging. The MRI finding of SRMA in dogs include enhancement of the meninges in the cervical region on T1-weighted (T1W) images after intravenous injection of gadolinium, and signal changes of the cervical muscle such as hyperintensity on T2-weighted (T2W) and short tau inversion recovery (STIR) (7), as well as contrast enhancement. The study by Remelli et al. highlights the usefulness of low and high-field MRI in complementing clinical and laboratory findings in the diagnosis of SRMA. In this retrospective study, including 70 dogs with SRMA, the MRI showed abnormalities in 98.6% of dogs, with the majority (87.1%) being MRI features suggestive of meningeal inflammation. T1W FAT-SAT sequences were particularly useful in detecting meningeal enhancement. In addition, the contrast enhancement of the synovium of the cervical articular facets and the epaxial muscles was detected in 48.6% of dogs.

Spinal epidural empyema (SEE) is characterized by the "accumulation of purulent material in the epidural space of the vertebral canal" (8). It can result in neurological deficits and even death if untreated or unresponsive to treatment (9). There is limited information on canine SEE in veterinary literature. A study by Laws et al. describes the clinical and diagnostic findings, treatment (conservative or surgical), and outcomes of dogs with SEE that were presented to five referral hospitals in the UK. This study provides detailed information on the presenting clinical signs, MRI findings, laboratory investigation results, treatment, and long-term outcomes. The results of this study inform client communication and clinical decisions on canine SSE management.

Various neurological conditions such as vertebral fractures and luxations, malformations, neoplasia, and intervertebral disc degenerative and infectious disorders can result in instability of the vertebral column. Different surgical techniques have been described to stabilize the vertebral column of dogs and cats. These procedures require specialistic equipment combined with advanced neurosurgical skills and expertise. One of the main risks of spinal stabilization is the violation of neurovascular structures during implant placement resulting in serious and potentially irreversible neurologic deficits for the patient. Reliable intra and post-operative evaluation of the accuracy of implant placement is necessary for the safe and successful treatment of patients undergoing stabilization of the vertebral column (10). A canine cadaveric imaging and anatomic study by Goffart et al. shows that end-on fluoroscopy, with or without inversion, is a highly accurate technique for the intraoperative evaluation of bicortically placed Steinmann pins' position in the canine thoracolumbar vertebral column. Three-dimensionally printed patient-specific drill guides have been used to improve the accuracy of implant placement in the canine spine (11).

Three-dimensionally printed patient-specific drill guides have recently been proposed to assist with another challenging neurosurgical procedure that involves a steep learning curve. The study by Escauriaza et al. investigated the accuracy of a 3-dimensional dog-specific printed surgical guide to support the surgeon performing transsphenoidal hypophysectomy, which is performed as surgical treatment of pituitary-dependent hyperadrenocorticism. Pituitary-dependent hyperadrenocorticism is a chronic and progressive disorder (12) that can be treated medically or surgically with or without radiation therapy. Surgical treatment to remove the pituitary neoplasm is increasingly used in dogs. However, this surgical procedure is challenging and requires prolonged training and advanced expertise. The methods described in the study by Escauriaza et al. support the identification of the area to drill in the basisphenoid bone to access the salle turcica and the pituitary mass.

This collection of articles promotes the work of female neurology and neurosurgery researchers and contributes to the advancement of diagnosis and treatment of different neurologic conditions (i.e., infectious, inflammatory, neoplastic) of the central and peripheral nervous system.

Author contributions

The author confirms being the sole contributor of this work and has approved it for publication.

Conflict of interest

LD is an employee of Linnaeus Veterinary limited, a provider of veterinary services.

Publisher's note

References

1. Vilela P, Rowley HA. Brain ischemia: CT and MRI techniques in acute ischemic stroke. *Eur J Radiol.* (2017) 96:162–72. doi: 10.1016/j.ejrad.2017.08.014

2. Fiebach JB, Schellinger PD, Jansen O, Meyer M, Wilde P, Bender J, et al. CT and diffusion-weighted MR imaging in randomized order: diffusionweighted imaging results in higher accuracy and lower interrater variability in the diagnosis of hyperacute ischemic stroke. *Stroke*. (2002) 33:2206–10. doi: 10.1161/01.STR.0000026864.20339.CB

3. Tipold A, Schatzberg SJ. An update on steroid responsive meningitis arteritis. *J Small Anim Pract*. (2010) 51:150–4. doi: 10.1111/j.1748-5827.2009.00848.x

4. Di Terlizzi R, Platt SR. The function, composition and analysis of cerebrospinal fluid in companion animals: part II—analysis. *Vet J.* (2009) 180:15–32. doi: 10.1016/j.tvjl.2007.11.024

5. Maiolini A, Carlson R, Schwartz M, Gandini G, Tipold A. Determination of immunoglobulin A concentrations in the serum and cerebrospinal fluid of dogs: an estimation of its diagnostic value in canine steroid-responsive meningitis–arteritis. *Vet J.* (2012) 191:219–24. doi: 10.1016/j.tvjl.2010.12.018

6. Spitzbarth I, Baumgärtner W, Beineke A. The role of pro- and anti-inflammatory cytokines in the pathogenesis of spontaneous canine CNS diseases. *Vet Immunol Immunopathol.* (2012) 147: 6–24. doi: 10.1016/j.vetimm.2012.04.005

7. Lau J, Nettifee JA, Early PJ, Mariani CL, Olby NJ, Muñana KR. Clinical characteristics, breed differences, and quality of life in North American dogs with acute steroid-responsive meningitis-arteritis. *J Vet Intern Med.* (2019) 33:1719–27. doi: 10.1111/jvim.15543

8. De Stefani A, Garosi LS, Mcconnell FJ, Diaz FJ, Dennis R, Platt SR. Magnetic resonance imaging features of spinal epidural empyema in five dogs. *Vet Radiol Ultrasound.* (2008) 49:135–40. doi: 10.1111/j.1740-8261.2008.00339.x

9. Lavely JA, Vernau KM, Vernau W, Herrgesell EJ, Lecouteur RA. Spinal epidural empyema in seven dogs. *Vet Surg.* (2006) 35:176–85. doi: 10.1111/j.1532-950X.2006.00129.x

10. Hettlich BF, Fosgate GT, Levine JM, Young BD, Kerwin SC, Walker M, et al. Accuracy of conventional radiography and computed tomography in predicting implant position in relation to the vertebral canal in dogs. *Vet Surg.* (2010) 39:680–7. doi: 10.1111/j.1532-950X.2010.00697

11. Elford JH, Oxley B, Behr S. Accuracy of placement of pedicle screws in the thoracolumbar spine of dogs with spinal deformities with three-dimensionally printed patient-specific drill guides. *Vet Surg.* (2020) 49:347–53. doi: 10.1111/vsu.13333

12. Sanders K, Galac S, Meij BP. Pituitary tumour types in dogs and cats. *Vet J.*(2021) 270:105623. doi: 10.1016/j.tvjl.2021.105623

frontiers in Veterinary Science

ORIGINAL RESEARCH
published: 07 March 2022
doi: 10.3389/fvets.2022.813316

Multicenter Study of Clinical Presentation, Treatment, and Outcome in 41 Dogs With Spinal Epidural Empyema

Emma J. Laws[1], Lluís Sánchez[2], Elsa Beltran[3], Elisabet Domínguez[4], Abel B. Ekiri[5], Josep Brocal[6] and Luisa De Risio[1]*

[1] Linnaeus Veterinary Limited, Solihull, United Kingdom, [2] Neurology/Neurosurgery Service, Willows Veterinary Centre and Referral Centre, Linnaeus Veterinary Limited, Solihull, United Kingdom, [3] Neurology/Neurosurgery Service, Queen Mother Hospital for Animals, Royal Veterinary College, Potters Bar, United Kingdom, [4] Diagnostic Imaging Service, Anicura ARS Hospital Veterinari, Barcelona, Spain, [5] Department of Veterinary Epidemiology and Public Health, School of Veterinary Medicine, University of Surrey, Guildford, United Kingdom, [6] Neurology/Neurosurgery Service, Anderson Moores, Linnaeus Veterinary Limited, Winchester, United Kingdom

OPEN ACCESS

Edited by:
Andrea Fischer, Ludwig Maximilian University of Munich, Germany

Reviewed by:
Lara Matiasek, AniCura Kleintierklinik Babenhausen, Germany
Silke Hecht, The University of Tennessee, Knoxville, United States

***Correspondence:**
Emma J. Laws
emma.laws@linnaeusgroup.co.uk

Specialty section:
This article was submitted to Veterinary Neurology and Neurosurgery, a section of the journal Frontiers in Veterinary Science

Received: *11 November 2021*
Accepted: *18 January 2022*
Published: *07 March 2022*

Citation:
Laws EJ, Sánchez L, Beltran E, Domínguez E, Ekiri AB, Brocal J and De Risio L (2022) Multicenter Study of Clinical Presentation, Treatment, and Outcome in 41 Dogs With Spinal Epidural Empyema. Front. Vet. Sci. 9:813316. doi: 10.3389/fvets.2022.813316

There is limited information on canine spinal epidural empyema (SEE). The aim of this multicenter retrospective study is to describe the clinical presentation and outcome of dogs undergoing spinal surgery or conservative management for SEE. Forty-one dogs met the inclusion criteria; the SEE was treated surgically in 17 dogs and conservatively in 24 dogs. Two dogs underwent spinal surgery after failure of conservative management, meaning that 19 dogs in total had spinal surgery. Long-term (i.e., >6 months) follow-up was available in 35 dogs (19 conservatively treated and 16 surgically treated dogs). Recovery to a functional pet status was achieved in 15/19 (78.9%) conservatively treated and 12/16 (75%) surgically treated dogs. There was no significant difference ($p = 1.000$) in long-term outcome between conservatively and surgically treated dogs (78.9 and 75%, respectively). However, significantly more surgically treated dogs were non-ambulatory at presentation (9/17 vs. 5/24, $p = 0.048$) compared with conservatively treated dogs. This study suggests that conservative treatment may be appropriate for dogs with SEE that are ambulatory at presentation and that surgically treated dogs generally have good outcomes. Age may be a negative prognostic indicator as dogs with poor long-term outcomes were significantly older than dogs with a good long-term outcome ($p = 0.048$). A larger prospective randomized study may provide further insight on treatment and outcome of SEE in dogs.

Keywords: empyema, infection, dog, spinal epidural empyema, spinal epidural abscess, epidural

INTRODUCTION

Spinal epidural empyema (SEE) is defined as the accumulation of purulent material in the epidural space of the vertebral canal (1). It can affect humans (2), dogs (3–7), and other species (8–13) leading to neurological disability and mortality (5).

Microorganisms enter the epidural space *via* hematogenous spread (2, 4, 14, 15), direct extension (2, 3, 5–7, 15–24), iatrogenic inoculation (2, 25), or trauma (2, 6, 15). Suggested

pathophysiological mechanisms to explain neuronal damage include ischemia from compression or disruption of vascular supply secondary to septic thrombophlebitis and secondary inflammation of neuroparenchyma itself, in particular in cases where the LS region is affected (e.g., secondary inflammation of the cauda equina) (26). Neurological symptoms and signs reported in human and canine SEE include spinal pain and progressive neurological dysfunction, including paresis, plegia, and incontinence (2, 5).

SEE can be treated surgically or conservatively (15, 27). Surgical treatment involves epidural pus drainage and appropriate antimicrobial therapy, while conservative treatment consists of adequate antibiotherapy (15, 27). In the human literature, it is unclear whether patients undergoing surgical drainage of paraspinal abscesses without direct spinal cord and/or cauda equina decompression are considered to be conservatively or surgically treated.

The choice between conservative and surgical management in humans remains controversial (28–31). Most human studies recommend that if surgery is performed, it is done within 24 h of diagnosis (28, 30, 32–35). However, conservative management can be successful (27, 28, 30, 33, 36–38), particularly in patients without neurological deficits (30, 35, 39, 40). In canine SEE, it is unknown whether superior clinical outcomes are achieved with conservative or surgical treatment. Most veterinary reports of SEE are single cases, with the largest case series comprising seven dogs (5). Of the 39 previously published canine SEE cases, 12 were managed conservatively (4, 15, 25, 41–43), 24 surgically (5–7, 14, 16–23), and 3 were not treated (3, 4, 24). Of the 12 conservatively treated dogs, only 2 had a poor outcome and were euthanized following respiratory arrest (4) and neurological deterioration (43). One of these two dogs also had intracranial involvement (4). Of the 24 surgically managed dogs, 4 had a poor outcome (5–7); however, one was euthanized without further investigations after relapse of severe spinal pain 1 week post-surgery (6), and one was euthanized due to an unrelated cervical intervertebral disc extrusion 1 month postoperatively (5). For the remaining two dogs, one was euthanized due to worsening neurological signs and pneumonia (5), and one died after cardiac arrest in the immediate postoperative period (7).

The aim of this study is to describe the clinical presentation and outcomes of conservatively and surgically treated dogs with SEE that presented to five referral hospitals. We hypothesized that dogs that presented as non-ambulatory were more likely to be treated surgically and that conservative treatment may be appropriate for dogs without neurological deficits.

MATERIALS AND METHODS

Study Sites

The clinical database of five UK veterinary referral centers was searched for dogs diagnosed with SEE. The time period searched varied depending on the availability of a neurology service and high-field MRI in each included institution: January 1, 2000–December 31, 2020 at the first institution; January 1, 2000–December 31, 2019 at the second institution; January 1, 2009–December 31, 2020 at the third institution; January 1, 2015–December 31, 2020 at both the fourth and fifth institutions.

Inclusion Criteria

The inclusion criteria were a diagnosis of SEE based on clinical presentations, MRI findings consistent with previously reported MRI features of SEE (6, 20, 23), and/or surgically confirmed SEE. Previously reported MRI features of SEE that were used included T2W high/mixed signal and T1W low signal epidural mass lesion with concurrent T2W hyperintensity within spinal cord gray matter (6, 20, 23). Only dogs that had undergone 1.5 T MRI were included. Each MRI study was reviewed by the same board-certified radiologist (ED) at the time of the study to further validate the diagnosis of SEE and to carefully evaluate all the MRI findings detailed in the MRI section that follows. Dogs with concomitant intracranial involvement were excluded.

Data Collection

The following data were obtained from the medical records and recorded in an Excel document: signalment, clinical signs observed by the dog owners, pre-referral treatment, general physical and neurological examination findings (at the referral centers), concurrent conditions, time from the onset of clinical signs to SEE diagnosis, laboratory and MRI findings, and details of treatment and outcome.

Data on laboratory investigations included hematology, serum biochemistry, urine and blood cultures, cerebrospinal fluid (CSF) analysis and culture, and histopathological examination and culture of epidural material (in surgically treated dogs). Anemia was classified as either mild [hematocrit (HCT): 0.30–0.36], moderate (HCT: 0.18–0.29), or severe (HCT: <0.18).

Data on high-field (1.5 T) MRI images of the vertebral column were collected for all enrolled dogs, which were reviewed by a board-certified diagnostic imaging specialist (ED). The regions of the vertebral column undergoing MRI were determined based on the neuro-anatomic localization following neurologic examination by a board-certified veterinary neurologist. MRI scanners at the different referral institutions were Signa EchoSpeed (GE Healthcare, Milwaukee, Wisconsin, USA), Intera (Philips Healthcare, Eindhoven, The Netherlands), Vantage ELAN (Canon Medical Systems, Tustin, California, USA), and Magnetom Essenza Dot (Siemens Healthcare, Munich, Germany).

T2-weighted (TR range 2,541–13,681 ms; TE range 81–120 ms) images in the transverse, sagittal, and/or dorsal planes were obtained for all dogs. T1-weighted (400–660 ms; 8–16 ms) (T1W), T1W fat saturated (8–620 ms; 4–15 ms) after intravenous gadolinium (0.1 mmol/kg gadobutrol, Gadovist; Bayer) administration, T2* gradient echo (300–440 ms; 9–15 ms), short tau inversion recovery (3,420–4,270 ms; 13–80 ms), and fluid-attenuated inversion recovery (6,000–8,002 ms; 98–120 ms) images were obtained at the discretion of the attending diagnostic imaging specialist and neurologist. The slice thickness was 1–10 mm. The following MRI features were recorded: SEE location (cervical, i.e., C1–C7 vertebral bodies; thoracic, i.e., T1–T13 vertebral bodies; and/or lumbosacral, i.e., L1–S3 vertebral bodies and cauda equina), the presence/absence of

abnormal intramedullary signal, the pattern of epidural material contrast enhancement, the presence of changes compatible with discospondylitis, and the presence of extra-spinal foci of suspected inflammation or infection.

The pre- and post-treatment neurological status was scored using a six-point grading scale [adapted from Scott (44)] based on the information detailed in the neurologic examination form of each dog (at the referral hospital): grade 0 (neurologically normal), 1 (pain without neurological deficits), 2 (ambulatory paresis), 3 (non-ambulatory paresis), 4 (plegia with nociception), or 5 (plegia without nociception). Dogs exhibiting a stiff gait and/or lameness without any further neurological deficits were classified as grade 1. Urinary and fecal continence were assessed separately.

The decision to treat SEE conservatively or surgically was at the discretion of the attending neurologist and dog's owner. Dogs were divided into two groups: dogs treated with spinal cord decompression plus antibiotic therapy (referred in this article as spinal surgical treatment group or surgically treated dogs), and dogs treated with antibiotics alone or combined with abdominal surgery to debride a paraspinal abscess (referred in this article as conservative treatment group or conservatively treated dogs). All dogs received anti-inflammatories [non-steroidal anti-inflammatory drugs (NSAIDs) or glucocorticoids] and analgesia (opioids, lidocaine, gabapentin, paracetamol, or ketamine).

Information regarding complications during hospitalization and duration of hospitalization was retrieved from the medical records. Neurological grade was determined at the time of discharge and at re-examination at the referral hospital 4–8 weeks post-discharge. Long-term follow-up was defined as a follow-up period of at least 6 months and was obtained *via* the referral centers' or referring practices' medical records and/or postal questionnaires sent to the dogs' owners. The outcome was considered successful if the dog was a functional pet (independently ambulatory, urinary and fecally continent, and considered by their owner to be pain-free with a good quality of life). The outcome was considered poor if the dog was euthanized or died due to SEE, was euthanized or died due to systemic disease potentially associated with SEE, or if it had not become a functional pet by $\geq$6 months post-discharge.

Statistical Analysis

Descriptive statistics were used to compare clinical presentation and outcome variables between the treatment groups. Fisher's exact test was used to compare categorical data, Mann–Whitney test to compare ordinal data, and two-sample *t*-test for continuous data (after checking for normality using the Shapiro–Wilk test). For all analyses, a two-sided *p*-value of <0.05 was considered significant, and all analyses were performed by a biostatistician using STATA (version 14.2; StataCorp, College Station, Texas, USA).

RESULTS

Forty-one dogs met the inclusion criteria: 24 were initially treated conservatively (including 3 who underwent surgical debridement of a paraspinal abscess without entering the vertebral canal) and 17 underwent decompressive spinal surgery (e.g., minihemilaminectomy, hemilaminectomy, or dorsal laminectomy and debridement of the empyema) shortly after MRI. Two dogs underwent spinal decompressive surgery after failure of conservative management; therefore, the total number of dogs undergoing spinal surgery was 19. These two dogs are included in the conservatively treated group for signalment and clinical presentation, location, and MRI findings, while in the surgical group for neurological status at discharge and outcome.

Signalment and Clinical Presentation

Median age at presentation was 6 years (range, 0.3–13.3years) for all 41 dogs included in the study, 7 years (range, 0.3–13.3 years) in the 24 dogs who underwent conservative treatment, and 4 years (range, 3–11 years) in the 17 dogs that underwent spinal surgery for SEE. There was no significant difference ($p = 0.298$) in age at presentation between the conservatively and surgically managed groups. Twenty-six dogs were male (17 conservatively treated and 9 surgically treated) and 15 dogs were female (7 conservatively treated and 8 surgically treated). Twenty-one dogs (51%) were entire [16/26 male dogs (61.5%) and 5/19 (26.3%) female dogs]. The most commonly represented breeds included springer spaniels ($n = 7$), rottweilers ($n = 4$), German shepherds ($n = 4$), border collies ($n = 3$), boxers ($n = 3$), crossbreeds ($n = 2$), bull terriers ($n = 2$), English bulldogs ($n = 2$), and French bulldogs ($n = 2$).

In 40/41 (97.5%) dogs, pain, lameness, and a stiff gait were the first neurological signs observed by the dog owners. Other owners reported clinical signs (in the 24 conservatively treated and 17 dogs who underwent spinal surgery, respectively) included lethargy (13/24 and 10/17 dogs), hyporexia (7/24 and 6/17 dogs), paresis (8/24 and 4/17 dogs), diarrhea (3/24 and 1/17 dogs), respiratory distress (2/24 and 1/17 dogs), and weight loss (2/24 and 1/17 dogs). In addition, 1 dog exhibited vomiting.

Information on pre-referral medications was available in 38 dogs (21 conservatively treated and 17 surgically treated dogs). Pre-referral antibiotics were prescribed to 8/21 conservatively treated and 7/17 surgically treated dogs. Pre-referral analgesia was prescribed to all 38 dogs with information available. Corticosteroids at varying doses had been administered to four dogs for non–SEE-related conditions. Three of these dogs had courses >12 months in duration, and one dog had a course for 1 month prior to referral. Clinical signs detected at the time of initial examination at the referral hospital are summarized in **Table 1**. The only significant finding was that more dogs in the conservatively treated group were ambulatory compared with the surgically treated group ($p = 0.048$). Other than the ambulatory status, there were no other significant differences in clinical presentation parameters between the two groups.

Table 1 Clinical signs detected at the time of presentation to the referral hospital of 41 dogs with SEE.

Concurrent conditions detected on presentation to the referral hospitals included (in the 24 conservatively treated and 17 dogs who underwent spinal surgery, respectively) bilateral otitis externa (1/24 and 1/17 dogs), a heart murmur (2/24 and 1/17 dogs), tense abdomen (2/24 and 2/17 dogs), orthopedic signs

TABLE 1 | Clinical signs detected at the time of presentation to the referral hospital of 41 dogs with SEE.

	All dogs (41)	Conservatively treated dogs (24)	Surgically treated dogs (17)	*P*-value
Hyperthermia	11 (26.8%)	5 (20.8%)	6 (35.3%)	0.476
Spinal hyperaesthesia (identified on neurologic examination)	38 (92.7%)	23 (95.8%)	15 (88.2%)	0.560
Neurological grade				0.058
0	0 (0.0%)	0 (0.0%)	0 (0.0%)	
1	7 (17.1%)	5 (20.8%)	2 (11.8%)	
2	20 (48.8%)	14 (58.3%)	6 (35.3%)	
3	11 (26.8%)	4 (16.7%)	7 (41.2%)	
4	3 (7.3%)	1 (4.2%)	2 (11.8%)	
5	0 (0.0%)	0 (0.0%)	0 (0.0%)	
Ambulatory	27 (65.9%)	19 (79.2%)	8 (47.1%)	0.048
Urinary incontinence	3 (7.3%)	1 (4.4%)	2 (11.8%)	0.565
Fecal incontinence	2 (4.9%)	1 (4.4%)	1 (5.9%)	1.000

(5/24 and 3/17 dogs), respiratory distress (0/24 and 1/17), and anal sac abscessation (0/24 and 1/17).

Two dogs in the surgical treatment group had undergone spinal surgery for intervertebral disc herniation prior to development of SEE; one dog developed lumbosacral SEE 749 days following cervical surgery and the other developed SEE at the thoracolumbar surgical site 15 days postoperatively.

The median time from the onset of clinical signs to SEE diagnosis was 12.5 days for all dogs (range 1–76 days), 16 days in conservatively treated dogs, and 11 days in surgically treated dogs.

Of the 41 dogs, only 2 dogs were tetraparetic (grades 2 and 3), 29 dogs were paraparetic (grade 2 in 19 dogs and grade 3 in 10 dogs), 3 dogs were paraplegic (grade 4), and 7 dogs had pain only (grade 1).

Laboratory Findings

Anemia was present in 9/34 (26.5%) dogs that underwent hematology, characterized as mild in 8 dogs and moderate in one other dog. The mean leukocyte count was 17.3×10^9/L (median 17.7×10^9/L, range: $4.5–31.8 \times 10^9$/L), reference interval $6.0–18.0 \times 10^9$, for all dogs with SEE. Neutrophilia was observed in 19/32 (59.4%) dogs with SEE. A left shift was present in 4/32 dogs. Serum biochemistry panels revealed no significant abnormalities in any dog.

Urine culture was performed in 16/41 dogs and was positive in 2/16 (12.5%) dogs. Pre-referral antibiotic therapy had been administered in 5/16 dogs. The urine culture results were positive for *Pasteurella* spp. in one dog and both *Streptococcus canis* and *Staphylococcus pseudointermedius* in the other dog. Neither dog had received pre-referral antibiotic therapy. Blood cultures were performed in 11/41 dogs. The blood cultures were positive in 7/11 (63.6%) dogs with SEE; six were coagulase-positive *Staphylococcus* spp. and one was *Pasteurella* spp. One of the seven dogs with a positive blood culture had been administered antibiotics prior to referral. Of the aforementioned dogs, eight dogs had both urine and blood cultures performed; both cultures were negative in 3/8 dogs (37.5%).

TABLE 2 | Laboratory findings of dogs treated conservatively and surgically for SEE at the time of admission to the referral hospital.

	All dogs	Conservatively treated	Surgically treated	*P*-value
Anemia	9/34 (26.5%)	6/19 (31.6%)	3/15 (20%)	0.697
Mean leukocyte count ($\times 10^9$/L)	17.7	16.5	18.3	0.425
Positive urine culture	2/16 (12.5%)	2/15 (13.3%)	0/1 (0.0%)	1.000
Positive blood culture	7/11 (63.6%)	5/8 (62.5%)	2/3 (66.7%)	1.000

CSF was collected in 10/41 dogs (four lumbar collection, two cisternal, one both lumbar and cisternal, and three undocumented). Analysis revealed neutrophilic pleocytosis in 4/11 samples, proteinosis in 4/11 CSF samples, and/or the presence of bacteria in 2/11 dogs (both a mixture of bacilli and cocci). CSF culture was positive in 2/6 (33.3%) dogs with SEE, with *Pasteurella* spp. found in one dog (with *Pasteurella* spp. also grown in the urine and blood) and non-hemolytic *Streptococcus* spp. found in another dog (urine culture was not performed, blood culture was negative). Neither of these dogs had received pre-referral antibiotic treatment.

Histopathological analysis of abnormal epidural material was performed in 15/19 (78.9%) surgically treated cases and confirmed SEE. Cytological examination of epidural material was performed in 12/19 surgically treated dogs, with bacteria observed in 2/12 cases. In 13/19 dogs, purulent epidural material was cultured. Eight of these dogs had received antibiotics. Bacterial growth was observed in 4/13 (30.7%) cultures; 1/8 (12.5%) dogs that had received antibiotics and 3/5 (60.0%) dogs that had not. The following bacteria were identified (one case each): *Enterobacter cloacae*, coagulase-positive *Staphylococcus* spp., coagulase-negative *Staphylococcus* spp., *Salmonella* spp., and *Pseudomonas aeruginosa*. Only one dog had blood, urine, and epidural material cultures all performed, with *Escherichia coli* and *Salmonella* spp. found epidurally and negative urine and blood cultures.

No significant differences in laboratory findings were observed between the two groups (**Table 2**).

MRI Findings

The sites affected by SEE and the abnormalities detected on MRI are summarized in **Table 3**. Of the 7 dogs with SEE in more than one spinal region, 6/7 had SEE in the T3–L3 and L4–S3 regions and one dog, with multifocal spinal localization, had SEE at C1–T2, T3–L3, and L4–S3. Intravenous gadolinium was administered to 23/24 conservatively treated and 13/17 surgically treated dogs. Contrast enhancement of epidural material was noted in 35/36 dogs (97.2%). Of the dogs with SEE contrast enhancement, the pattern was uniform/slightly heterogeneous in 24/36 (66.7%) dogs (17/23 conservatively treated and 7/13 surgically treated

TABLE 3 | Location and MRI findings of SEE.

	All dogs	Conservatively treated dogs	Surgically treated dogs	*P*-value
Location of SEE				
Cervical (C1–C7)	2/41 (4.9%)	1/24 (4.2%)	1/17 (5.9%)	
Thoracic (T1–T13)	22/41 (80.5%)	15/24 (62.5%)	7/17 (41.2%)	
Lumbosacral (L4–S3 and cauda equina)	32/41 (45%)	8/24 (33.3%)	14/17 (82.4%)	Not performed
Concurrent discospondylitis	22/41 (53.7%)	17/24 (70.8%)	5/17 (29.4%)	0.012
Concurrent paraspinal inflammation	33/41 (80.5%)	22/24 (91.7%)	11/16 (68.8%)	0.094
Paraspinal abscessation	18/40 (45%)	9/23 (39.1%)	9/17 (52.9%)	0.523
Contrast enhancement (epidural material)	35/36 (97.2%)	23/23 (100.0%)	12/13 (92.3%)	0.406

In some dogs, more than one spinal region was affected.

TABLE 4 | Neurological status at discharge and long-term outcome of dogs treated conservatively and surgically for SEE.

	All dogs	Conservatively treated dogs	Surgically treated dogs	*P*-value
Survived to discharge	37/41 (90.2%)	19/22 (86.4%)	18/19 (94.7%)	0.610
Neurological grade at discharge				
0	4/37 (10.8%)	3/19 (15.8%)	1/18 (5.6%)	0.221
1	9/37 (24.3%)	5/19 (26.3%)	4/18 (22.2%)	
2	18/37 (48.6%)	9/19 (47.4%)	9/18 (50.0%)	
3	5/37 (13.5%)	2/19 (10.5%)	3/18 (16.7%)	
4	1/37 (2.7%)	0/19 (0.0%)	1/18 (5.6%)	
5	0/37 (0%)	0/19 (0.0%)	0/18 (0.0%)	
Ambulatory at discharge	31/37 (83.8%)	17/19 (89.5%)	14/18 (77.8%)	0.405
Urinary/fecal incontinence	0/36 (0%)	0/19 (0.0%)	0/18 (0.0%)	1.000

dogs) and peripheral in 14/36 (39.0%) dogs (9/23 conservatively treated and 5/13 surgically treated dogs).

Treatment and Short-Term Outcome

Extraspinal Abscess Management

In addition to the SEE, 18 dogs presented with an extraspinal abscess, of which 15 dogs underwent surgery for abscess debridement. Of these 15 dogs having surgery for an extraspinal abscess, eight dogs had an exploratory laparotomy for a sublumbar abscess (3 are included in the conservatively treated group and 5 in the spinal decompressive surgery group) and the remainder had the extraspinal abscess surgically explored using the same approach as for the spinal surgery required to treat the SEE. Foreign bodies were identified in 3 dogs, all of which were a grass seed located outside the vertebral canal.

Conservatively Treated Dogs

Antibiotics were administered to all 24 conservatively managed dogs (amoxicillin–clavulanic acid, fluoroquinolones, cephalosporins, metronidazole, and/or clindamycin in 11, 10, 9, 7, and 2 dogs, respectively). Information on the duration of antibiotic therapy was available for 21/24 conservatively treated dogs with a median of 105 days (range: 9–651 days). Analgesia was administered to all 24 dogs (opioids, NSAIDs, gabapentin, lidocaine, paracetamol, and ketamine in 20, 15, 12, 5, 5, and 3 dogs, respectively). One dog presented to the referral center already on an anti-inflammatory dose of prednisolone, and this medication was tapered off over 7 days. Information on the duration of analgesia administration was available for 21/24 conservatively treated dogs with a median of 21 days (range: 0–385 days).

Of the 24 dogs that were initially allocated to the conservative treatment group, two dogs (presenting as grade 1 and grade 2) deteriorated neurologically (both to grade 3) during hospitalization and surgical intervention was deemed necessary. These two dogs were moved into the surgical treatment group with 22 dogs remaining in the conservatively managed group. Both dogs had a good short-term outcome and were ambulatory at discharge. One of these dogs was then lost to long-term follow-up, but the other dog was reported to have a good long-term outcome.

Three dogs (one grade 2 and two grade 3) deteriorated during hospitalization despite conservative treatment and were euthanized at their owner's request prior to discharge, meaning 19/22 conservatively managed dogs survived to discharge. The duration of hospitalization for these remaining 19 dogs managed conservatively ranged from 1 to 17 days (median 5 days), and the neurological status at discharge is presented in **Table 4**.

Two dogs received physiotherapy in a physiotherapy center for <1–3 months, starting within 2 weeks of SEE diagnosis. One of these dogs also received hydrotherapy.

Surgically Treated Dogs (i.e., Dogs That Underwent Spinal Surgery for SEE)

Two dogs undergoing conservative management deteriorated neurologically and surgery was performed. These dogs are therefore included in the surgical group, meaning the total number of surgically treated dogs is 19 as indicated in **Table 4** and the following descriptive statistics. Surgically treated dogs underwent minihemilaminectomy/hemilaminectomy (9/19) or dorsal laminectomy (10/19). Five of these dogs had a concurrent exploratory laparotomy to address an extraspinal abscess. No dog required vertebral column stabilization. A grass seed foreign body, external to the vertebral canal, was identified intraoperatively in 3/19 dogs. Sixteen dogs underwent spinal surgery <24 h after diagnosis.

Antimicrobials were administered to all 19 dogs (amoxicillin–clavulanic acid, metronidazole, cephalosporins, fluoroquinolones, clindamycin, and/or doxycycline in 11, 9, 9, 7, 3, and 1 dog, respectively) with a mean duration of 72 days (range: 11–270 days). Antimicrobial treatment was based on

culture and sensitivity in 7 dogs (based on blood cultures in 5 dogs, urinary culture in 1 dog, and both urinary/blood culture in 1 dog).

Analgesia was administered to all 19 dogs (opioids, NSAIDs, gabapentin, ketamine, lidocaine, glucocorticoids, paracetamol, and/or diazepam in 19, 15, 9, 7, 5, 4, 1, and 1 dog, respectively) for a median of 42 days (range: 6–79 days).

One dog, which presented non-ambulatory paraparetic (grade 3), did not improve and was euthanized during hospitalization. The duration of hospitalization for the remaining 18 dogs ranged from 4 to 23 days (median 8 days). The neurological status at discharge was available for all 18 dogs that survived to discharge (**Table 4**). Urinary incontinence had resolved in the dog that presented with this.

Comparison Between Conservatively and Surgically Treated Dogs

There were no significant differences between the treatment groups with respect to the survival to discharge, neurological grade at discharge, or presence of urinary/fecal incontinence. The hospitalization period for surgically treated dogs was longer than for those conservatively treated and more surgically treated dogs were non-ambulatory on presentation than the conservatively managed group.

Long-Term Outcome

Three dogs were lost to long-term follow-up in each group (six dogs in total) meaning that long-term outcome information was available for 19/22 dogs in the conservatively treated group and 16/19 dogs in the surgically treated group. The long-term follow-up ranged from 12 to 90 months (median 40 months) for conservatively treated dogs and 6–110 months (median 56 months) for surgically treated dogs.

There was no significant difference ($p = 1.000$) in long-term outcome between the conservatively and surgically treated dogs with a good long-term outcome in 15/19 (78.9%) conservatively treated and 12/16 (75%) surgically treated dogs. There was also no significant difference ($p = 1.000$) in time from onset of clinical signs to SEE diagnosis between dogs with a poor long-term outcome (onset to diagnosis mean time of 20.1 days) and dogs with a good long-term outcome (onset to diagnosis mean time of 19.4 days). Of the 7 dogs that had multiple regions affected by SEE (5 surgically treated and 2 conservatively treated), one was lost to follow-up and the other six dogs had a good long-term outcome. Mean leukocyte count, age, and ambulation status at presentation were compared between the good and poor long-term outcome groups to see if there were any significant differences. Results are summarized in **Table 5**.

Dogs with a poor long-term outcome were significantly older ($p = 0.039$) at presentation to the referral center than dogs with a good long-term outcome. Dogs with a successful long-term outcome had a mean age of 5.5 years (median 6.46, range: 0.3–11) and a mean leukocyte count of 17×10^9/L (median 17.5×10^9/L, range: 4.5–31.8×10^9/L), whereas dogs with a poor long-term outcome had a mean age of 8.19 years (median 8.25, range: 0.7–13.25) and a mean leukocyte count of 19.3×10^9/L (median 19.8×10^9/L, range: 13.3–24.5×10^9/L). Mean leukocyte count was not significantly associated with a poorer outcome and the number of dogs who had blood culture was too low to include this in the statistical analysis.

TABLE 5 | Mean leucocyte count, age, and ambulation status in dogs with good and poor long-term outcome.

	Good long-term outcome (27 dogs)	Poor long-term outcome (8 dogs)	*P*-value
Mean leukocyte count ($\times 10^9$/L)	17	19.3	0.527
Mean age (years)	5.54	8.19	0.039
Ambulation status at presentation			
Non-ambulatory	8/13 (61.5%)	5/13 (38.4%)	0.116
Ambulatory	19/22 (86.3%)	3/22 (13.6%)	

DISCUSSION

To the authors' knowledge, this study represents the largest investigation of canine SEE conducted to date.

Signalment and Clinical Presentation

In our study population, male dogs with SEE were overrepresented (63.4%), with a higher proportion of entire male dogs [16/26 (61.5%)] than entire female dogs [5/19 (26.3%)]. In previous studies on SEE in dogs, there was no apparent age, gender, or breed predisposition (5, 6).

Spinal hyperesthesia was a very common presenting finding (38/41 dogs, 92.7%), in agreement with previous reports in both animals and humans (4–6, 16, 29). Pyrexia at presentation was not common (11/41 dogs, 26.8%). The incidence of pyrexia is less common in our canine population than in the two large human studies, which reported fever in 37–66% of patients with SEE (28, 29).

Surgically treated dogs were significantly more likely to present non-ambulatory ($p = 0.048$), suggesting that the attending clinicians may have been more inclined to treat surgically non-ambulatory than ambulatory dogs. The extent of the empyema and financial considerations may also have influenced the decision to treat surgically or conservatively.

Laboratory Findings

Positive identification with culture and sensitivity is preferable for antibiotic stewardship and for optimizing outcomes in bacterial infections. In this study 15/41 dogs had received pre-referral antibiotic treatment. There was a higher percentage of positive blood cultures (7/11, 63.6%) than urine cultures (2/16, 12.5%); however, a higher percentage of dogs in the urine culture group had already received pre-culture antibiotics (5/16, 31%) compared with the blood culture group (1/11, 9%). This difference in pre-referral antibiotic treatment may explain the difference in positive culture rates. Over half (4/7) of the dogs with positive blood cultures had a concurrent urine culture and 3/4 of these urine cultures were negative. One dog had the same bacteria identified in both urine and blood cultures. Of the two

dogs with positive urine cultures, one dog had the same bacteria (*Pasteurella* spp.) identified on blood culture and the other did not have a blood culture performed. The sensitivity of blood and urine cultures for identification of causal organisms in SEE requires further investigation, but our findings suggest that blood culture may be beneficial despite a negative urine culture.

MRI Findings

SEE was more common in the lumbosacral (32/41 dogs, 78%) and thoracic vertebral column (22/41 dogs, 53.7%) than the cervical vertebral column (2/41, 4.9%). A possible explanation for the skew toward the lumbosacral vertebral column may be the proximity of the genitourinary tract, mobility within the L7/S1 disc space, and the lumbar region being a common place for sublumbar abscesses and foreign bodies. The L7–S1 intervertebral disc space seems to be the most common individual disc site affected by discospondylitis in a study of 513 dogs with discospondylitis (45).

Concurrent discospondylitis was common in our study population (53.7% of all dogs). This is similar to previous studies of SEE in dogs (5, 6). Discospondylitis is present in 95% of human patients with SEE (46). Discospondylitis was identified significantly ($p = 0.012$) more frequently in conservatively managed (17/24 dogs, 70.8%) than surgically managed cases (5/17, 29.4%). It is possible that the presence of discospondylitis was a negative factor in the decision-making process for surgery. The clinician may feel that discospondylitis could lead to more chance of instability following spinal surgery. This could lead them to pursue conservative management preferentially in these cases as the use of implants with an active bacterial infection is more prone to complications.

Contrast enhancement of the epidural material was very common in the 36/41 SEE cases that received contrast (35/36 dogs, 97.2%), which would be expected with the pathophysiology of the disease process and is consistent with findings in a previous study on MRI findings in SEE in dogs (6). The contrast enhancement pattern in our study was uniform/slightly heterogeneous in 24/36 (66.7%) dogs and peripheral in 14/36 (39.0%) dogs. The presence of two distinct contrast patterns (both diffuse and peripheral) in our study is similar to that described previously in a paper on MRI findings in five dogs with SEE (6).

Outcome

Despite greater clinical severity at presentation in surgically treated dogs, there was no significant difference in long-term outcome between conservatively and surgically treated dogs (78.9 and 75.0%, respectively). Our study suggests that conservative treatment may be appropriate for dogs with SEE that are ambulatory, provided there is no clinical progression during conservative management. These findings are clinically important because not every animal is a suitable surgical/anesthetic candidate and not every owner is prepared or financially able to pursue surgical treatment.

Most SEE studies in people also fail to demonstrate a significant difference in outcome between conservatively and surgically treated patients (1, 27, 33, 37, 47–51). However, some studies do not comment on the patients' pre-treatment neurological status (47–50), and in most studies, as in ours, surgically treated patients exhibit more severe pre-treatment neurological signs compared with conservatively treated patients (27, 33, 37, 51). Only Curry et al. (30) demonstrated a significant difference in outcome between conservatively and surgically managed patients, with the latter exhibiting a better outcome (13 vs. 60%) (30). Failure of conservative treatment and the subsequent need for surgery has been reported in 9.5–47.8% of human cases (27, 30, 33, 37, 47).

Risk factors for failure of conservative management in humans include diabetes mellitus, a C-reactive protein (CRP) >115 mg/L, a leukocyte count $>12 \times 10^9$/L, positive blood cultures, age >65 years, the presence of methicillin-resistant *Staphylococcus aureus*, and advanced neurological deficits (33, 39, 52). No such information exists in the veterinary literature.

As we only had two dogs in this study that failed conservative management, we looked for differences between the good and poor long-term outcome groups with respect to leukocyte count, positive blood culture, age, and neurological status at presentation. Positive blood cultures could not be evaluated statistically due to the small number of dogs ($n = 8$) having blood culture performed. There were no significant differences between the long-term outcome groups for leukocyte count or neurological status at presentation; however, dogs with a poor long-term outcome were significantly older. Only eight dogs had a poor outcome in our study, which meant that the statistical power in the outcome analysis was low. The percentage of dogs with a poor long-term outcome that presented non-ambulatory or ambulatory is quite different between the groups, and although we did not achieve statistical significance ($p = 0.116$), this may be a factor that does show significance with a larger sample size. A prospective study with larger case numbers looking at risk factors for poor outcome including CRP, leukocyte count, blood culture, age, and severity of neurological deficits would be indicated in the future to further help in the decision-making process of which dogs should be managed surgically compared with conservatively.

Of the dogs that survived to discharge, most were ambulatory (31/37) at the time of discharge. For the dogs (6/37) that were non-ambulatory at discharge, the exact time to regain ambulation is known in three dogs with a median of 7 days and a mean of 15.75 days (range 7–28 days). All but two dogs with a successful long-term outcome were neurologically normal at the time of data collection. Thus, our study suggests that most dogs that become neurologically normal with a successful long-term outcome are functional pets within a month of treatment initiation.

Limitations

The retrospective design of the study limited the investigation, with biases for data collection and variability in the evaluation of objective clinical outcome measures. A direct comparison of outcomes between the treatment groups must be interpreted cautiously due to the differences in presentation. A more severe neurological grading increased the likelihood of surgical treatment; therefore, the outcome in non-ambulatory dogs receiving conservative treatment is unknown. A prospective study would help to test this aspect more reliably; however, it

can be argued that it would be unethical not to provide spinal decompression to dogs with severe neurologic dysfunction when their owners are willing to pursue surgery. Furthermore, the study population was composed of five referral hospital caseloads, potentially introducing bias toward more severe clinical phenotypes and/or owners with fewer financial constraints than the general population. Although larger studies, permitting multivariate analyses, would be very valuable, SEE is a relatively rare condition and obtaining sufficient case numbers is problematic.

Not all clinical presentation, diagnostic, therapeutic, and outcome variables were available for all dogs. As these missing data may have affected the results obtained, this was also a study limitation.

Two dogs failed conservative management (becoming non-ambulatory after initially presenting with neurological grades 1 and 3) and were subsequently treated surgically. Unfortunately, case numbers in this study were insufficient to create a third group, namely, failed conservative management requiring surgery.

Larger prospective studies are required to identify prognostic factors associated with recurrence, treatment failure, and poor outcome in each treatment group.

Conclusions

Our data revealed no significant difference ($p = 1.00$) in long-term success rates between conservatively and surgically managed dogs; however, significantly more cases within the surgically treated group were non-ambulatory on presentation. This study suggests that conservative treatment may be appropriate for dogs with SEE that are ambulatory at presentation, although a further study evaluating whether dogs that fail conservative management and subsequently undergo spinal surgery also have good long-term outcomes would be indicated.

Despite the limitations of our study, it remains the largest study on spinal epidural empyema to date and the results can help in clinical decision-making and inform discussion with owners of dogs diagnosed with SEE. Further studies are needed to compare conservative and surgical treatment of SEE in a population of dogs with similar clinical presentations to determine prognostic indicators of treatment response and indicators of disease recurrence.

DATA AVAILABILITY STATEMENT

The raw data supporting the conclusions of this article will be made available by the authors, without undue reservation.

ETHICS STATEMENT

The animal study was reviewed and approved by Animal Health Trust Clinical Research Ethics Committee. Written informed consent was obtained from the owners for the participation of their animals in this study.

AUTHOR CONTRIBUTIONS

EL and LD: study design, data collection, data analysis, manuscript writing, and manuscript revision. LS: study design, data collection, manuscript writing, and manuscript revision. EB and JB: data collection and manuscript revision. ED: data collection, data analysis, and manuscript revision. AE: manuscript revision. All authors contributed to the article and approved the submitted version.

ACKNOWLEDGMENTS

We are very grateful to our colleague Tim Sparks at the Waltham Petcare Science Institute for his contribution to the statistical analysis within this study. The authors are very grateful to Anita Shea for her contribution to the part of this project conducted at the Animal Health Trust.

REFERENCES

1. Adogwa O, Karikari IO, Carr KR, Krucoff M, Ajay D, Fatemi P, et al. Spontaneous spinal epidural abscess in patients 50 years of age and older: a 15-year institutional perspective and review of the literature: clinical article. *J Neurosurg Spine.* (2014) 20:344–9. doi: 10.3171/2013.11.SPINE13527
2. Defroda SF, Depasse JM, Eltorai AE, Daniels AH, Palumbo MA. Evaluation and management of spinal epidural abscess. *J Hosp Med.* (2016) 11:130–5. doi: 10.1002/jhm.2506
3. Ndikuwera J, Knottenbelt DC, Lawrence J, Hill FW. Spinal abscess in a dog. *Vet Rec.* (1987) 120:554–5. doi: 10.1136/vr.120.23.554
4. Dewey CW, Kortz GD, Bailey CS. Spinal epidural empyema in two dogs. *J Am Anim Hosp Assoc.* (1998) 34:305–8. doi: 10.5326/15473317-34-4-305
5. Lavely JA, Vernau KM, Vernau W, Herrgesell EJ, Lecouteur RA. Spinal epidural empyema in seven dogs. *Vet Surg.* (2006) 35:176–85. doi: 10.1111/j.1532-950X.2006.00129.x
6. De Stefani A, Garosi LS, Mcconnell FJ, Diaz FJ, Dennis R, Platt SR. Magnetic resonance imaging features of spinal epidural empyema in five dogs. *Vet Radiol Ultrasound.* (2008) 49:135–40. doi: 10.1111/j.1740-8261.2008.00339.x
7. Nykamp SG, Steffey MA, Scrivani PV, Schatzberg SJ. Computed tomographic appearance of epidural empyema in a dog. *Can Vet J.* (2003) 44:729–31. doi: 10.1111/j.1740-8261.2003.tb00502.x
8. Granger N, Hidalgo A, Leperlier D, Gnirs K, Thibaud JL, Delisle F, et al. Successful treatment of cervical spinal epidural empyema secondary to grass awn migration in a cat. *J Feline Med Surg.* (2007) 9:340–5. doi: 10.1016/j.jfms.2007.01.004
9. Maeta N, Kanda T, Sasaki T, Morita T, Furukawa T. Spinal epidural empyema in a cat. *J Feline Med Surg.* (2010) 12:494–7. doi: 10.1016/j.jfms.2010.01.015
10. Crawford AH, Hedley JE, Lam R, Drozdzynska MJ, De Decker S. Surgical treatment of a paraspinal abscess with osteomyelitis and spinal cord compression in a rabbit. *J Am Anim Hosp Assoc.* (2017) 251:340–4. doi: 10.2460/javma.251.3.340
11. Braun U, Gerspach C, Kühn K, Bünter J, Hilbe M. Abscess of the cervical spine secondary to injection site infection in a heifer. *Acta Vet Scand.* (2017) 59:10. doi: 10.1186/s13028-017-0278-z
12. Braun U, Suarez J, Gasparini S, Warislohner S, Dennler M. Magnetic resonance imaging in a lamb with compression of the thoracic spinal cord by an abscess. *Schweiz Arch Tierheilkd.* (2016) 158:573–7. doi: 10.17236/sat00079
13. Zani DD, Romano L, Scandella M, Rondena M, Riccaboni P, Morandi N, et al. Spinal epidural abscess in two calves. *Vet Surg.* (2008) 37:801–8. doi: 10.1111/j.1532-950X.2008.00454.x

14. Schmiedt CW, Thomas WB. Spinal epidural abscess in a juvenile dog. *Vet Compar Orthopaedics Traumatol.* (2005) 18:186–8. doi: 10.1055/s-0038-1632944
15. Monteiro SR, Gallucci A, Rousset N, Freeman PM, Ives EJ, Gandini G, et al. Medical management of spinal epidural empyema in five dogs. *J Am Anim Hosp Assoc.* (2016) 249:1180–6. doi: 10.2460/javma.249.10.1180
16. Cherrone KL, Eich CS, Bonzynski JJ. Suspected paraspinal abscess and spinal epidural empyema in a dog. *J Am Anim Hosp Assoc.* (2002) 38:149–51. doi: 10.5326/0380149
17. Jerram RM, Dewey CW. Suspected spinal epidural empyema and associated vertebral osteomyelitis (physitis) in a dog. *J Vet Emerg Crit Care.* (1998) 8:216–21. doi: 10.1111/j.1476-4431.1998.tb00127.x
18. Adamo PF, Cherubini GB. Discospondylitis associated with three unreported bacteria in the dog. *J Small Animal Prac.* (2001) 42:352–5. doi: 10.1111/j.1748-5827.2001.tb02473.x
19. Linon E, Geissbuhler U, Karli P, Forterre F. Atlantoaxial epidural abscess secondary to grass awn migration in a dog. *Vet Compar Orthopaedics Traumatol.* (2014) 27:155–8. doi: 10.3415/VCOT-13-07-0095
20. Whitty CC, Milner HR, Oram B. Use of magnetic resonance imaging in the diagnosis of spinal empyema caused by a migrating grass awn in a dog. *N Z Vet J.* (2013) 61:115–8. doi: 10.1080/00480169.2012.731717
21. Gemmill TJ. What is your diagnosis? Epidural empyema. *J Small Animal Prac.* (2008) 49:110–2. doi: 10.1111/j.1748-5827.2007.00498.x
22. Sutton A, May C, Coughlan A. Spinal osteomyelitis and epidural empyema in a dog due to migrating conifer material. *Vet Rec.* (2010) 166:693–4. doi: 10.1136/vr.b4829
23. Plessas IN, Jull P, Volk HA. A case of canine discospondylitis and epidural empyema due to Salmonella species. *Can Vet J.* (2013) 54:595–8. Available online at: https://www.ncbi.nlm.nih.gov/pmc/articles/PMC3659457/
24. Varotsis G, Milne E, Marioni-Henry K. What is your neurologic diagnosis? *J Am Vet Med Assoc.* (2017) 250:979–82. doi: 10.2460/javma.250.9.979
25. Remedios AM, Wagner R, Caulkett NA, Duke T. Epidural abscess and discospondylitis in a dog after administration of a lumbosacral epidural analgesic. *Can Vet J.* (1996) 37:106–7.
26. Baker AS, Ojemann RG, Swartz MN, Richardson EP Jr. Spinal epidural abscess. *N Engl J Med.* (1975) 293:463–8. doi: 10.1056/NEJM197509042931001
27. Siddiq F, Chowfin A, Tight R, Sahmoun AE, Smego RA Jr. Medical vs surgical management of spinal epidural abscess. *Arch Intern Med.* (2004) 164:2409–12. doi: 10.1001/archinte.164.22.2409
28. Rigamonti D, Liem L, Sampath P, Knoller N, Namaguchi Y, Schreibman DL, et al. Spinal epidural abscess: contemporary trends in etiology, evaluation, and management. *Surg Neurol.* (1999) 52:189–96. doi: 10.1016/S0090-3019(99)00055-5
29. Reihsaus E, Waldbaur H, Seeling W. Spinal epidural abscess: a meta-analysis of 915 patients. *Neurosurg Rev.* (2000) 23:175–204. doi: 10.1007/PL00011954
30. Curry WT, Hoh BL, Amin-Hanjani S, Eskandar EN. Spinal epidural abscess: clinical presentation, management, and outcome. *Surg Neurol.* (2005) 63:364–71. doi: 10.1016/j.surneu.2004.08.081
31. Danner RL, Hartman BJ. Update on spinal epidural abscess: 35 cases and review of the literature. *Rev Infect Dis.* (1987) 9:265–74. doi: 10.1093/clinids/9.2.265
32. Darouiche RO. Spinal epidural abscess. *N Engl J Med.* (2006) 355:2012–20. doi: 10.1056/NEJMra055111
33. Patel AR, Alton TB, Bransford RJ, Lee MJ, Bellabarba CB, Chapman JR. Spinal epidural abscesses: risk factors, medical versus surgical management, a retrospective review of 128 cases. *Spine J.* (2014) 14:326–30. doi: 10.1016/j.spinee.2013.10.046
34. Sendi P, Bregenzer T, Zimmerli W. Spinal epidural abscess in clinical practice. *QJM.* (2008) 101:1–12. doi: 10.1093/qjmed/hcm100
35. Epstein NE. Timing and prognosis of surgery for spinal epidural abscess: a review. *Surg Neurol Int.* (2015) 6:S475–86. doi: 10.4103/2152-7806.166887
36. Alton TB, Patel AR, Bransford RJ, Bellabarba C, Lee MJ, Chapman JR. Is there a difference in neurologic outcome in medical versus early operative management of cervical epidural abscesses? *Spine J.* (2015) 15:10–7. doi: 10.1016/j.spinee.2014.06.010
37. Savage K, Holtom PD, Zalavras CG. Spinal epidural abscess: early clinical outcome in patients treated medically. *Clin Orthop Relat Res.* (2005) 439:56–60. doi: 10.1097/01.blo.0000183089.37768.2d
38. Sengul G, Akar A, Alper F, Uslu H. Nonsurgically treated cervical brucellar epidural abscess causing spinal cord compression. *J Clin Neurosci.* (2008) 15:1411–4. doi: 10.1016/j.jocn.2007.05.023
39. Arko LT, Quach E, Nguyen V, Chang D, Sukul V, Kim BS. Medical and surgical management of spinal epidural abscess: a systematic review. *Neurosurg Focus.* (2014) 37:E4. doi: 10.3171/2014.6.FOCUS14127
40. Duarte RM, Vaccaro AR. Spinal infection: state of the art and management algorithm. *Euro Spine J.* (2013) 22:2787–99. doi: 10.1007/s00586-013-2850-1
41. Escriou C, Duchene LS, Gilbert S, Seurin MJ. Spinal epidural infection medically treated in 3 dogs: MRI features and follow-up. *J Vet Internal Med.* (2012) 26:843. doi: 10.1111/j.1939-1976.2012.00938.x
42. Romero-Fernandez N, José-López R, Durand A, Gutierrez-Quintana R. Successful medical management of an epidural abscess in a dog. *Vet Rec Case Rep.* (2017) 5:27–9. doi: 10.1136/vetreccr-2017-000448
43. Levshin S, Davies ES, Van Hatten R, Williamson BG. What is your neurologic diagnosis? *J Am Vet Med Assoc.* (2017) 251:787–90. doi: 10.2460/javma.251.7.787
44. Scott HW. Hemilaminectomy for the treatment of thoracolumbar disc disease in the dog: a follow-up study of 40 cases. *J Small Animal Pract.* (1997) 38:488–94. doi: 10.1111/j.1748-5827.1997.tb03303.x
45. Burkert BA, Kerwin SC, Hosgood GL, Pechman RD, Fontenelle JP. Signalment and clinical features of diskospondylitis in dogs: 513 Cases (1980-2001). *J Am Vet Med Assoc.* (2005) 227:268–75. doi: 10.2460/javma.2005.227.268
46. Pilkington SA, Jackson SA, Gillett GR. Spinal epidural empyema. *Br J Neurosurg.* (2003) 17:196–270 doi: 10.1080/0268869031000108990
47. Khanna RK, Malik GM, Rock JP, Rosenblum ML. Spinal epidural abscess: evaluation of factors influencing outcome. *Neurosurgery.* (1996) 39:958–64. doi: 10.1227/00006123-199611000-00016
48. Tang HJ, Lin HJ, Liu YC, Li CM. Spinal epidural abscess—experience with 46 patients and evaluation of prognostic factors. *J Infect.* (2002) 45:76–81. doi: 10.1053/jinf.2002.1013
49. Karikari IO, Powers CJ, Reynolds RM, Mehta AI, Isaacs RE. Management of a spontaneous spinal epidural abscess: a single-center 10-year experience. *Neurosurgery.* (2009) 65:919–23. doi: 10.1227/01.NEU.0000356972.97356.C5
50. Chen SH, Chang WN, Lu CH, Chuang YC, Lui CC, Chen SF, et al. The clinical characteristics, therapeutic outcome, and prognostic factors of non-tuberculous bacterial spinal epidural abscess in adults: a hospital-based study. *Acta Neurol Taiwan.* (2011) 20:107–13. Available online at: https://pubmed.ncbi.nlm.nih.gov/21739389/
51. Connor DE Jr, Chittiboina P, Caldito G, Nanda A. Comparison Of Operative and nonoperative management of spinal epidural abscess: a retrospective review of clinical and laboratory predictors of neurological outcome. *J Neurosurg Spine.* (2013) 19:119–27. doi: 10.3171/2013.3.SPINE12762
52. Kim SD, Melikian R, Ju KL, Zurakowski D, Wood KB, Bono CM, et al. Independent predictors of failure of nonoperative management of spinal epidural abscesses. *Spine J.* (2014)14:1673–9. doi: 10.1016/j.spinee.2013.10.011

Conflict of Interest: EL, LD, LS, and JB were employed by Linnaeus Veterinary Limited.

The remaining authors declare that the research was conducted in the absence of any commercial or financial relationships that could be construed as a potential conflict of interest.

frontiers in Veterinary Science

CASE REPORT
published: 23 March 2022
doi: 10.3389/fvets.2022.828083

Case Report: Ventriculoperitoneal Shunting and Radiation Therapy Treatment in a Cat With a Suspected Choroid Plexus Tumor and Hypertensive Hydrocephalus

Elizabeth Mahon[1]*, *Aldara Eiras-Diaz*[2], *Sarah Mason*[3], *Fabio Stabile*[1] and *Ane Uriarte*[1]

[1] Department of Neurology and Neurosurgery, Southfields Veterinary Specialists, Essex, United Kingdom, [2] Department of Internal Medicine, Southfields Veterinary Specialists, Essex, United Kingdom, [3] Department of Oncology/Radiation Therapy, Southfields Veterinary Specialists, Essex, United Kingdom

OPEN ACCESS

Edited by:
Andrea Tipold,
University of Veterinary Medicine
Hannover, Germany

Reviewed by:
Miyoko Saito,
Azabu University, Japan
Sam Long,
Veterinary Referral Hospital, Australia
Michael Sean Kent,
University of California, Davis,
United States

***Correspondence:**
Elizabeth Mahon
beth.mahon@southfields.co.uk

Specialty section:
This article was submitted to Veterinary Neurology and Neurosurgery, a section of the journal Frontiers in Veterinary Science

Received: 02 December 2021
Accepted: 14 February 2022
Published: 23 March 2022

Citation:
Mahon E, Eiras-Diaz A, Mason S, Stabile F and Uriarte A (2022) Case Report: Ventriculoperitoneal Shunting and Radiation Therapy Treatment in a Cat With a Suspected Choroid Plexus Tumor and Hypertensive Hydrocephalus. Front. Vet. Sci. 9:828083. doi: 10.3389/fvets.2022.828083

A 14-year-old male neutered domestic short-hair cat was presented for a history of behavioral changes and episodes of urinary retention. Neurological examination was consistent with a multifocal intracranial neuroanatomical localization, with suspected right sided lateralisation and suspected raised intracranial pressure (ICP). Brain magnetic resonance imaging (MRI) revealed an intraventricular multilobulated well-defined T2W-hyperintense and T1W-isointense, markedly contrast enhancing mass lesion within the dorsal aspect of the III ventricle extending into the left lateral ventricle, causing hypertensive obstructive hydrocephalus. A ventriculoperitoneal shunt (VPS) was placed within the left lateral ventricle, followed by a radiation therapy (RT) course of 45 Gy total dose in 18 daily fractions. Six-months post-RT, computed tomography revealed mild reduction in mass size and resolution of the hydrocephalus. The patient was neurologically normal with no medical treatment. Raised ICP causes severe clinical signs, can lead to brain ischaemia and herniation, and significantly increases anesthetic risk during RT. Placement of a VPS in cats with hypertensive obstructive hydrocephalus may allow improvement of neurological signs due to raised ICP, and therefore making the patient a more stable candidate for anesthesia and radiation therapy.

Keywords: ventriculoperitoneal shunt, hydrocephalus, choroid plexus tumor, radiation therapy, cat

INTRODUCTION

Radiation therapy (RT) is an established treatment choice for inoperable intracranial tumors in cats (1). Ventriculoperitoneal shunt (VPS) placement has been described for the treatment of obstructive hypertensive hydrocephalus secondary to intraventricular tumors (2–4). To the best of the authors' knowledge, this is the first report of successful VPS placement and subsequent RT treatment in a cat with III ventricle tumor causing hypertensive obstructive hydrocephalus.

CASE PRESENTATION

A 14-year-old, male neutered, domestic short hair cat presented after a 2-month history of episodes

of urinary retention and behavioral changes. Before referral, the cat had been catheterised by the referring veterinary surgeon on several occasions after presenting with a distended, not easily expressible bladder. In between these episodes, it was reported that the cat would urinate once every 24 h and no periuria, stranguria or pollakiuria was noticed. There had been a gradual change in behavior, being more affectionate and disorientated at times. The disorientation increased and progressed to colliding into stationary objects the day before referral following sedation for abdominal imaging. Pre-referral, the following medications had been trialed: meloxicam (0.05 mg/kg q24 h PO) given for several days consecutively at various times in the two-month period when clinical signs began, prazosin (0.17 mg/kg q8–12 h PO) given for 7 weeks, two courses of amoxicillin-clavulanic (12.5 mg/kg q12 h PO) for a week each time and dantrolene (0.5 mg/kg q12 h PO). None of these had resulted in resolution of his urinary signs or altered behavior

On clinical exam, vital parameters were within normal limits. The body condition score was 5/9. On cardiac auscultation there was a grade 4/6 left apical systolic heart murmur. No abnormalities were detected on abdominal palpation. Neurological exam revealed mild obtundation and compulsive pacing with a tendency to circle to the right. There were inconsistent proprioceptive deficits mainly on the left side of the body. The menace response and oculocephalic reflexes were reduced bilaterally, and the pupillary light reflexes absent bilaterally. The neurological examination was consistent with multifocal intracranial neuroanatomical localization, with suspected right sided lateralisation. The main differential diagnoses at this stage were neoplasia or inflammatory granuloma.

Systolic blood pressure measurement was 130 mmHg. Serum biochemistry revealed raised creatinine kinase (2,241 U/L, reference range 50–200 U/L), alanine transaminase (111 IU/L, reference range 0–40 IU/L) and alkaline phosphatase (33 U/L, reference range 0–25 U/L). Hematology was unremarkable. Abdominal ultrasonography did not reveal any abnormalities and retrograde urethrocystogram did not show any obvious filling defects of the urethral lumen or urinary bladder. Urinalysis of a sample obtained by cystocentesis revealed a urine specific gravity of 1.042 (reference >1.035), a urine protein: creatine ratio of 2 (reference 0–0.2) and on dipstick evaluation a pH of 6, protein 3+ and hemoglobin-RBC 4+. The urine sample was grossly haematuric. Urine sediment analysis showed the presence of >100 red blood cells (reference <5/hpf) but was otherwise unremarkable. There was no growth on urine bacterial culture. Although glomerular disease could not be completely excluded, given the presence of gross haematuria, together with the absence of hypoalbuminemia, hypercholesterolemia or azotaemia, the increased urine protein:creatine ratio was considered most likely secondary to blood contamination due to the cystocentesis technique (5, 6).

Three-view, thoracic radiographs showed mild cardiomegaly with no radiographic evidence of congestive heart failure. Echocardiography was declined by the owner. Magnetic resonance imaging (MRI) was acquired from a 1.5-Tesla Philips Achieva Magnetic Resonance Imaging Scanner (Phillips Medical System, Eindhoven, Netherlands). Dorsal, transverse and sagittal T2-weighted images, dorsal, transverse and sagittal T1-weighted images plus T1-weighted images with Gadolinium contrast media, fluid-attenuated inversion recovery transverse images and T2*-weighted transverse images of the brain were obtained. MRI revealed a multilobulated, well defined T2-weighted hyperintense and T1 weighted isointense mass measuring 1.7 × 1.3 × 1.5 cm within the dorsal aspect of the III ventricle. There was marked heterogenous contrast enhancement. The mass extended within the left lateral ventricle and compressed the rostral aspect of the cerebellum caudally, the inter-thalamic adhesion rostro-ventrally and the pons ventrally. The lateral ventricles and olfactory recess were severely distended with normal signal intensity and sulcal effacement was noticed through the forebrain (**Supplementary Figure 1**). The MRI was consistent with an extra-axial mass within the III ventricle causing obstructive hypertensive hydrocephalus. The main differentials were a choroid plexus carcinoma/papilloma, ependymoma, subependymoma, meningioma, neurocytoma, pilocytic astrocytoma and oligodendroglioma. The collection of a cerebrospinal fluid (CSF) sample was not performed as it is contraindicated in cases of raised intracranial pressure as it increases the risk of brain herniation (7).

Treatment with 0.1 mg/kg of dexamethasone intravenously and 1 g/kg of mannitol intravenously was commenced followed 24 h later by 1.1 mg/kg of prednisolone PO q24 h and prazosin at 0.17 mg/kg PO q8 h which was continued until surgery 5 days later. At admission for surgery, the demeanor was slightly brighter, but the neurological exam was similar to presentation. No more episodes of urinary retention were observed. Under general anesthesia, a lateral approach to the parietal bone was performed. The temporal muscle was retracted, and a small, circular craniotomy was performed. The shunt was placed within the left lateral ventricle to the abdominal peritoneum (miniNAV® SHUNTSYSTEM with pediatric burrhole reservoir and differential pressure unit of 10 cm H_20). The craniotomy was sutured routinely without complications. Under the same anesthesia, a computerized tomography (CT) (Siemens Somatom Spirit) at 2 mm slice thickness and 1 mm collimation confirmed successful placement of the VPS and radiation therapy planning was performed. Intraoperatively, 20 mg/kg IV cefuroxime was given every 90 mins. After the procedure and overnight, treatment included 2 ml/kg/h of Hartmann's solution, 1 mcg/kg/ medetomidine as a constant rate infusion and 0.1 mg/kg methadone according to pain score using the Glasgow Feline Composite Measure Pain Scale.

The day after VPS placement, neurological exam had improved. There was still a tendency to circle to the right. The menace response and proprioception were normal and there were bilaterally reduced pupillary light reflexes. Twenty-four hours after surgery an episode of opisthotonos and ear twitching was observed. Seizure activity was suspected and 22 mg/kg of levetiracetam q8 h PO was therefore started. Twelve days after VPS placement, RT began. The gross tumor volume (GTV) was contoured to include all contrast enhancing tissue (Eclipse version 15). The clinical target volume (CTV) was agreed by two boarded radiation oncologists and was contoured to include the

VPS and the lateral ventricles. A planning target volume of 3 mm was applied in all dimensions (see **Supplementary Table 1**). A bespoke dental mold bite block was made and fixed to a rigid Perspex positioning bridge. Prescription isocentre was to the midpoint of the PTV. No shielding was used. No bolus was used. Port intervals were performed at regular intervals during treatment. 45 Gy total dose was delivered using 6 MV photons in 18 daily fractions (total length over 23 days). The plan comprised of three wedged beams at G0G90G20.

Post VPS placement, 1.1 mg/kg prednisolone q24 h PO was continued for 2 months before tapering over 10 days and discontinuing. Levetiracetam was continued for 6 months. Six months after RT, no more seizure activity or urinary issues were reported. The behavioral changes had gradually returned to normal. On clinical and neurological examination no abnormalities were detected. Follow-up CT of the head at this time revealed a stable disease ($1.7 \times 1.3 \times 1.3$ cm compared with $1.7 \times 1.3 \times 1.5$ cm previously) (**Supplementary Figure 2**) (8). The cerebellar shape was rounded in sagittal reformat and there was no trans tentorial herniation identified. The lateral ventricles were only slightly distended. The CT confirmed resolution of the hypertensive hydrocephalus.

At the time of writing, 10 months after VPS placement, the cat was on no medication and still according to the owner, free of clinical signs.

DISCUSSION

Choroid plexus tumors are rare tumors in cats, and the reported clinical signs are variable including seizures, blindness and altered mental status (1, 9). Although not mentioned if the cats in these studies had increased ICP, in people and dogs choroid plexus tumors are widely associated with raised ICP (2, 10). Ventricular shunt placement has been shown to significantly improve clinical symptoms of human patients with increased ICP secondary to brain tumors (11). A retrospective case series describing four dogs with brain tumors affecting the III ventricle reported that clinical signs such as abnormal mental status, unlocalizable pain, decreased menace response and impaired vision improved after VPS placement, demonstrating that these clinical signs were likely due to the raised ICP rather than the brain tumors themselves (2). Furthermore, a retrospective study reporting 45 dogs treated with VPS due to hypertensive hydrocephalus found that decreases in ventricular volume and increases in brain parenchyma after VPS placement have been associated with improvement in one or more pre-operative clinical signs in dogs (12). The cat in this case report had an improvement in neurological examination and clinical signs post VPS placement, demonstrating that the raised ICP was likely causing the presenting clinical signs.

There have been no previous reports of urinary retention in cats associated with brain tumors and/or hypertensive hydrocephalus. The micturition process involves the storage and emptying phases of the bladder and is controlled by both the autonomic and somatic nervous system (13). Urinary retention can be caused by both neurogenic and non-neurogenic disease, with the latter due to anatomic urethral outflow obstruction (14). The thorough investigations into bladder function, including urine analysis and culture, abdominal ultrasound and retrograde urethrocystogram, did not reveal a non-neurogenic cause. In the absence of consistent clinical signs or response to appropriate therapy, feline lower urinary tract disease was considered unlikely. Therefore, neurological disease was presumed to be influencing the cat's urine retention, particularly as there was resolution of clinical signs post treatment of raised ICP.

The voiding of urine is coordinated by the micturition center and involves detrusor muscle contraction and urethral sphincter relaxation. Afferent impulses are transmitted to the sacral spinal cord when stretch receptors in the bladder wall are stimulated. These impulses ascend to the pontine reticular formation (the micturition center) and the cerebral cortex. Voluntary control of urination is the response of inhibitory influence from the cerebral cortex, basal nuclei, thalamus, hypothalamus and cerebellum on the micturition center (13, 15). In people, urinary tract retention has been described secondary to structural disorders in the frontal lobe, posterior fossa, hypothalamus, basal nuclei, paraventricular white matter, internal capsule, cerebellum, brainstem and thalamus (16–19). In cats, severe cluster seizures have also been associated with neurogenic urinary retention (20). In our case, the urinary signs resolved when the raised ICP was treated. It is thought that the urinary retention was caused by increased pressure on the intracranial structures involved in micturition, potentially the thalamus due to the location of the tumor. Lesions in the thalamus in people have been associated with urinary retention, but to the best of the authors knowledge, this has never been reported in veterinary medicine (18, 19).

Increased ICP can be caused by trauma, ischaemia or space occupying lesions such as neoplasia, cysts or inflammation. As ICP increases, cerebrovascular autoregulation is impaired causing a decrease in the cerebral perfusion and ischaemic damage. Additionally, there may be herniation of brain tissue and this ultimately can be life threatening (21, 22). The use of anesthetic agents can affect cerebral blood flow and further increase ICP, therefore increasing the chance of fatality (23). Multiple anesthetics are required for RT and so it is vital that increases in ICP are treated before commencing the course.

Medical management of increased ICP involves reducing CSF production through glucocorticoid and diuretics but this often only results in short-term improvement of signs. Electrolytes must be carefully monitored with the use of diuretics, particularly in combination with glucocorticoids, as electrolyte depletion is a common sequalae (21, 24). Frusemide, acetazolamide, mannitol and hypertonic saline have been described, with mannitol and hypertonic saline used in cases where it is required to rapidly reduce ICP (21, 25). Omeprazole has also been proposed as a possible treatment to decrease CSF production. It has been demonstrated in dogs and rabbits that CSF production decreases when treated with omeprazole by ventriculocisternal or intravenous administration (26, 27). However, a pilot study with 15 healthy beagles given oral omeprazole for 14 days suggested that CSF production was not affected by this medication (28). Further studies are therefore required to assess its effectiveness in reducing CSF production in cases of hydrocephalus, thus it

was not used in this case. This cat received glucocorticoids and a dose of mannitol (1 g/kg IV) during general anesthesia when the images from the MRI demonstrated obstructive hypertensive hydrocephalus. This was sufficient to stop further deterioration before VPS placement.

Placement of a VPS is often the preferred option for hydrocephalus treatment, although this too comes with various complications such as mechanical shunt failure, infection, hemorrhage and over drainage (2, 21). In human medicine, rarely metastatic spread of neoplastic cells in the CSF through the VPS from the brain to the abdomen have been reported (29). Literature on VPS placement success and complication rate in cats is lacking. One study in human medicine suggested a complication rate of 23.8% in patients treated with a VPS secondary to both communicating and non-communicating hydrocephalus (30). A comparison between dogs with congenital hydrocephalus treated with VPS or medical management showed similar outcomes, although the median follow up time was only 9 months for medical and 15 months for surgical management (31). However, a case series with dogs with hydrocephalus secondary to tumors of the third ventricle found that the ICP measured considerably higher (28 mmHg and 31 mmHg) than the intracranial pressures found in dogs with communicating internal hydrocephalus (mean 8.8 mmHg, range from 3 to 18 mmHg) (2, 32). In these dogs with hydrocephalus secondary to III ventricle tumors, their clinical signs were not improved by medical management but significantly improved after being treated with VPS placement (2). This supports the use of VPS placement in obstructive hypertensive hydrocephalus patients particularly if not responding to initial medical management. In this case, the intracranial pressure of the cat was not measured, but the limited response to medical management in the interim between diagnosis and VPS placement was another indicator to proceed with the VPS placement.

Successful surgical removal of intracranial tumors has been well described in cats (1, 33). Nonetheless, for tumors in less accessible areas, radiation therapy is a viable alternative with one study finding that 95% of cats had an improvement in clinical signs after treatment (1). However, the lack of histological diagnosis for the tumor in this case and therefore the potential response to RT is a limitation of the case report. For tumors in the III ventricle, surgical resection has been successfully attempted in veterinary medicine (34, 35). However, due to the very challenging location, it carries a high rate of complications and post-operative mortality, hence was not attempted in this case (4, 36, 37). There has been one case report of successful surgical removal of a tumor from the III ventricle in a cat which was later diagnosed histologically as an ependymoma. In this particular case, RT was not available and so a left rostral tentorial craniotomy was performed and the III ventricle approached via the dilated left lateral ventricle (35).

Palliative VPS placement has been described in a cat with a later histopathological diagnosed ependymomas causing hypertensive obstructive hydrocephalus. However, the cat presented 6 months later with reoccurrence of neurological signs and was euthanised 10 months after VPS placement due to rapid deterioration (4). In dogs, both RT and VPS placement have been described for the treatment of ventricular tumors, but direct comparison of survival times is difficult due to variations in detailed reports of tumor location and clinical condition (2, 38). Our case presented a rapid improvement and 10 months after diagnosis, the cat was still neurologically normal and free of clinical signs.

This case report describes successful VPS placement in a cat with obstructive hypertensive hydrocephalus due to a mass lesion within the III ventricle. The cat's clinical signs improved after VPS placement and was therefore a more stable candidate for multiple general anesthetics for RT.

CONCLUSION

VPS placement should be considered for cases of obstructive hypertensive hydrocephalus to improve clinical signs and the safety of multiple general anesthetics for RT. The combined treatment of VPS placement and RT makes for good long-term outcomes.

DATA AVAILABILITY STATEMENT

The original contributions presented in the study are included in the article/**Supplementary Material**, further inquiries can be directed to the corresponding author/s.

ETHICS STATEMENT

Ethical review and approval was not required for the animal in this study because it is a retrospective case report. Written informed consent was obtained from the owners for the participation of their animal in this study.

AUTHOR CONTRIBUTIONS

EM: article writing. AU: main clinician during case presentation and performed the surgery. AE-D: performed internal medicine consultation. SM: radiation planning. FS: clinical support. All authors contributed to the article and approved the submitted version.

ACKNOWLEDGMENTS

We would like to thank the supporting clinicians and nursing team at Southfields Veterinary Specialists.

SUPPLEMENTARY MATERIAL

The Supplementary Material for this article can be found online at: https://www.frontiersin.org/articles/10.3389/fvets.2022.828083/full#supplementary-material

REFERENCES

1. Körner M, Roos M, Meier VS, Soukup A, Cancedda S, Parys MM, et al. Radiation Therapy for Intracranial Tumours in Cats with Neurological Signs. *J Feline Med Surg.* (2019) 21:765–71. doi: 10.1177/1098612X18801032
2. Orlandi R, Vasilache CG, Mateo I. Palliative ventriculoperitoneal shunting in dogs with obstructive hydrocephalus caused by tumors affecting the third ventricle. *J Vet Intern Med.* (2020) 34:1556–62. doi: 10.1111/jvim.15818
3. Stefani AD. Surgical technique, postoperative complications and outcome in 14 dogs treated for hydrocephalus by ventriculoperitoneal shunting. *Vet Surg.* (2011) 40:183–91. doi: 10.1111/j.1532-950X.2010.00764.x
4. DeJesus A, Cohen EB, Galban E, Suran JN. Magnetic resonance imaging features of intraventricular ependymomas in five cats. *Vet Radiol Ultrasound.* (2017) 58:326–33. doi: 10.1111/vru.12464
5. Couëtil L, Hoffman A, Hodgson J, Buechner-Maxwell V, Viel L, Wood J, et al. ACVIM consensus statement. *J Vet Intern Med.* (2007) 21:356–61. doi: 10.1111/j.1939-1676.2007.tb02975.x
6. Vientós-Plotts A, Behrend E, Welles E, Chew D, Gaillard P, Busler J, et al. Effect of blood contamination on results of dipstick evaluation and urine protein-to-urine creatinine ratio for urine samples from dogs and cats. *Am J Vet Res.* (2018) 79:525–31. doi: 10.2460/ajvr.79.5.525
7. Dewey CW. *A Practical Guide to Feline and Canine Neurology*. Second Add. Iowa, USA: Wiley-Blackwell (2008).
8. Biller B, Berg J, Garrett L, Ruslander D, Wearing R, Abbott B, et al. 2016 AAHA Oncology Guidelines for Dogs and Cats. *J Am Anim Hosp Assoc.* (2016) 52:181–204. doi: 10.5326/JAAHA-MS-6570
9. Troxel MT, Vite CH, van Winkle TJ, Newton AL, Tiches D, Dayrell-Hart B, et al. Feline intracranial neoplasia: retrospective review of 160 cases (1985–2001). *J Vet Intern Med.* (2003) 17:850–59. doi: 10.1111/j.1939-1676.2003.tb02525.x
10. Jaiswal S, Vij M, Mehrotra A, Kumar B, Nair A, Jaiswal AK, et al. Choroid plexus tumors: a clinico-pathological and neuro-radiological study of 23 cases. *Asian J Neurosurg.* (2013) 8:29–35. doi: 10.4103/1793-5482.110277
11. Nigim F, Critchlow JF. Role of ventriculoperitoneal shunting in patients with neoplasms of the central nervous system: an analysis of 59 cases. *Mol Clin Oncol.* (2015) 3:1381–86. doi: 10.3892/mco.2015.627
12. Schmidt MJ, Hartmann A, Farke D, Failling K, Kolecka M. Association between improvement of clinical signs and decrease of ventricular volume after ventriculoperitoneal shunting in dogs with internal hydrocephalus. *J Vet Int Med.* (2019) 33:1368–75. doi: 10.1111/jvim.15468
13. Coates JR. BSAVA manual of canine and feline neurology. In: Platt S and Olby S, eds. *British Small Animal Veterinary Assosiation*. Glouster, GL2 2AB (2012).
14. Hostutler RA, Chew DJ, DiBartola SP. Recent concepts in feline lower urinary tract disease. *Vet Clin North Am Small Animal Pract.* (2005) 35:147–70. doi: 10.1016/j.cvsm.2004.08.006
15. Nickel RF, Venker-van Haagen AJ. Functional anatomy and neural regulation of the lower urinary tract in female dogs: a review. *Vet Q.* (1999) 21:83–5. doi: 10.1080/01652176.1999.9694999
16. Sakakibara R. *Lower Urinary Tract Dysfunction in Patients with Brain Lesions. Handbook of Clinical Neurology*. 1st ed. Vol. 130. Amsterdam: Elsevier BV (2015).
17. Fowler CJ. Neurological disorders of micturition and their treatment. *Brain.* (1999) 122:1213–31. doi: 10.1093/brain/122.7.1213
18. Sakakibara R, Hattori T, Yasuda K, Yamanishi T. Micturitional disturbance after acute hemispheric stroke: analysis of the lesion site by CT and MRI. *J Neurol Sci.* (1996) 137:47–56. doi: 10.1016/0022-510X(95)00322-S
19. Umemura T, Ohta H, Yokota A, Yarimizu S, Nishizawa S. Urinary retention associated with stroke. *J UOEH.* (2016) 38:263–9. doi: 10.7888/juoeh.38.263
20. Balducci F, Risio LD. Neurogenic urinary retention in cats following severe cluster seizures. *J Feline Med Surg.* (2017) 19:246–50. doi: 10.1177/1098612X15602739
21. Coates JR, Axlund TW, Dewey CW, Smith J. Hydrocephalus in dogs and cats. *Advances*. (2006) 28:136–46. doi: 10.1016/j.cvsm.2009.09.008
22. Lyons MK. Cerebrospinal fluid physiology and the management of increased intracranial pressure. *Mayo Clin Proc.* (1990) 65:684–707. doi: 10.1016/S0025-6196(12)65131-3
23. Armitage-Chan EA, Wetmore LA, Chan DL. Anesthetic management of the head trauma patient: state of the art review. *J Vet Emerg Critic Care.* (2007) 17:5–14. doi: 10.1111/j.1476-4431.2006.00194.x
24. Shihab N, Davies E, Kenny PJ, Loderstedt S, Volk HA. Treatment of hydrocephalus with ventriculoperitoneal shunting in twelve dogs. *Vet Surg.* (2011) 40:477–84. doi: 10.1111/j.1532-950X.2011.00832.x
25. Pigott A, Rudloff E. Traumatic brain injury—a review of intravenous fluid therapy. *Front Vet Sci.* (2021) 8:1–12. doi: 10.3389/fvets.2021.643800
26. Javaheri S, Corbett WS, Simbartl LA, Mehta S, Khosla A. Different effects of omeprazole and Sch 28080 on canine cerebrospinal fluid production. *Brain Res.* (1997) 754:321–24. doi: 10.1016/S0006-8993(97)00175-3
27. Lindvall-Axelsson M, Nilsson C, Owman C, Winbladh B. Inhibition of cerebrospinal fluid formation by omeprazole. *Exp Neurol.* (1992) 115:394–99. doi: 10.1016/0014-4886(92)90204-4
28. Girod M, Allerton F, Gommeren K, Tutunaru AC, de Marchin J, Soens I, et al. Evaluation of the effect of oral omeprazole on canine cerebrospinal fluid production: a pilot study. *Vet J.* (2016) 209:119–24. doi: 10.1016/j.tvjl.2015.10.045
29. Rickert CH. Abdominal metastases of pediatric brain tumors via ventriculo-peritoneal shunts. *Child's Nervous Syst.* (1998) 14:10–4. doi: 10.1007/s003810050166
30. Merkler AE, Ch'ang J, Parker WE, Murthy SB, Kamel H. The rate of complications after ventriculoperitoneal shunt surgery. *World Neurosurg.* (2017) 98:654–8. doi: 10.1016/j.wneu.2016.10.136
31. Gillespie S, Gilbert Z, Decker SD. Results of oral prednisolone administration or ventriculoperitoneal shunt placement in dogs with congenital hydrocephalus: 40 cases (2005–2016). *J Am Vet Med Assoc.* (2019) 254:835–42. doi: 10.2460/javma.254.7.835
32. Kolecka M, Farke D, Failling K, Kramer M, Schmidt MJ. Intraoperative measurement of intraventricular pressure in dogs with communicating internal hydrocephalus. *PLoS ONE.* (2019) 14:1–12. doi: 10.1371/journal.pone.0222725
33. Cameron S, Rishniw M, Miller AD, Sturges B, Dewey CW. Characteristics and survival of 121 cats undergoing excision of intracranial meningiomas (1994–2011). *Vet Surg.* (2015) 44:772–76. doi: 10.1111/vsu.12340
34. Lehner L, Czeibert K, Benczik J, Jakab C, Nagy G. Transcallosal removal of a choroid plexus tumor from the lateral ventricle in a dog. Case report. *Front Vet Sci.* 7 (September):1–7. doi: 10.3389/fvets.2020.00536
35. Simpson DJ, Hunt GB, Tisdall PLC, Govendir M, Zaki S, France MP, et al. Surgical removal of an ependymoma from the third ventricle of a cat. *Aust Vet J.* (1999) 77:645–48. doi: 10.1111/j.1751-0813.1999.tb13150.x
36. Heidner GL, Kornegay JN, Page RL, Dodge RK, Thrall DE. Analysis of survival in a retrospective study of 86 dogs with brain tumors. *J Vet Intern Med.* (1991) 5:219–26. doi: 10.1111/j.1939-1676.1991.tb00952.x
37. Marino DJ, Dewey CW, Loughin CA, Marino LJ. severe hyperthermia, hypernatremia, and early postoperative death after transethmoidal cavitron ultrasonic surgical aspirator (CUSA)-assisted diencephalic mass removal in 4 dogs and 2 cats. *Vet Surg.* (2014) 43:888–94. doi: 10.1111/j.1532-950X.2014.12238.x
38. Mariani CL, Schubert TA, House RA, Wong MA, Hopkins AL, Barnes Heller HL, et al. Frameless stereotactic radiosurgery for the treatment of primary intracranial tumours in dogs. *Vet Comp Oncol.* (2015) 13:409–23. doi: 10.1111/vco.12056

Conflict of Interest: The authors declare that the research was conducted in the absence of any commercial or financial relationships that could be construed as a potential conflict of interest.

frontiers | Frontiers in Veterinary Science

ORIGINAL RESEARCH
published: 18 May 2022
doi: 10.3389/fvets.2022.880038

Retrospective Preliminary Assessment of Routine Follow-Up Low-Field Magnetic Resonance Imaging in Dogs Presumptively Diagnosed With Discospondylitis

Maria Ines de Freitas, Enzo Vettorato, Elena Scarpante, Giunio Bruto Cherubini and Abby Caine*

Dick White Referrals, Linnaeus Veterinary Ltd, Cambridgeshire, United Kingdom

Background: The usefulness of routine follow-up Magnetic Resonance Imaging (MRI-2) in asymptomatic dogs treated for discospondylitis is unknown.

Methods: This cross-sectional retrospective study investigated the features of MRI-2 in a heterogeneous group of dogs treated for discospondylitis, and if these were associated with the presence or absence of clinical signs. After comparing initial MRI (MRI-1) and MRI-2, an observer, blinded to the dog's clinical signs, described the MRI-2 findings. The study population was then divided into symptomatic or asymptomatic at the time of MRI-2. Two separate observers subjectively classified the discospondylitis as active or inactive. Repeatability and interobserver agreement were evaluated.

Results: A total of 25 dogs were included. At the time of MRI-2 16 (64%) dogs were asymptomatic and 9 (36%) were symptomatic. Based on MRI-2, 20 (80%) and 18 (72%) out of 25 dogs were considered to have active discospondylitis by the first and second observers, respectively. Interobserver agreement was moderate. No MRI-2 features were associated with the clinical status. The subjective classification of inactive discospondylitis was significantly associated with asymptomatic clinical status, but the classification of active discospondylitis was evenly distributed between groups.

Conclusion: This study did not identify a meaningful association between the clinical status of dogs treated for presumptive discospondylitis and MRI-2 results. There were no specific MRI-2 features which were associated with the clinical status.

Keywords: discospondylitis, MRI, vertebral endplate, dog, spine, intervertebral disc

OPEN ACCESS

Edited by:
Luisa De Risio,
Linnaeus Veterinary Limited,
United Kingdom

Reviewed by:
Steven De Decker,
Royal Veterinary College (RVC),
United Kingdom
John Henry Rossmeisl,
Virginia Tech, United States

****Correspondence:***
Maria Ines de Freitas
ines.defreitas@dwr.co.uk

Specialty section:
This article was submitted to Veterinary Neurology and Neurosurgery, a section of the journal Frontiers in Veterinary Science

Received: *20 February 2022*
Accepted: *19 April 2022*
Published: *18 May 2022*

Citation:
de Freitas MI, Vettorato E, Scarpante E, Cherubini GB and Caine A (2022) Retrospective Preliminary Assessment of Routine Follow-Up Low-Field Magnetic Resonance Imaging in Dogs Presumptively Diagnosed With Discospondylitis. Front. Vet. Sci. 9:880038. doi: 10.3389/fvets.2022.880038

INTRODUCTION

Discospondylitis is an infection of one, or more, intervertebral disc (IVD) spaces and adjacent vertebral endplates (1). The infection may also affect the vertebral bodies and surrounding soft tissues or extend into the vertebral canal and cause epidural empyema (2). Diagnosis of discospondylitis may be challenging as clinical signs are often unspecific (1). Magnetic resonance imaging (MRI) is the most sensitive and specific modality for the detection of infections of the vertebral column in human patients (3, 4) and its use in dogs with discospondylitis has been well documented (5–8).

Treatment for discospondylitis generally consists of administration of antibiotic(s), but surgical intervention may be necessary in some dogs (2, 9, 10). While various antibiotic protocols have been proposed, the appropriate length of the treatment is unknown (1, 11, 12). Relapse of the condition is likely to occur if antibiotics are discontinued prematurely (13). Furthermore, clinical signs and diagnostic imaging findings are often incongruent during disease progression, complicating the decision regarding when to interrupt treatment. Radiographic deterioration of discospondylitis was reported despite improvement of clinical signs in dogs (14).

While MRI is more sensitive than radiography for diagnosing discospondylitis (5, 15, 16), the value of routine follow-up MRI (MRI-2) to assist clinical decision making regarding the appropriate time point of antibiotic therapy discontinuation in asymptomatic dogs has not been evaluated. In human medicine, the usefulness of routine MRI-2 in asymptomatic patients is questionable with multiple studies reporting progressive imaging deterioration despite successful clinical response to the treatment (17–19). In fact, the clinical practice guidelines of the Infectious Disease Society of America do not recommend follow-up MRI in patients with a favorable clinical response to therapy in vertebral osteomyelitis (20).

The aim of our study is to describe MRI-2 features in a heterogeneous group of dogs presumptively diagnosed with discospondylitis and to investigate if there is an association between the MRI-2 features and the clinical status. We hypothesize that MRI-2 findings will be unspecific and not associated with the clinical status.

MATERIALS AND METHODS

The medical records of dogs diagnosed with and treated for discospondylitis by an ECVN board-certified neurologist, or ECVN resident, at Dick White Referrals from 2010 to 2019 were retrieved from the electronic database. Signed owner consent for the use of clinical information was obtained at the time of the animal admission to the hospital. No ethical approval was obtained due to the retrospective nature of this cross-sectional study, and prior acquisition of written owner consent for patient data to be included in scientific studies.

Cases were immediately excluded if: (1) clinical records were not complete up to the time of MRI-2; (2) antibiotics were not administered as part of the treatment; (3) MRI-2 of the affected vertebral column region was not performed at least 28 days from diagnosis.

Of the remaining cases, the MRI study obtained on initial presentation (MRI-1) was reviewed by an ECVDI-certified veterinary radiologist (AC) unaware of the dog's clinical signs. Only cases that fulfilled the criteria for presumptive diagnosis of discospondylitis were included in the study. Specifically, involvement of the intervertebral disc and adjacent vertebral endplates, a short-tau inversion recovery (STIR) hyperintense signal and/or contrast enhancement of the paravertebral soft-tissues and at least one of the following features: presence of a STIR hyperintense signal and/or contrast enhancement of the IVD, STIR hyperintense signal or T2-Weighted (T2w) hypointense or hyperintense signal of the adjacent endplate(s) (6, 7, 21).

Of the final population of dogs included in the study, signalment and clinical information (**Table 1**), culture results from urine, blood, or affected IVD samples were recorded. The IVD samples were collected by ultrasound-guided percutaneous fine-needle-aspiration or intraoperatively. Treatment following diagnosis was recorded as medical, if only antibiotic therapy and analgesic drugs were administered; or surgical, if surgery preceded the antibiotic therapy. The type of medical treatment following MRI-1, including antibiotic and/or analgesic therapy was recorded, as well as whether antibiotic therapy was continued following MRI-2. The time elapsed between MRI-1 and MRI-2 was also recorded.

The cases were divided into two groups based on the clinical status at the time of MRI-2. Dogs were assigned to the "asymptomatic" group if clinical signs had resolved and MRI-2 was performed only as part of a re-examination, or to the "symptomatic" group if response to the treatment was unsatisfactory due to either clinical deterioration or failure to clinically improve.

Both MRI-1 and MRI-2 were performed under general anesthesia using a low-field, 0.4 T, permanent, open magnet (Aperto Lucent, Hitachi Medical Corporation, Tokyo, Japan) to include the portion of the spinal cord indicated by the clinical neuro-localization on MRI-1, and to include the previously diagnosed discospondylitis site on MRI-2. Dogs were positioned in dorsal recumbency with the pelvic limbs in a neutral position. The first observer (AC), blinded to the dog's clinical status, reviewed the acquired images and documented the location of affected disc space and presence or absence of specific features, all of which are summarized in **Table 2**.

Two observers (AC and ES), unaware of the dog's clinical status, compared MRI-1 and MRI-2 and subjectively classified each case as active or inactive discospondylitis, based on the overall interpretation of the MRI-2 findings. To assess intra-observer repeatability of this subjective assessment, the images were re-assessed 2 months later by the first observer (AC), and the scores repeated.

Whilst no single feature independently led to a case being assigned "active" or "inactive", the lack of regional lymphadenomegaly; the lack of STIR hyperintense signal and/or contrast enhancement of the perilesional soft tissues, beyond the tissues dissected during the previous surgical approach; well defined endplates with no-to-mild STIR hyperintensity; lack of STIR hyperintense epidural material; no-to-mild only enhancement of the affected vertebrae; T2-W and STIR hypointense intravertebral discs compared to spinal cord were findings considered to be suggestive of inactive disease. In contrast, regional lymphadenomegaly; STIR hyperintensity and/or contrast enhancement of the perilesional soft tissues, beyond the tissues dissected during the previous surgical approach; ill-defined and effaced endplates with strong STIR hyperintensity; STIR hyperintense epidural material; strong contrast enhancement of the endplates and bodies of the affected vertebrae were features which were considered to be suggestive

of active disease (6–8, 21). In cases where the features suggestive of active and inactive overlapped, the classification was awarded based on observer's subjective assessment.

Statistical Analysis

The distribution of continuous variables was assessed using D'Agostino and Pearson test and results are reported as mean ± standard deviation or median [95% confidence intervals (CI)], accordingly. Mann-Whitney U test was used to compare the time between MRI-1 and MRI-2 between symptomatic and asymptomatic groups.

McNemar test was used to analyze paired ordinal variables and to assess the presence of systematic difference between: (1) specific features detected on MRI-1 and MRI-2; (2) presence of active discospondylitis or inactive discospondylitis on MRI-2 between symptomatic and asymptomatic groups; (3) repeatability of identifying active discospondylitis or inactive discospondylitis on MRI-2.

The Cohen's Kappa (k) coefficient was calculated to measure inter-observer agreement.

Fisher's exact test was used to analyze unpaired ordinal variables: (1) type of treatment (medical or surgical) between symptomatic and asymptomatic groups; (2) type of treatment and active or inactive discospondylitis on MRI-2.

A $p < 0.05$ was considered statistically significant. Odd ratio (OR) and 95% CI, sensitivity and specificity are reported when appropriate.

To study if any of the MRI-2 features were associated with the presence of clinical signs a backward stepwise regression was performed. Variables with variance inflation factor (VIF) > 5 were excluded because of multicollinearity. Hosmer-Lemshow test and Likelyhood ratio test were used to confirm the good fitness of the model used.

RESULTS

A total of 168 dogs presumptively diagnosed with discospondylitis were initially identified, but only 25 fulfilled the inclusion criteria (**Figure 1**).

Demographic and clinical data of the population of dogs included in this study are summarized in **Table 1**. Spinal hyperesthesia and paresis were reported in 96 and 40% of the dogs, respectively. Clinical signs were present for a median of 30 days before hospital admission. Discospondylitis was naturally occurring in 20/25 (80%) cases and developed after spinal surgery to address spinal cord compression secondary to intervertebral disc disease in 5/25 (20%) cases: 2 dogs following lumbosacral (LS) dorsal laminectomy, annulectomy (1/2) and IVD fenestration (1/2); 2 dogs following IVD fenestration performed at the time of thoracolumbar hemilaminectomy; and 1 dog following a cervical ventral slot. Time between surgery and development of discospondylitis was 9, 30, 75, 93, and 102 days. Dogs who underwent L7-S1 dorsal laminectomy (2/25) were diagnosed with discospondylitis based on clinical deterioration despite lack of neural tissue compression, presence of STIR hyperintense and/or enhancing soft tissues surrounding to the affected IVD, as well as abnormal IVD space and adjacent vertebral bodies (**Figure 2**). Dogs diagnosed with discospondylitis following thoracolumbar IVD fenestration (2/25) were diagnosed with discospondylitis based on marked IVD and endplate changes, and absence of similar changes in the remainder of the fenestrated discs (**Figure 3**). The dog that underwent ventral slot was subsequently diagnosed with discospondylitis based on severe endplate changes, characterized by strong STIR hyperintense signal which extended within the vertebral body and heterogenous, ill-defined endplate margins, as well as presence of STIR hyperintense epidural material and lack of neural tissue compression to explain the clinical deterioration (**Figure 4**).

In 56% of the dogs, discospondylitis affected the LS intervertebral disc. Treatment between MRI-1 and MRI-2 was medical in 13 (52%) dogs and surgical in 12 (48%) dogs. Surgical treatment was pursued at the clinician's discretion to address spinal cord compression secondary to disc extrusion or empyema (10/12), and/or curettage and acquisition of samples for culture (10/12). Surgical treatment consisted of: C6-C7 ventral slot revision for curettage and sample collection in 1/12 dogs; T12-T13 hemilaminectomy, spinal cord decompression and IVD fenestration in 1/12 dogs; L2-L3 IVD fenestration and curettage in 1/12 dogs; L3-L4 hemilaminectomy, spinal cord decompression and IVD fenestration in 1/12 dogs; L6-L7 mini-hemilaminectomy, spinal cord decompression and IVD fenestration in 1/12 dogs; exploratory laparotomy to treat a sublumbar abscess secondary to migrating foreign body in 1/12 dogs; lumbosacral dorsal laminectomy, IVD fenestration and curettage in 5/12 dogs; revision of the previous lumbosacral dorsal laminectomy in 1/12 dogs.

Samples for culture of different tissues were taken in 22/25 (88%) dogs. Urine culture was performed in 14/25 (56%) dogs and was positive in 3 dogs: Proteus mirabilis ($n = 2$) and Escherichia coli ($n = 1$). A total of 13/25 (52%) dogs had blood culture performed, which was positive in 5 dogs: *Staphylococcus species* ($n = 4$) and *Acinetobacter species* ($n = 1$). Culture of ultrasound guided fine needle aspirates of the affected intervertebral disc was performed in 2/25 (8%) dogs and resulted negative. A total of 10/25 (40%) dogs underwent surgical sampling of the affected disc and culture was positive in 5/10 dogs: *Staphylococcus species*. ($n = 3$), *Sphingomonas paucimobilis* ($n = 1$) and *Corynebacterium efficiens* ($n = 1$).

Dogs who had a negative tissue culture, or in which no samples were taken, were presumptively diagnosed with discospondylitis based on a combination of history, clinical presentation, neurological examination findings and diagnostic imaging findings.

The median (95% CI) time between MRI-1 and MRI-2 was 123 (28–860) days. In all dogs, STIR and T2-W sequences were performed during both MRI-1 and MRI-2. However, T1-W sequences were not performed in 8 dogs and 4 dogs during MRI-1 and MRI-2, respectively. Contrast (Gadobutrol 1 mmol/ml, Gadovist, Bayer®, Germany) at a dose of 0.1 ml/kg was not administered to 10 out 25 (40%) dogs during MRI-1 and 5 out of 25 (20%) dogs during MRI-2. The presence or absence of specific MRI features detected on MRI-1 and MRI-2 are summarized in **Table 2**.

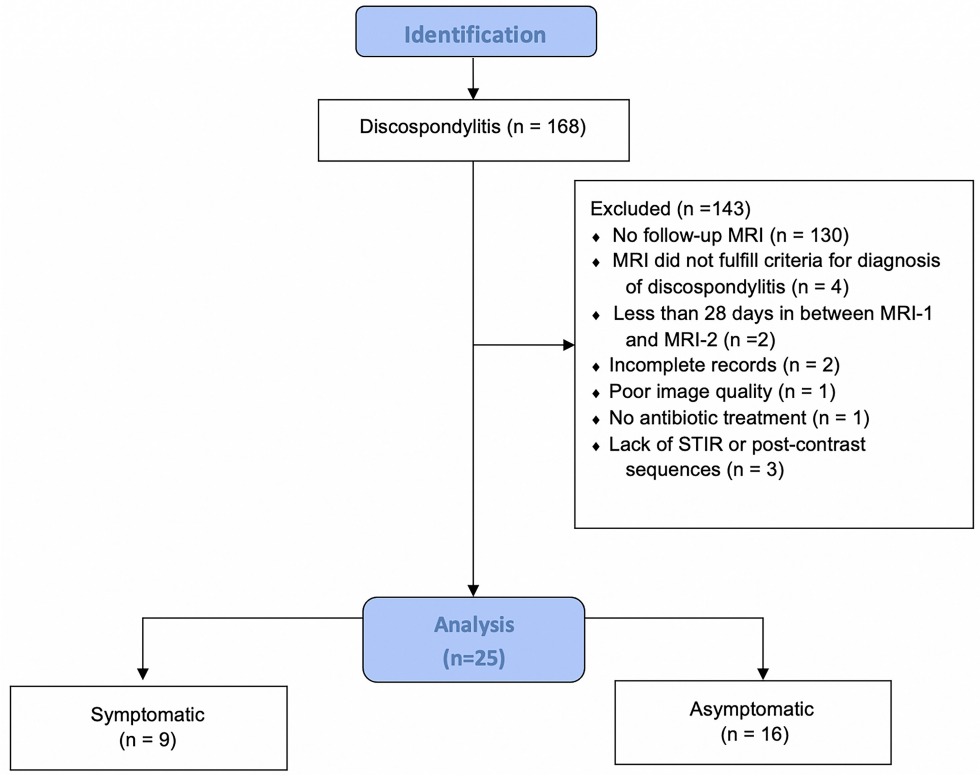

FIGURE 1 | Flow diagram illustrating the inclusion and distribution of dogs in this study. MRI, magnetic resonance imaging; MRI-2, follow-up MRI; STIR, short-tau inversion recovery; *n*, number of dogs.

At the time of MRI-2, 16 dogs were asymptomatic and 9 were symptomatic. The time between MRI-1 and MRI-2 did not differ ($p = 0.813$) between symptomatic [123(34–620) days] and asymptomatic dogs [136 (28–860) days]. Furthermore, the type of treatment (medical or surgical) following MRI-1 was not different between symptomatic and asymptomatic dogs (**Table 3**).

At the time of MRI-2 22/25 dogs were receiving treatment, which consisted of antibiotic-therapy in 10/22 dogs, analgesic therapy in 2/22 dogs and a combination of the two in 10/22. All except three symptomatic cases (7/10) were receiving antibiotics and pain relief at the time or MRI-2, and 1/15 cases was receiving analgesic medication alone. Two (2/15) symptomatic cases were not receiving medication. Thirteen (13/15) asymptomatic dogs were receiving antibiotics, which was combined with analgesic therapy in 4/15 cases. One (1/15) asymptomatic case was not receiving any treatment, and one case was receiving analgesic medication alone (1/15).

Based on MRI-2, 20 out of 25 (80%) and 18 out of 25 (72%) dogs were considered to have presumptive active discospondylitis at the first and second assessment by observer 1, respectively ($p = 0.62$). Observer 2 classified 7/25 (72%) cases as active discospondylitis. The Cohen's kappa (k) coefficient was 0.6 and 0.4 indicating a moderate agreement between the observers on first and second assessment, respectively.

After first assessment of MRI-2 by observer 1, 10/13 medically treated and 10/12 dogs surgically treated dogs were considered to have active discospondylitis ($p > 0.99$). After the second assessment of MRI-2 by observer 1, 8/13 medically treated and 10/12 dogs surgically treated were considered to have active discospondylitis ($p = 0.38$). Following attribution of the classification of active and inactive, it was noted that all dogs with lymphadenomegaly (7/25) on MRI-2 had been attributed an active classification. All dogs with soft tissue STIR hyperintensity on MRI-2 (16/25) and 13/14 dogs with STIR epidural hyperintensity had also been classified as active. A total of 17/20 with STIR hyperintense endplates were also classified as active.

A systematic difference between MRI evaluation of active and inactive discospondylitis in symptomatic and asymptomatic dogs was found on MRI-2 after both assessments by observer 1 (**Table 3**). At first assessment, the sensitivity and specificity of the association between active and inactive scores and symptomatic or asymptomatic clinical status were 40% (21.88–61.34) and 80% (37.55–98.97), respectively. On the second assessment, the sensitivity was 38.9% (20.31–61.38) and the specificity was 71.4% (35.89–94.92).

The antibiotic therapy was continued in 8/15 asymptomatic dogs, 7 of which were considered to have active disease on MRI-2; antibiotic therapy was not continued in 6/15 asymptomatic dogs,

TABLE 1 | Demographic information and clinical data of 25 dogs with discospondylitis included in this study.

Demographic information and clinical data	
Breeds (*n*)	
- Labrador Retriever	8
- Springer Spaniel	4
- German Shepherd Dog	3
- Basset hound	1
- Beagle	1
- Boxer	1
- Crossbreed	1
- Miniature Dachshund	1
- English Bull Terrier	1
- Hungarian Vizsla	1
- Siberian Husky	1
- Rhodesian Ridgeback	1
- West Highland White Terrier	1
Sex (*n*)	
- Female entire-Female neutered	4–6
- Male entire-Male neutered	13–2
Clinical signs (*n*)	
- Spinal pain	24
- Paresis	10
- Lameness	1
Age (months) [mean (± standard deviation)]	78 (±23)
Weight (kg) [mean (± standard deviation)]	29.2 (±10.3)
Duration of clinical signs (days) [median (95% confidence intervals)]	30 (7–75)
Cause of discospondylitis (*n*)	
- Natural	20
- Post-surgical	5
Time from surgery to discospondylitis (days) [median (95% confidence intervals)]	75 (9–102)
Affected disc spaces (*n*)	
- L7-S1	13
- L8-S1	1
- T12-13	2
- L2-3	2
- L3-4	2
- C6-7	1
- L1-2	1
- L1-3	1
- L5-6	1
- L6-7	1

Data are reported as mean (± standard deviation) or median (95% confidence intervals). n, number of dogs; C, cervical; T, thoracic; L, lumbar; S, sacral.

3 of which were classified as active. One asymptomatic case was euthanised due to unrelated disease. The antibiotic therapy was continued in 8/10 symptomatic dogs, 5 of which were considered to have active disease on MRI-2. One (1/10) symptomatic case was euthanised due to disease progression and one (1/10) was not continued on antibiotic-therapy: both cases had MRI-2 classified as active disease.

A total of 4/25 dogs underwent urine (2/4), intervertebral disc (1/4) and blood cultures (1/4): 2/4 of the cases were symptomatic and 0/4 of the cultures were positive.

From the logistic regression, MRI-2 epidural contrast enhancement ($p = 0.997$), epidural STIR hyperintensity ($p = 0.997$), endplate T2-W hyperintensity ($p = 0.281$), endplate STIR hyperintensity ($p = 0.998$), medical treatment ($p = 0.392$) were included in the final model and were not associated with the clinical status. Hosmer-Lemshow test ($p = 0.78$) and Likelyhood ratio test ($p = 0.016$) confirmed the good fitness of the model used.

DISCUSSION

This study assessed the MRI-2 findings in a group of dogs presumptively diagnosed with, and treated for, discospondylitis. According to our results, no systematic difference was found between MRI-1 and MRI-2 features. There was a systematic difference between the subjective classification of active and inactive disease on MRI-2 and the presence of clinical signs with a sensitivity and specificity of 38.9–40 and 71.4–80% respectively. Whilst a systematic difference was found, these findings illustrate that "inactive disease" on MRI is associated with asymptomatic cases. However, the low sensitivity illustrates the subjective and likely inaccurate imaging classification of "active disease" which was evenly distributed between the symptomatic and asymptomatic groups. Therefore, routine MRI-2 might not provide useful information in asymptomatic dogs treated for discospondylitis in the clinical setting, as no specific features were associated with the presence or absence of clinical resolution.

Despite the low number of dogs included in this study, the population reflected previous findings (1, 12, 22): discospondylitis affected mainly the lumbosacral IVD of intact male dogs; presenting clinical signs were unspecific but spinal pain was the most frequent; *Staphylococcus species* were the most frequent infectious agents isolated on available tissue samples.

Both MRI-1 and MRI-2 were available to the observers for comparison, as they would be in the clinical setting. Active or inactive discospondylitis scores were attributed based on the presence or absence of a regional inflammatory process, that is commonly used to distinguish a degenerative from an infectious process during the diagnosis of discospondylitis (7, 21–23). However, the authors recognize that the presence of an active infection cannot be discarded purely based on the absence of paravertebral soft tissue changes and regional inflammatory changes (ex: lymphadenomegaly), as resolution of soft tissue infection may precede that of the avascular IVD (24, 25). In the present study, the classification of "inactive" discospondylitis score was mostly attributed to asymptomatic cases. However, this study revealed that while a dog without signs of active disease on MRI-2 is probably asymptomatic, the opposite might not be true: a dog with features interpreted as active discospondylitis on MRI-2 may be symptomatic or asymptomatic, suggesting that presumptive inflammatory changes may be present in the absence of an active infectious process. In addition, asymptomatic dogs were not more likely to have presumptive inactive disease on MRI-2. Especially in clinically improved cases, routine follow up MRI will likely prove challenging to be interpreted and may lead to additional testing or unnecessary interventions. These findings are consistent with previous studies in human medicine in which routine

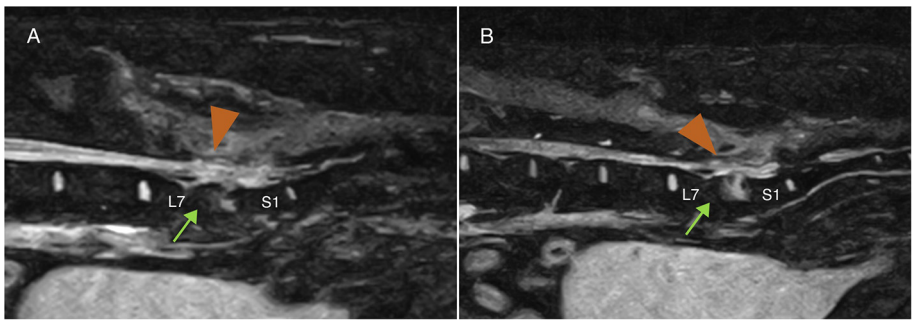

FIGURE 2 | Midline **(A)** and 4 mm from midline **(B)** MRI-1 short-tau inversion recovery (STIR) sagittal images of a dog that developed discospondylitis post-operatively, 4 months following dorsal laminectomy and IVD annulectomy. The diagnosis was based on the combination of severe and progressive clinical signs, lack of significant persistent IVD protrusion causing neural tissue compression and changes affecting the epidural space (arrow-head) and the vertebral body (arrow), and erosion of the end plates.

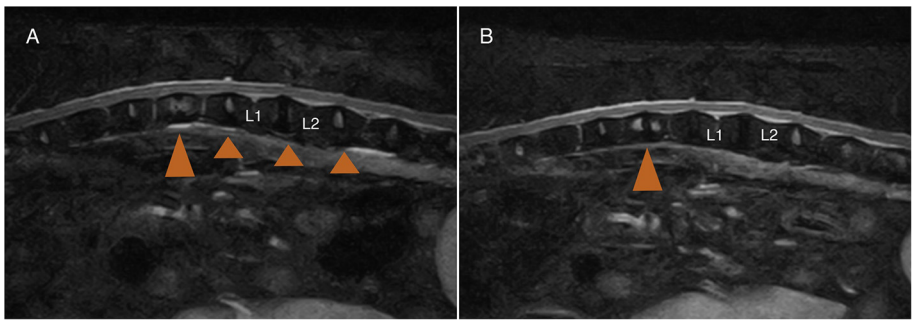

FIGURE 3 | MRI-1 **(A)** 2 months post-surgery, and MRI-2 **(B)** 10 months post-surgery of a dog that underwent L1-L2 left hemilaminectomy and T12-L3 IVD fenestrations. The dog developed marked spinal pain and on MRI-1 **(A)** there was no evidence of neural tissue compression at the previous IVD extrusion site (L1-L2), and evidence of T12-T13 discospondylitis (large arrowhead) corresponding to a previously fenestrated disc site. Note the lack of STIR abnormalities in the other fenestrated discs (small arrowhead).

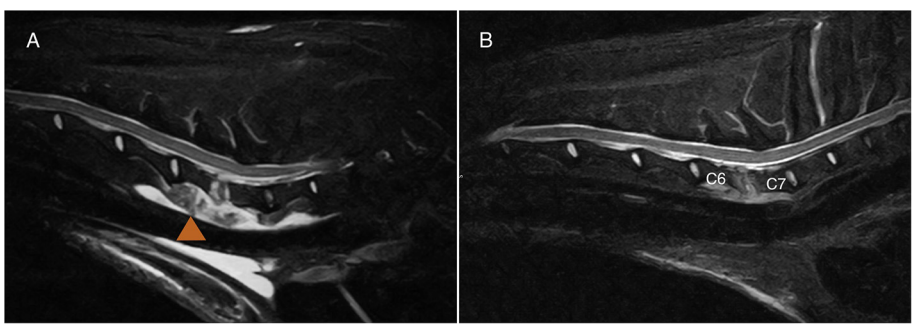

FIGURE 4 | MRI-1 **(A)** and MRI-2 **(B)** midline sagittal short-tau inversion recovery (STIR) images of the case diagnosed with C6-C7 discospondylitis following ventral slot. One month separates MRI-1 and MRI-2. Note the extensive soft tissue changes (arrowhead) which my be associated with surgical exposure. The degree of effacement and STIR hyperintensity affecting the endplates, as well as the STIR hyperintense material in the epidural space were considered beyond what is expected following surgery. The dog had cervical spinal pain despite lack of obvious neural tissue compression. The dog was "symptomatic" at the time of MRI-2 and both observers classified the case as "active."

follow-up MRIs in asymptomatic patients were of questionable value (18–20).

While this study was retrospective, interpretation of symptomatic and asymptomatic cases was straight forward in all instances as the clinician clearly specified the clinical status during the request for MRI-2. However, we cannot categorically exclude that some dogs with neural tissue compression secondary to degenerative disease, such as intervertebral disc protrusion, may have been included in the symptomatic group based on the presence of neuropathic pain. Given that neural tissue

compression was evenly distributed through the symptomatic and asymptomatic groups, and that the majority of our cases was asymptomatic, it is unlikely that this would have significantly affected the findings of our study. The even distribution of dogs with neural tissue impingement between groups supports the previously reported low association between presence of neural tissue compression and clinical signs in dogs with degenerative spinal disease (26–29).

In the present study, discospondylitis was presumptively diagnosed after 9 to 102 days from spinal surgery in 20% of dogs. To the authors' knowledge, post-operative MRI soft tissue changes have not been described in dogs, and interpretation between the expected normal post-operative inflammation or presence of infection is challenging. In theory, the soft tissue damage and inflammation caused by the surgical approach is foreseeable to cause short- and long-term MRI changes associated with inflammation and fibrosis of the paravertebral tissues, respectively. It is therefore possible that we may have included false-positive cases where the MRI changes were associated with normal post-surgical inflammation and not with an infectious process. However, the presumptive diagnosis of discospondylitis in each case was a combination of history, clinical signs, laboratory data and MRI findings. A study reporting post-operative MRI changes in dogs following lumbosacral dorsal laminectomy described a high frequency of contrast enhancing epidural tissue which suppressed fully on fat saturation sequences (29). In our study, the included post-operative cases were presumptively diagnosed with discospondylitis based on presence of clinical signs indicating neurological deterioration despite previous successful decompressive surgery, absence of neural tissue compression on MRI-1, and changes involving the vertebral endplates and vertebral body beyond the expected following surgery (29). In our study, two dogs developed discospondylitis following L7-S1 dorsal laminectomy, two dogs following thoraco-lumbar hemilaminectomy and one dog following a cervical ventral slot. The soft tissue changes detected on MRI-1 were considered significantly more extensive than expected for a normal post-operative MRI study and, for this reason, they were considered representative of an infectious process (29). Similarly, the dogs treated surgically after MRI-1 could have been a source of bias as the post-surgical soft tissue changes could have been considered a sign of an active discospondylitis process on MRI-2. There was no difference in the proportion of dogs classified with active or inactive discospondylitis on MRI-2 between the treatment groups but it cannot be categorically excluded that a difference may be present with a larger sample size group.

In human medicine, suspected infectious diseases with negative tissue culture, such as spondylodiscitis, vertebral osteomyelitis, sepsis, endocarditis and periprosthetic joint infections, have been widely reported (30–34). In our study, 10 out of 12 dogs in which discospondylitis was treated surgically, had an IVD sample taken. The culture was negative in five of them. Negative culture on canine discospondylitis is not an uncommon finding (5, 9) and the following causative factors should be considered: (1) lack of sensitivity of culture medium to detect all infecting bacteria; (2) different types of infectious organisms (i.e. fungal or parasitic) for which specific cultures were not acquired, (3) prior antibiotic exposure; (4) slow-growing or fastidious bacteria, (5) intracellular bacteria that cannot be cultured with the available methods; (6) sampling error or insufficient sample (30–32). Further studies are needed to understand the driving cause for negative culture on dogs affected with discospondylitis.

TABLE 2 | Type of treatment between MRI-1 (magnetic resonance imaging at initial presentation) and MRI-2 (follow-up), defined subjectively as active or inactive discospondylitis after MRI-2 in symptomatic and asymptomatic dogs.

	Symptomatic (*n* = 9)	**Asymptomatic (*n* = 16)**	***p*-value**	**OR (95%CI)**
Treatment	5 Medical 4 Surgical	8 Medical 8 Surgical	0.99	
1st assessment of discospondylitis on MRI-2 (*n*)	8 Active 1 Inactive	12 Active 4 Inactive	0.005*	12(1.77–512.97)
2nd assessment of discospondylitis on MRI-2 (*n*)	7 Active 2 Inactive	11 Active 5 Inactive	0.026	5.5(1.20–51.06)

n, number of dogs; OR, odd ratio; CI, 95% confidence intervals.

Vertebral endplate contrast enhancement is frequently reported in the diagnosis of discospondylitis (7, 21, 22). In the present study, vertebral endplate enhancement was present in all dogs on MRI-2 that received intravenous contrast medium, despite the presence or absence of clinical signs. This finding suggests that vertebral endplate enhancement is likely present in the absence of active infectious disease and may therefore be an unreliable feature when analyzing MRI-2 for evidence of active infection. The underlying reason for the presence of contrast enhancement on a higher proportion of dogs on MRI-2 compared to MRI-1 is unclear. A plausible hypothesis may be the presence of greater vascular supply and increasing granulation tissue associated with healing results in this finding. These findings are in line with previous reports in human literature (18, 20).

In a previous study, a high incidence of contrast enhancement of the vertebral endplates was also reported in reactive, but not infectious, endplate disorders and highlighted that there is overlap between the signal patterns of degenerative, infectious, and neoplastic diseases (21). However, in that study, no dogs had contrast enhancement of the IVD, except if they had discospondylitis. In our study, no difference on IVD contrast enhancement was found between symptomatic and asymptomatic dogs on MRI-2. Intervertebral disc enhancement may, therefore, likely be present in inactive discospondylitis and should therefore be interpreted with caution on follow-up MRI. This finding is further supported by a previous study which reported a high frequency of intervertebral disc enhancement in follow-up MRI in dogs who underwent dorsal lumbosacral laminectomy (29). Neovascularisation of

TABLE 3 | Magnetic resonance imaging (MRI) features detected on initial presentation (MRI-1) and follow-up (MRI-2) in 25 dogs with discospondylitis.

MRI features	MRI-1	MRI-2	Presence on MRI-1 vs. MRI-2				
	(*n*)	(*n*)	Not in MRI-1-Yes in MRI-2	Yes in MRI-1—Not in MRI-2	Yes in MRI-1—Yes in MRI-2	No in MRI-1—Not in MRI-2	*p*-value
Paravertebral tissue STIR hyperintensity	20	16	1	5	15	4	0.22
Paravertebral tissue contrast enhancement	14*	16*	0	3	8	1	0.25
Epidural contrast enhancement	12*	15*	0	0	8	1	n/a
Epidural STIR hyperintensity	14	11	2	5	9	9	0.45
IVD STIR hyperintensity	15	9	2	8	7	8	0.11
IVD contrast enhancement	12*	10*	1	3	6	1	0.62
Vertebral endplate T2-W hyperintensity	10	9	2	3	7	13	1
Vertebral endplate T2-W hypointensity	10	7	1	4	6	14	0.37
Vertebral endplate STIR hyperintensity	20	16	0	4	16	5	0.13
Vertebral endplate T1-W hypointensity	13∇	15∇	3	5	7	3	0.72
Vertebral endplate T1-W eroded	12∇	11∇	2	2	9	5	0.62
Vertebral endplate T1-W destroyed	3∇	5∇	2	1	2	13	1
Vertebral endplate T1-W eroded + destroyed	14∇	16∇	1	0	14	3	1
Length of vertebral body changes >25%	11	8	1	4	7	13	0.37
Vertebral endplate contrast enhancement	14*	20*	1	0	11	0	n/a
Lymphadenomegaly	13	7	2	7	5	10	0.18
Neural tissue compression	19	15	0	4	15	6	0.13

n, number of dogs; STIR, short-tau inversion recovery; IVD, intervertebral disc; T2-W, T2-Weighted; T1-W, T1-Weighted; n/a, not applicable.

**A total of 15 and 20 dogs were administered contrast during MRI-1 and MRI-2, respectively.*

∇ A total of 17 and 21 dogs had T1-W sequence performed during MRI-1 and MRI-2, respectively.

the intervertebral disc during healing is also hypothesized as a potential underlying pathophysiological mechanism for contrast enhancement in cases who have been successfully treated for discospondylitis.

The retrospective nature of this study is a limitation as well as the low number of subjects allocated to the symptomatic and asymptomatic group. This is likely a result of the low incidence of discospondylitis in the general population of dogs (1). Furthermore, as discospondylitis carries an overall good prognosis (1, 12), the ambiguous utility of follow up MRI paired with its challenging interpretation, the need for a general anesthetic, and the associated monetary and emotional implications to the owners, are likely to have been driving causes for the limited number of cases that underwent MRI-2.

The MRI protocols were not standardized and some of the cases did not receive intravenous contrast. This lack of homogeneity likely stems from the fact that once the clinicians involved in the case consider the images diagnostic, they may refrain from performing additional sequences due to monetary restraints, as well as to prevent unnecessary prolonging of anesthesia.

The two observers had a moderate interindividual agreement during the classification of active or inactive MRI-2. The lack of a perfect agreement likely stems from the ambiguity of MRI-2 findings, in part due to the frequent presence of overlapping imaging features which are suspected to represent presence and absence of infection. This finding highlights the importance of combining clinical, laboratory and imaging data during clinical decision making as MRI features alone are subject to individual interpretation. It is possible that the inclusion of a greater number of reviewers or review of serial MRI studies would have yielded different results.

Information regarding patient outcomes following MRI-2, especially in asymptomatic cases, would have been of value to understand if these cases have indeed inactive disease, or if the clinical signs relapsed further down the line indicating persistent infection. Given the retrospective nature of this study and that most dogs were continued on antibiotics despite the classification of "inactive" disease, the ability to draw any conclusions is hindered. Further studies should include a set protocol regarding the length of treatment and interval of time between MRI-1 and MRI-2 so that conclusions can be inferred regarding usefulness of MRI-2 in clinical decision making.

Lastly, considering the influence of field strength on the tissue contrast (35), the changes reported in this study may not be applicable to high field MRI.

In conclusion, this study did not identify meaningful evidence to support routine MRI-2 in dogs treated for discospondylitis and in which clinical signs have resolved. In addition, this study did not identify specific MRI characteristics which are associated with the clinical status of dogs presumptively diagnosed with discospondylitis. The utility of MRI in assessing patients that

continue to have clinical signs, and specifically the role of contrast in evaluating these cases, remains unclear at this stage. Considering the small population size, the heterogenicity of the cases and MRI protocols, and the fact that not all dogs received contrast, further studies are required to evaluate the clinical relevance of intervertebral disc and vertebral endplate enhancement on follow-up MRI.

DATA AVAILABILITY STATEMENT

The raw data supporting the conclusions of this article will be made available by the authors, without undue reservation.

ETHICS STATEMENT

Ethical review and approval was not required for the animal study because no ethical approval was obtained considering the retrospective nature of this cross-sectional study, and prior acquisition of owner consent for patient data to be included in scientific studies. Written informed consent was obtained from the owners for the participation of their animals in this study.

AUTHOR CONTRIBUTIONS

MdF, AC, and ES acquired the data. MdF and EV analyzed and interpreted the data. MdF drafter the article. All authors contributed to the conception and design of the study, contributed to manuscript revision, read, and approved the submitted version.

ACKNOWLEDGMENTS

The abstract of the present study was presented at the 2021 ECVN Symposium as a flash presentation.

REFERENCES

1. Burkert BA, Kerwin SC, Hosgood GL, Pechman RD, Fontenelle JP. Signalment and clinical features of diskospondylitis in dogs: 513 cases (1980-2001). *J Am Vet Med Assoc.* (2005) 227:268–75. doi: 10.2460/javma.2005.227.268
2. De Stefani A, Garosi LS, McConnell FJ, Diaz FJ, Dennis R, Platt SR. Magnetic resonance imaging features of spinal epidural empyema in five dogs. *Vet Radiol Ultrasound.* (2008) 49:135–40. doi: 10.1111/j.1740-8261.2008.00339.x
3. Hovi I, Lamminen A, Salonen O, Raininko R. MR imaging of the lower spine. Differentiation between infectious and malignant disease. *Acta Radiol.* (1994) 35:532–40. doi: 10.1080/02841859409173318
4. Dagirmanjian A, Schils J, McHenry MC. MR imaging of spinal infections. *Magn Reson Imaging Clin N Am.* (1999) 7:525–38. doi: 10.1016/S1064-9689(21)00573-0
5. Ruoff CM, Kerwin SC, Taylor AR. Diagnostic Imaging of Discospondylitis. *Vet Clin North Am Small Anim Pract.* (2018) 48:85–94. doi: 10.1016/j.cvsm.2017.08.007
6. Harris JM, Chen AV, Tucker RL, Mattoon JS. Clinical features and magnetic resonance imaging characteristics of diskospondylitis in dogs: 23 cases (1997-2010). *J Am Vet Med Assoc.* (2013) 242:359–65. doi: 10.2460/javma.242.3.359
7. Carrera I, Sullivan M, McConnell F, Gonçalves R. Magnetic resonance imaging features of discospondylitis in dogs. *Vet Radiol Ultrasound.* (2011) 52:125–31. doi: 10.1111/j.1740-8261.2010.01756.x
8. Cherubini GB, Cappello R, Lu D, Targett M, Wessmann A, Mantis P, et al. findings in a dog with discospondylitis caused by Bordetella species. *J Small Anim Pract.* (2004) 45:417–20. doi: 10.1111/j.1748-5827.2004.tb00259.x
9. Adamo PF, Cherubini GB. Discospondylitis associated with three unreported bacteria in the dog. *J Small Anim Pract.* (2001) 42:352–5. doi: 10.1111/j.1748-5827.2001.tb02473.x
10. Tipold A, Stein VM. Inflammatory diseases of the spine in small animals. *Vet Clin North Am Small Anim Pract.* (2010) 40:871–9. doi: 10.1016/j.cvsm.2010.05.008
11. Betbeze C, McLaughlin R. Canine diskospondylitis: its etiology, diagnosis, and treatment. *Vet Med.* (2002) 97:673–8.
12. Gilmore DR. Lumbosacral diskospondylitis in 21 dogs. *J Am Anim Hosp Assoc.* (1987) 23:57–61.
13. Schwartz M, Boettcher IC, Kramer S, Tipold A. Two dogs with iatrogenic discospondylitis caused by meticillin-resistant Staphylococcus aureus. *J Small Anim Pract.* (2009) 50:201–5. doi: 10.1111/j.1748-5827.2008.00720.x
14. Shamir MH, Tavor N, Aizenberg T. Radiographic findings during recovery from discospondylitis. *Vet Radiol Ultrasound.* (2001) 42:496–503. doi: 10.1111/j.1740-8261.2001.tb00976.x
15. Kraft SL, Mussman JM, Smith T, Biller DS, Hoskinson JJ. Magnetic resonance imaging of presumptive lumbosacral discospondylitis in a dog. *Vet Radiol Ultrasound.* (1998) 39:9–13. doi: 10.1111/j.1740-8261.1998.tb00318.x
16. Gonzalo-Orden JM, Altonaga JR, Orden MA, Gonzalo JM. Magnetic resonance, computed tomographic and radiologic findings in a dog with discospondylitis. *Vet Radiol Ultrasound.* (2000) 41:142–4. doi: 10.1111/j.1740-8261.2000.tb01467.x
17. Carragee EJ. The clinical use of magnetic resonance imaging in pyogenic vertebral osteomyelitis. *Spine.* (1997) 22:780–85. doi: 10.1097/00007632-199704010-00015
18. Gillams AR, Chaddha B, Carter AP. MR appearances of the temporal evolution and resolution of infectious spondylitis. *Am J Roentgenol.* (1996) 166:903–07. doi: 10.2214/ajr.166.4.8610571
19. Veillard E, Guggenbuhl P, Morcet N, Meadeb J, Bello S, Perdriger A, et al. Prompt regression of paravertebral and epidural abscesses in patients with pyogenic discitis. Sixteen cases evaluated using magnetic resonance imaging. *Joint Bone Spine.* (2000) 67:219–27. doi: 10.1016/S1169-8330(00)80034-4
20. Berbari EF, Kanj SS, Kowalski TJ, Darouiche RO, Widmer AF, Schmitt SK, et al. 2015 Infectious Diseases Society of America (IDSA) clinical practice guidelines for the diagnosis and treatment of native vertebral osteomyelitis in adults. *Clin Infect Dis.* (2015) 61:e26–46. doi: 10.1093/cid/civ482
21. Gendron K, Doherr MG, Gavin P, Lang J. Magnetic resonance imaging characterization of vertebral endplate changes in the dog. *Vet Radiol Ultrasound.* (2012) 53:50–6. doi: 10.1111/j.1740-8261.2011.01861.x
22. Thomas WB. Diskospondylitis and other vertebral infections. *Vet Clin North Am Small Anim Pract.* (2000) 30:169–82. doi: 10.1016/S0195-5616(00)50008-4
23. Ledermann HP, Schweitzer ME, Morrison WB, Carrino JA. MR imaging findings in spinal infections: rules or myths? *Radiology.* (2003) 228:506–14. doi: 10.1148/radiol.2282020752
24. Daly C, Ghosh P, Jenkin G, Oehme D, Goldschlager T. A review of animal models of intervertebral disc degeneration: pathophysiology, regeneration, and translation to the clinic. *Biomed Res Int.* (2016) 2016:5952165. doi: 10.1155/2016/5952165
25. Jackson AR, Eismont A, Yu L, Li N, Gu W, Eismont F, et al. Diffusion of antibiotics in intervertebral disc. *J Biomech.* (2018) 76:259–62. doi: 10.1016/j.jbiomech.2018.06.008
26. Mukherjee M, Jones JC, Holaskova I, Raylman R, Meade J. Phenotyping of lumbosacral stenosis in Labrador retrievers using computed tomography. *Vet Radiol Ultrasound.* (2017) 58:565–80. doi: 10.1111/vru.12520
27. Linn LL, Bartels KE, Rochat MC, Payton ME, Moore GE. Lumbosacral stenosis in 29 military working dogs: epidemiologic findings and outcome after surgical intervention (1990–1999). *Vet Surg.* (2003) 32:21–9. doi: 10.1053/jvet.2003.50001

28. De Decker S, Gielen IM, Duchateau L, van Bree HJ, Waelbers T, Bavegems V, et al. Morphometric dimensions of the caudal cervical vertebral column in clinically normal doberman pinschers, english foxhounds and doberman pinschers with clinical signs of disk-associated cervical spondylomyelopathy. *Vet J.* (2012) 191:52–7. doi: 10.1016/j.tvjl.2010.12.017
29. Rapp M, Ley CJ, Hansson K, Sjöström L. Postoperative computed tomography and low-field magnetic resonance imaging findings in dogs with degenerative lumbosacral stenosis treated by dorsal laminectomy. *Vet Comp Orthop Traumatol.* (2017) 30:143–52. doi: 10.3415/VCOT-16-06-0096
30. Tattevin P, Watt G, Revest M, Arvieux C, Fournier PE. Update on blood culture-negative endocarditis. *Med Mal Infect.* (2015) 45:1–8. doi: 10.1016/j.medmal.2014.11.003
31. Thorndike J, Kollef MH. Culture-negative sepsis. *Curr Opin Crit Care.* (2020) 26:473–7. doi: 10.1097/MCC.0000000000000751
32. Palan J, Nolan C, Sarantos K, Westerman R, King R, Foguet P. Culture-negative periprosthetic joint infections. *EFORT Open Rev.* (2019) 4:585–94. doi: 10.1302/2058-5241.4.180067
33. Kasalak Ö, Adams HJA, Jutte PC, Overbosch J, Dierckx RAJO, Wouthuyzen-Bakker M, et al. Culture yield of repeat percutaneous image-guided biopsy after a negative initial biopsy in suspected spondylodiscitis: a systematic review. *Skeletal Radiol.* (2018) 47:1327–35. doi: 10.1007/s00256-018-3006-5
34. Dogan M, Simsek AT, Yilmaz I, Karaarslan N. Evaluation of Empirical Antibiotic Treatment in Culture Negative Pyogenic Vertebral Osteomyelitis. *Turk Neurosurg.* (2019) 29:816–22. doi: 10.5137/1019-5149.JTN.25018-18.2
35. Jensen TS, Bendix T, Kjaer P. Characteristics and natural course of vertebral endplate signal (Modic) changes in the Danish general population. *BMC Musculoskelet Disord.* (2009) 10:1–9. doi: 10.1186/1471-2474-10-81

Conflict of Interest: All authors were employed by company Dick White Referrals, part of Linnaeus Veterinary Ltd.

The remaining authors declare that the research was conducted in the absence of any commercial or financial relationships that could be construed as a potential conflict of interest.

Publisher's Note: All claims expressed in this article are solely those of the authors and do not necessarily represent those of their affiliated organizations, or those of the publisher, the editors and the reviewers. Any product that may be evaluated in this article, or claim that may be made by its manufacturer, is not guaranteed or endorsed by the publisher.

frontiers | Frontiers in Veterinary Science

CASE REPORT
published: 03 June 2022
doi: 10.3389/fvets.2022.869082

Case Report: A Novel Lateral Approach to the C7, C8, and T1 Intervertebral Foramina for Resection of Malignant Peripheral Nerve Sheath Neoplasia, Followed by Adjunctive Radiotherapy, in Three Dogs

Oliver Marsh[1]*, *Naomi Shimizu*[2], *Sarah L. Mason*[3] and *Ane Uriarte*[1]

[1] Linnaeus Veterinary Limited, Neurology and Neurosurgery Service, Southfields Veterinary Specialists, Essex, United Kingdom, [2] Linnaeus Veterinary Limited, Orthopaedic and Soft Tissue Surgery Service, Southfields Veterinary Specialists, Essex, United Kingdom, [3] Linnaeus Veterinary Limited, Oncology Service, Southfields Veterinary Specialists, Essex, United Kingdom

OPEN ACCESS

Edited by:
Luisa De Risio,
Linnaeus Veterinary Limited,
United Kingdom

Reviewed by:
Takeshi Aikawa,
Aikawa Veterinary Medical Center, Japan
Paul Freeman,
University of Cambridge,
United Kingdom

***Correspondence:**
Oliver Marsh
oliver.marsh@southfields.co.uk

Specialty section:
This article was submitted to Veterinary Neurology and Neurosurgery, a section of the journal Frontiers in Veterinary Science

Received: 03 February 2022
Accepted: 06 May 2022
Published: 03 June 2022

Citation:
Marsh O, Shimizu N, Mason SL and Uriarte A (2022) Case Report: A Novel Lateral Approach to the C7, C8, and T1 Intervertebral Foramina for Resection of Malignant Peripheral Nerve Sheath Neoplasia, Followed by Adjunctive Radiotherapy, in Three Dogs. Front. Vet. Sci. 9:869082. doi: 10.3389/fvets.2022.869082

This case report describes the diagnosis, management and outcome of three dogs with peripheral nerve sheath tumors (PNSTs) involving the brachial plexus, C7 (case 1), C8 (case 2), and C8 and T1 (case 3) spinal nerves and nerve roots with intrathoracic invasion. Surgical resection required thoracic limb amputation and removal of the first rib, facilitating a novel lateral approach to the spinal nerves and foramina in all cases. This was followed by hemilaminectomy and rhizotomy in cases 1 and 2. Adjunctive radiotherapy was then performed in all dogs. All three dogs regained a good quality of life in the short-term following surgery. Two were euthanased after 3 and 10 months, following detection of a pulmonary mass in one case and multiple thoracic and abdominal masses in the other. The third dog was alive and well at the time of writing (7 months post-surgery). This surgical approach facilitated good access and allowed gross neoplastic tissue to be resected. The ease of surgical access was dependent, to a degree, on the size of the patient. This surgical approach can be considered in cases of PNSTs involving the caudal cervical or cranial thoracic spinal nerves and nerve roots. Adjunctive radiotherapy should be considered as part of a multi-modal approach to these challenging tumors due to the difficulty of achieving clean margins, particularly proximally, even with optimal surgical access.

Keywords: peripheral nerve sheath tumor, surgery, radiotherapy, dog, brachial plexus

INTRODUCTION

Peripheral nerve sheath tumors (PNSTs) are malignant mesenchymal tumors arising from the myelin sheath or connective tissues surrounding nerves. Historically, terms such as Schwannoma and neurofibroma have been used (1, 2). Since 2013, World Health Organization guidelines have suggested the use of the term peripheral nerve sheath tumor in human medicine (3), and veterinary nomenclature has followed this lead.

In dogs, PNSTs most commonly affect the brachial plexus and its contributing spinal nerves, and less frequently the pelvic limb (4). Typical clinical signs are insidious and include progressive lameness, monoparesis, muscle atrophy, a palpable mass and pain of variable severity (4–9). A presumptive diagnosis is usually achieved *via* CT (7) or MRI (8), or less commonly ultrasound (10), with or without confirmation *via* biopsy or fine needle aspirate (11).

Common treatment options for PNSTs include surgery with or without radiotherapy, and palliative therapy. Optimal treatment for canine brachial plexus tumors is not supported by strong evidence, and is also debated in human medicine (12). Surgery as the sole treatment in dogs has been associated with a poor prognosis due to short times to recurrence and death, reported to be 7.5 and 12 months, respectively (4). With nerve root involvement, the mean disease-free interval is 1 month and survival time around 5 months (4). However, short disease-free and survival times are not universal, and cases have been reported in which surgery has conferred prolonged survival and excellent quality of life. This appears to be particularly associated with complete mass resection (6). Where complete resection is not possible, there is some evidence that the use of adjunctive radiotherapy prolongs disease-free and survival times (13). Radiotherapy as a sole treatment appears to give a similar outcome to surgery alone (9).

Surgical resection is challenging when the caudal cervical and cranial thoracic spinal nerves and nerve roots are involved due to three main factors: the presence of the scapula, vertebral canal involvement and potentially intra-thoracic extension. A lateral approach to resect PNSTs involving the C6–C7, C7–T1, and T1–T2 intervertebral foramina, with intra-thoracic extension, has not been described. Here, we provide a description of the clinical presentation, imaging findings, surgical procedures, radiotherapy and outcome in three dogs with PNSTs involving the brachial plexuses, first rib and C7, C8, and T1 spinal nerves.

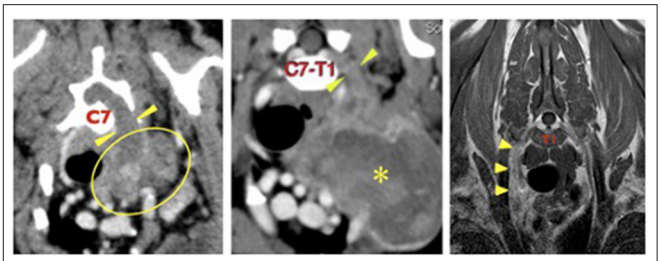

FIGURE 1 | Left, case 1: transverse CT image at the level of the C7 vertebral body. There is a large, irregular soft tissue attenuating mass in the left axilla (outlined) which extends dorsally (arrowheads) through the enlarged C6–C7 intervertebral foramen to enter the vertebral canal. Middle, case 2: transverse CT image at the level of the C7–T1 intervertebral formamina showing a large, irregular mass (asterisk in its center) in the left axilla, extending proximally (arrowheads) through the C7–T1 intervertebral foramina to enter the vertebral canal. Right, case 3: transverse T1 weighted post-contrast image at the level of the mid T1 vertebral body. The right C8 spinal nerve (arrowheads) is enlarged and irregular and shows mild, homogenous contrast uptake. The right side of the dog is on the left side of each image.

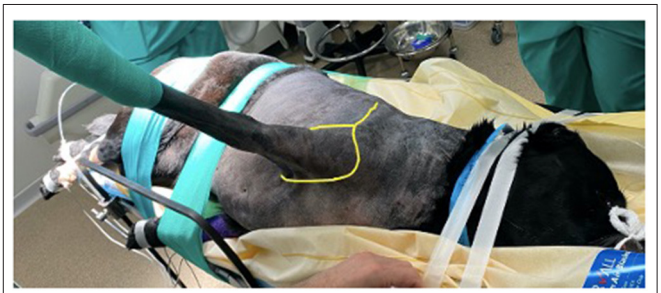

FIGURE 2 | Patient positioning prior to surgery. Both thoracic limbs are retracted caudally to allow the surgeon closer and more comfortable access. The dog is held securely to the table using tape and elasticated bandage, to prevent movement when the table is tilted. Sandbags (not visible in this image) are placed under the dog's cervical region to maintain the vertebral column in horizontal alignment. The yellow line shows how the initial incision is performed- dorsoventrally over the spine of the scapula and then in a circumflex manner around the limb.

CASE 1

Signalment and Clinical Presentation

A 12-year old, female neutered West Highland White Terrier weighing 9.25 kg presented with a 5-month history of progressive left thoracic limb lameness and pain that had shown no response to meloxicam and a mild, short-lived response to gabapentin. Neurological examination was limited due to the severity of the dog's pain. Left thoracic limb non-weight bearing lameness was observed. There was marked discomfort upon any attempt to touch the left thoracic limb. There was severe wastage of the left thoracic limb musculature. No other neurological deficits were present. Hematology and biochemistry profiles were unremarkable.

Imaging

A pre-referral CT scan of the thorax and thoracic limbs revealed a poorly defined, soft tissue attenuating mass extending from the left axilla dorsally as a thick cord toward the vertebral canal (**Figure 1**). It passed through the widened C6–C7 intervertebral foramen to form a mass that compressed and displaced the spinal cord to the right. The mass was closely associated with the first rib and invaded the entrance to the thorax. There was no evidence of pulmonary metastatic disease.

Surgical Procedure

Thoracic limb amputation and rib resection were performed following previously described techniques (14). An incision was made over the scapula and in a circumflex manner around the left thoracic limb (**Figure 2**). The cephalic vein was ligated and divided where it passed deep to the cleidobrachialis muscle. The omotransversarius, trapezius, rhomboideus and serratus dorsalis muscles were incised at their insertions on the scapula. At the caudal aspect of the axillary space, the insertions of the latissimus dorsi, teres major, and cutaneous trunci muscles were transected at their insertions on the teres tubercle of the humerus. With the dorsal aspect of the scapula held in abduction, the thoracodorsal, axillary and lateral thoracic arteries, and brachial, thoracodorsal,

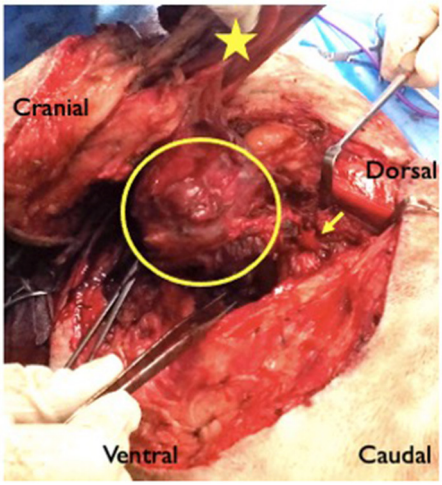

FIGURE 3 | Intraoperative image from case 2 showing a large ovoid axillary mass (circled) with extension (arrow) toward the C7–T1 intervertebral foramen. The star shows the medial aspect of the scapula. The forceps in the surgeon's right hand show the region of the osteotomised rib.

and axillary veins were ligated and transected. The superficial and deep pectoral muscles were transected from their insertions on the humerus. With the scapula abducted, the mass could be visualized medial to it. The carotid, jugular, esophagus and vagosympathetic trunk were identified and were not invaded by the mass. The mass was encircling the first rib. The rib and mass were isolated from surrounding soft tissue and the intercostal artery ligated dorsally and ventrally. The tubercule and head of the rib were disarticulated and an osteotomy was performed distally using bone cutters. A combination of sharp and blunt dissection was performed around the mass (**Figure 3**). The abnormal spinal nerve was identified and transected just ventral to the vertebral body allowing removal of the distal part of the mass, the rib and the limb. The table was tilted from horizontal to around 20 degrees toward the vertical plane, improving access and visualization for the following part of the surgery. The approach to the hemilaminectomy was made by bluntly dissecting, cutting or cauterizing the serratus ventralis, deep scalenus, longissimus cervicis, intertransversarii dorsalis, and intermedius cervicis muscles. A C6–C7 hemilaminectomy was then performed. The mass could be visualized compressing and invading into the spinal cord. A rhizotomy was performed as close to the spinal cord as possible and the abnormal spinal nerve was resected. The surgical site was copiously lavaged prior to placement of a chest drain and routine closure.

Recovery and Follow-Up

The dog was bright and comfortable the day following surgery, was eating well and was able to stand unaided. The dog was discharged 2 days after surgery. Two weeks later, definitive intent radiotherapy was performed (51 Gy over 18 daily fractions). The dog was reported to be bright and happy at home for a further 6 weeks, before acutely becoming painful. There were no obvious neurological deficits on re-examination, but the dog was painful on being handled. Thoracic radiographs were performed which revealed a single 2.5 cm diameter well-defined soft tissue opacity in the right middle lung lobe most consistent with a neoplastic mass. The owner declined further investigations including advanced imaging and biopsy of the mass and instead requested euthanasia, declining post-mortem.

CASE 2

Signalment and Clinical Presentation

A 7-year old, male entire, English Springer Spaniel weighing 20 kg presented with a 10 month history of progressive left thoracic limb lameness unresponsive to meloxicam and gabapentin. Examination revealed non-weight bearing lameness of the left thoracic limb. In this limb, the postural reactions were absent, the withdrawal reflex was incomplete and the muscle mass was markedly reduced. The cutaneous trunci reflex was present on the right and absent on the left. Miosis and third eyelid protrusion was seen in the left eye (partial Horner syndrome). A firm, round, painful mass was palpable in the left axilla. Hematology and biochemistry profiles were unremarkable.

Imaging

Pre-referral CT of the neck, thorax, and elbows had revealed the presence of an ovoid, 8 × 7 cm diameter soft tissue attenuating mass in the left axilla, extending to the thoracic inlet where it displaced the trachea, esophagus, common carotid, and left subclavian arteries. It surrounded the left axillary artery and circumference of the first rib, where it was causing cortical lysis and periosteal reaction. The C8 spinal nerve was thickened and was extending into the vertebral canal where it was indenting the spinal cord (**Figure 1**). The axillary portion of the mass showed marked contrast enhancement and the abnormal C8 nerve showed mild contrast enhancement. There was no evidence of pulmonary metastatic disease.

Surgery

Forequarter amputation and first rib removal were performed in the same manner as in case 1. The mass was followed proximally and the abnormal C8 spinal nerve identified, prior to transecting it and removing the distal part of the mass and the limb. The approach to the hemilaminectomy site was as in case 1. A left C7–T1 hemilaminectomy was then performed. The enlarged C8 nerve roots were resected ∼1–2 mm distal to their attachment to the spinal cord, which appeared macroscopically normal. Lavage, chest drain placement and closure were performed as in case 1.

Recovery and Follow-Up

The dog was comfortable the day following surgery and was discharged after 5 days. At 2-week re-examination there were no neurological abnormalities present and the Horner syndrome had resolved. Definitive intent radiotherapy was then performed (49.4 Gy over 19 daily fractions). Adjunctive metronomic chemotherapy (cyclophosphamide 50 mg/m^2/48 h) and meloxicam (0.1 mg/kg/24 h) was started 3 months post-surgery. The dog was reported to be well, without obvious

abnormalities, for 9 months, before becoming acutely dyspnoeic. Investigations revealed multiple thoracic and abdominal masses, which were not sampled, leading to euthanasia.

CASE 3

Signalment and Clinical Presentation

A 10-year old, male neutered, Labrador weighing 39.7 kg was presented with a 3 month history of progressive right thoracic limb lameness and paresis. Examination revealed intermittent non-weight bearing lameness, severe paresis, spontaneous knuckling, absent postural reactions, reduced withdrawal reflex, and poor muscle mass in the right thoracic limb. No obvious discomfort or masses were detected on palpation. Hematology and biochemistry profiles were unremarkable. The clinical signs progressed despite 2-week courses of gabapentin (8 mg/kg/8 h) and prednisolone (0.5 mg/kg/24 h).

Imaging

Pre-referral radiographs of the thorax, cervical spine, and thoracic limbs were normal. MRI of the cervical and cranial thoracic vertebral column, spinal cord and brachial plexuses revealed that the right C8 and T1 nerve roots, spinal nerves, and brachial plexus were enlarged and irregularly marginated, were STIR hyperintense, mildly T2 hyperintense and T1 isointense compared to normal muscle, and showed mild contrast enhancement (**Figure 1**). The abnormal T1 spinal nerve was closely associated with the first rib. No obvious spinal cord involvement was observed. There was no evidence of pulmonary metastatic disease.

Surgery

Forequarter amputation and first rib removal were performed in the same manner as in case 1. The enlarged, hard and nodular brachial plexus and C8 and T1 spinal nerves were identified and followed proximally, then transected, allowing removal of the distal part of the mass. The approach to a planned C7–T2 hemilaminectomy was similar to that described in case 1, though the size of the patient made muscle dissection and retraction challenging. The C7–T2 vertebrae were identified and the hemilaminectomy was commenced but during drilling significant hemorrhage occurred from the vertebral venous sinus. The drilling of the hemilaminectomy window was incomplete at this stage and it was thought that the sinus was displaced due to the presence of the mass. Bleeding was controlled using bone wax and fibrillar collagen (Lyostypt). Given this complication, the decision was made to discontinue with the hemilaminectomy and transect the abnormal nerves as close as possible to their entry to their respective foramina. Lavage, chest drain placement and closure were performed as in case 1.

Recovery and Follow-Up

The dog was comfortable the morning following surgery and was discharged after 4 days. At 2-week re-examination there were no neurological abnormalities present. Definitive intent radiotherapy was performed (50 Gy over 20 daily fractions). At time of writing, 7 months after surgery, the dog was coping well on three legs without any other abnormalities.

HISTOPATHOLOGY

All three masses showed similar histopathological features. All were moderately cellular and composed of fusiform cells arranged in intersecting bundles, streams and whorls, supported by a moderate amount of fibrovascular stroma. Neoplastic cells had indistinct borders, a small to moderate amount of pale eosinophilic cytoplasm, ovoid nuclei with finely stippled chromatin and 1–2 distinct nucleoli. There was moderate anisocytosis and anisokaryosis with 4–19 mitotic figures in 10 400× fields. There was individual cellular and regional necrosis. There were areas of myxomatous fibrovascular stroma and peripheral infiltration of lymphocytes. In cases 1 and 3 the mass was unencapsulated whereas that in case 2 was encapsulated. In cases 1 and 2 neoplastic cells were seen extending to the borders of the nerve root samples. In case 2 neoplastic cells were also seen in adipose tissue surrounding the nerve roots. In case 3, neoplastic cells were separated from the peripheral tissue borders by a rim of adipose tissue, ∼1 mm in width, with no neoplastic cells at the proximal border. The histopathological diagnosis in all three cases was malignant PNST.

DISCUSSION

This report demonstrates the feasibility of a lateral approach to remove PNSTs involving the C7, C8, and T1 spinal nerve and nerve roots, with intra-thoracic invasion. Crucial to the procedure is the input of a multidisciplinary team for limb amputation, thoracotomy and rib removal. Patient positioning and tilting of the table was key as it allowed optimal, adaptable positioning throughout the procedure. The lateral approach facilitated good access, particularly in the two smaller patients, allowing gross tumor resection and in case 3, complete removal.

The objective of the surgery in all cases was to achieve resection of as much of the PNST as possible, while recognizing that complete resection would be very challenging, particularly in cases with spinal cord involvement. Hence, adjunctive radiotherapy was recommended. We sought to follow the principle of oncological surgery of reducing tumor burden as far as possible, thereby increasing the efficacy of non-surgical adjuvant therapies intended to eliminate microscopic disease, and consequently reducing the likelihood of local spread or widespread metastasis (15). In case 3, the planned hemilaminectomy part of the procedure was not completed due to hemorrhage from the vertebral venous sinus, which may have been distorted or displaced. It was considered safer to control hemorrhage and resect the tumor as close as possible to the foramina, rather than persist with the hemilaminectomy. The approach to the hemilaminectomy site was challenging in this particular case. This was because of the patient's large size and muscle mass, which limited visualization and made it difficult to adequately retract the muscles. While it is possible to perform

a caudal cervical or cranial thoracic hemilaminectomy in large dogs, it is considerably more difficult and time-consuming than in smaller patients.

This surgical procedure was planned to permit optimal access for efficacious tumor removal. It did not, however, lead to complete proximal resection in cases 1 and 2. It is possible that performing a durotomy would have allowed more neoplastic tissue to be removed. Durotomy in these cases, while possible, would be challenging as the extent of the hemilaminectomies had to be relatively conservative. This was due to limitations imposed by muscle mass and vascular anatomy. The vertebral venous sinuses were likely to be displaced due to the enlarged infiltrated nerve root and had to be avoided. The vertebral artery and vein located within the transverse foramen of C6 were another impediment to ventral access (16). Durotomy may have led to iatrogenic damage to the spinal cord and, given the locally invasive nature of these tumors, durotomy is unlikely to permit complete resection in cases with intramedullary invasion.

Despite the decision not to proceed with a hemilaminectomy in case 3, this was the only tumor that was completely removed. On the basis of the MRI, nerve root involvement was thought possible and the clean histological margins were unexpected. It is possible that MRI is relatively non-specific for detection of nerve root involvement. Abnormalities on electromyography (EMG) of the epaxial muscles in dogs with PNSTs have been shown to be significantly associated with nerve root or spinal cord involvement (5). Interpreting EMG findings alongside advanced imaging may, therefore, provide superior information regarding nerve root and spinal cord involvement compared to imaging alone and should ideally be performed in cases of PNST.

In order to remove the thoracic limb to permit access and visualization for the hemilaminectomy, the affected spinal nerve had to be transected, contrary to the broad principle of oncological surgery of avoiding incision into macroscopic tumor (17) which could potentially lead to tumor cell seeding. We do not have evidence of local tumor recurrence in any of our cases. Tumor seeding was therefore not documented to have occurred, despite incision into the neoplastic nerves. However, tumor regrowth may have been delayed by radiotherapy, rather than completely inhibited, and its possibility cannot be discounted, particularly in the absence of follow-up imaging.

Due to the difficulty of clean resection, radiotherapy may be valuable in cases of PNST with involvement of the vertebral canal. Radiotherapy could be considered even in cases with clean histopathological margins, due to the typical narrow margin of resection and the possibility of "skip" lesions (18). These are foci of neoplastic cells in tissue surrounding the primary mass, that are not connected to it- essentially, they are local metastases that may not be apparent on imaging or during surgery. Inadvertent damage to local tissue, including that of the central nervous system is a rare but potentially serious complication of radiation therapy in the vicinity of the spinal cord (19). Measures taken to mitigate this risk include meticulous radiotherapy planning with precisely targeted and conformed delivery, administration of multiple, low-dose fraction, and administration of anti-inflammatories to address the inflammatory component of radiation injury. These measures were taken in all our cases.

The immediate post-operative outcome in all cases was favorable as relief of pain occurred very quickly in both painful dogs (cases 1 and 2) and case 3 has continued to enjoy an excellent quality of life. In case 1 and 2, good quality of life was achieved but this was only of relatively short duration due to the development of masses in the lungs (cases 1 and 2) and abdomen (case 2). The disease-free and survival times in these two cases fell in the range that have been previously reported for surgery (4) and radiotherapy (9) alone.

It could not be determined whether the new masses in cases 1 and 2 were related to the PNSTs, as post-mortem, and histopathology were not performed. While PNSTs are typically described as of low metastatic potential, distant metastases have occasionally been reported (20), and concurrent lung masses were found in 3/24 dogs with a histologically confirmed PNST (7). It is likely that metastatic potential exists in dogs with PNST and owners should be informed of this before embarking on invasive and expensive treatment. The signs of deterioration in case 1 (i.e., vocalizing in pain) are not typical of a lung lesion so it is possible that other undetected pathology was present, or even local recurrence of the PNST, though this remains speculative in the absence of further imaging, histopathology of the lung mass, or post-mortem.

Other possible differential diagnoses for the brachial plexus lesions in these cases included neuritis and lymphoma. Neuritis was thought unlikely as this would not typically be associated with intrathoracic involvement as seen in cases 1 and 2. In case 3, the clinical signs progressed despite corticosteroid administration, making inflammatory disease less likely. Lymphoma was also a possibility, though brachial plexus lymphoma appears to be very rare in dogs. It may occur as part of a more widespread neoplastic disease (21). In our cases, PNST was the most likely differential diagnosis for a single localized mass lesion affecting the brachial plexus region. Biopsy would ideally have been performed prior to radical surgery. Biopsy was discussed with, offered to, and declined by all owners prior to proceeding with radical surgery. In cases 1 and 2, pre-referral CT, rather than MRI, was performed. It is possible that MRI might have allowed more accurate assessment of spinal cord invasion and therefore superior pre-operative planning compared to CT. On the other hand, CT does have advantages over MRI including its speed, wider availability and capacity for detailed assessment of the thorax in the same procedure. Repeat advanced imaging would ideally comprise part of the follow up in cases of PNST; this was not performed in our cases. A topic of interest with respect to advanced imaging in cases of human PNST is the use of MRI to distinguish benign from malignant lesions (22). This has not been reported in dogs, but extrapolation to canine cases merits future investigation.

At our clinic, chemotherapy has generally not previously been employed for PNSTs, due to assertions (2, 4) that these tumors are not typically widely metastatic. Local treatment has therefore been thought to be more appropriate. In case 2, chemotherapy was instituted at a different center, chosen by the owner for follow-up care for geographical reasons, and

the rationale for the decision to use chemotherapy was not available to us. Unfortunately, this case developed suspected metastatic disease despite chemotherapy. It is unknown whether the use of chemotherapy had any efficacy- it may not have been beneficial; conversely, it may have delayed the onset of the suspected metastatic disease. The metastatic potential of PNST is unknown, and a large number of cases, systematically screened for metastatic disease, would be required for clear information on this.

Very little information is available regarding chemotherapy for canine PNST. Some response has been reported in isolated cases treated with nitrosylcobalamin (23), and cyclophosphamide with piroxicam (20). Chemotherapy is used in some human PNSTs, with doxorubicin and cyclophosphamide/ifosfamide showing the greatest efficacy (12, 24–26) though the evidence supporting the use of conventional chemotherapeutic agents is mixed (27). Novel molecular-targeting agents that target growth factor and other receptors involved in oncogenesis and tumor proliferation (12, 28–32) have been described, though clinical benefit has not yet been reported. Gene-based therapies, currently under investigation in a laboratory setting, are another area of interest (12). Importantly, the efficacy of chemotherapy in human PNST is profoundly affected by the patient's neurofibromatosis type 1 (NF1) tumor predisposition syndrome status (25). It has been suggested that dogs with PNST may represent a naturally occurring model of NF1, though genetic studies to confirm this are lacking (33). This presents an intriguing topic for future research. The use of chemotherapy for PNST is a subject of debate amongst human oncologists. Information on its use in canine PNST is sparse and is an area that warrants further investigation.

In conclusion, the reported cases demonstrate the feasibility of a lateral approach for resection of PNSTs involving the C7–T1 spinal nerves. The completeness of tumor resection, as well as disease-free and survival times, was variable. Two of three cases developed presumed metastasis or secondary neoplasia, which was unexpected considering previously available data on PNST. The benefit of radiotherapy in addition to surgery remains to be confirmed. A larger study is required to determine the efficacy of this treatment regime for canine PNST.

DATA AVAILABILITY STATEMENT

The raw data supporting the conclusions of this article will be made available by the authors, without undue reservation.

ETHICS STATEMENT

Ethical review and approval was not required for the animal study because this report provides only a description of clinical care provided to patients according to best practice. Owners consented for data related to the patients to be published. Written informed consent was obtained from the owners for the participation of their animals in this study.

AUTHOR CONTRIBUTIONS

AU, OM, and NS were involved in the surgeries. SM planned and oversaw radiotherapy. AU, OM, NS, and SM involved in the assessment and management of the cases reported. All authors listed have made a substantial, direct, and intellectual contribution to the work and approved it for publication.

FUNDING

Linnaeus Veterinary Limited supported the costs of the open access publication charges.

REFERENCES

1. DeLahunta A, Glass E, Kent M. *Veterinary Neuroanatomy and Clinical Neurology*. 5th edition. Philadelphia, PA: Elsevier (2021).
2. Vandevelde M, Higgins R, Oevermann A. *Veterinary Neuropathology: Essentials of Theory and Practice.* Chichester: Wiley-Blackwell (2012).
3. Chikkannaiah P, Boovalli MM, Nathiyal V, Venkataramappa S. Morphological spectrum of peripheral nerve sheath tumors: an insight into world health organization 2013 classification. *J Neurosci Rural Pract.* (2016) 7:346–54. doi: 10.4103/0976-3147.182768
4. Brehm DM, Vite CH, Steinberg HS, Haviland J, van Winkle T. A retrospective evaluation of 51 cases of peripheral nerve sheath tumors in the dog. *J Am Anim Hosp Assoc.* (1995) 31:349–59. doi: 10.5326/15473317-31-4-349
5. le Chevoir M, Thibaud JL, Labruyère J, Uriarte A, Fornel-Thibaud P De, Moissonnier P, et al. Electrophysiological features in dogs with peripheral nerve sheath tumors: 51 cases (1993–2010). *J Am Vet Med Assoc.* (2012) 241:1194–201. doi: 10.2460/javma.241.9.1194
6. van Stee L, Boston S, Teske E, Meij B. Compartmental resection of peripheral nerve tumours with limb preservation in 16 dogs (1995–2011). *Vet J.* (2017) 226:40–5. doi: 10.1016/j.tvjl.2017.07.002
7. Rudich SR, Feeney DA, Anderson KL, Walter PA. Computed tomography of masses of the brachial plexus and contributing nerve roots in dogs. *Vet Radiol Ultrasound.* (2004) 45:46–50. doi: 10.1111/j.1740-8261.2004.04007.x
8. Kraft S, Ehrhart EJ, Gall D, Klopp L, Gavin P, Tucker R, et al. Magnetic resonance imaging characteristics of peripheral nerve sheath tumors of the canine brachial plexus in 18 dogs. *Vet Radiol Ultrasound.* (2007) 48:1–7. doi: 10.1111/j.1740-8261.2007.00195.x
9. Dolera M, Malfassi L, Bianchi C, Carrara N, Finesso S, Marcarini S, et al. Frameless stereotactic volumetric modulated arc radiotherapy of brachial plexus tumours in dogs: 10 cases. *Br J Radiol.* (2017) 90:20160617. doi: 10.1259/bjr.20160617
10. Rose S, Long C, Knipe M, Hornof B. Ultrasonographic evaluation of brachial plexus tumours in five dogs. *Vet Radiol Ultrasound.* (2005) 46:514–7. doi: 10.1111/j.1740-8261.2005.00093.x
11. da Costa R, Parent J, Dobson H, Ruotsalo K, Holmberg D, Duque C, et al. Ultrasound-guided fine needle aspiration in the diagnosis of peripheral nerve sheath tumors in 4 dogs. *Can Vet J.* (2008) 49:77–81. doi: 10.4141/cjas 69-011
12. Prudner BC, Ball T, Rathore R, Hirbe AC. Diagnosis and management of malignant peripheral nerve sheath tumors: current practice and future perspectives. *Neuro Oncol Adv.* (2019) 2 (Suppl. 1):40–9. doi: 10.1093/noajnl/vdz047
13. Lacassagne K, Hearon K, Berg J, Séguin B, Hoyt L, Byer B, et al. Canine spinal meningiomas and nerve sheath tumours in 34 dogs (2008-2016): distribution and long-term outcome based upon histopathology and treatment modality. *Vet Comp Oncol.* (2018) 16:344–51. doi: 10.1111/vco.12385

14. Tobias KM, Johnston SA. *Veterinary Surgery: Small Animal*. St Louis, MO: Elsevier (2012).
15. Pollock R, Morton D. Principles of surgical oncology. In: Kufe D, Pollock R, Weichselbaum R, editors. *Holland-Frei Cancer Medicine*. 6th Edition. Hamilton, CA: BC Decker (2003)
16. Hermanson J, de Lahunta A, Evans H. *Miller and Evans' Anatomy of the Dog*. Fifth edition. St Louis, MO: Elsevier (2020).
17. Johnston S TK. *Veterinary Surgery Small Animal*. Second edition. Vol. 1. St Louis, MO: Elsevier (2018).
18. Chou D, Bilsky MH, Luzzati A, Fisher CG, Gokaslan ZL, Rhines LD, et al. Malignant peripheral nerve sheath tumors of the spine: results of surgical management from a multicenter study. *J Neurosurg Spine.* (2017) 26:291–8. doi: 10.3171/2016.8.SPINE151548
19. Schultheiss TE. Repair of radiation damage and radiation injury to the spinal cord. In: Jandial R, Chen M, editors. *Regenerative Biology of the Spine and Spinal Cord*. First edition. New York, NY: Springer (2012). doi: 10.1007/978-1-4614-4090-1_6
20. Son J, Park S, Choi SH, Kim G. Treatment of malignant peripheral nerve sheath tumour using surgery and metronomic chemotherapy in a dog. *J Vet Clin.* (2011) 28:310–3.
21. Ueno H, Miyoshi K, Fukui S, Kondo Y, Matsuda K, Uchide T. Extranodal lymphoma with peripheral nervous system involvement in a dog. *J Vet Med Sci.* (2014) 76:723–7. doi: 10.1292/jvms.13-0159
22. Yun JS, Lee MH, Lee SM, Lee JS, Kim HJ, Lee SJ, et al. Peripheral nerve sheath tumor: differentiation of malignant from benign tumors with conventional and diffusion-weighted MRI. *Eur Radiol.* (2021) 31:1548–57. doi: 10.1007/s00330-020-07234-5
23. Bauer JA, Frye G, Bahr A, Gieg J, Brofman P. Anti-tumor effects of nitrosylcobalamin against spontaneous tumors in dogs. *Invest New Drugs.* (2010) 28:694–702. doi: 10.1007/s10637-009-9282-0
24. Ferrari A, Bisogno G, Carli M. Management of childhood malignant peripheral nerve sheath tumor. *Pediatr Drugs.* (2007) 9:239–48. doi: 10.2165/00148581-200709040-00005
25. Carli M, Ferrari A, Mattke A, Zanetti I, Casanova M, Bisogno G, et al. Pediatric malignant peripheral nerve sheath tumor: the Italian and german soft tissue sarcoma cooperative group. *J Clin Oncol.* (2005) 23:8422–30. doi: 10.1200/JCO.2005.01.4886
26. Zehou O, Fabre E, Zelek L, Sbidian E, Ortonne N, Banu E, et al. Chemotherapy for the treatment of malignant peripheral nerve sheath tumors in neurofibromatosis 1: a 10-year institutional review. *Orphanet J Rare Dis.* (2013) 8:1–7. doi: 10.1186/1750-1172-8-127
27. Durbin AD, Ki DH, He S, Look AT. Malignant peripheral nerve sheath tumors. *Adv Exp Med Biol.* (2016) 916:495–530. doi: 10.1007/978-3-319-30654-4_22
28. Widemann BC, Salzer WL, Arceci RJ, Blaney SM, Fox E, End D, et al. Phase I trial and pharmacokinetic study of the farnesyltransferase inhibitor tipifarnib in children with refractory solid tumors or neurofibromatosis type I and plexiform neurofibromas. *J Clin Oncol.* (2006) 24:507–16. doi: 10.1200/JCO.2005.03.8638
29. Kalamarides M, Acosta MT, Babovic-Vuksanovic D, Carpen O, Cichowski K, Gareth Evans D, et al. Neurofibromatosis 2011: a report of the children's tumor foundation annual meeting. *Acta Neuropathol.* (2012) 123:369–80. doi: 10.1007/s00401-011-0905-0
30. Yamashita AS, Baia GS, Ho JSY, Velarde E, Wong J, Gallia GL, et al. Preclinical evaluation of the combination of mTOR and proteasome inhibitors with radiotherapy in malignant peripheral nerve sheath tumors. *J Neurooncol.* (2014) 118:83–92. doi: 10.1007/s11060-014-1422-5
31. Karajannis MA, Legault G, Hagiwara M, Giancotti FG, Filatov A, Derman A, et al. Phase II study of everolimus in children and adults with neurofibromatosis type 2 and progressive vestibular schwannomas. *Neuro Oncol.* (2014) 16:292–7. doi: 10.1093/neuonc/not150
32. Holtkamp N, Okuducu AF, Mucha J, Afanasieva A, Hartmann C, Atallah I, et al. Mutation and expression of PDGFRA and KIT in malignant peripheral nerve sheath tumors, and its implications for imatinib sensitivity. *Carcinogenesis.* (2006) 27:664–71. doi: 10.1093/carcin/bgi273
33. Osum SH, Watson AL, Largaespada DA. Spontaneous and engineered large animal models of neurofibromatosis type 1. *Int J Mol Sci.* (2021) 22:1954. doi: 10.3390/ijms22041954

Conflict of Interest: All authors were employed by company Linnaeus Veterinary Limited.

The handling Editor declared a past co-authorship and past collaboration with one of the authors, OM.

frontiers | Frontiers in Veterinary Science

ORIGINAL RESEARCH
published: 20 June 2022
doi: 10.3389/fvets.2022.930856

A 3-Dimensional Printed Patient-Specific Surgical Guide to Facilitate Transsphenoidal Hypophysectomy in Dogs

*Leticia Escauriaza[1], Joe Fenn[2], John McCue[3], Darren Roper[1], Helene Vandenberghe[1], George Nye[1], Bill Oxley[4] and Nicolas Granger[1]**

[1] Neurology Department, Bristol Veterinary Specialists at Highcroft, CVS Referrals, Bristol, United Kingdom, [2] Department of Clinical Science and Services, Royal Veterinary College, Hertfordshire, United Kingdom, [3] Animal Medical Centre, New York, NY, United States, [4] Vet3D, Kendal, United Kingdom

Objective: Hypophysectomy in dogs is a difficult surgery that requires specific learning and training. We aimed to evaluate the accuracy of a 3-dimensional printed patient-specific surgical guide to facilitate choosing the entry point in the basisphenoid bone before approaching the *sella turcica* during transsphenoidal hypophysectomy in dogs.

Methods: Two canine cadavers and 8 dogs undergoing transsphenoidal hypophysectomy for Cushing's disease treatment, involving design and fabrication of a 3-dimensional printed guide. The ideal entry point in the basisphenoid bone outer cortical layer was determined in each dog pre-operatively; its anatomical location was described with a set of measurements then compared to post-operative computed tomography measures describing the location of the outer cortical window created in the basisphenoid bone.

Results: Several guide designs were proposed, and a consensus reached based on surgeons' experience performing hypophysectomy. The device chosen could be applied to the size and shape of skulls encountered in this case series. The pre-planned measurements were comparable to post-operative measurement (there was also no statistical difference), with median of differences <0.1 mm, which we judged as clinically acceptable.

Clinical Significance: Hypophysectomy in dogs is a challenging procedure that has a learning curve and needs to be performed by specialist neurosurgeons. We propose that a low-profile 3-dimensional printed surgical guide can aid the specialist neurosurgeon to locate the burring site of the outer cortical layer of the basisphenoid bone at a pre-defined location and with good accuracy. It does not alleviate the need to understand the anatomy of the region and to know how to create a slot within the basisphenoid bone, which remains essential to enter the *sella turcica.* This device could help specialist veterinary neurosurgeons wishing to be trained to perform hypophysectomy.

Keywords: 3D printing, computed tomography, companion dogs, pituitary dependent hyperadrenocorticism, neurosurgery, hypophysectomy

OPEN ACCESS

Edited by:
Luisa De Risio,
Linnaeus Veterinary Limited,
United Kingdom

Reviewed by:
Paul Freeman,
University of Cambridge,
United Kingdom
Ane Uriarte,
Southfields Veterinary Specialist,
United Kingdom

***Correspondence:**
Nicolas Granger
Nicolas.granger@cvsvets.com

Specialty section:
This article was submitted to Veterinary Neurology and Neurosurgery, a section of the journal Frontiers in Veterinary Science

Received: *28 April 2022*
Accepted: *23 May 2022*
Published: *20 June 2022*

Citation:
Escauriaza L, Fenn J, McCue J, Roper D, Vandenberghe H, Nye G, Oxley B and Granger N (2022) A 3-Dimensional Printed Patient-Specific Surgical Guide to Facilitate Transsphenoidal Hypophysectomy in Dogs. Front. Vet. Sci. 9:930856. doi: 10.3389/fvets.2022.930856

INTRODUCTION

Pituitary-dependent hyperadrenocorticism is a chronic, progressive, and eventually fatal condition, present in 80–85% of dogs with naturally occurring hyperadrenocorticism (1–3). It is caused by the presence of a functional corticotroph pituitary mass secreting the adrenocorticotropic hormone (ACTH) and subsequent adrenal cortisol release (4). These tumours are usually classified histologically as adenoma, invasive adenoma, or adenocarcinoma (5). Rarely, they can secrete other hormones such as somatotropin or prolactin, or be non-functional (5, 6). Historically, pituitary masses have been classified using computed tomography (CT) or magnetic resonance imaging (MRI) by the pituitary height (mm)/brain area (mm^2) ratio (P/B); a P/B ratio $>$ 0.31 defines enlarged adenomas, whereas a P/B ratio $<$ 0.31 defines non-enlarged adenomas. Enlarged adenomas can cause compression of adjacent brain structures and lead to a variety of neurological signs (7–9).

Treatment of pituitary-dependent hyperadrenocorticism can be medical or surgical with or without radiotherapy. Etiological treatment requires a transsphenoidal craniectomy (i.e., hypophysectomy) to remove the pituitary gland and associated neoplasm. Transsphenoidal hypophysectomy is becoming increasingly popular for dogs with pituitary-dependent hyperadrenocorticism, judging by recent publications, and is considered the treatment of choice for dogs with Cushing's disease (1, 9–17). According to Hanson et al. (12) looking at 150 dogs, a remission rate of 84% is seen after surgery and the 1, 2, 3, and 4-year survival rates are 83.5, 76.1, 71.5, and 67.8%, respectively (12). The same authors extended their data to 306 dogs and found the 1, 2, 3, 4, and 5-year survival rates after surgery to be 86, 79, 74, 72, and 64%, respectively (4). The mortality rate within 4 weeks of transsphenoidal hypophysectomy has been quoted to range from 8.8 to 19% (4, 14). Recently, a 5-point MRI-based grading system for pituitary masses has been proposed by Sato et al. (18), using the height and width of the pituitary tumour, extension cranio-caudally toward the optic chiasm and mamillary bodies, respectively, and extension dorsally toward the third ventricle or inter-thalamic adhesion (18). Sato et al. further classified these lesions as "type A" when there is no involvement of the surrounding arterial circle of Willis or cavernous sinus, and as "type B" when the vascular structures are involved (18). This classification is useful because dogs with grade 1 or 2 lesions can be cured (3 out of 3 grade 1A cases, 3 out of 3 grade 2A cases), grade 3 lesions may be removed fully macroscopically (22 out of 23 grade 3A cases and one grade 3B case) but recurrence can be observed (3 out of 22 grade 3A cases where the lesion had been macroscopically removed), grade 4 lesions can only be partially removed (two 4B cases were incompletely removed and one dog relapsed), and grade 5 were considered not suitable for transsphenoidal surgical treatment because only a partial resection could be expected without cure (18). In the largest case series so far published and capturing 306 dogs with Cushing's disease treated with hypophysectomy, 27 dogs died within 4 weeks and had a median P/B ratio of 0.54 (therefore above the accepted cut-off of $>$0.31 defining enlarged adenoma), whereas dogs that survived more than 4 weeks after surgery had a median P/B ratio of 0.38 (4, 19). In another large case series of 150 dogs from the same authors, dogs with a pituitary height $>$10 mm only had a survival rate of 50% in the year after surgery (12). Furthermore, in Mamelak et al. study, 4 dogs had a P/B ratio above 1, and 3 of these dogs died in the first 3 days after surgery, while one survived for 1,095 days (14).

Transsphenoidal hypophysectomy remains a challenging surgery regardless of the size of the mass because of the deep location of the *sella turcica* at the base of the skull. The surgeon needs to identify an adequate point of entry into the basisphenoid bone, while the space through the open mouth to visualise it is limited. To identify the location of the *sella turcica* and determine an entry point in the basisphenoid bone, veterinary surgeons have used palpation of the *hamuli* processes (along with other techniques discussed later), but this is challenging because of the position of the head in the surgery, usually held tilted from horizontal (9, 15, 20). The surgeon can use the inter-sphenoidal suture as an anatomical landmark, but its location varies depending on the dog's skull shape and size, or the location of the emissary vein, although, again, this vein is inconsistently present in dogs (9, 16, 21). The vascular structures (the arterial circle of Willis and cavernous venous sinus) surrounding the *sella turcica* limit the size of the window that the surgeon can create within the basisphenoid bone (1, 16). If the entry point is too far rostral, one risks entering the pre-sphenoid bone below the optic chiasm, and if the entry point is too caudal, one risks penetrating the promontory of the dorsum sellae and damage to the caudal communicating arteries (1, 4, 12, 14). Large lesions are intimately associated with the vasculature and surgical reports clearly establish occurrence of severe haemorrhage in surgery in dogs with large pituitary masses (4, 12, 14, 20).

The objective of this study was to create a low-profile (i.e., thin) and versatile system that would aid the surgeon to accurately locate the burring site and its size in the outer cortical layer of the basisphenoid bone, before continuing the approach through the basisphenoid bone and inner cortex and into the *sella turcica*. To achieve this, a 3-dimensional (3D) printed surgical guide was designed for each dog. The location and dimension of the bone window created on the outer cortex of the basisphenoid bone was compared to pre-operatively determined measures.

MATERIALS AND METHODS

Cadaver Study

Two cadavers were donated by the pathology service at the Royal Veterinary College (London, UK) in 2018. Head dissections were performed with the use of a scalpel, periosteal elevator, and Gelpi retractors to incise the soft palate, basisphenoid mucosa and periosteum and allow visualisation of the basisphenoid bone. This was performed first to aid deciding what landmarks could easily be used to hold a surgical guide in place, and secondly, to assess whether dummy guides would permit burring of the outer basisphenoid cortical layer. Given the limited space in the oral cavity, a device occupying the least possible space was

Abbreviations: P/B, pituitary height/brain area.

a key requirement. A CT scan of both heads was performed with the mouth held open with a 16-s line multidetector CT scanner (Siemens, Somatom Scope, Erlangen, Germany), and the following parameters were applied: pitch 0.6, rotation speed 1.5 seconds, Kvp 130, mAs static 200, slice thickness and number of slices per rotation 16 × 0.75 mm. The oral cavity was held open to avoid contact between the upper and lower arcade teeth, to allow optimal surface rendering of the teeth when reconstructing the images. The 3D printed guides for each cadaver were designed (see result section) and mock transsphenoidal hypophysectomy performed in both cadavers. Another CT scan was then taken after the mock hypophysectomy to cheque the accuracy of the burring sites.

Construction of the 3D Printed Patient-Specific Guide

The burring guides were manufactured by Vet3D (Coventry, UK) using the following protocol. For each case, the CT DICOM images from a medical imaging software (Osirix, Pixmeo, SARL; Geneva, Switzerland) (**Figure 1A**) were exported to a computer aided design (CAD) software (Netfabb professional, Netfabb GmbH: Parsberg, Germany) and a surface rendered virtual 3D model of the skull was created, which also allowed to 3D print the skull (**Figure 1B**). To design a patient-specific guide, we focused on the anatomy of the upper arcade including the upper teeth, the basisphenoid bone, *hamuli* processes of the pterygoid bone, vomer, and pituitary fossa. The skull and the guide were 3D printed in methacrylate photopolymer resin with Form 3 printers using High Temperature and BioMed Amber resin, respectively (Formlabs, Somerville, Massachusetts, United States). The BioMed Amber resin used to print the guide is certified as autoclavable and biocompatible (EN ISO 10993-1:2018; 10993-3:2014; 10993-5:2009). Prior to surgery, the guides and skull model were sterilised in ethylene oxide for 24 h or in an autoclave (121°C for 20 min).

In vivo Study

Eight cases were recruited between 2019 and 2022 from two institutions.

Pituitary Imaging

The pituitary lesions and bony anatomy were assessed *via* CT in all dogs. The CT from one hospital was a 16-s line multidetector CT scanner (Siemens, Somatom Scope, Erlangen, Germany) used with the following parameters: Kvp 130, pitch 0.55, mAs modulation Care Cose 4D^{TM} turned on quality ref 220, rotation speed 1.5 s, slice thickness and number of slices per rotation 16 × 0.75 mm (with both bone and soft tissue reconstruction) and medium sharpening kernel algorithm. Dogs received an intravenous contrast injection of 1.7 ml per kg of body weight of iohexol (Omnipaque; GE Healthcare AS, Norway). The CT scan from the other hospital was a 320-s line multidetector CT scanner (Aquilion One Genesis, Canon Medical Systems). The settings used were pitch 0.625, rotation speed 0.75 s, kVp 120, slice thickness 2 mm, slice interval 1 mm, 40 slices, mA 300. The height of the lesion contained in the *sella turcica* and the area of the brain taken from the same image (thus defining the P/B ratio) were measured on transverse soft-tissue window post-contrast CT image, using the P/B cut-off of 0.31 to define non-enlarged *vs.* enlarged pituitary tumours (19). Following pituitary imaging, dogs were recovered from general anaesthetic and returned for surgery when the guide was ready.

Surgical Technique

All dogs were positioned in sternal recumbency with their head held by hooking the canine teeth on a bar supported by a metal frame secured to the surgical table ($n = 4$, **Figure 2**) or using a commercially available surgical headframe ($n = 4$; Brainsight^{TM}, Rogue Research, Canada), while avoiding pressure to the jugular veins, as previously described (1, 8, 15, 16, 20, 22). The mandible was kept hanging to allow opening of the mouth during the different steps of the surgery. The cuffed armed endotracheal tube was attached to the lower jaw and retracted to the side of the mandible out of the surgical field. Following draping, a swab with a radio-opaque marker was placed in the pharynx to prevent leakage of fluids into the airways in 4 dogs. The soft palate was incised with a n°15 blade ($n = 4$) or monopolar diathermy ($n = 4$) in the midline (taking care not to section the soft palate along its entire length) following palpation of the pterygoid *hamuli* processes. Mini Gelpi retractors were placed in the soft palate wound to visualise the palatine mucosa and mucoperiosteum overlying the basisphenoid bone and these were elevated with a freer. The 3D printed guide was then inserted into the oral cavity, adjusting it to the upper arcade molars and making sure that the arm of the guide extended to make contact with the basisphenoid bone (see result section below). Once in place, the air-powered drill was brought in contact with the basisphenoid bone to burr the window depicted by the arm of the surgical guide. During that step, the surgeon needs to maintain the burr hand piece relatively horizontal in order to burr the basisphenoid bone with an angle of ∼45 degrees while the head is held tilted in position (**Figure 2**). Once the margins of the slot were created, the 3D patient specific surgical guide was removed from the oral cavity and the burring was continued through the cancellous bone toward the inner cortical layer until the dura underneath the pituitary gland was visible. Between burring, the surgical field was flushed with sterile saline NaCl 0.9% (B|Braun, Melsungen, Germany). Haemorrhage from the cancellous bone was controlled with bone wax (Ethicon, Johnson&Johnson Medical GmbH, Germany). The dura mater was incised with a n°11 surgical blade, after which the pituitary gland / mass lesion was visible through the incision. The pituitary gland and pituitary neoplasm were slowly and carefully removed as much as possible using blunt dissection and suction. Visualisation of the third ventricle, normal brain tissue or cerebrospinal fluid leak gave evidence of debulking of the mass. The slot created in the basisphenoid bone was covered by an absorbable collagen fleece (Lyostypt, B|Braun, Spain) or a corneal disc from porcine urinary bladder (Vetrix BioSIS ECM-BioSIS Plus^{+} 15 mm Multi-layer Ocular Discs- Vetrix, West Lafayette, IN 47906 USA) at the end of the surgery. The internal and external layers of the soft palate were closed in two planes with polyglactin suture (Vicryl 2-0 or 3-0, Johnson&Johnson, Belgium).

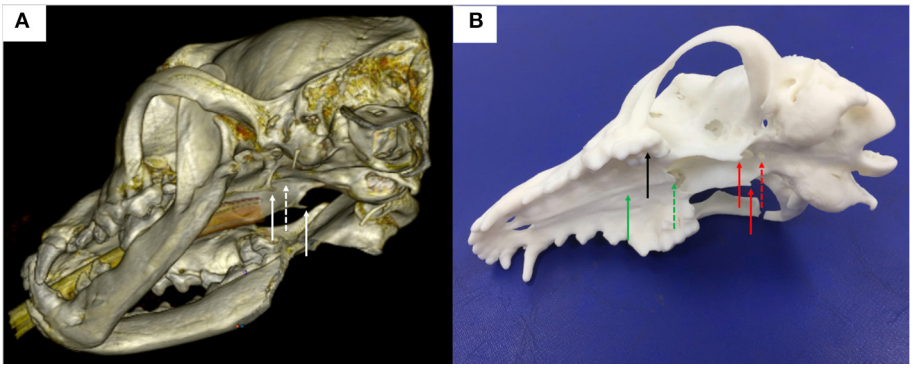

FIGURE 1 | (A) 3-dimensional reconstruction of a canine head in a bone window using DICOM images generated from CT and the medical imaging software Horos; note the *hamuli* processes, part of the pterygoid bone (plain white arrows) and the basisphenoid bone where a window needs to be burred (dashed white arrow) in the midline between the *hamuli* processes; **(B)** 3-dimension printed skull from the DICOM images; note again the *hamuli* processes (plain red arrows) and the basisphenoid bone where a window has been burred (dashed red arrow) in the midline between the *hamuli* processes; other anatomical landmarks used for the surgical guide design were the upper teeth (black plain arrow), the hard palate (green plain arrow) and the vomer (green dashed arrow).

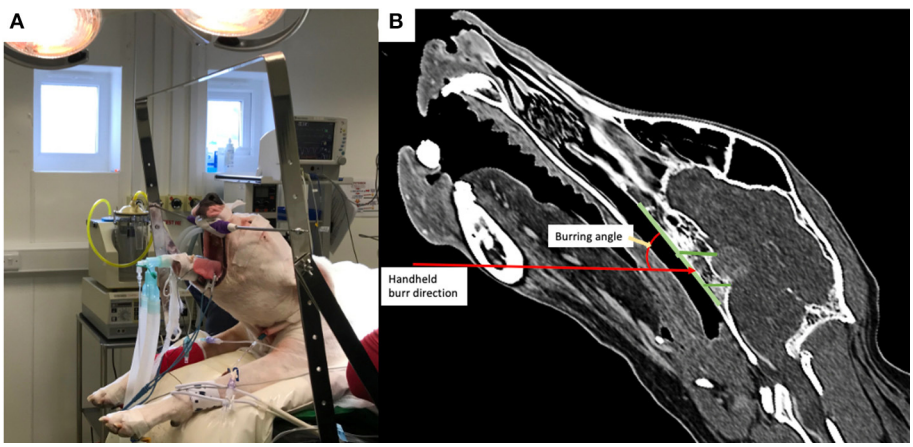

FIGURE 2 | (A) Photograph of a dog positioned in theatre with the head attached by the canine teeth to a metallic bar; note the head is therefore tilted from horizontal; **(B)** post-operative reconstructed sagittal CT image in a bone window showing the angulation required for burring with the handheld drill into the basisphenoid bone.

Pre- and Post-surgical Measurements of the Burring Site

Pre-operatively, we defined and measured (**Figures 3A,B**): (i) the distance between the vomer and the rostral aspect of the burring window depicted by the guide (named A1); (ii) the length (named B1) and the width (named C1) of the burring window into the basisphenoid outer cortical bone layer, as depicted by the guide in place; and (iii) the length of cortical bone removed from the second cortex forming the *sella turcica* (in a sagittal plane, named D1) and chosen to be the same as B1 (**Figures 3C–E**). All cases underwent a post-operative CT-scan [before and after intravenous injection of iohexol contrast at a dose of 1.7 ml/kg (Omnipaque, GE Healthcare, USA)] immediately after surgery to assess completeness of the hypophysectomy (**Figure 3F**). From the DICOM images, the following parameters were measured again (see **Figures 4A,B**): (i) the distance between the vomer and the rostral aspect of the achieved burred window in the basisphenoid outer cortex (named A2); (ii) the length (named B2) and width (named C2) of the achieved window in the basisphenoid outer cortex, and (iii) the length of cortical bone removed from the second cortex forming the *sella turcica*, named D2. Assessment of the accuracy of the burred window was evaluated by comparing the pre- and post-operative measures.

For the measurements, the median and the range are reported. Comparison of pre- and post-operative measures was done with the non-parametric Wilcoxon test for paired data with a p value of 0.05 considered significant and using GraphPad Prism version 9.0.0 for Windows (GraphPad Software, San Diego, California USA, www.graphpad.com).

We defined that a variation from baseline to post-operative measures of a magnitude of <10% would be acceptable and safe based on the distance left between the margins of the burred window and the cavernous sinuses and arterial circle of Willis measured on the post-contrast CT images.

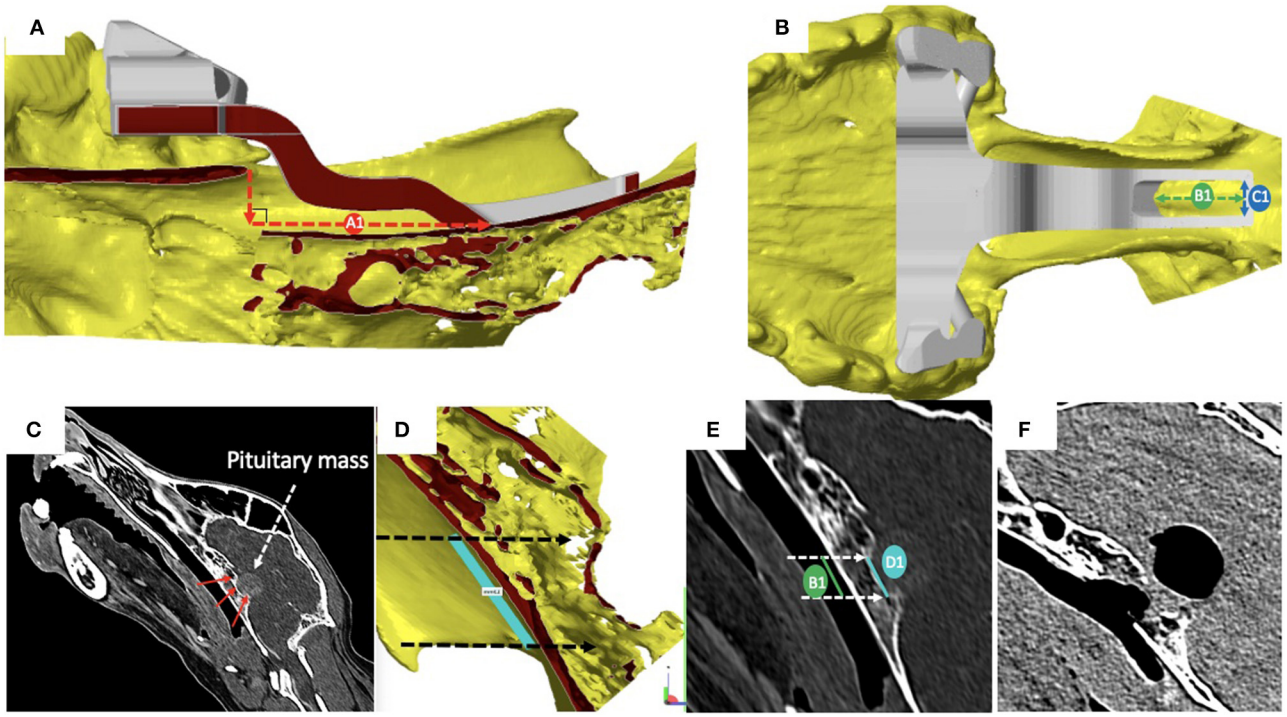

FIGURE 3 | (A) Sagittal section of the skull visualised with the CAD software Netfabb professional (rostral is to the left in the figure); cortical surfaces appear in yellow and the 3-dimensional printed guide in place is in grey: the distance between the vomer and the rostral aspect of the burring window depicted by the guide (A1) was measured by drawing a vertical line from the tip of the vomer to basisphenoid and another line, perpendicular to the first and extending to the rostral margin of the surgical guide; **(B)** dorsal view of the skull and surgical guide in place, visualised with the CAD software: the length (B1) and the width (C1) of the burring window into the basisphenoid first cortical bone layer appear as the green and blue double head dashed arrows, respectively; **(C)** the length of bone to remove from the inner cortical layer of the basisphenoid bone (red arrows) forming the *sella turcica* was defined to match that of the outer cortical layer to burr; **(D)** light blue line chosen to be no longer than the *tuberculum sellae* and the *dorsum sellae*); **(E)** the length of inner and outer cortical layers to be removed where defined as equal; **(F)** sagittal reconstructed post-operative post-contrast CT image obtained to assess completeness of the hypophysectomy; note the signal void region suggesting presence of air.

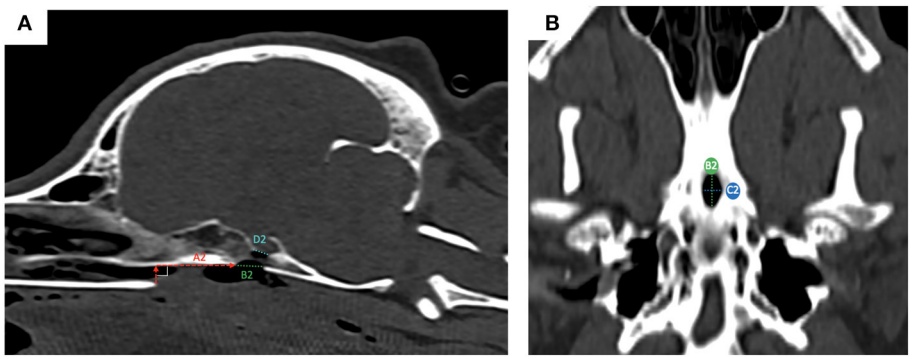

FIGURE 4 | post-operative measures from reconstructed sagittal CT images in a bone window; the measured obtained were: **(A)** the distance between the vomer and the rostral aspect of the achieved window in the basisphenoid outer cortex (A2, red dashed horizontal line); (ii) the length of bone removed from the outer cortical layer (B2, green dashed line) and the length of bone remove from the inner cortical layer (D2, light blue dashed line); **(B)** ventral view of the basisphenoid bone: the width (C2, blue dashed line) of the achieved window is visible, as well as the length (B2, green dashed line).

RESULTS

Case Signalment

Eight dogs with pituitary-dependent hyperadrenocorticism underwent transsphenoidal hypophysectomy with the help of a 3D printed surgical guide. Five patients were male (4 neutered and 1 entire) and 3 were neutered females. The age at the time of surgery ranged from 5.8 to 12.4 years (median age was 8 years old). The body weight ranged from 8.65 to 34.3 kg (median body weight was 29 kg). The breeds were: Labrador retriever

TABLE 1 | Signalment, pituitary height/brain area ratio (P/B ratio), and clinical outcome in the eight dogs in which transsphenoidal hypophysectomy was performed with the use of the 3D-patient-specific surgical guide.

Cases	Breed	Age (years)	Sex	Body Weight (kg)	P/B ratio (mm^{-1})	Outcome; survival to date	Histopathology
Case 1	Greyhound	7.3	FN	32	0.80	Clinical remission (absent hyperadrenocorticism); 34 months	Chromophobic enlarged adenoma
Case 2	Labrador retriever	5.8	MN	34.3	0.36	Clinical remission (absent hyperadrenocorticism); 29 months	Sinusoidal chromophobe adenoma
Case 3	Border terrier	12.4	MN	9.7	0.85	Mild persistent right-sided head tilt; persistent hyperadrenocorticism; 20 months	Sample of non-diagnostic quality
Case 4	Boxer	8	ME	26.3	0.78	Euthanasia 7 months post-operatively	Sinusoidal adenoma
Case 5	Labrador retriever	9	MN	29	0.70	Euthanasia 24 h post-operatively	Sample of non-diagnostic quality
Case 6	Labrador retriever	8	MN	30.6	0.30	Clinical remission (absent hyperadrenocorticism); 8 months	Sinusoidal adenoma
Case 7	English springer spaniel	11	FN	20.7	0.38	Clinical remission (absent hyperadrenocorticism); 8 months	Acidophil adenoma
Case 8	Bichon frise	9	FN	8.65	0.29	Clinical remission (absent hyperadrenocorticism); 6 months	Sinusoidal chromophobe adenoma

FN, female neutered; MN, male neutered; ME, male entire.

($n = 3$), Greyhound ($n = 1$), Border terrier ($n = 1$), Boxer ($n = 1$), English springer spaniel ($n = 1$), and Bichon frise ($n = 1$). The two cadavers were a Boxer and a Greyhound. The median P/B ratio was 0.37 and ranged from 0.29 to 0.85 for the eight clinical cases (**Table 1**); therefore, two cases were classified as non-enlarged adenoma and six were classified as enlarged adenoma. There was no involvement of the arterial circle of Willis or cavernous sinus in any of the cases, except in case 4.

Guide Design and Placement in Surgery

Following dissection of the cadavers, CT, and study of the 3D printed skulls in the CAD software (**Figures 1A,B**), multiple ideas were discussed between the authors in terms of what would be the most convenient design and location for the guide within the oral cavity (**Figure 5**). It appeared that locking the guide onto the upper arcade molars was the best option because the ventral aspect of the molars offers a well-contoured surface for purchase of the guide and is unique to each dog (**Figure 6**). This would ensure stability of the surgical guide and the molar teeth are easily reachable with the oral cavity open whilst doing open mouth surgery. Even if an animal was lacking one of the molars, the guide could be designed to be fitted onto a more rostral tooth. The abaxial aspects of the guide therefore comprised a contact of footprint which was an inverted representation of the maxillary molars (**Figure 5B**). We then designed an arm extending toward the basisphenoid bone with a shape following the anatomical contour of the hard palate, while avoiding the vomer bone and eventually reaching the region of the basisphenoid bone we wished to burr away (**Figure 6C**). Several designs were considered for the guide "foot" (**Figure 5**), including a U-shape, a round shape, a tunnel shape that could accommodate a burr or a pin and/or a rectangular shape. Eventually, the rectangular shape was retained, as it was the one restricting the least the surgeon's view once the guide was in place. The base of this foot was an inverted representation of the cortical contours of the basisphenoid bone at that point, thus providing a third point of contact to optimise guide fit and stability. The length of the rectangular window was designed to match the distance between the *tuberculum sellae* and the *dorsum sellae* (**Figures 3C–E**) and the width was dictated by the width of the *sella turcica* and need to avoid vascular structures. The angle of the rostral wall of the guide window was designed to match the necessary angle for the bone tunnel to emerge at the rostral aspect of the *sella turcica* and could be used as guide by the surgeon. We initially planned to use surgical glue to hold the guide in position, but this was discarded after the experience of the first surgery because it was felt to be convenient to be able to move the guide in and out of the mouth during the approach. Indeed, the guide was designed to indicate the burring site in the outer cortical layer of the basisphenoid bone and then removed to continue the approach through the basisphenoid bone. It was concluded that the guide could be held in place by a surgical assistant by applying gentle pressure toward the molars until the burring window was completed (**Figure 7** and **Supplementary Video 1**); Gelpi retractors placed to maintain the soft palate wound open also helped to maintain the guide. The variation between A1-A2, B1-B2, C1-C2, and D1-D2 was 0.03, 0.10, 0.00, and 0.30 cm, respectively, for the first cadaver and 0.00, 0.30, 0.10, 0.30 cm, respectively, for the second cadaver.

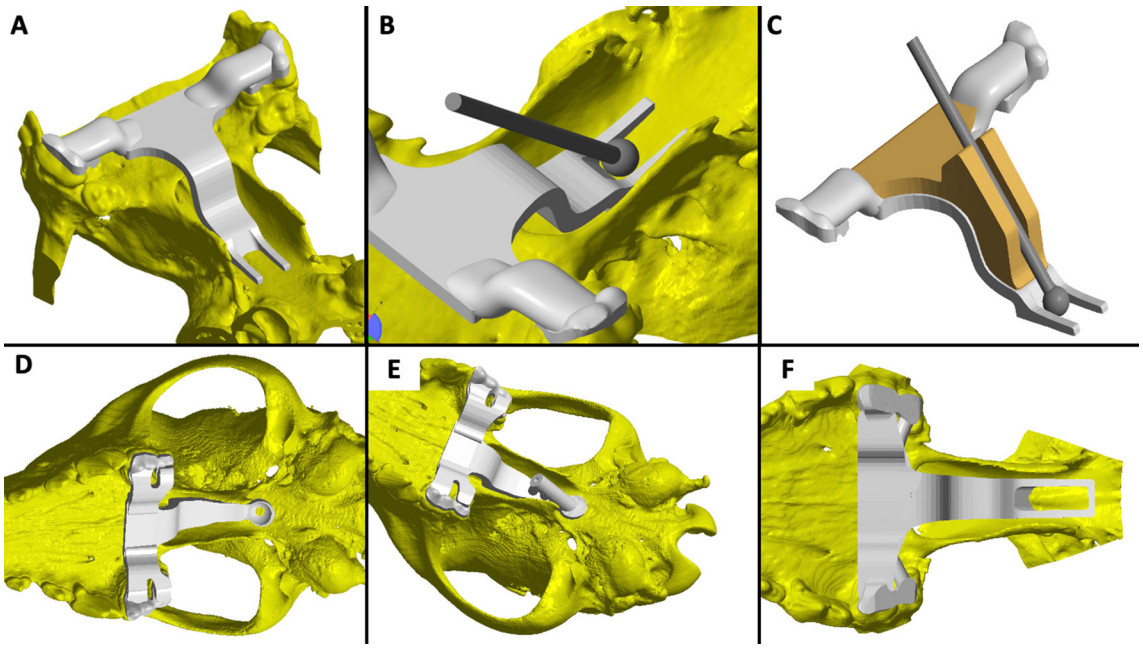

FIGURE 5 | Examples of the various iterations of the guide discussed by the authors: **(A)** the caudal aspect of the guide window left open; **(B)** placement of a slight slope at the rostral edge of the burring window to aid with burring trajectory; **(C)** use of a semi-opened channel to guide the bur; **(D)** guide offering solely a pilot hole position; **(E)** full channel to guide a pin and place a pilot hole; **(F)** final and preferred design.

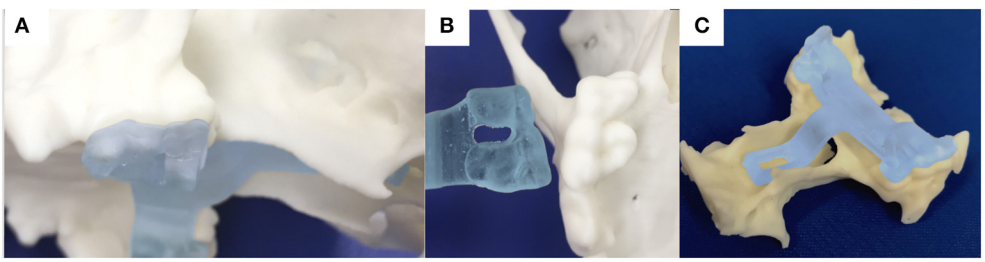

FIGURE 6 | photograph of the 3-dimensional printed skull showing the surface of the molar teeth on the left side in sagittal **(A)** and ventral **(B)** views; **(C)** the printed guide can lock on the molar teeth and contains an arm extending toward the basisphenoid bone with a shape following the anatomical contour of the hard palate, while avoiding the vomer bone and eventually reaching the outer cortex of the basisphenoid bone.

Trial in more cadavers was not considered necessary, since in case the guide would fail, the surgery could still be performed as previously described (15, 20).

When used *in vivo*, the guide was successfully held in place by the assistant. The surgeons observed that depending on the thickness of the soft palate and pre-planned contour of the guide, further dissection of the rostral aspect of the soft palate and even the hard palate in case 4 (a Boxer where the view was restricted due the brachycephalic shape of the head), was required for a perfect fit. This also facilitated the guide's stability.

Pre- and Post-operative Measures in Operated Cases

For the pre-operative measures, we found that A1 had a median of 2.22 cm and ranged from 1.30 to 3.05 cm; B1 had a median of 1.25 cm and ranged from 0.7 to 1.45 cm, C1 had a median of 0.5 cm and ranged from 0.40 to 0.60 cm and D1 had a median of 1.25 cm and ranged from 0.70 to 1.45 cm. For the post-operative measures, we found that A2 had a median of 2.2 cm and ranged from 1.10 to 3.06 cm, B2 had a median of 1.17 cm and ranged from 0.60 to 1.60 cm, C2 had a median of 0.55 cm and ranged from 0.40 to 0.70 cm and D2 had a median of 1.17 cm and ranged 0.7 to 1.35 cm. We entered the *sella turcica* in all cases and did not breach into the *tuberculum sellae* rostrally or *dorsum sellae* caudally. For A2 and A1, the median of differences was −0.075 mm (ranging from 0.00 to 0.20 cm); for B2 and B1 the median of differences was −0.05 mm (ranging from 0.00 to 0.30 cm); for C2 and C1 the median of differences was −0.015 mm (ranging from 0.00 to 0.20 cm); and for D1 and D2 the median of differences was −0.1 mm (ranging from 0.00 to 0.20 cm) (**Table 2**). The median of differences for the 4 parameters studied were all <10% of variation from baseline.

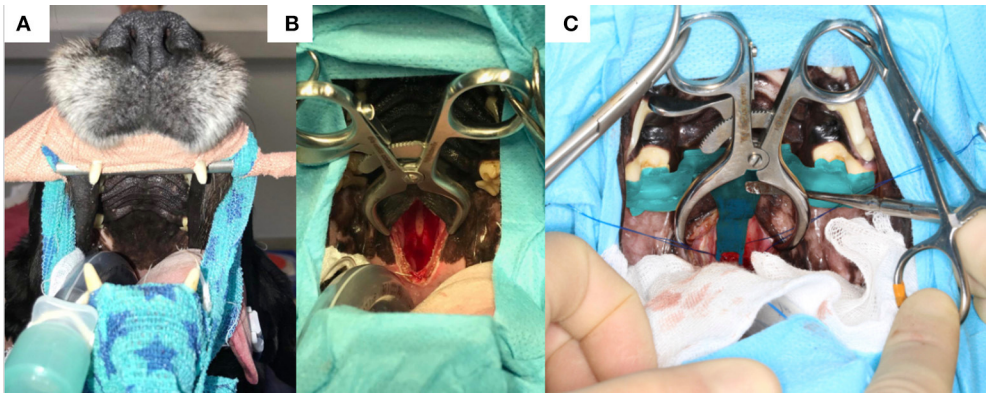

FIGURE 7 | (A) Photograph of the head of one of the dogs before surgery with the canines hooked on a bar attached to a frame and the surgical table; **(B)** incomplete incision in the soft palate and palatine mucosa exposing the basisphenoid bone; **(C)** 3-dimensional printed surgical guide *in situ* held by an assistant with a surgical instrument; note the foot of the guide extending toward the planned burring window; the Gelpi retractors also help to maintain the guide in place.

There was no significant difference between the pre- and post-operative measures: (i) A1 vs. A2: $p = 0.1875$, $W = -16$; (ii) B1 vs. B2: $p = 0.2031$, $W = -16$; (iii) C1 vs. C2: $p = 0.6250$, W = 6; (iv) D1 vs. D2: $p = 0.2344$, $W = -15$ (Wilcoxon test).

Clinical Outcome

For all 10 dogs, including both cadavers, entry into the *sella turcica* was achieved allowing removal of the pituitary gland and all ($n = 6$) or some of the mass lesion ($n = 2$).

None of the cases had intra-operative complications or died during surgery. Case 1 suffered from a cerebrovascular accident 5 days post- operatively and 5 months later was in clinical remission and has remained so since then. At 4 weeks after surgery, ACTH level was < 5pg/ml in this case, confirming the absence of hypercortisolism. Case 2 also had an ACTH measurement < 5 pg/ml 4 weeks after surgery, which confirmed absence of hypercortisolism. This case remains in remission. Case 3 developed post-operative right-sided vestibular signs which gradually improved. In this case, complete excision of the mass was not possible, therefore this patient remains with clinical signs of hyperadrenocorticism (ACTH 4 weeks after surgery was 64 pg/ml) and with a subtle head tilt to the right. Case 4 developed severe aspiration pneumonia 72 h after surgery which resolved with medical treatment. However, 7 months following surgery the patient had severe haemorrhagic diarrhoea and vomiting which led to decreased mentation and generalised weakness and the owner elected euthanasia. Case 5 showed loss of vision and pupillary light reflexes post-operatively, which was suspected to be secondary to haemorrhage and the owner elected euthanasia. Cases 6 and 7 are in clinical remission and both had ACTH levels 4 weeks after surgery <5 pg/ml and are not showing any sign of Cushing's disease. Case 8 had surgery in October 2021 and is neurologically normal 6 months later.

The follow-up in this case series ranges from 1 day to 34 months and the survival at 6 months is 75% (**Table 1**).

On histopathology, 5 dogs were diagnosed with a pituitary chromophobe sinusoidal adenoma, 1 dog with a pituitary acidophil adenoma and 2 dogs (cases 3 and 5) were diagnosed with pituitary neoplasia, however the sample was insufficient to adequately differentiate between benign or malignant pituitary neoplasia.

DISCUSSION

This study shows that the use of a 3D patient specific surgical guide is a possible method to localise the burring site along the outer cortical layer of the basisphenoid bone during hypophysectomy. The described technique was accurate to a tenth of a millimetre, which we consider satisfactory. This is similar to the accuracy desired for some brain surgeries in humans and reached with the use of 3D printed surgical guides, for example for implantation of deep brain stimulation electrodes (23).

A recent study from colleagues in Korea, using experimental dogs under 8.5 kg, performed coincidentally and in parallel to ours, also reports that a 3D surgical guide for transsphenoidal hypophysectomy provides an accurate reading of the entry point into the outer cortical layer of the basisphenoid bone (24). These authors have not tested their device in companion dogs affected by pituitary dependent-hyperadrenocorticism (24). They focus on the accuracy of a single pilot hole indicating the center of the *sella turcica* that is later extended in a rectangular shape in cranio-caudal and latero-lateral directions (24). The pre-operative planned measures were 6 mm in width and 8 mm in length, and the post-operative measures had a median of 5.17 mm width and 7.51 mm length, therefore similar to the precision we achieved (24).

It is important to recognise that the device we propose only gives the location of the burring site at the level of the outer basisphenoid cortical layer. Whilst it can provide the surgeon with a burring trajectory or angle through the basisphenoid bone to reach the inner cortical layer and therefore the *sella turcica*, indicated by the rostral wall of the guide window, it is a small surface that is difficult to follow and may not be reliable. In addition, the head position of the dog, tilted ∼45

TABLE 2 | Pre- (A1, B1, C1, D1) and post-operative (A2, B2, C2, D2) measures obtained from eight cases undergoing hypophysectomy with the use of a 3-dimensional printed guide.

Case number	Parameter	Pre-operative measures (A1; B1; C1; D1) (cm)	Post-operative numbers (A2; B2; C2; D2) (cm)	Difference between A1-A2, B1-B2, C1-C2 and D1-D2 (cm)	Variation from baseline (%)
	A	2.10	2.20	0.10	4.7
1	B	1.30	1.25	0.05	3.8
	C	0.50	0.60	0.10	20
	D	1.30	1.10	0.20	15
	A	3.05	3.06	0.01	0.3
2	B	1.45	1.43	0.22	1.3
	C	0.60	0.70	0.10	16.6
	D	1.45	1.30	0.15	10.3
	A	1.30	1.10	0.20	15.3
3	B	1.40	1.60	0.20	14.3
	C	0.40	0.60	0.20	50
	D	1.40	1.30	0.10	7.1
	A	2.35	2.20	0.15	6.3
4	B	1.20	1.10	0.10	8.3
	C	0.50	0.41	0.09	18
	D	1.20	1.15	0.05	4.1
	A	2.60	2.70	0.10	3.8
5	B	1.00	1.00	0.00	0
	C	0.43	0.40	0.03	6.9
	D	1.00	1.20	0.20	20
	A	2.40	2.40	0.00	0
6	B	1.20	0.90	0.30	25
	C	0.46	0.43	0.03	6.5
	D	1.20	1.10	0.10	8.3
	A	1.90	1.70	0.20	10.5
7	B	1.45	1.40	0.05	3.4
	C	0.60	0.60	0.00	0
	D	1.45	1.35	0.10	6.8
	A	1.8	1.63	0.17	9.4
8	B	0.7	0.6	0.10	14.2
	C	0.6	0.5	0.10	16.6
	D	0.7	0.7	0.00	0

degrees from horizontal, renders burring in the basisphenoid bone challenging. It is possible that other intraoperative tools such as goniometers could be thought to ascertain the optimal angle of approach of the *sella turcica* based on preoperative CT imaging. It might be that modification of the guide, to visualise the burring angle more clearly is possible too and something we are working on. Eventually, we did enter the *sella turcica* in all cases with a precision of a tenth of a centimetre. This seems small, however, the space we wished to create in the inner layer of the basisphenoid bone ranged from 0.7 to 1.35 cm and therefore, in some cases, a 0.1 mm variation would be above the 10% we considered acceptable. This is an imprecision we need to resolve through further research. Other clinicians using neuronavigation systems have also reported errors in localisation both in dogs and in humans, due to the variation in size, shape and thickness of the skull conformation, making the application of surgical systems challenging (25, 26). This also serves to highlight the importance of good surgical technique and clear understanding of the skull base anatomy required to perform this procedure. The impact of the use of this device on the outcome of the dogs was not a goal in this study and should be investigated as we continue to use this system. The post-operative mortality we recorded within 4 weeks was 12.5% (case 5, with a P/B ratio = 0.7 mm^{-1}, was euthanised 24 h after surgery). Eighty seven percent of the dogs (7 dogs) survived more than 4 weeks and of those cases, all but one (case 4), are alive at the time of writing. These survivals are similar to those previously published (4, 8, 9, 18). Further, in our cases (except case 4), there was no involvement of the arterial circle of Willis or cavernous sinus, similar to grade 2 and 3A cases presented by Sato et al. (18) and for which a good clinical outcome is expected (18).

Historically, hypophysectomy *via* an intracranial transtemporal route was used in experimental dogs but was later replaced by the transsphenoidal route (3). Reported

transsphenoidal techniques in experimental "normal" dogs include: (i) the placement of three small self-threading screws in the basisphenoid bone used as radiographic markers and followed by cranial sinus venogram outlining the *sella turcica* (16); (ii) a ventral paramedian approach using CT images obtained with the tip of a radiopaque feeding tube placed in the nasopharynx near the *hamuli* processes (10); (iii) the use of a stereotactic neuro-navigation system (27); and (iv) the use of a 3D surgical guide using CT and MRI images for the design and planning of the device (24). In practise, the reported transsphenoidal techniques in pet dogs with pituitary dependent hyperadrenocorticism include: (i) using anatomical landmarks such as the *hamuli* processes and emissary vein; and (ii) placement of pilot holes in the outer cortical layer of the basisphenoid bone followed by CT imaging (4, 12, 14, 20). These procedures can be invasive, imply peri-surgical imaging and therefore the need to take the animal out of theatre to CT and back to theatre, therefore increasing surgical time. Even then, the gain in precision for the surgeon to burr the basisphenoid bone hole accurately remains unknown. For the technique used by Owen et al. (9) the neuro-navigation system involves an expensive investment that is unlikely to be acceptable for medium-sized referral hospitals and comes with the need to place a frame around the head in the dog, which requires creating skin wounds to place the fixing pins (27). In comparison, the device we are proposing has a low profile (i.e., is thin enough) that leaves the burring site visible to the surgeon, is non-invasive and is rapidly deployable in surgery. It can be placed for practise, removed, and replaced in the mouth at will. It is also individually customised to the patient taking into account anatomical variations. We believe that this technique adds a useful option for neurosurgeons performing this procedure, thanks to the advances offered by 3D printing and the direct use of CT DICOM images within CAD software. Further, this surgical guide could be designed to fit varying skull sizes and shapes—our smallest patient was 9.7 kg dog and the largest patient was 34.3 kg—and if the patient is lacking any of the molar teeth, the guide could be designed using other teeth. The present study did not compare surgery duration with other surgical techniques due to the small number of cases available. However, we feel that the device, regardless of the gain in surgical time, can offer additional comfort to the surgeon and increase accuracy in locating the entry point in the basisphenoid bone, thereby increasing the surgeon's confidence.

Another limitation of this surgical guide is the cost, which, in the UK veterinary market, adds ∼10% to the total cost of the procedure. On the other hand, the use of the guide might remove the need for peri-operative CT or other neuronavigation techniques.

Hypophysectomy is typically an elective procedure to treat a chronic condition hence there is no need for a fast turn-around. The time needed to design and produce a guide can be as low as 3 days; it took on average 1 week to do in the cases presented.

It is known that pituitary surgery requires a learning curve for the surgeon to become confident in performing the approach. In 1999, Meij et al. clearly recognised this issue and reported five deaths related to the procedure in their first series of 26 cases, whereas they faced no death in their second series of 26 cases (1). Mamelak et al. also reported this in 26 operated dogs where the mortality rate was 50% in the first 10 cases and 0% in the next 16 dogs (14). Without replacing the need for training for this surgery, we propose that the extra help provided by our device in locating the entry point in the basisphenoid could improve the learning curve, although this is something we would need to study in another case series. A multicenter study would allow to collect a greater number of cases to better assess this theory. The use of 3D printing technology to train doctors to perform trans-nasal sphenoid endoscopy and hypophysectomy in people has been reported too (28). In that instance, 3D printing is used to model the hard and soft tissues of the skull region of interest and the neurosurgeon can then navigate their endoscope in the replica of the patient's head to gain familiarity with the anatomy.

Anecdotally, we have used the surgical guide for one feline acromegalic patient undergoing hypophysectomy, a treatment previously described (2, 3, 6, 22). We obtained the same precision as in the dogs of this study to locate the entry point in the basisphenoid bone. That cat has remained in clinical remission at the time of writing (16 months) with normalised insulin-like growth factor. To form a homogenous case series, we have decided to exclude this cat from the study since it would not add any meaningful data. But this suggests that the surgical device could be used in cats and is something we wish to test.

In conclusion, this surgical device provides an accurate method to localise the burring site in the outer layer of the basisphenoid bone when performing transsphenoidal hypophysectomy in dogs. It is versatile, non-invasive, and easy to apply. Whilst it does not replace the need for a thorough understanding of the surgical technique and relevant anatomy, and the need for training, it may prove useful as a teaching tool for veterinary specialist neurosurgeons wishing to learn to perform a hypophysectomy.

DATA AVAILABILITY STATEMENT

The original contributions presented in the study are included in the article/**Supplementary Material**, further inquiries can be directed to the corresponding authors.

ETHICS STATEMENT

Ethical review and approval was not required for the animal study because the authors perform hypophysectomy routinely in their clinics as a treatment for Cushing's disease. The dogs presented in the manuscript have undergone hypophysectomy as part of their treatment plan and for their direct benefit. The interventions therefore were done under the Veterinary Surgeons Act (VSA) 1966. The guides used in the dog's mouth were a visual aid, as much as loupes we use for this surgery or other surgical tools, and did not require any additional intervention; it does not involve breaching the skin, mucosa or any invasive action on the dog. We have explained the surgery to all clients and collected informed consent from the owners of these cases and permission to use medical data. Written informed consent was obtained from the owners for the participation of their animals in this study.

AUTHOR CONTRIBUTIONS

BO, NG, and LE designed the guide. NG designed the study. BO ran the CAD software and 3D printing to manufacture the guide. JF, JM, and NG contributed to the article by using the device in surgery. LE, JF, HV, GN, JM, NG, and DR were involved in the clinical management of the cases. LE and NG wrote the manuscript. DR contributed to the article by performing the diagnostic investigations and advising on CT technique for later 3D printing. All authors proof read and helped correcting the manuscript. All authors contributed to the article and approved the submitted version.

FUNDING

The publication fees was funded by CVS Group PLC Company.

ACKNOWLEDGMENTS

We would like to thank the veterinary specialists and specialists in training who have helped manage the cases presented in this series: Jeremy Rose BA VetMB DipECVN AFHEA MRCVS, Sarah Caulfied BVMedSci(Hons) BVM BVS(Hons) PGDipVCP MRCVS, Emma Roberts BVetMed(Hons) MVM DipECVIM-CA MRCVS, Guillaume Ruiz DVM CEAV-MI DipECVIM-CA MRCVS, Jennifer Stallwood BVSc BSc (Hons) Cert AVP (ECC), DipECVIM-CA MRCVS, Paul Higgs MA VetMB CertSAM DipECVIM-CA MRCVS as well as the anaesthesia and the diagnostic imaging teams.

SUPPLEMENTARY MATERIAL

The Supplementary Material for this article can be found online at: https://www.frontiersin.org/articles/10.3389/fvets.2022.930856/full#supplementary-material

REFERENCES

1. Meij BP. Hypophysectomy in dogs: a review. *Vet Q.* (1999) 21:134–41. doi: 10.1080/01652176.1999.9695008
2. Meij BP, Voorhout G, Van Den Ingh TS, Rijnberk A. Transsphenoidal hypophysectomy for treatment of pituitary-dependent hyperadrenocorticism in 7 cats. *Vet Surg.* (2001) 30:72–86. doi: 10.1053/jvet.2001.17843
3. Meij BP, Voorhout G, Rijnberk Ad. Progress in transsphenoidal hypophysectomy for treatment of pituitary-dependent hyperadrenocorticism in dogs and cats. *Mol Cell Endocrinol.* (2002) 197:89–96. doi: 10.1016/S0303-7207(02)00283-6
4. van Rijn SJ, Galac S, Tryfonidou MA, Hesselink JW, Penning LC, Kooistra HS, et al. The influence on pituitary size on outcome after transsphenoidal hypophysectomy in a large cohort of dogs with pituitary-dependent hypercortisolism. *J Vet Intern Med.* (2016) 30:989–95. doi: 10.1111/jvim.14367
5. Sanders K, Galac S, Meij BP. Pituitary tumour types in dogs and cats. *Vet J.* (2021) 270:105623. doi: 10.1016/j.tvjl.2021.105623
6. Blackman G. Hypophysectomy; ground breaking treatment for acromegaly in cats-an overview of cutting edge surgery. *Vet Nurs J.* (2018) 33:192–6. doi: 10.1080/17415349.2018.1470912
7. Menchetti M, De Risio L, Galli G, Bruto Cherubini G, Corlazzoli D, Baroni M, et al. Neurological abnormalities in 97 dogs with detectable pituitary masses. *Vet Q.* (2019) 39:57–64. doi: 10.1080/01652176.2019.1622819
8. Hara Y. Transsphenoidal surgery in canines: safety, efficacy and patient selection. *Vet Med.* (2020) 11:1–14. doi: 10.2147/VMRR.S175995
9. Owen TJ, Martin LG, Chen AV. Transsphenoidal surgery for pituitary tumors and other sellar masses. *Vet Clin North Am Small Anim Pract.* (2017) 48:129–51. doi: 10.1016/j.cvsm.2017.08.006
10. Axlund TW, Behrend EN, Sorjonen DC, Simpson ST, Kemppainen RJ. Canine hypophysectomy using a ventral paramedian approach. *Vet Surg.* (2005) 34:179–89. doi: 10.1111/j.1532-950x.2005.00029.x
11. Ganong RF, Hume DM. The effect of graded hypophysectomy on thyroid, gonadal and adrenocortical function in the dog. *Endocrinology.* (1956) 59:293–301. doi: 10.1210/endo-59-3-293
12. Hanson JM, van't Hoofd MM, Voorhout G, Voorhout G, Teske E, Kooistra HS, et al. Efficacy of transsphenoidal hypophysectomy in treatment of dogs with pituitary-dependent hyperadrenocorticism. *J Vet Intern Med.* (2005) 19:687–94. doi: 10.1111/j.1939-1676.2005.tb02747.x
13. Hara Y, Tagawa M, Masuda H, Sako T, Koyama H, Orima H, et al. Transsphenoidal hypophysectomy for four dogs with pituitary ACTH-producing adenoma. *J Vet Med Sci.* (2005) 65:801–4. doi: 10.1292/jvms.65.801
14. Mamelak AN, Facs MD, Owen TJ. Transsphenoidal surgery using a high definition video telescope for pituitary adenomas in dogs with pituitary dependent hypercortisolism: methods and results. *Vet Surg.* (2013) 43:369–79. doi: 10.1111/j.1532-950X.2014.12146.x
15. Meij BP, Voorhout G, Van den Ingh TS, Hazewinkel HA, Van't Verlaat JW. Transsphenoidal hypophysectomy in Beagle dogs: evaluation of a microsurgical technique. *Vet Surg.* (1997) 26:295–309. doi: 10.1111/j.1532-950X.1997.tb01502.x
16. Niebauer GW, Evans SM. Transsphenoidal hypophysectomy in the dog. A new technique. *Vet Surg.* (1988) 17:296–303. doi: 10.1111/j.1532-950X.1988.tb01021.x
17. Behrend. E. Canine hyperadrenocorticism. *In: Canine and feline endocrinology and reproduction.4th edn. Eds. Feldman E.C, Nelson R, Reusch.C, Scott-Moncrieff.C, Saunders, St Louis.* (2015) p.377-451 doi: 10.1016/B978-1-4557-4456-5.00010-9
18. Sato A, Teshima T, Ishino H, Harada Y, Yogo T, Kanno N, et al. A magnetic resonance imaging-based classification system for indication of trans-sphenoidal hypophysectomy in canine pituitary-dependent hypercortisolism. *J Small Anim Pract.* (2016) 57:240–6. doi: 10.1111/jsap.12474
19. Kooistra HS, Voorhout G, Mol JA, Rijnberk A. Correlation between the impairment of glucocorticoid feedback and the size of the pituitary gland in dogs with pituitary -dependent hyperadrenocorticism. *J Endocrinol.* (1997) 152:387–94. doi: 10.1677/joe.0.1520387
20. Meij BP, Voorhout G, Van den Ingh TS, Hazewinkel HA, Teske E, Rijnberk A. Results of transsphenoidal hypophysectomy in 52 dogs with pituitary-dependent hyperadrenocorticism. *Vet Surg.* (1998) 27:246–61. doi: 10.1111/j.1532-950X.1998.tb00123.x
21. Barker FG, Klibanski A, Swearingen B. Transsphenoidal surgery for pituitary tumors in the United States, 1996-2000: mortality, morbitidy and the effects of hospital and surgeon volume. *J Clin Endocrinol Metab.* (2003) 88:4709–19. doi: 10.1210/jc.2003-030461
22. Fenn J, Kenny PJ, Scudder CJ, Hazuchova K, Gostelow R, Fowkes RC, et al. Efficacy of hypophysectomy for the treatment of hypersomatotropism-induced diabetes mellitus in 68 cats. *J Vet Intern Med.* (2021) 35:823–33. doi: 10.1111/jvim.16080
23. Rusheen AE, Barath AS, Goyal A, Barnett JH, Gifford BT, Bennetet KE, et al. A compact stereotactic system for image-guided surgical intervention. *J Neural Eng.* (2020) 17:10.1088/1741-2552/abc743. doi: 10.1088/1741-2552/abc743
24. Roh Y, Kim D, Jeong S, Lee H. Evaluation of the accuracy of three-dimensional printed patient-specific guides for transsphenoidal hypophysectomy in small-breed dogs. *Am J Vet Res.* (2022) 83:465–72. doi: 10.2460/ajvr.21.09.0154

25. Wininger F. Neuronavitation in small animals: development, techniques, and applications. *J Vet Clin North Am Small Anim Pract.* (2014) 44:1235–48. doi: 10.1016/j.cvsm.2014.07.015
26. Wang M, Song Z. Classification and analysis of errors in neuronavigation. *Neurosurgery.* (2011) 68:1131–43. doi: 10.1227/NEU.0b013e318209cc45
27. Owen TJ, Chen AV, Frey S, Martin LG, Kalebaugh T. Transsphenoidal surgery: accuracy of an image-guided neuronavigation system to approach the pituitary fossa (sella turcica). *Vet Surg.* (2018) 47:664–71. doi: 10.1111/vsu.12906
28. Waran V, Menon R, Pancharatnam D, Rathinam AK, Balakrishnan YK, Tung TS, et al. The creation and verification of cranial models using three-dimensional rapid prototyping technology in field of transnasal sphenoid endoscopy. *Am J Rhinol Allergy.* (2012) 26:132–6. doi: 10.2500/ajra.2012.26.3808

Conflict of Interest: BO is the manufacturer of the surgical device through the company Vet3D and NG undertakes paid consultancy work for Vet3D in relation to the guide system.

The remaining authors declare that the research was conducted in the absence of any commercial or financial relationships that could be construed as a potential conflict of interest.

Publisher's Note: All claims expressed in this article are solely those of the authors and do not necessarily represent those of their affiliated organizations, or those of the publisher, the editors and the reviewers. Any product that may be evaluated in this article, or claim that may be made by its manufacturer, is not guaranteed or endorsed by the publisher.

frontiers | Frontiers in Veterinary Science

CASE REPORT
published: 22 June 2022
doi: 10.3389/fvets.2022.825525

Case Report: Diffuse Lumbar Hyperostosis Causing Vertebral Canal Stenosis in a Dog With Concurrent Multicentric T-Cell Lymphoma

Max Foreman[1]*, *Audrey Belmudes*[2], *Elizabeth Villiers*[3] and *Elena Scarpante*[1]

[1] Neurology and Neurosurgery Service, Dick White Referrals, Part of Linnaeus Veterinary Limited, Cambridgeshire, United Kingdom, [2] Diagnostic Imaging Service, Dick White Referrals, Part of Linnaeus Veterinary Limited, Cambridgeshire, United Kingdom, [3] Clinical Pathology Service, Dick White Referrals, Part of Linnaeus Veterinary Limited, Cambridgeshire, United Kingdom

A 4-year-old female spayed Bullmastiff-cross presented with a 24-h history of progressive paraparesis. Neurological examination was consistent with L4–S3 myelopathy. On magnetic resonance imaging (MRI), all vertebrae showed homogenously increased short tau inversion recovery (STIR) signal with strong contrast enhancement. The vertebral canal was concentrically narrowed along the length of the L5 vertebra secondary to bony proliferation of the vertebral pedicles, dorsal lamina, and vertebral body. Cytological analysis of the peripheral lymph nodes and subsequent flow cytometry was consistent with T-cell lymphoma. The dog was euthanised due to poor prognosis. Necropsy confirmed the presence of stage V multicentric T-cell lymphoma, as well as diffuse hyperostosis of the vertebral bodies. This is the first report of presumed paraneoplastic lumbar skeletal hyperostosis.

Keywords: magnetic resonance imaging (MRI), neoplasia, neurology, paraparesis, paraneoplastic

OPEN ACCESS

Edited by:
Luisa De Risio,
Linnaeus Veterinary Limited,
United Kingdom

Reviewed by:
Marc Vandevelde,
University of Bern, Switzerland
Emma Laws,
Linnaeus Veterinary Limited,
United Kingdom

***Correspondence:**
Max Foreman
max.foreman@dwr.co.uk

Specialty section:
This article was submitted to Veterinary Neurology and Neurosurgery, a section of the journal Frontiers in Veterinary Science

Received: *30 November 2021*
Accepted: *27 May 2022*
Published: *22 June 2022*

Citation:
Foreman M, Belmudes A, Villiers E and Scarpante E (2022) Case Report: Diffuse Lumbar Hyperostosis Causing Vertebral Canal Stenosis in a Dog With Concurrent Multicentric T-Cell Lymphoma. Front. Vet. Sci. 9:825525. doi: 10.3389/fvets.2022.825525

INTRODUCTION

Lymphoma is one of the most frequently diagnosed malignancies in the dog, with medium-sized and larger breeds being overrepresented. A familial occurrence has been reported in several breeds, including the Bullmastiff (1). The most common clinical presentation is the multicentric form affecting multiple peripheral lymph nodes, however extranodal forms exist within all other body systems. Primary osseous lymphoma is rarely reported in dogs (2). More commonly, osseous and vertebral lymphoma in dogs is diagnosed as part of a multicentric process (3–6). T-cell and stage V lymphomas carry a poorer prognosis (1) when compared to B-cell or lower stage lymphomas. T-cell lymphoma appears to be rarely associated with osseous involvement, with only one out of a 46 cases of T-cell lymphoma involving bone in one study (7). Spinal extradural T-cell lymphoma has also been reported in dogs, however there was no evidence of bony infiltration in these cases (8, 9).

Osseous lymphoma in dogs may be radiographically silent (6, 10), or may show a variety of non-specific radiological changes, most commonly osetolysis (2, 4, 10). Diffuse smooth diaphyseal periosteal reaction was seen in the long bones of one dog with polyostotic lymphoma (4), and irregular osteoproductive lesions were present associated with the vertebrae of another (5). Vertebral changes on MRI may be confined to the medullary cavity (3) or may extend into the extradural and paraspinal tissues (6).

Various paraneoplastic syndromes have been reported associated with canine lymphoma. Hypercalcaemia is most common (1, 11), however other conditions reported include neuropathy

(12), polycythaemia (13), hypoglycaemia (14), monoclonal gammopathy (15), eosinophilia (8) and immune-mediated diseases (16). Hyperostosis can occur as a paraneoplastic condition most commonly secondary to both neoplastic and non-neoplastic pulmonary disease - hypertrophic osteopathy (HO) - and causes a painful periosteal reaction and associated soft tissue swelling of the distal limbs (17). Extrapulmonary neoplastic causes have been reported as well, including tumours of the bladder and kidney. (18–21). In human medicine, axial skeletal hyperostosis has been reported in a case of systemic Hodgkin's lymphoma (18).

To the authors' knowledge, a hyperostotic syndrome has not been reported in association with canine lymphoma. Therefore, this case report describes the presence of an unusual distribution of hyperostosis in a dog concurrently affected by atypical multicentric T-cell lymphoma.

CASE DESCRIPTION

A 4-year-old female spayed Bullmastiff-cross was referred with a 24-h history of progressive paraparesis. The dog was reported to have had a two-month history of intermittent vomiting and frequent diarrhoea, weight loss of 2 kilograms and more recently suspected polyuria-polydipsia - the referring veterinary surgeon had diagnosed hypocobalaminaemia and initiated supplementation. Subsequently, the dog had become progressively unable to stand on the pelvic limbs.

General physical examination documented poor body condition, generalised peripheral lymphadenomegaly affecting the mandibular, superficial cervical and popliteal lymph nodes, and instability of the right stifle. On neurological examination, the patient was ambulatory paraparetic with reduced pelvic limb, tail and anal tone, reduced patella and pelvic limb withdrawal reflexes and absent pelvic limb proprioception. Focal lumbar pain was present. Neuroanatomical localisation was consistent with L4–S3 myelopathy, with differentials for the paraparesis considered including degenerative, inflammatory, neoplastic and infectious diseases. Differential considered for the peripheral lymphadenomegaly included neoplastic, reactive, inflammatory and infectious diseases.

DIAGNOSTIC INVESTIGATIONS AND OUTCOME

Complete blood count, biochemistry and electrolyte profiles were unremarkable, however a moderate proportion of lymphocytes appeared reactive on smear examination. Total calcium was within the reference range, hence ionised calcium was not assessed. C-Reactive Protein was elevated (21 mg/L; reference range <10). Urinalysis showed the urine to be well concentrated with a specific gravity of 1.033, trace protein and evidence of a urinary tract infection, with 10–20 white blood cells/high power field (Ref. 0–2). Urine culture was positive for *E. coli*.

Under general anaesthesia, magnetic resonance examination of the lumbosacral vertebral column was performed (Hitachi Aperto Lucente 0.4 Tesla, Berkshire, UK). Imaging was performed in dorsal recumbency with the pelvic limbs in extension. The following multiplanar MR sequences were performed: sagittal T2-weighted (T2W; TE=120 ms; TR=3290 ms; 3 mm thick with no interslice gap), transverse T2-weighted (T2W; TE=100 ms; TR=5653 ms; 4 mm thick with no interslice gap), sagittal short-tau inversion recovery (STIR; TE=60 ms; TR=3014 ms; 3 mm thick with no interslice gap), sagittal and transverse T1-weighted (T1W; TE=13 ms; TR=745 ms; 3 mm and 4 mm thick respectively with no interslice gap). Following intravenous administration of 0.1 mmol/kg gadolinium-based contrast agent (Dotarem, Guerbet LLC, Ohio, USA), sagittal and transverse T1-weighted sequences were obtained (T1W; TE=13 ms; TR=745 ms; 3 mm and 4 mm thick respectively with no interslice gap). Sagittal sequences were acquired from L2 to Cd4, and transverse sequences acquired from L4–5 to L6. Transverse T2-weighted sequence was also acquired across L7–S1.

Diffusely abnormal bone signal was observed in all visible vertebrae, showing an increase in STIR signal and normal to increased T2 signal (**Figure 1**) with diffuse and homogenous contrast enhancement (**Figure 2**). The signal intensity changes were associated with circumferential concentric thickening of the vertebral pedicles, dorsal lamina and vertebral body, leading to marked circumferential narrowing of the vertebral canal along the length of L5 with secondary spinal cord compression. There was complete circumferential attenuation of the CSF signal surrounding the spinal cord at this level (**Figure 1**). There were similar but less marked changes affecting the L4 and L6 vertebrae. The normal shape of the vertebral bodies was maintained, with persistent visualisation of the external cortical bone but loss of visualisation of the inner cortex. Moderate flowing ventral ossification was also noted along the length of the lumbar spine, bridging the vertebral bodies from L3 to L7 with absence of extensive changes of degenerative disc disease. Additionally, moderate bilateral medial iliac lymphadenomegaly was noted. Differential diagnoses considered for concentric osseous thickening included generalised osteoproliferative disease (osteochondromatosis, atypical hypertrophic osteopathy), myeloproliferative disorders (myelofibrosis), osteopetrosis, hypervitaminosis D, metabolic disease (hypoparathyroidism, hypervitaminosis A) or less likely neoplastic infiltration (round cell neoplasia). The changes noted along the ventral aspect of the lumbar spine were consistent with diffuse idiopathic spinal hyperostosis (DISH).

Right lateral radiographs of the vertebral column from T6 to Cd2 (**Figure 3**) showed normal to decreased bone radiopacity of the lumbar vertebrae, and loss of visualisation of the dorsal cortex of the vertebral body from L1 to L6. Moderate new bone formation around the spinous processes of T11 and T12, and the articular facets at the level of T11–12 and T12–13, and more mildly at L1–2 and L2–3 was noted. Furthermore, the same flowing ossification along the ventral aspects of the vertebral bodies from L3–L7 was noted, as well as ventral bridging spondylosis at the levels of T9–11, T7–8 and L7–S1.

Bone biopsy of the new bone around the vertebral articular facets at T11–13 consisted of mature cartilage and bone, which

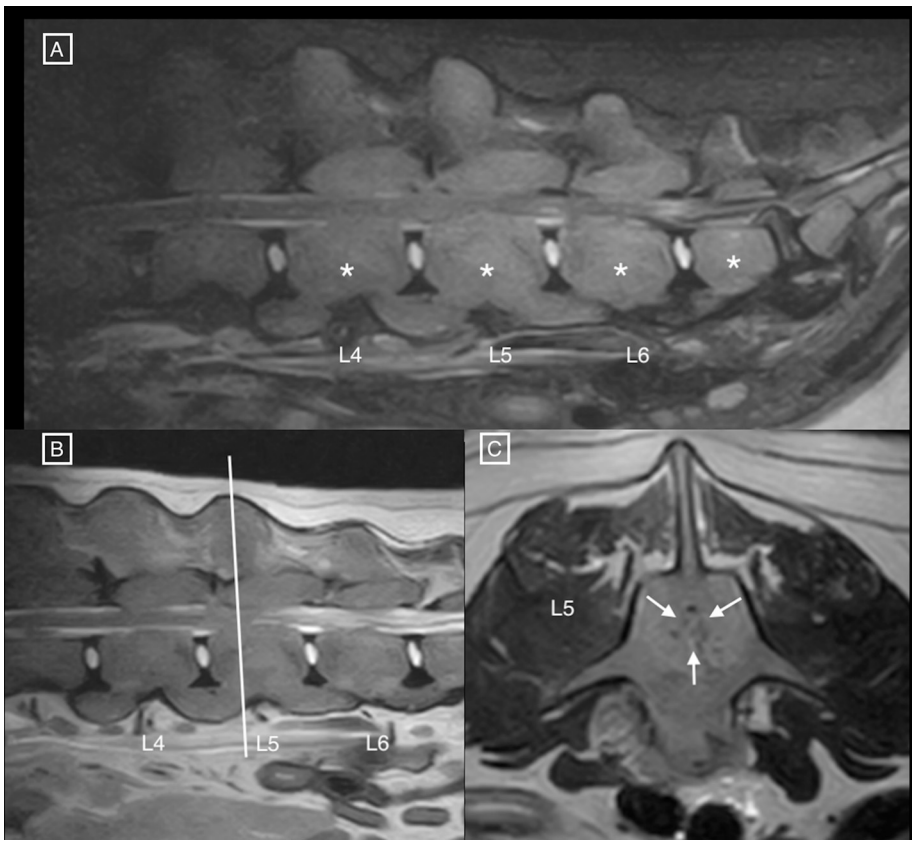

FIGURE 1 | (A) Sagittal STIR and **(B)** T2 MR images of the lumbar spine, and **(C)** transverse T2 MR image at the level of mid-L5. Notice the diffuse hyperintensity of the vertebral structures (asterisks), associated with circumferential concentric bone thickening, and secondary narrowing of the vertebral canal (white arrows) leading to circumferential compression of the spinal cord. The nucleus pulposus is also decreased in intensity at L7–S1, and the annulus fibrosus protrudes dorsally in the vertebral canal.

was disorganised and forming thick trabeculae. There was no evidence of inflammation or malignant neoplasia.

Fine needle aspiration of the popliteal lymph nodes showed significant expansion in the proportion of intermediate-sized lymphoid cells which were approximately 1.5 times the diameter of small lymphocytes. They had a round and slightly irregular shaped nucleus, slightly dispersed chromatin but no nucleoli, and a small to moderate amount of pale-staining cytoplasm. The cytological diagnosis was most suggestive of lymphoma although an atypical hyperplasia was not excluded. Flow cytometry was performed, using leukocyte marker CD45, B-cell markers CD21 and CD79a, T-cell markers CD3 and CD5, T-helper cell marker CD4, cytotoxic T-cell marker CD8, early precursor marker CD34 as well as MHC II. The cells assessed were CD45 positive in 99%, with 98% positive for CD3 and 21% positive for CD4. The cells were negative for CD5 and MHC II. This atypical immunophenotype (CD3+ / CD5- / variable CD4) confirmed a T-cell lymphoma and excluded hyperplasia.

The owner elected for euthanasia. On gross necropsy the lumbar vertebrae were thickened (hyperostosis), with the articular surfaces covered in smooth osseous proliferation (**Figure 4**). Following sectioning, narrowing of the spinal canal was seen, and the vertebral bodies of the L4–6 vertebrae were enlarged. Additionally, a multinodular proliferation was present, adhered to the left cranial dorsal lung and expanding the mediastinal space, the liver showed a diffuse lobular pattern, the spleen was diffusely enlarged, and the mesenteric and retroperitoneal lymph nodes were enlarged.

All major body organs were examined histopathologically. Proliferations of densely cellular, infiltrative round cells were present in the thymus, liver, spleen, lymph nodes and gastric wall. These neoplastic cells were arranged in sheets on a fine fibrovascular stroma, were approximately 1–1.5xRBC, round with distinct cell borders and scant eosinophilic cytoplasm. Nuclei were round to oval with coarsely stippled chromatin. There was mild anisocytosis and anisokaryosis and marked multifocal necrosis. Frequently neoplastic cells were seen migrating across vascular adventitial layers. The bone marrow of L5 was diffusely expanded and hypercellular and was infiltrated with the same monomorphic population of monocytic cells. Multifocally within the epidural adipose tissue was a similar mononuclear infiltrate. Smaller clusters of rounds cells appeared next to nerve roots within the

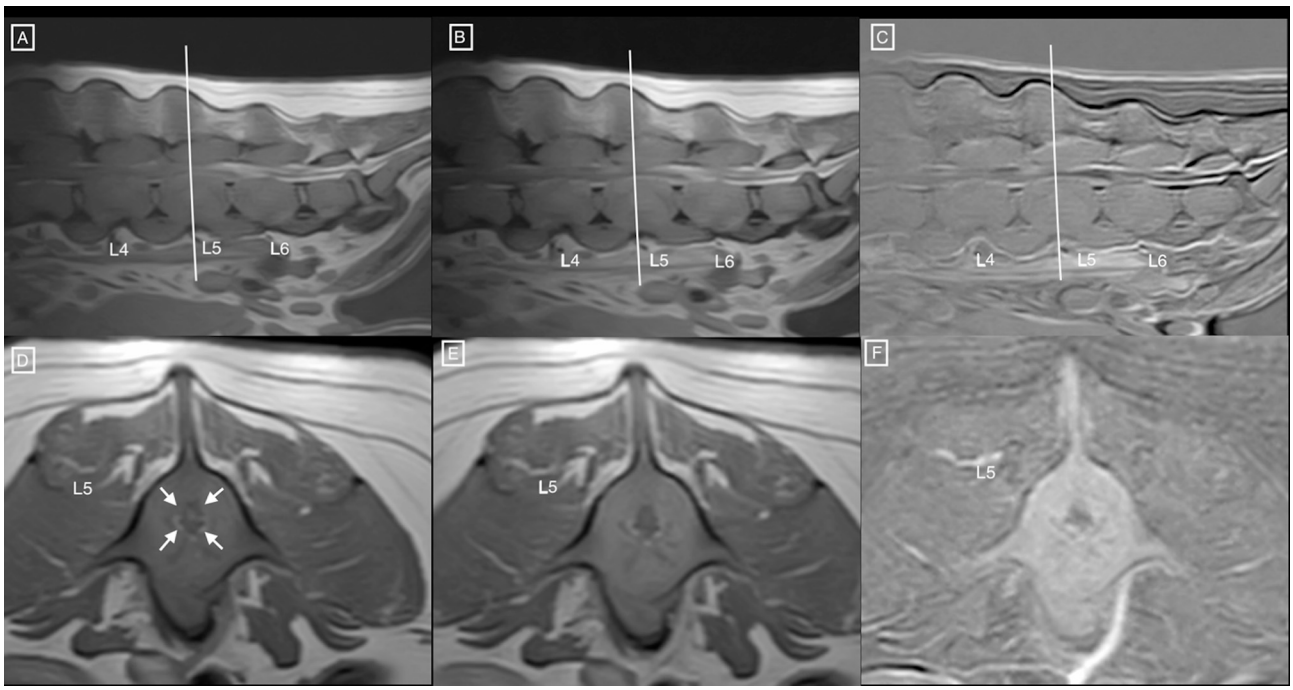

FIGURE 2 | Sagittal T1 weighted **(A)** pre and **(B)** post contrast MR images of the lumbar spine, and **(C)** corresponding subtraction image. **(D)** Transverse T1 weighted pre and **(E)** post contrast MR images at the level of mid-L5 and **(F)** corresponding subtraction image. Notice the diffuse hyperintensity, homogeneous enhancement of the vertebral structures, associated with circumferential concentric bone thickening, and secondary narrowing of the vertebral canal (white arrows) leading to circumferential compression of the spinal cord. Similar changes are noted at L4 and L6.

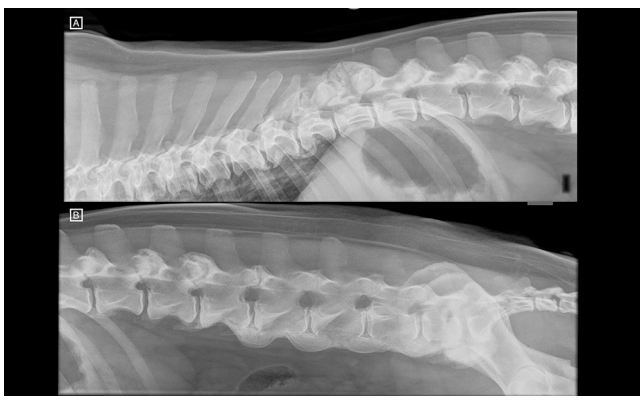

FIGURE 3 | (A) Right lateral radiographs of the thoracolumbar and **(B)** lumbosacral spine. T13 has the last pair of ribs. Notice the new bone formation around the spinous process of T11 and T12 and the articular processes at T11–12 and T12–13. The lumbar vertebrae appear decreased in radiopacity, and the dorsal cortex of the vertebral bodies is not identified. There is ventral bridging spondylosis along the ventral aspect of the lumbar spine, from L3 to LS (ventrally to the endplates but extending ventrally to the vertebral body as well) causing a flowing ossicification consistent with diffuse idiopathic skeletal hyperostosis (DISH). There is further ventral bridging spondylosis at the level of T7–T8 and T9–T11.

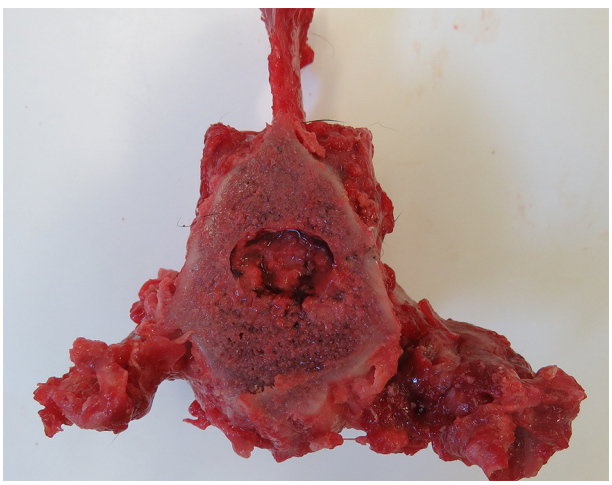

FIGURE 4 | Post-mortem specimen; transverse section at the level of mid-L5 vertebral body. Note the concentric narrowing of the vertebral canal, as well as the hyperostosis and smooth osseous proliferation of the articular surfaces.

intradural space (intradural, extramedullary). No neoplastic invasion of the hyperostotic cortical bone was noted. The necroscopic findings were consistent with stage V multicentric lymphoma with concurrent vertebral hyperostosis. The cell size, lack of auxiliary plasma cells and amyloid production was consistent with T-cell differentiation, as suspected from the flow cytometry.

DISCUSSION

T-cell lymphoma (TCL) represents around 30–40% of canine lymphomas, with prevalence varying among breeds (22). Most TCL are peripheral, with the nodal form being the most common (23). The case presented here had a typical multicentric distribution for a TCL, with the mediastinal involvement having also been associated with the T-cell phenotype (24). The flow cytometry performed was atypical for a TCL, as the cells were positive for the CD3 T-cell marker, but negative for CD5 T-cell marker and MCH II. The flow cytometry was repeated in this case to confirm the immunotype. Among peripheral TCLs, MHC II loss is frequent. Loss of CD5 is reported to aberrantly occur and may have a prognostic Implication (25).

The medullary cavity changes on MRI in the case reported here are consistent with those previously described (3), being T1 isointense, T2 iso to hyperintense and STIR hyperintense, and strongly contrast enhancing. These findings are compatible with replacement of the medullary bone fat with malignant cellular infiltrate. What is novel about this case is the presence of diffuse, bilateral and symmetrical periosteal new bone formation affecting the lumbar vertebrae in the absence of osteolysis or focal vertebral lesions. Most unusually, this hyperostosis caused circumferential narrowing of the vertebral canal and secondary spinal cord compression, which to the authors' knowledge has not previously been reported. The changes however appear analogous to a human case report of meningeal Hodgkins lymphoma, with adjacent calvarial hyperostosis without histological evidence of tumour cell invasion (18). It is not clear in this case whether the rapid onset of neurological signs relates to the bony compression, or otherwise due to the concurrent infiltration of the epidural and intradural spaces compounding the spinal cord compression.

Hypertrophic osteopathy is a well characterised syndrome in humans and animals that may develop in response to neoplastic and non-neoplastic pulmonary disease, as well as in extra-pulmonary neoplastic disease (17–21). Despite its frequency, the underlying pathogenesis is still not well understood. Recently, most attention has been given to the role of vascular endothelial growth factor (VEGF) and platelet-derived growth factor (PDGF) in this condition, with over-expression and activation inducing the stromal and vascular changes seen in HO (26). Both VEGF and PDGF overexpression has been associated with non-Hodgkin's lymphoma in humans (27, 28). It is therefore possible that the case presented here represents a novel form of paraneoplastic HO, with the changes instead affecting the axial skeleton. Imaging of the distal appendicular skeleton was not performed in this case, and the long bones were not examined during necropsy. Despite there being no clinical findings to suggest it, concurrent typical changes of HO in the distal appendicular skeleton cannot be ruled out.

In addition to the diffuse enlargement and hyperostosis affecting the vertebral bones of L4–6, both MRI and radiographic imaging of the spine demonstrated changes typical of diffuse idiopathic skeletal hyperostosis (DISH). These include calcification and ossification along the ventral aspects of three contiguous vertebral bodies, absence of extensive radiographic changes of degenerative disc disease, peri-articular osteophytes around vertebral joints and calcification and ossification of soft tissue attachments in both the axial and peripheral skeleton (19). Therefore, the mature cartilage and bone proliferation found around the articular facets of the thoracic vertebrae were considered a component of DISH rather than part of the proposed paraneoplastic syndrome. DISH is a common non-inflammatory systemic disease of the spine and abaxial skeleton of dogs, which is often incidental although can rarely be associated with clinical signs (20–22). Hyperostosis of the internal vertebral cortical bone causing vertebral canal narrowing is not reported in DISH, however it is possible that all of the bony changes reported here may represent a novel presentation of DISH that is unrelated to the lymphoma.

To the authors' knowledge, this is the first reported case of suspected paraneoplastic hyperostosis in the axial skeleton of a dog with confirmed stage V T-cell lymphoma, leading to circumferential spinal cord compression.

DATA AVAILABILITY STATEMENT

The original contributions presented in the study are included in the article/supplementary material, further inquiries can be directed to the corresponding author/s.

ETHICS STATEMENT

Ethical review and approval was not required for the animal study because this is a retrospective clinical case report. Written informed consent was obtained from the owners for the participation of their animals in this study.

AUTHOR CONTRIBUTIONS

Conception and design: MF and ES. Acquisition of data, analysis and interpretation of data, revising article for intellectual content, and final approval of the completed article: MF, AB, EV, and ES. Drafting the article: MF. All authors contributed to the article and approved the submitted version.

FUNDING

Funding for this publication was provided by Linnaeus Veterinary Limited. The funder was not involved in the study design, collection, analysis, interpretation of data, the writing of this article or the decision to submit it for publication.

ACKNOWLEDGMENTS

The authors would like to acknowledge Mr. Adrian Dodoiu (MRCVS) for referring the case, as well as Drs. Kian Guerzoni (MRCVS) and Kerstin Baiker (MRCVS, DECVP) and the staff at the University of Nottingham Pathology Service.

REFERENCES

1. Zandvliet M. Canine lymphoma: a review. *Vet Quart.* (2016) 36:76–104. doi: 10.1080/01652176.2016.1152633
2. Lamagna B, Lamagna F, Meomartino L, Paciello O, Fatone G. Polyostotic lymphoma with vertebral involvement and spinal extradural compression in a dog. *J Am Anim Hosp Assoc.* (2014) 42:71–6. doi: 10.5326/0420071
3. Allett B, Hecht S. Magnetic resonance imaging findings in the spine of six dogs diagnosed with lymphoma. *Vet Radiol Ultrasoun.* (2016) 57:154–61. doi: 10.1111/vru.12340
4. Langley-Hobbs SJ, Carmichael S, Lamb CR, Bjornson AP DAY MJ. Polyostotic lymphoma in a young dog: a case report and literature review. *J Small Anim Pract.* (1997) 38:412–6. doi: 10.1111/j.1748-5827.1997.tb03495.x
5. Vascellari M, Tasca S, Furlanello T, Carli E, Patron C, Mutinelli F, et al. Vertebral polyostotic lymphoma in a young dog. *J Vet Diagn Invest.* (2007) 19:205–8. doi: 10.1177/104063870701900214
6. Kornder J, Platt SR, Eagleson J, Kent M, Holmes SP. Imaging diagnosis — vertebral polyostotic lymphoma in a geriatric dog. *Vet Radiol Ultrasoun.* (2016) 57:E42–5. doi: 10.1111/vru.12312
7. Fournel-Fleury C, Ponce F, Felman P, Blavier A, Bonnefont C, Chabanne L, et al. Canine T-cell lymphomas: a morphological, immunological, and clinical study of 46 new cases. *Vet Pathol.* (2002) 39:92–109. doi: 10.1354/vp.39-1-92
8. McNaught KA, Morris J, Lazzerini K, Millins C, José-López R. Spinal extradural T-cell lymphoma with paraneoplastic hypereosinophilia in a dog: clinicopathological features, treatment, and outcome. *Clin Case Reports.* (2018) 6:999–1005. doi: 10.1002/ccr3.1503
9. Ortega M, Castillo-Alcala F. Hind-limb paresis in a dog with paralumbar solitary T-cell lymphoma. *Can Vet J La Revue Vétérinaire Can.* (2010) 51:480–4.
10. Blackwood L, Sullivan M, Lawson H. Radiographic abnormalities in canine multicentric lymphoma: a review of 84 cases. *J Small Anim Pract.* (1997) 38:62–9. doi: 10.1111/j.1748-5827.1997.tb02989.x
11. Bergman PJ. Paraneoplastic Hypercalcemia. *Top Companion Anim M.* (2012) 27:156–8. doi: 10.1053/j.tcam.2012.09.003
12. Presthus J, Teige J. Peripheral neuropathy associated with lymphosarcoma in a dog. *J Small Anim Pract.* (1986) 27:463–9. doi: 10.1111/j.1748-5827.1986.tb03964.x
13. Durno AS, Webb JA, Gauthier MJ, Bienzle D. Polycythemia and inappropriate erythropoietin concentrations in two dogs with renal T-cell lymphoma. *J Am Anim Hosp Assoc.* (2011) 47:122–8. doi: 10.5326/JAAHA-MS-5614
14. Zhao D, Yamaguchi R, Tateyama S, Yamazaki Y, Ogawa H. Bilateral renal lymphosarcoma in a dog. *J Vet Med Sci.* (1993) 55:657–9. doi: 10.1292/jvms.55.657
15. Giraudel JM, Pagès J-P, Guelfi J-F. Monoclonal gammopathies in the dog: a retrospective study of 18 cases (1986–1999) and literature review. *J Am Anim Hosp Assoc.* (2014) 38:135–47. doi: 10.5326/0380135
16. Evans J, Levesque D, Shelton GD. canine inflammatory myopathies: a clinicopathologic review of 200 cases. *J Vet Intern Med.* (2004) 18:679–91. doi: 10.1111/j.1939-1676.2004.tb02606.x
17. Withers SS, Johnson EG, Culp WTN, Rodriguez CO, Skorupski KA, Rebhun RB. Paraneoplastic hypertrophic osteopathy in 30 dogs. *Vet Comp Oncol.* (2015) 13:157–65. doi: 10.1111/vco.12026
18. Paiva J, King J, Chandra R. Extra-axial Hodgkin's lymphoma with bony hyperostosis mimicking meningioma. *J Clin Neurosci.* (2011) 18:725–7.
19. Morgan J, Stavenborn M. Disseminated idiopathic skeletal hyperostosis (DISH) in a dog. *Vet Radiol Ultrasoun.* (1991) 32:65–70. doi: 10.1111/j.1740-8261.1991.tb00082.x
20. Taylor-Brown F, Decker SD. Diffuse idiopathic skeletal hyperostosis causing L4 and L5 nerve root entrapment. *J Small Anim Pract.* (2017) 58:724–724. doi: 10.1111/jsap.12729
21. Oh J, Lee J, Cho K, Choi J. Diffuse idiopathic skeletal hyperostosis with prominent appendicular bone proliferation in a dog. *J Vet Med Sci.* (2015) 77:493–7. doi: 10.1292/jvms.14-0115
22. Ciepluch MF, Costa RC da, Russell D. Imaging Diagnosis — An atypical presentation of diffuse idiopathic skeletal hyperostosis (DISH) in a dog. *Vet Radiol Ultrasoun.* (2015) 56:E5–8. doi: 10.1111/vru.12124
23. Valli VE, San Myint M, Barthel A, Bienzle D, Caswell J, Colbatzky F, et al. Classification of canine malignant lymphomas according to the World Health Organization criteria. *Vet Pathol.* (2011) 48:198–211. doi: 10.1177/0300985810379428
24. Moore EL, Vernau W, Rebhun RB, Skorupski KA, Burton JH. Patient characteristics, prognostic factors and outcome of dogs with high-grade primary mediastinal lymphoma. *Vet Comp Oncol.* (2018) 16:E45–51. doi: 10.1111/vco.12331
25. Comazzi S, Riondato F. Flow Cytometry in the diagnosis of canine T-cell lymphoma. *Front Vet Sci.* (2021) 8:600963. doi: 10.3389/fvets.2021.600963
26. Atkinson S, Fox SB. Vascular endothelial growth factor (VEGF)-A and platelet-derived growth factor (PDGF) play a central role in the pathogenesis of digital clubbing. *J Pathol.* (2004) 203:721–8. doi: 10.1002/path.1565
27. Yang J, Li W, He X, Zhang G, Yue L, Chai Y, et al. overexpression is a valuable prognostic factor for non-Hodgkin's lymphoma evidence from a systemic meta-analysis. *Dis Markers.* (2015) 2015:786790. doi: 10.1155/2015/786790
28. Güler N, Yilmaz S, Ayaz S, Yilmaz M, Aki Z, Dagdaş S, et al. The platelet-derived growth factor level (PDGF) in Hodgkin's disease and non-Hodgkin's lymphoma and its relationship disease activation. *Hematology.* (2005) 10:53–7. doi: 10.1080/10245330400020405

Conflict of Interest: All authors were employed by company Linnaeus Veterinary Limited.

Publisher's Note: All claims expressed in this article are solely those of the authors and do not necessarily represent those of their affiliated organizations, or those of the publisher, the editors and the reviewers. Any product that may be evaluated in this article, or claim that may be made by its manufacturer, is not guaranteed or endorsed by the publisher.

frontiers | Frontiers in Veterinary Science

TYPE Case Report
PUBLISHED 16 August 2022
DOI 10.3389/fvets.2022.966853

OPEN ACCESS

EDITED BY
Andrea Tipold,
University of Veterinary Medicine Hannover, Germany

REVIEWED BY
Rigoberto Hernandez-Castro,
Hospital General Dr. Manuel Gea Gonzalez, Mexico
Daisuke Hasegawa,
Nippon Veterinary and Life Science University, Japan

*CORRESPONDENCE
Silke Hecht
shecht@utk.edu

SPECIALTY SECTION
This article was submitted to Veterinary Neurology and Neurosurgery, a section of the journal Frontiers in Veterinary Science

RECEIVED 11 June 2022
ACCEPTED 21 July 2022
PUBLISHED 16 August 2022

CITATION
Hecht S, Michaels JR and Simon H (2022) Case report: MRI findings with CNS blastomycosis in three domestic cats. *Front. Vet. Sci.* 9:966853. doi: 10.3389/fvets.2022.966853

Case report: MRI findings with CNS blastomycosis in three domestic cats

Silke Hecht[1]*, Jennifer R. Michaels[2] and Heather Simon[1]

[1]Department of Small Animal Clinical Sciences, University of Tennessee, Knoxville, TN, United States, [2]Department of Neurology and Neurosurgery, Angell Animal Medical Center, Boston, MA, United States

Blastomycosis is a systemic mycotic infection caused by dimorphic fungi. The disease is rare in cats, and reports on imaging findings with central nervous system (CNS) involvement are limited. Magnetic resonance imaging (MRI) was performed antemortem in three feline patients. Imaging findings that may allow prioritization of intracranial blastomycosis over other differential diagnoses included focal or multifocal intra-axial mass lesions with dural contact, lesion hypointensity on T2-weighted images and diffusion-weighted imaging/apparent diffusion coefficient map (DWI/ADC), strong and homogeneous contrast enhancement of the lesion(s), concurrent meningeal enhancement, marked perilesional edema and mass-effect, and ocular abnormalities. One cat was managed successfully and had a recurrence of CNS blastomycosis more than 4.5 years after the initial diagnosis. Repeat MRI at that point revealed both new and persistent (chronic) abnormalities.

KEYWORDS

feline, brain, central nervous system, fungal, encephalitis, magnetic resonance imaging, *Blastomyces dermatitidis*

Introduction

Blastomycosis is a systemic mycotic infection caused by dimorphic fungi. *Blastomyces dermatitidis* and *Blastomyces gilchristii* have an endemic distribution in the Mississippi, Missouri, and Ohio River valleys, the mid-Atlantic states, and some Canadian provinces with sporadic cases reported in other regions (1–3). Disease transmission occurs predominantly through inhalation, resulting in infection of the respiratory system. Other organ systems that may be involved include the regional lymph nodes, the skin, the urogenital system, the eyes, and the central nervous system (CNS) (4–9).

Unlike dogs, the disease is uncommon in domestic cats (2, 3, 10, 11). Clinical signs are variable and include dyspnea, increased respiratory sounds, visual impairment, draining skin lesions, and weight loss (2). Inflammatory ocular lesions or neuro–ophthalmic abnormalities such as Horner's syndrome, anisocoria, or an absent menace are common (7, 9, 12). The involvement of the central nervous system has been reported in 30–41% of cats and results in ataxia, paresis, circling and head tilt (6, 7, 9). Even though uncommon, CNS infection may occur in isolation without active systemic disease (13).

Computed tomography (CT) and magnetic resonance imaging (MRI) findings in dogs with intracranial blastomycosis are variable and include solitary or multifocal mass lesions that can be intra- and/or extra-axial and may extend from the nasal cavity or orbit into the cranial vault, perilesional edema, mass–effect and brain herniation, meningeal thickening and contrast enhancement, and ventricular lesions characterized by ventriculomegaly, ependymal or periventricular contrast enhancement, and evidence of increased intracranial pressure (14–19). Reports of imaging findings in cats with intracranial blastomycosis are limited. The CT findings in one domestic cat included a large peripheral intra-cranial strongly contrast-enhancing mass with associated meningeal enhancement, perilesional edema, mass-effect, and associated midline shift (13). The MRI findings reported in a tiger (*Panthera tigris*) included asymmetric hydrocephalus with marked contrast enhancement of the ventricular lining (20).

In this case series, we report the MRI findings in three domestic cats diagnosed with CNS blastomycosis. Case 2 was included in a previous publication on ocular blastomycosis (12), but diagnostic imaging findings were not included in the prior study and are presented here.

The MRI scans were performed using a 1.0 T MRI system (MAGNETOM Harmony™, Siemens Medical Solutions, Malvern, PA) (Case 1 first scan and Case 2) or a 1.5T MRI system (MAGNETOM Espree™, Siemens Medical Solutions, Malvern, PA) (Case 1 second scan and Case 3). Intravenous contrast medium was administered in all cases (Cases 1 and 2: 0.1 mmol/kg IV gadopentetate meglumine, Magnevist®, Bayer Schering Pharma; Case 3: 0.1 mmol/kg IV gadodiamide, Omniscan®, GE Healthcare). The MRI protocols varied slightly between the cases. The sequences acquired in all patients included sagittal T2-weighted spin echo (SE); transverse T2-weighted SE, T1-weighted SE, proton-density (PD)-weighted SE, T2-FLAIR, and T2*-weighted gradient recalled echo (GRE); transverse postcontrast volume interpolated GRE images with fat saturation (FatSat); and postcontrast transverse, dorsal FatSat and sagittal T1-weighted SE images. Diffusion-weighted imaging (DWI) and apparent diffusion coefficient (ADC) maps were available for review for the second scan in Case 1 and Case 3.

Case descriptions

Case 1

An 11-year-old male castrated 5.7-kg domestic shorthair cat presented to the internal medicine service after experiencing two seizures (believed to be tonic–clonic). The medical record information prior to this presentation is limited. The patient was feline immunodeficiency virus (FIV) positive and had been seen at the referring veterinarian 3 months prior with a presenting complaint of fever and ataxia. Pulmonary nodules were identified on thoracic radiographs at that time. A diagnosis of systemic blastomycosis was made based on fine-needle aspiration (FNA) of an enlarged popliteal lymph node. A *Blastomyces* urine antigen enzyme immunoassay (*Blastomyces* quantitative antigen EIA; MiraVista Diagnostics; range of quantification 0.2–14.7 ng/ml) was performed and was highly positive (above the limit of quantification). The clinical signs and lung nodules had improved with treatment (itraconazole and amphotericin B; dose regimen unknown). The reported tonic–clonic seizures occurred after the most recent antifungal treatment had been administered. At presentation, no abnormalities were noted on physical and neurologic examination.

On MRI of the brain, three separate intra-axial lesions were identified (Figure 1). A round ≈0.8-cm diameter nodule was associated with the ventral aspect of the left temporal lobe. This lesion was iso-to-slightly hypointense to gray matter, with a hyperintense rim on T2-weighted and T2-FLAIR images, was slightly hypointense on T1-weighted images, did not show evidence of susceptibility artifact on T2*-weighted images, and was strongly homogeneously contrast enhancing. There was moderate indistinct perilesional T2 hyperintensity, consistent with perilesional edema. A second well-circumscribed ≈0.4-cm diameter T2 hypointense and T1 isointense lesion was associated with the right cerebellar hemisphere and exhibited moderate ring enhancement following contrast medium administration. A third ≈0.2-cm diameter ring-enhancing lesion was noted in the cerebellar vermis, not seen on precontrast images. There was no evidence of perilesional edema associated with the cerebellar lesions. There was no evidence of meningeal enhancement or any abnormalities of the ventricular system, skull, nasal cavity, paranasal sinuses, tympanic bullae, orbits, ocular structures, and soft tissues of the head and cranial neck including regional lymph nodes.

A cisternal cerebrospinal fluid (CSF) tap was obtained and yielded a diagnosis of probably iatrogenic hemorrhage without other cytologic abnormalities. A *Blastomyces* urine antigen EIA was moderately positive (3.04 ng/ml).

Corticosteroid treatment was initiated (prednisolone 5-mg/head PO q 24 h × 3 days, 2.5-mg/head PO q 24 h × 3 days, and 1.25-mg/head PO q 24 h × 3 days) for treatment of perilesional edema and to help manage the inflammatory effects caused by fungal die-off. The patient was also started on phenobarbital (2.5-mg/kg PO BID of 20-mg/ml suspension), levetiracetam (20-mg/kg PO of 100-mg/ml suspension q 8 h), and fluconazole (50-mg/head PO q 12 h). Amphotericin B was discontinued. Phenobarbital was discontinued the following day due to the patient being very lethargic.

The cat showed improvement over the next months and was considered clinically normal aside from an occasional cough and unrelated chronic gingivitis 2 months after the MRI examination (5 months after initial diagnosis). The previously seen pulmonary abnormalities had resolved.

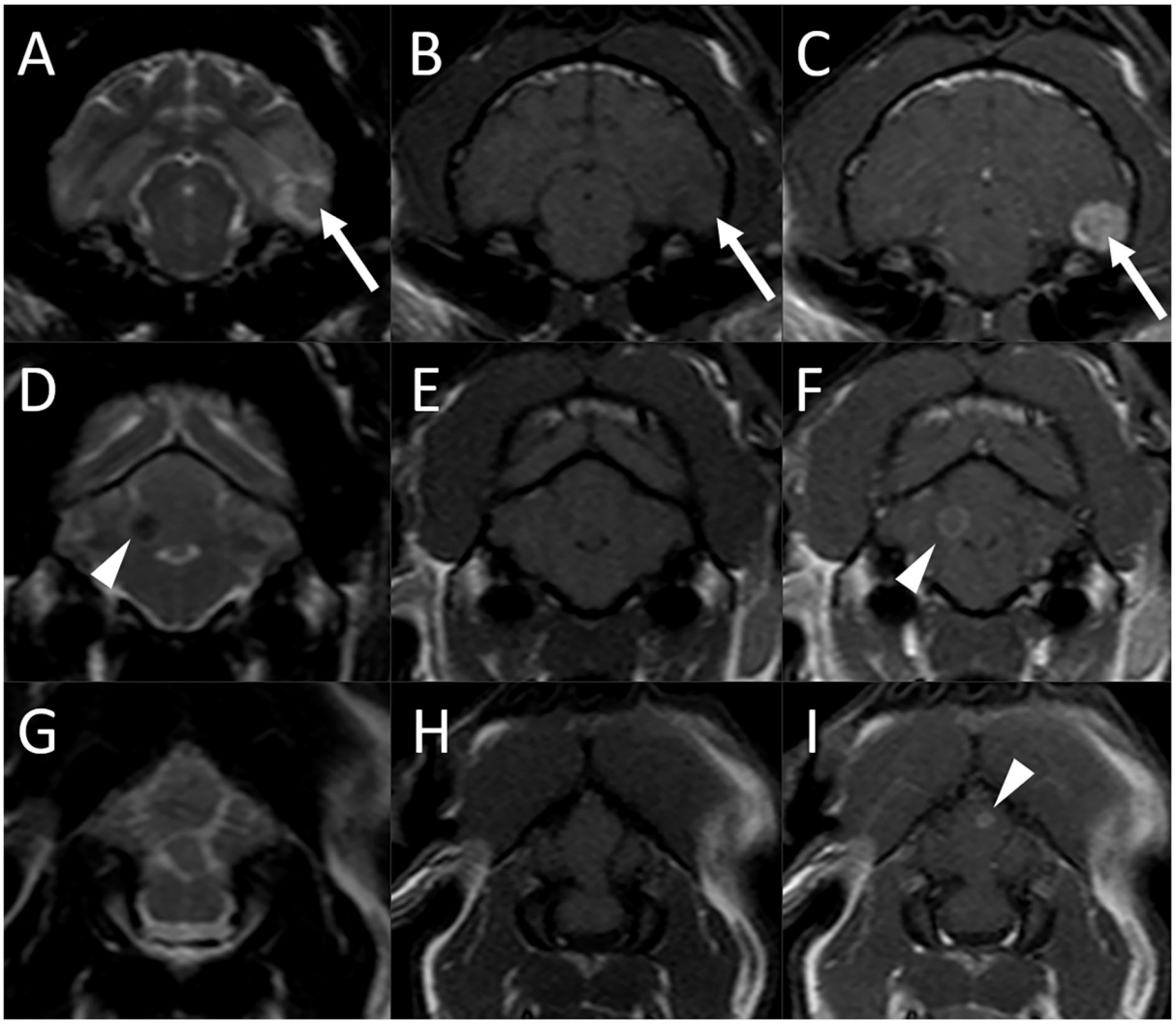

FIGURE 1
Brain MRI in an 11-year-old male castrated domestic shorthair cat (Case 1) 3 months after the diagnosis of systemic blastomycosis and after experiencing two seizures after the latest antifungal treatment. Transverse T2-weighted **(A)**, **(D)**, and **(G)**, T1-weighted **(B)**, **(E)**, and **(H)**, and postcontrast T1-weighted **(C)**, **(F)**, and **(I)** images. **(A)–(C)** A round ≈0.8-cm diameter nodule is associated with the ventral aspect of the left temporal lobe (arrows) which is iso-to slightly hypointense to gray matter, with a hyperintense rim on T2-weighted image **(A)**, slightly hypointense on T1-weighted image **(B)**, and has strong and homogeneous contrast enhancement **(C)**. There is moderate indistinct perilesional T2 hyperintensity, consistent with perilesional edema. **(D)–(E)** A second well-circumscribed ≈0.4-cm diameter T2 hypointense **(A)** and T1 isointense **(B)** lesion is associated with the right cerebellar hemisphere and exhibits moderate ring enhancement **(C)** following contrast medium administration (arrowheads). **(G)–(I)** A third ≈0.2-cm diameter ring-enhancing lesion is noted in the cerebellar vermis [**(I)**, arrowhead], not seen on the precontrast images.

There was no recurrence of seizures, and no other neurologic abnormalities were reported. A *Blastomyces* urine antigen EIA was greatly improved but still mildly positive (0.73 ng/ml).

The patient remained neurologically normal. Levetiracetam was gradually tapered from 5 to 8 months after the initial diagnosis without recurrence of seizure activity. A *Blastomyces* urine antigen EIA was still mildly positive after 7 and 9 months. Fluconazole was discontinued 15 months after the initial diagnosis (12 months after the first MRI examination) based on 2 consecutive negative *Blastomyces* urine antigen EIA tests.

The cat represented 3 years later (4 years and 7 months after initial diagnosis) to the emergency service for a 24-h history of circling to the right and behavior changes. On neurologic examination, the patient was circling to the right and had a bilaterally absent menace response. Possible hyperesthesia of the head was also noted. Neurolocalization was to the

10.3389/fvets.2022.966853

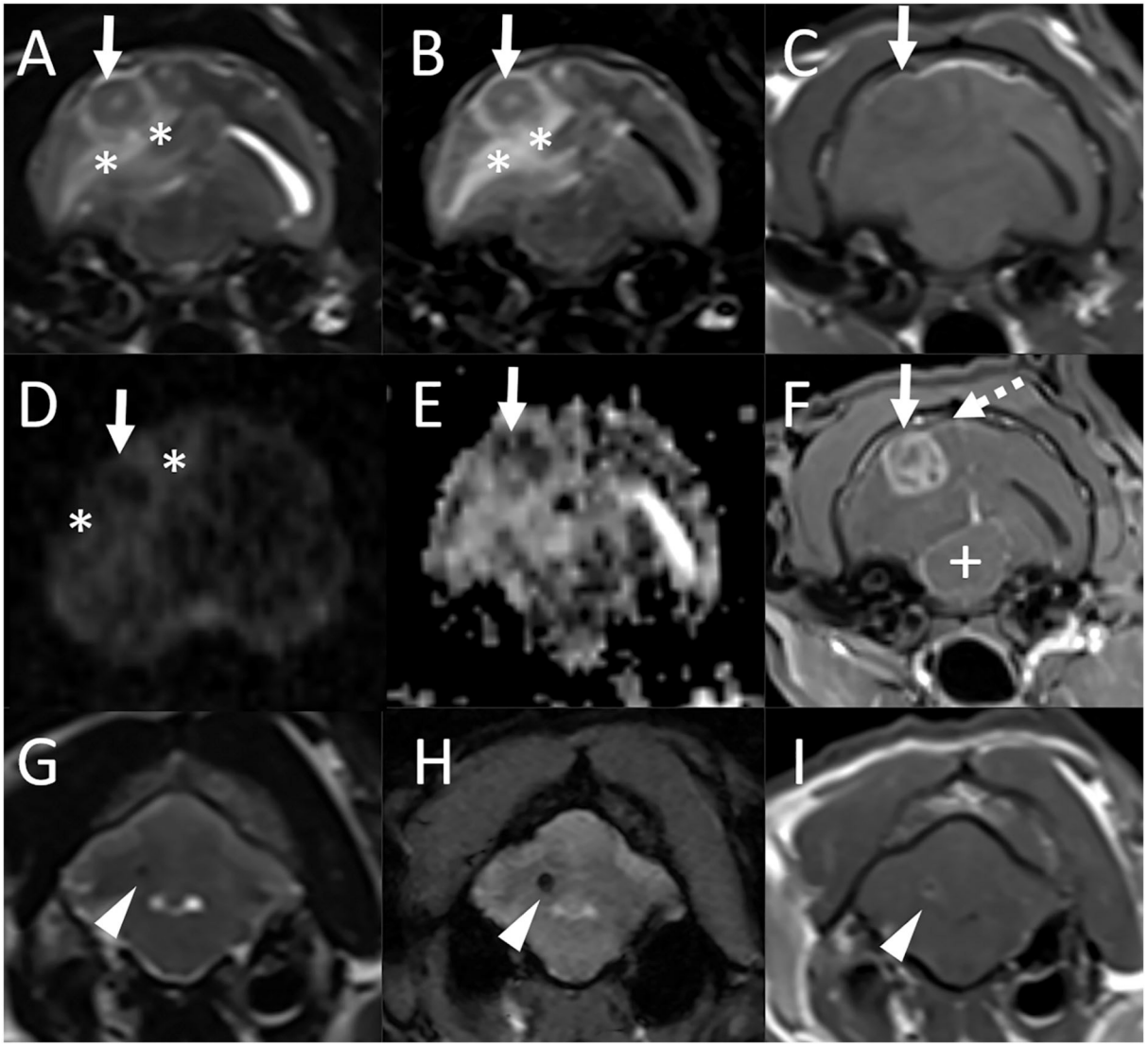

FIGURE 2
Repeat MRI examination of the cat in Figure 1 (Case 1), 4 years and 4 months after the initial MRI study. Transverse T2-weighted **(A)**, T2-FLAIR **(B)**, T1-weighted **(C)**, diffusion-weighted imaging [DWI, **(D)**] and corresponding apparent diffusion coefficient (ADC) map **(E)**, and postcontrast T1-weighted GRE with fat suppression **(F)** images at the level of the tympanic bullae and temporal lobes, and transverse T2-weighted **(G)**, T2*-weighted GRE **(H)**, and postcontrast T1-weighted **(I)** images at the level of the cerebellum. **(A)–(F)** There is a new finding of an ≈1.2 × 1.4 cm ovoid mass in the right temporal lobe (solid arrows) which is predominantly T2, T2-FLAIR, and T1 isointense to gray matter with a small centrally located T2 hyperintense and T1 hypointense focus which does not suppress on T2-FLAIR [**(A)–(C)**]. The lesion is hypointense both on DWI and ADC maps [**(D)**, **(E)**]. There is marked perilesional T2 and FLAIR hyperintensity following the white matter tracts of the right cerebral hemisphere (*) with a moderate to marked mass effect characterized by compression of the right lateral ventricle, leftward midline shift, and compression of the mesencephalon (+). Following contrast medium administration, the mass displays marked heterogeneous contrast enhancement **(F)**. Mild focal pachymeningeal contrast enhancement is identified adjacent to the lesion (dashed arrow). An incidental small amount of fluid is noted within the bilateral tympanic bulla. **(G)–(I)** An ≈0.2-cm diameter well-defined T2 hypointense ovoid nodule is observed in the region of the previously seen cerebellar hemispheric lesion and is decreased in size from previous [**(G)**, arrowhead]. This lesion is associated with a susceptibility artifact on T2*-weighted images **(H)** and has mild rim contrast enhancement **(I)**.

right forebrain. Thoracic radiographs did not reveal any significant abnormalities.

Magnetic resonance imaging was repeated. There was a new finding of an ≈1.2 × 1.4 cm ovoid mass in the right temporal lobe (Figure 2) which was predominantly T2 and T1 isointense to gray matter with a small centrally located T2 hyperintense and T1 hypointense focus which did not suppress on T2-FLAIR. The lesion was hypointense on both DWI and ADC maps. There was marked perilesional T2 and FLAIR hyperintensity following the white matter tracts

of the right cerebral hemisphere with a moderate to marked mass effect characterized by compression of the right lateral ventricle, leftward midline shift, and caudal transtentorial and foramen magnum herniations. Following contrast medium administration, the mass displayed marked heterogeneous contrast enhancement. Mild focal pachymeningeal contrast enhancement was identified adjacent to the lesion. An ≈0.2-cm diameter well-defined T1, T2, and T2-FLAIR hypointense ovoid nodule was observed in the region of the previously seen cerebellar hemispheric lesion and was decreased in size. This lesion was associated with a susceptibility artifact on T2*-weighted images and had mild rim contrast enhancement. The lesion within the cerebellar vermis was no longer visible. An incidental small amount of fluid was noted within the bilateral tympanic bulla. The remaining structures of the head and cranial neck remained normal.

The patient received a tapering dosing regimen of prednisolone (5-mg/head PO q 24 h × 3 days, 2.5-mg/head PO q 24 h × 3 days, and 1.25-mg/head PO q 24 h × 3 days). Fluconazole treatment was resumed empirically (50-mg/head PO q 12 h) while awaiting urine antigen testing results. A repeat *Blastomyces* urine EIA test was positive (4.24 ng/ml), and fluconazole treatment was continued. The patient improved, and the client reported the cat as being back to normal 5 weeks after the second MRI examination. On neurologic examination at that time, menace response was noted in both eyes. The pupillary light responses were decreased. Additional findings during this visit included weight loss, hypoalbuminemia, anemia, a soft heart murmur, and an irregular heartbeat. The patient represented for a work-up of these new problems to the internal medicine service 2 weeks later and at that point was diagnosed with large cell gastrointestinal (GI) lymphoma. Chemotherapy was started and initially well-tolerated. The owners did not report a recurrence of neurologic abnormalities, and the physical examinations performed by the oncology service over the next weeks did not reveal any obvious neurologic abnormalities. A full neurologic exam was not performed. Urine blastomycosis antigen tests were also not repeated during that time due to the inability to acquire sufficient urine samples. The patient started declining ≈2 months after the diagnosis of GI lymphoma and was euthanized 3 months later. An autopsy was not performed. The overall survival time after the initial diagnosis of systemic blastomycosis was ≈5 years.

Case 2

A 3-year-old 4.7-kg female spayed domestic shorthair cat presented to the emergency service after a mass was noted associated with the conjunctiva of her right eye. Two weeks prior she had been seen by the ophthalmology service for uveitis and secondary glaucoma of the right eye (Oculus Dexter; OD). Physical examination findings and a complete blood count (CBC) performed at that point were normal. The infectious disease testing for feline leukemia virus (FeLV), FIV, and toxoplasmosis were negative. The patient was managed with topical medications. At the current presentation, the cat had worsened uveitis OD and blindness in both eyes (Oculus Uterque; OU) with a fixed dilated pupil of the left eye (Oculus Sinister; OS). Thoracic radiographs revealed a single ≈2.5-cm diameter ill-defined soft tissue opacity mass associated with the left caudal lung lobe. A fine-needle aspiration of the conjunctival mass was performed and yielded a diagnosis of blastomycosis. Due to concern for intracranial involvement, MRI of the brain was performed (Figure 3).

There were marked abnormalities of the right eye including severe thickening and contrast enhancement of the periocular tissues, thickening and enhancement of the wall of the globe, retinal detachment, diffuse heterogeneous alteration in signal intensity of the ocular structures with abnormal contrast enhancement, and multifocal susceptibility artifacts, mostly in the posterior chamber, consistent with hemorrhage. There was diffuse thickening of the right optic nerve (up to 5 mm) and marked enlargement of the optic chiasm (1.3 cm). Two additional intracranial lesions were noted. A round 0.5 cm diameter intra-axial nodule was associated with the caudal aspect of the right frontal lobe. An irregularly shaped ≈0.8 × 0.7 cm nodule was associated with the left parietal lobe. This lesion was in contact with the falx and meningeal surface of the brain but formed an acute angle with both. Both lesions were iso- to mildly hypointense to gray matter on both T1- and T2-weighted images. Bordering the lesions and extending extensively throughout the cerebral white matter bilaterally, there were parenchymal hyperintensities consistent with vasogenic edema. There was evidence of increased intracranial pressure characterized by attenuation of the CSF signal in the cerebral sulci, compression of the lateral ventricles, a mild midline shift, and caudal transtentorial and foramen magnum herniations. Following contrast medium administration, the right globe, abnormal tissues within the right orbit, right optic nerve, optic chiasm, and intracranial nodules showed strong and homogeneous contrast enhancement. There was no evidence of abnormal meningeal contrast enhancement and no evidence of a dural tail sign adjacent to the brain lesions. Moderate enlargement of the right and mild enlargement of the left medial retropharyngeal lymph nodes were noted.

The patient was euthanized, and an autopsy was performed, confirming the clinical diagnosis of blastomycosis. There was marked pyogranulomatous panophthalmitis of the right eye with involvement of the optic nerve and the optic chiasm. Both cerebral nodules were intra-axial in location, and a diagnosis of a marked pyogranulomatous meningoencephalitis with intralesional yeasts was made. Additional lesions were found in the lungs (as suspected based on radiographs), the thoracic lymph nodes, and the fourth and fifth digits of the right front limb.

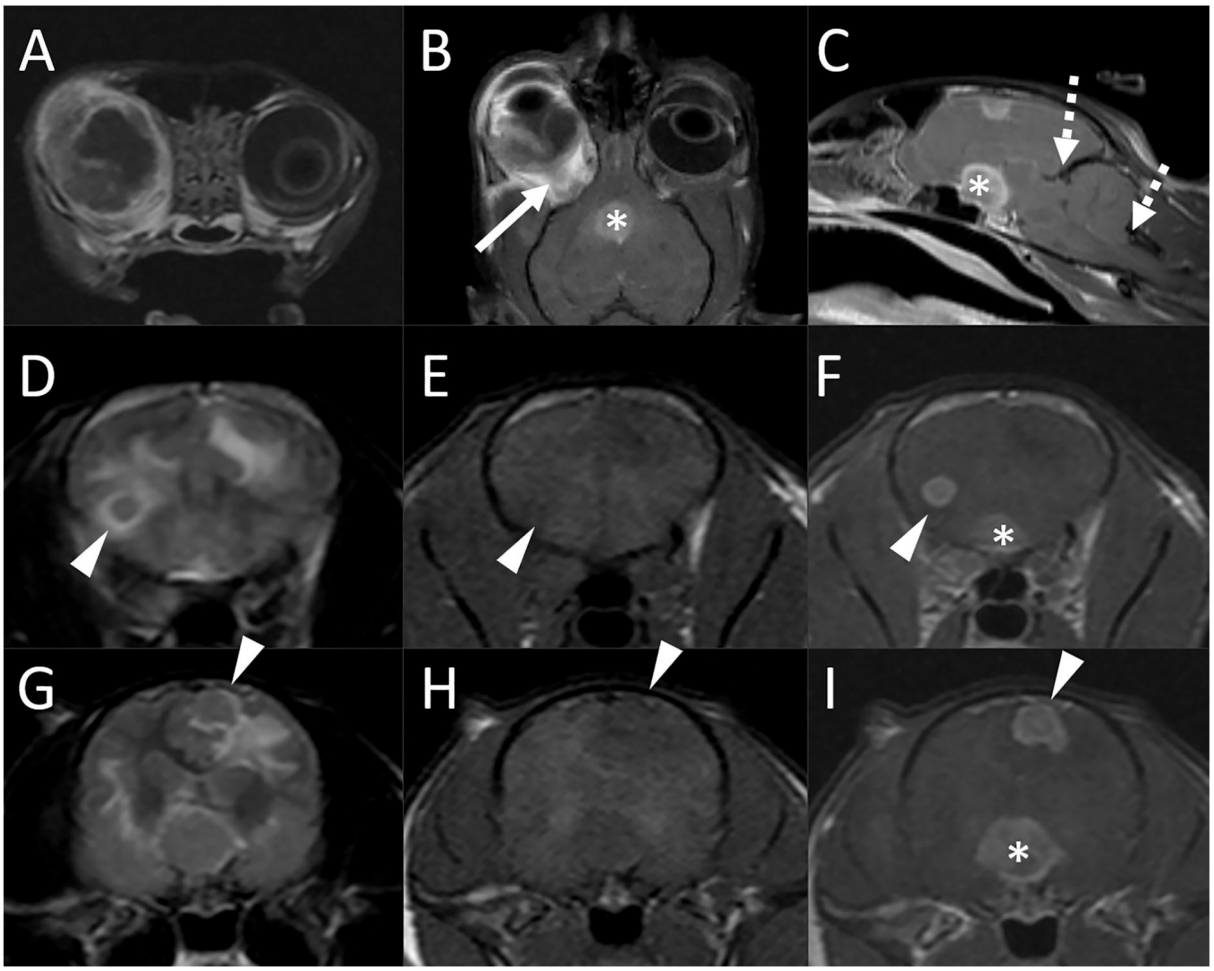

FIGURE 3
Brain MRI in a 3-year-old domestic shorthair cat (Case 2) following a diagnosis of ocular blastomycosis and with concern for intracranial involvement. Transverse **(A)**, dorsal **(B)**, and midline sagittal **(C)** postcontrast T1-weighted images; transverse T2-weighted images [**(D)** and **(G)**], transverse T1-weighted images before [**(E)** and **(H)**] and after [**(F)** and **(I)**] contrast medium administration. There is severe thickening, diffuse heterogeneous alteration in signal intensity, abnormal contrast enhancement of the periocular and tissues, thickening and enhancement of the wall of the globe, and retinal detachment [**(A)** and **(B)**]. There is diffuse thickening of the right optic nerve [**(B)**, arrow] and marked enlargement of the optic chiasm [* in **(B)**, **(C)**, **(F)**, and **(I)**]. A round 0.5-cm diameter intra-axial nodule is associated with the caudal aspect of the right frontal lobe [arrowheads, **(D)–(F)**] and an irregularly shaped ≈0.8 cm × 0.7 cm nodule is associated with the left parietal lobe [**(G)–(I)**, arrowheads]. Both lesions are iso- to mildly hypointense to gray matter on both T2 and T1-weighted images [**(D)**, **(E)**, **(G)**, **(H)**]. Bordering the lesions and extending extensively throughout the cerebral white matter bilaterally, there are parenchymal hyperintensities consistent with vasogenic edema. There is evidence of increased intracranial pressure characterized by attenuation of the CSF signal in the cerebral sulci, compression of the lateral ventricles, a mild midline shift, and caudal transtentorial and foramen magnum herniations [**(C)**, dashed arrows].

Case 3

An estimated 7-year-old 6.1-kg male castrated domestic shorthair cat presented to a local emergency clinic for head pressing. Complete blood count and blood chemistry panel were normal, and FeLV/FIV testing was negative. The patient was referred for progressive neurologic abnormalities. Upon presentation, the cat was bright, alert, and responsive. One hind limb had been amputated previously for unknown reasons. Neurological deficits included a lack of menace response of the left eye (OS) and intermittent loss of the right eye (OD), bilateral (OU) loss of direct and indirect pupillary light reflexes, and circling to the right. Neurolocalization was to the right forebrain and bilateral optic nerves/optic chiasm. A mild diffuse bronchointerstitial pattern was identified on thoracic radiographs.

On MRI examination of the brain, there was an ≈1-cm diameter mass associated with the periphery of the right temporal lobe, in contact with the dural surface (Figure 4). The lesion was iso-to-mildly hypointense to gray matter on both T1- and T2-weighted images, was not associated with susceptibility artifact on T2*-weighted images, and was

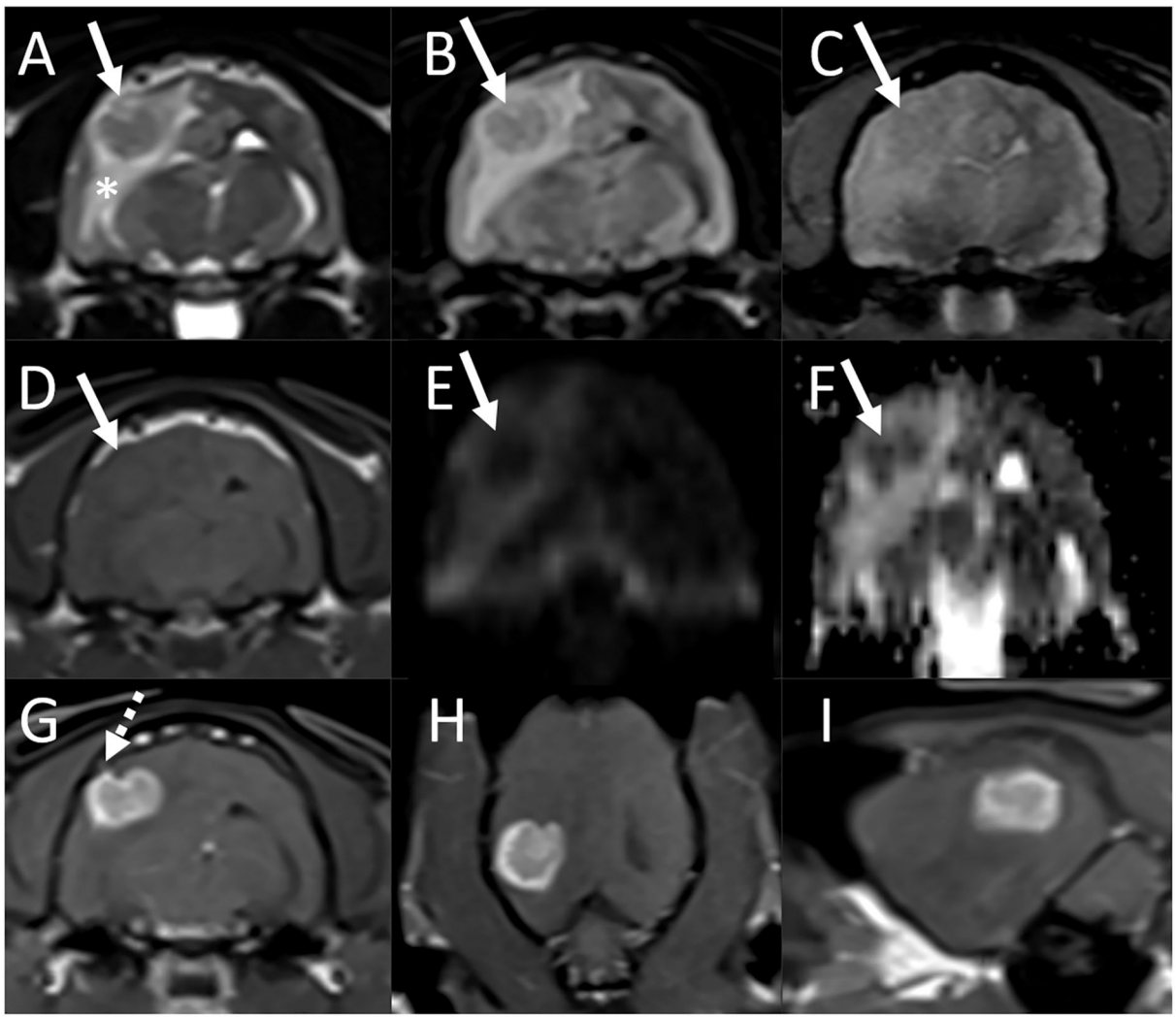

FIGURE 4
Brain MRI in an estimated 7-year-old cat (Case 3) with presenting complaints of head pressing and progressive neurologic deficits. Transverse T2-weighted **(A)**, T2-FLAIR **(B)**, T2*-weighted GRE **(C)**, T1-weighted **(D)**, diffusion-weighted imaging [DWI, **(E)**] and corresponding ADC map **(F)**, and postcontrast T1-weighted images in the transverse **(G)**, dorsal **(H)**, and sagittal **(I)** planes. **(A)–(F)** There is an ≈1-cm diameter mass associated with the periphery of the right temporal lobe, in contact with the dural surface (arrows). The lesion is T2, T2-FLAIR, and T1 iso- to mildly hypointense to gray matter [**(A)**, **(B)**, **(D)**], is not associated with susceptibility artifact on T2*-weighted image **(C)**, and is hypointense both on DWI and ADC maps [**(E)** and **(F)**]. There is marked perilesional T2 hyperintensity extending along the white matter tracts of the right cerebral hemisphere, consistent with vasogenic edema, resulting in compression of the right lateral ventricle, and a midline shift toward the left. A small volume of fluid is present in the nasopharynx, considered incidental. **(G)–(I)** Following contrast medium administration, the mass shows strong and fairly homogeneous contrast enhancement. The majority of the lesion is centered on brain parenchyma, with acute angles between the ventral, rostral, and caudal aspects of the mass and the calvarium. At the dorsal aspect of the mass, there is mild focal thickening and contrast enhancement of the pachymeninges [**(G)**, dashed arrow].

hypointense on both DWI and ADC maps. There was marked perilesional T2 hyperintensity extending along the white matter tracts of the right cerebral hemisphere, consistent with vasogenic edema, resulting in compression of the right lateral ventricle, a midline shift toward the left, caudal transtentorial, and mild foramen magnum herniations. Following contrast medium administration, the mass showed strong and fairly homogeneous contrast enhancement. The majority of the lesion was centered on brain parenchyma, with acute angles between the ventral, rostral, and caudal aspects of the mass and the calvarium. At the dorsal aspect of the mass and best seen on thin section postcontrast T1-weighted FatSat GRE images, there was mild focal thickening and contrast enhancement of the pachymeninges. A small volume of fluid was present in the nasopharynx, considered incidental. There were no abnormalities of the skull, nasal cavity, paranasal sinuses,

tympanic bullae, orbits, ocular structures, and soft tissues of the head and cranial neck including lymph nodes.

A CSF tap was not performed. The patient was administered mannitol (0.5 g/kg IV) and dexamethasone sodium phosphate (0.1 mg/kg IV). Blood and urine samples were submitted for cryptococcosis and blastomycosis testing, respectively. The patient was discharged the following day on prednisolone (2-mg/head PO q 24 h) and levetiracetam (20-mg/kg PO of 100 mg/ml suspension q 8 h).

A cryptococcus antigen latex test was negative. A *Blastomyces* urine antigen EIA was positive (6.11 ng/ml). The patient was prescribed fluconazole (50-mg/head PO q 24 h). Two days after the start of treatment, the owner reported sudden deterioration of the patient followed by death. An autopsy was not performed.

Discussion

Inflammatory and neoplastic etiologies account for the majority of brain diseases in cats (21, 22), and an imaging diagnosis may not always be straightforward. This study aims at describing imaging features in cats with blastomycosis, an uncommon cause of meningoencephalitis in this species.

Even though the imaging findings in the three cats included in this case series differed, some commonalities were observed. All animals had focal or multifocal mass lesions associated with the forebrain. Contact with the brain surface was common, resulting in difficulty classifying a lesion as intra-axial vs. extra-axial in some instances. Ultimately, intra-axial lesion location was considered most likely in all cats based on lesion centering on brain parenchyma, infiltrative rather than expansile growth of the mass, the presence of additional intra-axial lesions in the majority of cases including cerebellar lesions in one cat, and the acute rather than the obtuse angle formed between the periphery mass and the skull (comparable to the radiographic differentiation of a pulmonary vs. an extrapleural mass based on contact with the thoracic wall on radiographs). An autopsy was only performed on one cat, confirming the intra-axial location of the lesion. Difficulty in distinguishing intra- from extra-axial lesion location was mentioned in a previous study describing CT findings in a cat with an intracranial blastomycosis granuloma (13) and has also been described in dogs and cats with CNS coccidiomycosis (23). Dural contact has been described as an MRI finding that may help increase the index of suspicion for intracranial granuloma over glioma in dogs (19).

In the acute stage, brain lesions were iso- to mildly hypointense to gray matter on T2-weighted images, variable but generally isointense on T1-weighted images, and strongly contrast-enhancing. The T2 hypointensity has previously been reported with fungal granulomas (17, 19, 23, 24). This may be an important consideration when prioritizing differential diagnoses considering the myriad possibilities for single or multifocal intra-axial mass(es). Gliomas are intra-axial tumors that are rare in cats and are reported to be T2 hyperintense and characterized by rim rather than homogeneous contrast enhancement (25). Intralesional T2 hypointensity may be seen with meningiomas if mineralization or hemorrhage is present (25, 26). These tumors are also commonly strongly and homogeneously contrast-enhancing. However, the T2 hypointensities are typically foci within an overall iso- to hyperintense mass, unlike the Blastomyces granulomas described here which were more uniformly T2 hypointense. In addition, meningiomas are extra-axial and characterized by broad-based or plaque-like contact with the skull. Intracranial melanoma metastases or hemorrhagic lesions (benign or malignant) may be T2 hypointense (27). However, those types of lesions are rare in cats and will typically exhibit marked susceptibility artifacts on T2*-weighted GRE images which were not seen in the cases described here. CNS lymphoma has a variable imaging appearance in cats, with intra- and/or extra-axial masses of varying intensity and contrast enhancement patterns. While T2 hyperintensity is a more common feature and T2 hypointensity has not been reported, T2 isointensity is possible (28). Other substances and lesions that may appear hypointense on T2-weighted images are gadolinium-based contrast agents, mucous- or protein-containing lesions, highly cellular lesions, lesions containing mineral substances such as calcium, copper, or iron, turbulent and rapid blood (or CSF) flow, and air-containing spaces or lesions (29). The T2 hypointensity seen with fungal granulomas can be explained by their high cellularity and density limiting the mobility of intralesional hydrogen protons. Other contributing factors (such as the presence of protein or mineralization) are possible but are not supported by the lesion appearance on other sequences.

Other common imaging features of acute granulomas in this case series were strong contrast enhancement of the main lesion, meningeal enhancement, perilesional edema, and mass effect. This is similar to the findings of previous reports (13, 14, 16–19). Vasogenic edema in Case 1 at first presentation was attributed to a flare-up of a granuloma following antifungal treatment. Chronic granulomas otherwise did not have evidence of perilesional edema, similar to previous reports (17), and were ring-enhancing. The extension of ocular blastomycosis into the cranial vault to affect the optic chiasm in one cat was similar to a case of intracranial extension of a retrobulbar fungal granuloma reported in a dog (14). The appearance of the fungal granulomas in two cases where DWI was performed was interesting. A restricted diffusion (characterized by hyperintensity on DWI and hypointensity on the ADC map) has been reported in some intracranial fungal infections in people (30). The hypointense appearance of the granulomas on both DWI and ADC in our cases is most likely attributable to "T2 blackout effects," where the true diffusion signal is reduced on DWI images by the presence of a very low signal in a lesion. This has been reported in acute and early subacute intracerebral hematomas

in people (31). Interestingly, neither of our cases exhibiting this imaging feature had evidence of susceptibility artifact in the lesion indicative of hemorrhage. It appears that the T2 hypointense nature of the granuloma was accentuated by surrounding vasogenic edema which was most evident on DWI/ADC.

Although there are a variety of imaging descriptions of intracranial blastomycosis in dogs, it is worth mentioning one particular manifestation centered on the ventricular system and resulting in periventricular edema, periventricular and meningeal contrast enhancement, and ventriculomegaly (15). Although this appearance has not been described in domestic cats with CNS blastomycosis, similar MR abnormalities have been reported in a tiger (20). It warrants particular discussion in regards to feline patients, as this imaging manifestation would be similar to and possibly indistinguishable from feline infectious peritonitis (FIP) (32). The presence and type of concurrent systemic disease, FNA and cytology of lesions, CSF abnormalities, and fungal antigen testing would all be useful in differentiating between systemic fungal disease and FIP in a given feline patient.

The presence or absence of additional lesions outside the CNS is an important consideration when ranking differential diagnoses for intracranial lesions and prognostication. Most animals with CNS blastomycosis have systemic disease. Two of the cats in this study had evidence of single or multiple pulmonary masses. It is unclear if the mild bronchointerstitial pattern seen in the third patient was related or unrelated to fungal disease. Even though the prognosis for dogs and cats with blastomycosis is generally good, the two prognostic factors for survival are the severity of lung disease and CNS involvement (2). The long-term treatment and survival of one immunocompromised cat with both pulmonary and CNS blastomycosis is somewhat surprising but supports the suggestion that prolonged duration of treatment is indicated in patients with fungal encephalitis (33).

There were several limitations to this study. The case number is small, which is likely due to the relative rarity of blastomycosis in cats. In addition, it is likely that many animals with systemic disease present with other clinical signs and may not undergo brain MRI even if neurologic abnormalities are present. The diagnosis of blastomycosis in two cats was based on cytology, and additional testing (mycological isolation or polymerase chain reaction) was not performed. This is representative of clinical veterinary practice, where organism identification through cytologic or histopathologic evaluation is preferred over serology due to the associated cost for the client (2). The identification of medium-sized, spherical, 8–20 μm in diameter, deeply basophilic organisms with a refractile double wall and occasional broad-based budding suggests blastomycosis (2, 34). Fungal serology is typically recommended when direct visualization of the organism is not possible (24). Most cases of blastomycosis in humans, dogs, and cats are thought to be caused by *B. dermatitidis*; however, in 2013, *B. gilchristii*, which is genetically distinct, was reported to also be a possible cause (35, 36). Because of morphological and clinical similarities between *B. dermatitidis* and *B. gilchristii*, there is no clinical need for genetic sequencing to differentiate the two species (12). In people, atypical blastomycosis is occasionally caused by *Blastomyces helicus* in western parts of North America and *Blastomyces percursus* in Africa (36). Neither of these organisms has been reported in small animals in the Southeastern United States to date. For these reasons, and considering the geographic distribution of various species of Blastomyces, *B. dermatitidis* was considered the most likely infectious agent seen in our case population. The diagnosis in one case was based on a positive result for a *Blastomyces* urine antigen EIA. This assay is only labeled for use in dogs, and it is known to cross-react with *Histoplasma capsulatum* antigen as well as possibly other infectious agents (*Paracoccidioidomyces*, *Penicillium*, less frequently in *Coccidiooidomyces*, rarely *Aspergillus*, and possibly *Sporotrichium*) (37, 38). However, most of these are not endemic in Tennessee, many have not been reported in cats, and CNS involvement in cats has to our knowledge not been reported in any of them (39, 40). Intracranial blastomycosis, therefore, remains the most likely diagnosis in our patient. Finally, the MRI protocols were not standardized, and DWI/ADC images were only available for review in two scans. Despite these limitations, this study provides important information on MRI findings in cats with CNS blastomycosis.

In summary, the imaging features that may suggest blastomycosis over other intracranial diseases in cats include focal or multifocal intra-axial mass lesions with dural contact, hypointensity on T2-weighted images and DWI/ADC, strong and homogeneous contrast enhancement of the lesion(s), concurrent meningeal enhancement, marked perilesional edema and mass-effect, and ocular abnormalities. Future studies with larger case numbers are warranted to confirm these findings and identify possible other imaging manifestations of CNS blastomycosis in feline patients.

Data availability statement

The original contributions presented in the study are included in the article/supplementary material, further inquiries can be directed to the corresponding author/s.

Ethics statement

Ethical review and approval was not required for the animal study because it is not required for retrospective case reports. Written informed consent was obtained from owners for participation of their animals.

Author contributions

SH identified the cases to be included in the study, performed the image evaluation, and drafted the initial manuscript. JM and HS assisted with the medical record review of the patients and reviewed and revised the manuscript. All authors contributed to the manuscript's final revision and approved the submitted manuscript.

Acknowledgments

The authors would like to acknowledge the Diagnostic Imaging, Neurology, and Ophthalmology services of the University of Tennessee College of Veterinary Medicine.

Conflict of interest

The authors declare that the research was conducted in the absence of any commercial or financial relationships that could be construed as a potential conflict of interest.

Publisher's note

References

1. Gnat S, Lagowski D, Nowakiewicz A, Dylag M, A. global view on fungal infections in humans and animals: infections caused by dimorphic fungi and dermatophytoses. *J Appl Microbiol.* (2021) 131:2688–704. doi: 10.1111/jam.15084

2. Legendre AM. Blastomycosis. In: Greene CE, editor. *Infectious Diseases of the Dog and Cat*. 4th edn. St. Louis: Elsevier Saunders (2012). p. 606–13.

3. Schwartz IS. Blastomycosis in mammals. In: Seyedmousavi S, de Hoog G, Guillot J, Verweij P, editors. *Emerging and Epizootic Fungal Infections in Animals*. Cham: Springer International Publishing AG, part of Springer Nature (2018). p. 159–76. doi: 10.1007/978-3-319-72093-7_8

4. Arceneaux KA, Taboada J, Hosgood G. Blastomycosis in dogs: 115 cases (1980–1995). *J Am Vet Med Assoc*. 1998;213:658.

5. Breider MA, Walker TL, Legendre AM, Vanee RT. Blastomycosis in cats – 5 cases (1979–1986). *J Am Vet Med Assoc.* (1988) 193:570–2.

6. Davies C, Troy GC.Deep mycotic infections in cats. *J Am Anim Hosp Assoc.* (1996) 32:380–91. doi: 10.5326/15473317-32-5-380

7. Gilor C, Graves TK, Barger AM, O'Dell-Anderson K. Clinical aspects of natural infection with Blastomyces dermatitidis in cats: 8 cases (1991–2005). *JAVMA-J Am Vet Med A.* (2006) 229:96–9. doi: 10.2460/javma.229.1.96

8. Legendre AM, Walker M, Buyukmihci N, Stevens R. Canine Blastomycosis – a review of 47 clinical cases. *J Am Vet Med Assoc.* (1981) 178:1163–8.

9. Miller PE, Miller LM, Schoster JV. Feline Blastomycosis – a report of 3 cases and literature-review (1961 to 1988). *J Am Anim Hosp Assoc.* (1990) 26:417–24.

10. Davies JL, Epp T, Burgess HJ. Prevalence and geographic distribution of canine and feline blastomycosis in the Canadian prairies. *Can Vet J-Revue Veterinaire Canadienne.* (2013) 54:753–60.

11. Lloret A, Hartmann K, Pennisi MG, Ferrer L, Addie D, Belak S, et al. Rare systemic mycoses in cats: blastomycosis, histoplasmosis and coccidioidomycosis: ABCD guidelines on prevention and management. *J Feline Med Surg.* (2013) 15:624–7. doi: 10.1177/1098612X13489226

12. Morris JM, Sigmund AB, Ward DA, Hendrix DVH. Ocular findings in cats with blastomycosis: 19 cases (1978-2019). *JAVMA-J Am Vet Med A.* (2022) 260:422–7. doi: 10.2460/javma.21.03.0135

13. Smith JR, Legendre AM, Thomas WB, LeBlanc CJ, Lamkin C, Avenell JS, et al. Cerebral Blastomyces dermatitidis infection in a cat. *JAVMA-J Am Vet Med A.* (2007) 231:1210–4. doi: 10.2460/javma.231.8.1210

14. Baron ML, Hecht S, Westermeyer HD, Mankin JM, Novak JM, Donnell RL. Intracranial extension of retrobulbar blastomycosis (*Blastomyces dermatitidis*) in a dog. *Vet Ophthalmol.* (2011) 14:137–41. doi: 10.1111/j.1463-5224.2010.00850.x

15. Bentley RT, Reese MJ, Heng HG, Lin TL, Shimonohara N, Fauber A. Ependymal and periventricular magnetic resonance imaging changes in four dogs with central nervous system blastomycosis. *Vet Radiol Ultrasound.* (2013) 54:489–96. doi: 10.1111/vru.12049

16. Hecht S, Adams WH, Smith JR, Thomas WB. Clinical and imaging findings in five dogs with intracranial blastomycosis (*Blastomyces dermatiditis*). *J Am Anim Hosp Assoc.* (2011) 47:241–9. doi: 10.5326/JAAHA-MS-5573

17. Lipitz L, Rylander H, Forrest LJ, Foy DS. Clinical and magnetic resonance imaging features of central nervous system blastomycosis in 4 dogs. *J Vet Int Med.* (2010) 24:1509–14. doi: 10.1111/j.1939-1676.2010.0581.x

18. Saito M, Sharp NJH, Munana K, Troan BV, Tokuriki M, Thrall DE, et al. findings of intracranial blastomycosis in a dog. *Vet Radiol Ultrasound.* (2002) 43:16–21. doi: 10.1111/j.1740-8261.2002.tb00436.x

19. Diangelo L, Cohen-Gadol A, Heng HG, Miller MA, Hague DW, Rossmeisl JH, et al. Glioma mimics: magnetic resonance imaging characteristics of granulomas in dogs. *Front Vet Sci.* (2019) 6:286. doi: 10.3389/fvets.2019.00286

20. Hecht S, Cushing AC, Williams-Hagler DA, Craig LE, Thomas WB, Anderson KM, et al. Magnetic resonance imaging in 50 captive non-domestic felids-Technique and imaging diagnoses. *Front Vet Sci.* (2022) 9:827870. doi: 10.3389/fvets.2022.827870

21. Bradshaw JM, Pearson GR, Gruffydd-Jones TJ, A. retrospective study of 286 cases of neurological disorders of the cat. *J Comp Pathol.* (2004) 131:112–20. doi: 10.1016/j.jcpa.2004.01.010

22. Nakamoto Y, Uemura T, Hasegawa H, Nakamoto M, Ozawa T. Feline neurological diseases in a veterinary neurology referral hospital population in Japan. *J Vet Med Sci.* (2019) 81:879–85. doi: 10.1292/jvms.18-0447

23. Bentley RT, Heng HG, Thompson C, Lee CS, Kroll RA, Roy ME, et al. Magnetic resonance imaging features and outcome for solitary central nervous system coccidioides granulomas in 11 dogs and cats. *Vet Radiol Ultrasound.* (2015) 56:520–30. doi: 10.1111/vru.12258

24. Lavely J, Lipsitz D. Fungal infections of the central nervous system in the dog and cat. *Clin Tech Small an P.* (2005) 20:212–9. doi: 10.1053/j.ctsap.2005.07.001

25. Troxel MT, Vite CH, Massicotte C, McLear RC, Van Winkle TJ, Glass EN, et al. Magnetic resonance imaging features of feline intracranial neoplasia: retrospective analysis of 46 cats. *J Vet Intern Med.* (2004) 18:176–89. doi: 10.1111/j.1939-1676.2004.tb00158.x

26. Martin-Vaquero P, Da Costa RC, Aeffner F, Oglesbee MJ, Echandi RL. Imaging diagnosis—Hemorrhagic meningioma. *Vet Radiol Ultrasound.* (2010) 51:165–7. doi: 10.1111/j.1740-8261.2009.01645.x

27. Orton T, Gaillard F. *Intracranial Metastatic Melanoma*. Radiopaedia (2021). doi: 10.53347/rID-4935 (accessed May 13, 2022).

28. Durand A, Keenihan E, Schweizer D, Maiolini A, Guevar J, Oevermann A, et al. Clinical and magnetic resonance imaging features of lymphoma involving the nervous system in cats. *J Vet Int Med.* (2022) 36:679–93. doi: 10.1111/jvim.16350

29. Zimny A, Neska-Matuszewska M, Bladowska J, Sasiadek MJ. Intracranial lesions with low signal intensity on T2-weighted MR images – review of pathologies. *Pol J Radiol.* (2015) 80:40–50. doi: 10.12659/PJR.892146

30. Starkey J, Moritani T, Kirby P, MRI. of CNS fungal infections: review of aspergillosis to histoplasmosis and everything in between. *Clin Neuroradiol.* (2014) 24:217–30. doi: 10.1007/s00062-014-0305-7

31. Silvera S, Oppenheim C, Touze E, Ducreux D, Page P, Domigo V, et al. Spontaneous intracerebral hematoma on diffusion-weighted images: influence of T2-shine-through and T2-blackout effects. *Am J Neuroradiol.* (2005) 26:236–41.

32. Crawford AH, Stoll AL, Sanchez-Masian D, Shea A, Michaels J, Fraser AR, et al. Clinicopathologic features and magnetic resonance imaging findings in 24 cats with histopathologically confirmed neurologic feline infectious peritonitis. *J Vet Int Med.* (2017) 31:1477–86. doi: 10.1111/jvim.14791

33. Bentley RT, Taylor AR, Thomovsky SA. Fungal infections of the central nervous system in small animals. Clinical features, diagnosis, and management. *Vet Clin N Am-Small.* (2018);48:63. doi: 10.1016/j.cvsm.2017.08.010

34. Lane LV, Yang PJ, Cowell RL. Selected infectious agents. In: Valenciano AC, editor. *Cowell and Tyler's Diagnostic Cytology and Hematologyof the Dog and Cat.* 5th edn. St. Louis, MO: Elsevier (2020). p. 44–64. doi: 10.1016/B978-0-323-53314-0.00003-1

35. Brown EM, McTaggart LR, Zhang SX, Low DE, Stevens DA, Richardson SE. Phylogenetic analysis reveals a cryptic species Blastomyces gilchristii, sp. nov within the human pathogenic fungus Blastomyces dermatitidis. *PLoS ONE.* (2013) 8:e59237. doi: 10.1371/journal.pone.0059237

36. Schwartz IS, Kauffman CA. Blastomycosis. *Semin Respir Crit Care Med.* (2020) 41:31–41. doi: 10.1055/s-0039-3400281

37. Connolly P, Hage CA, Bariola JR, Bensadoun E, Rodgers M, Bradsher RW, et al. Blastomyces dermatitidis antigen detection by quantitative enzyme immunoassay. *Clin Vaccine Immunol.* (2012) 19:53–6. doi: 10.1128/CVI.05248-11

38. MiraVistaLabs [cited 2022 July 1]. Available from: https://miravistalabs.com/medical-fungal-infection-testing/antigen-detection/blastomyces-dermatitidis-quantitative-eia-test/

39. Aulakh HK, Aulakh KS, Troy GC. Feline histoplasmosis: A retrospective study of 22 cases (1986–2009). *J Am Anim Hosp Assoc.* (2012) 48:182–7. doi: 10.5326/JAAHA-MS-5758

40. Bromel C, Sykes JE. Histoplasmosis in dogs and cats. *Clin Tech Small an Pract.* (2005) 20:227–32. doi: 10.1053/j.ctsap.2005.07.003

frontiers | Frontiers in Veterinary Science

TYPE Original Research
PUBLISHED 19 August 2022
DOI 10.3389/fvets.2022.956648

OPEN ACCESS

EDITED BY
Luisa De Risio,
Linnaeus Veterinary Limited,
United Kingdom

REVIEWED BY
Edward E. Patterson,
University of Minnesota Twin Cities,
United States
Anna Knebel,
University Hannover, Germany

*CORRESPONDENCE
Tina Loncarica
tina.loncarica@anicura.it

SPECIALTY SECTION
This article was submitted to Veterinary Neurology and Neurosurgery, a section of the journal Frontiers in Veterinary Science

RECEIVED 30 May 2022
ACCEPTED 02 August 2022
PUBLISHED 19 August 2022

CITATION
Loncarica T, Balducci F and Bernardini M (2022) Prevalence of idiopathic epilepsy and structural epilepsy in 74 Boxer dogs in a referral hospital. *Front. Vet. Sci.* 9:956648. doi: 10.3389/fvets.2022.956648

Prevalence of idiopathic epilepsy and structural epilepsy in 74 Boxer dogs in a referral hospital

Tina Loncarica[1]*, Federica Balducci[1] and Marco Bernardini[1,2]

[1]Neurology Unit, Anicura Portoni Rossi Veterinary Hospital, Bologna, Italy, [2]Department of Animal Medicine, Production and Health, Clinical section, University of Padua, Legnaro, Italy

The prevalence of idiopathic epilepsy and structural epilepsy in Boxer dogs is unknown. The aim of this retrospective study was to evaluate the prevalence of structural and idiopathic epilepsy in the Boxer population. A total of 74 Boxer dogs were included in the study from the database of one referral hospital and the following were recorded: signalment, history, clinical findings and results of advanced diagnostic imaging. Five dogs (6.8%) were diagnosed with idiopathic epilepsy, of which one was in the <6 months age group, three were in the 6–72 months age group and one was in the >72 months age group. Sixty-nine dogs (93.2%) were diagnosed with structural epilepsy. Sixty-six had a suspected intracranial neoplasia: Eight were in the 6–72 months age group and represent 66.7% of the dogs in that age group. The other fifty-eight were in the >72 months age group and represent 96.7% of the dogs in that age group. In our Boxer population, 81.8% of the patients had a suspected intra-axial tumor and 22.7% of dogs with an intracranial pathology nevertheless had a normal neurological examination. In conclusion, in the majority of boxer patients the cause of epilepsy is a suspected intracranial neoplasia regardless of the age at presentation. Considering the finding in this study of a low prevalence of presumed idiopathic epilepsy in the Boxer breed, it is recommended that patients who satisfy Tier I confidence level of the "International Veterinary Epilepsy Task Force" (IVETF) also undergo an MRI study of the brain.

KEYWORDS

Boxer, etiology, seizure, dog, structural epilepsy, idiopathic epilepsy

Introduction

Epilepsy is a common disorder in veterinary medicine and is defined as the predisposition to develop epileptic seizures (1). According to the International Veterinary Epilepsy Task Force (IVETF), epilepsy can be classified based on the underlying etiology into two categories: idiopathic or structural. Idiopathic epilepsy (IE) is diagnosed when a genetic background is identified or suspected, or an underlying cause has not been found (1). Numerous epidemiologic and genetic studies have been conducted to date, revealing a predisposition for genetic or suspected genetic epilepsy in Vizlas, Finnish Spitz, English Springer Spaniels, Belgian Tervurens, Belgian Sheepdogs, Bernese Mountain dogs, Labrador Retrievers, Lagotto Romagnolo, Border Collies and Irish Wolfhounds, among other breeds (2–13).

Structural epilepsy (SE) is characterized by the presence of epileptic seizures caused by an intracranial pathology (vascular, inflammatory/infectious, traumatic, congenital, neoplastic or degenerative anomaly), confirmed through an MRI study of the brain, examination of the cerebrospinal fluid, genetic tests or necropsy (1).

One recent study evaluated the prevalence of IE and SE in a large general population of dogs undergoing MRI for epileptic seizures; it found that 53.8% of dogs had IE and 45.1% had SE (14). 75.5% of the patients aged between 7 and 72 months were diagnosed with IE and 3% were diagnosed with intracranial neoplasia. In the >72 months age group, 34.1% of dogs were diagnosed with IE and 63,9% with SE, of which 43.2% had intracranial neoplasia (14). Another study conducted in a referral center found that 52.1% of dogs were affected by SE, 31.2% of them due to a neoplastic condition (15).

Two recent studies identified the Boxer as the breed with the highest prevalence of seizures (16, 17). In addition, a predisposition for Boxer dogs to develop intracranial tumors, both intra-axial and extra-axial, is reported (15, 17–24), as well as a predisposition for hereditary epilepsy (25).

There are currently no data regarding the prevalence of IE and SE in Boxer dogs. The aim of this study was to provide estimates of the prevalence of IE and SE in a population of Boxers that presented to our hospital and underwent MRI for epileptic seizures.

Materials and methods

Data were retrospectively collected between February 2007 and December 2020 from the database of the AniCura I Portoni Rossi Veterinary Hospital by searching for boxer dogs and then using the following keywords: "seizure(s)," "epileptic seizure(s)" or "epilepsy." Only dogs that underwent MRI of the brain were included in the study. Dogs were excluded if the medical records were incomplete; if the records were diagnostic or suggestive for a metabolic/toxic pathology; or if the MRI study was not available for re-examination. The medical records were reviewed and the following data were recorded: signalment, clinical history, results of physical and neurological examination, hematology and serum biochemistry results, age at the first seizure, MRI findings, and cerebrospinal fluid (CSF) analysis. Dogs were divided into categories based on the age of the first seizure: ≤6 months, 7–72 months, and >72 months, following a published paper (14). All cases were managed by a board-certified neurologist or a resident in neurology under supervision. The neurological examination was defined as normal, abnormal, or not evaluable (because of a recent seizure). The MRI was performed with a 0.22 T (MrJ, Paramed Health Service, Genua, Italy) from February 2007 to March 2018 and with a 1.5 T (Vantage Elan, Canon Medical Systems Europe, The Netherlands) from April 2018 to December 2020. The acquired sequences had to include at least: sagittal and transverse T2-weighted; transverse FLAIR; and transverse T1-weighted before and after the administration of a gadolinium-based contrast medium. The MRI studies were then reviewed by a board-certified neurologist to determine whether seizures were due to structural pathology. Based on the history, the neurological examination, the MRI results, and the CSF analysis, each dog was categorized as affected by IE or one of the following structural conditions: congenital malformation, inflammatory disease, vasculopathy, degenerative disease, trauma and neoplasm. Within the neoplastic group, patients were further divided into two groups based on the intra- or extra-axial localization of the mass lesion.

Descriptive statistics were performed utilizing Microsoft Excel for Mac. Mean was used for all descriptive statistics: gender, age at first seizure, neurological examination (altered, normal or not evaluable), MRI findings (altered or normal), etiology, age at which the patient was subjected to MRI, and localization of the neoplastic lesion (extra-axial or intra-axial).

Results

One thousand and seventy-two boxers presented to our hospital during the study period, 368 (34.3%) of which had a neurological examination for a suspected neurological disease and 91 (8.5%) had seizures. Of these 91 patients, 16 were excluded due to the lack of an MRI study and 1 because of reactive seizures. Thus, 74 patients (6.9%) were included in the study.

Two out of 74 cases were <6-months old. There was a 6-month old female patient diagnosed with IE and a 5-month old male patient diagnosed with a meningoencephalocele (MEC).

Twelve out of 74 patients (16.2%) were aged between 7 and 72 months. Five were males (41.7%) and 7 females (58.3%). The mean age of presentation of the first epileptic seizure was 44.8 months and the mean age at which they were subjected to advanced diagnostic procedures was 49.3 months. Eight out of 12 patients (66.7%) had an MRI study showing a presumptive neoplastic lesion (2 extra-axial, 1 suspected extra-axial, and 5 intra-axial). The mean age of these patients was 59 months. Of these eight patients, 2 (25.0%) had a normal and 6 (75%) had an abnormal neurological examination. Three out of 12 patients (25.0%) had a normal neurological examination with a normal MRI study and a normal cerebrospinal fluid examination (performed in only one out of 3 patients). In these cases, the suspected diagnosis was IE. The mean age of these patients was 19.3 months. The remaining dog in this age group was 7-months old and the MRI was suggestive of an ischemic event.

Sixty out of 74 patients (81.1%) were older than 72 months. Twenty-nine were male (48.3%) and 31 were female (51.7%). The mean age of presentation of epileptic seizures was 107.7

months and the mean age at which they were subjected to advanced diagnostics was 109.1 months. Fifty-eight of 60 patients (96.7%) had an MRI study suggestive of a neoplastic condition. The mean age of these patients was 108.4 months. Of these 58 dogs, 13 (22.4%) had a normal neurological examination and 38 (65.5%) had an abnormal neurological examination. In 7 dogs (12.1%) the neurological examination was either not performed because of the recent administration of antiepileptic drugs, or was not reliable because of a recent seizure. One out of 60 patients (1.7%) had a suspected diagnosis of IE. The age of this patient was 98 months. One out of 60 patients (1.7%), aged 74 months, had an MRI suggestive of an ischemic event.

Overall, the majority of patients (89.2%) were diagnosed with suspected neoplastic disease. Of this group, 12.1% were aged between 7 and 72 months and 87.9% were older than 72 months. We found a total of 54 intra-axial neoplasms and 12 extra-axial neoplasms. Eleven dogs underwent a histological examination, which confirmed the neoplastic nature of the lesions. There were 6 meningiomas, 1 glioma, 1 ependymoma, 1 leptomeningeal lymphomatosis and 2 metastases (1 hemangiosarcoma and 1 carcinoma). IE accounted for 5 out of 74 cases (6.8%), of which 3 (60%) were aged between 7 and 72 months, 1 (20%) was younger than 6 months and 1 was over 72 months. Two out of 74 patients (2.7%) had a suspected vascular disease, one of which was aged between 7 and 72 months and the other was older than 72 months. One out of 74 patients (1.4%) had a diagnosis of congenital disease, at <6 months old.

Discussion

This study analyzes the causes of epilepsy in the Boxer dogs. The motivation behind the study is the authors' impression that this breed presents epidemiologic and etiologic peculiarities among dogs affected by epileptic seizures.

Across the 14 year study period, of all the Boxers presented to our hospital 34.3% had a neurological examination for a suspected neurological disease. A previous study, conducted in Switzerland, found that 33% of general canine population had a presumptive neurological diagnosis (26). This data was in agreement with the results of our study, but it is possible that within this large group the pathologies were distributed in a different way according to the breed and the age range taken into consideration. In fact, when focusing on epilepsy, our data differed from that present in the literature. In our population of Boxer dogs fulfilling the inclusion criteria, the prevalence of epileptic seizures was found to be 6.9%. However, of the 17 patients that were excluded, only 1 was diagnosed with reactive seizures. In the remaining 16, clinical history and blood work were not suggestive of a metabolic condition, so either IE or SE would be a likely diagnosis. The real prevalence of epileptic seizures in our population of Boxer dogs might consequently be higher, close to 8.4% (90/1,072). The prevalence of epileptic Boxers in a referral institution has not been investigated to date. Two studies conducted on the prevalence of epileptic seizures in the general canine population in primary veterinary care reported a percentage of 0.75–0.82% and identified the Boxer as the breed with the highest seizure prevalence (1.8–2.3%, respectively) (16, 17).

In our population there were only two puppies aged between 0 and 6 months. In a paper on dogs aged <1 year, the mean age at the first seizure in dogs with IE was 6.8 months, while in dogs with SE it was 7.5 months, and in dogs experiencing reactive seizures it was 4 months (27). As such, one plausible reason for the low prevalence of epileptic dogs aged <6 months is that reactive seizures could be more common in this age group. This low prevalence strictly overlaps that found in another study, where 20 of 900 dogs were aged <6 months at the time of their first seizure (14). In the same study, 70% of the dogs (14/20) were diagnosed with SE, mostly due to congenital malformations, and 30% with IE (14).

The main causes of epileptic seizures in pediatric patients are congenital malformations and inflammatory conditions (28). The Boxer is not among the breeds with the highest incidence of the most common congenital conditions, such as hydrocephalus and lissencephaly (28, 29). The puppy with SE in our data set had a MEC, a sporadically occurring disease potentially underdiagnosed because diagnosis requires advanced imaging (30). Seizures are the main presenting neurologic sign in dogs with MEC (30). In our dog, MRI showed an intranasal MEC with robust meningeal post-contrast enhancement, possibly due to inflammation. Infiltration of inflammatory cells contributing to abnormal excitability of cortical neurons is one of the pathogenetic mechanisms hypothesized to explain seizures in patients with MEC (31).

The lack of pediatric patients with an inflammatory condition in our study is likely due to several causes. Autoimmune encephalitis is uncommon at this age (28, 32) and Boxers are not at a higher risk of this kind of inflammation (32). Infectious encephalitis was regarded as a frequent cause of seizures in dogs in the recent past and Canine Distemper virus was the most common form (33, 34). Although vaccination for Canine Distemper virus does not ensure a total immunity against the neurological form of the disease and not all dogs are vaccinated, in recent decades its use has become so widespread that there has been a severe reduction in the occurrence of CDV-related seizures.

A previous study reported that IE was the final diagnosis in 75.5% of cases in a canine population affected by epileptic seizures, aged between 6 months and 6 years (14). In the same study, neoplasia was diagnosed or suspected in only 3% of dogs. These data differ considerably from those found in our study, where 66.7% of Boxers had an MRI suggestive of brain neoplasia and only 25% had a diagnosis of IE. Among the dogs

diagnosed with or suspected of having a brain tumor, one quarter showed a normal neurological examination. The average age of dogs in this age group with suspected intracranial neoplasia was 59 months.

In a recent paper, the predictive value of age at the time of the first epileptic seizure to differentiate between IE and SE was investigated combining and analyzing the data from two previously published studies (1, 35). It found that a 6-year cut off was a better predictor than a 5-year cut off to determine the likelihood of a dog being affected by IE. We have not performed statistical analysis on our dataset. However, based on our data it seems reasonable that in Boxers a 6-year cut off is too high and we recommend performing an MRI of the brain, after the exclusion of reactive seizures, in Boxers 5 years old or even younger, independent of the results of the neurological examination.

With regard to the age group over 72 months, we found that 96.7% of our Boxers had a diagnosis of epilepsy due to a histologically confirmed or an MRI suspected neoplasia, and only 1.7% had a diagnosis of IE. In a published study on patients over 6 years of age, intracranial neoplasia was diagnosed in 43.2% of the cases and was the primary differential diagnosis for this age group (14). A similar study investigated the etiology of epilepsy in dogs 5 years of age and older and found that 49.5% of patients had a diagnosis of intracranial neoplasia (36). If we set the lower age limit of our population at 5 years, patients with a confirmed or suspected diagnosis of intracranial neoplasia equaled 96.9% (63 out of 65). In other words, lowering the age limit to 5 years did not cause any change in the percentage of epileptic Boxers in this age group who had intracranial neoplasia.

According to our data, regardless of the age of the first seizure, Boxers have a 93.2% chance to suffer from SE and a 90.4% chance of being affected by a suspected or confirmed neoplastic condition. A recent study investigated the prevalence of IE and SE in the canine population, where it emerged that the Boxer is the fourth most common breed to have structural pathologies underlying the development of epileptic seizures (14).

These data may reflect the high predisposition of Boxer dogs for developing brain neoplasia compared to the general population (15, 17–24). However, it is the authors' opinion that other causes have to be hypothesized to justify such a high prevalence. The first factor could be related to the referral nature of our hospital. It is likely that many of these dogs have been initially investigated by their referring veterinarians, that no clinically significant abnormalities on blood or urinalysis were found, and it was decided to either evaluate the response to an antiepileptic treatment or to wait and observe the frequency and the severity of the seizures. In this way, treatment-responders, i.e., dogs with mild neurological impairment and dogs with low frequency seizures, were not referred, generating a severe bias in our dataset. A second factor which again relates to the referral nature of our hospital could lead to an opposite clinical situation; for example, cases showing a very quick clinical evolution toward either cluster seizures / status epilepticus or severe neurological deficits may actually not be referred. A severe clinical scenario may discourage owners from pursuing a final diagnosis through often expensive investigations. Vascular and inflammatory conditions and, in some instances, IE could constitute the cause of such severe clinical conditions (37–39) and, again, bias the overall prevalence when not investigated.

Two recent studies, which considered dogs that have undergone intracranial surgery for tumor removal, highlighted the Boxer as one of the most affected breeds, representing 12.9–18.2% of patients (23, 24). Eighty-five percent of the Boxers had an intra-axial tumor (20). In our study, 81.8% of Boxers with an MRI-suspected neoplasia had an intra-axial lesion and 18.2% had an extra-axial lesion. This finding agrees with a previous study, where Boxers are the most represented breed amongst patients with intra-axial tumors (14, 20). In an older study it was hypothesized that the predisposition of the ancestral bulldog, from which the Boxer breed derives, to certain diseases (chemodectomas, proliferation of fibrillar astrocytes) is caused by the altered anatomy of the respiratory tract. This alteration leads to prolonged hypoxia, which in humans can stimulate the development of fibrillar gliosis (22). The same study also argues that some brachycephalic breeds (English bulldog, Boxer and Boston terrier) are more likely than other brachycephalic breeds to develop glial tumors. The neurological examination is usually expected to be abnormal in dogs with intracranial disease, yet it is known that a normal neurological examination does not exclude a structural brain lesion. In a previous study, 23% of dogs <6 years old at the onset of seizures and 22% of dogs over 6 years old at the onset of seizures had a normal neurological examination with abnormal MRI results (40). In our Boxer population we found similar results, since 22.7% of patients with an intracranial neoplasia had a normal neurological examination. In light of this evidence, we recommend performing an MRI in epileptic Boxers in spite of a normal neurological examination, especially if they experience the first epileptic seizure in adulthood.

In the Boxer dog a genetic predisposition to IE has been proposed, on the basis of a high mortality rate in seizuring subjects of 4 years of age or less (25). No diagnostic procedures were performed in that study to rule out SE and support this hypothesis. Indeed, the Boxer is not listed among the breeds for which IE has a demonstrated or supposed predisposition. Evidence to support a predisposition for IE was not found in our study. Only 6.8% of patients were diagnosed with IE out of the entire Boxer population, regardless of age, and 25% of patients in the range between 6 months and 6 years. However, if we lower the upper age limit of this group to 5 years based on the previously discussed

prevalence of tumors, the proportion of IE rises to 47%, approximating but not equaling what is found in the general canine population in the same age group (14). Again, it is likely that subjects with good control of epileptic seizures after IVETF Tier 1 protocols will not be referred to specialist centers for a complete diagnostic workup and this may lead to an underestimation of the real incidence of IE in Boxers. However, this may not be sufficient to explain the low level of IE seen here in Boxers; our institution sees many dogs of other breeds referred for refractory epilepsy and so it is possible that Boxers are less affected by this condition. Further studies are needed to determine the real prevalence of IE in Boxers.

Our study has several limitations, mainly related to its retrospective nature. In the 14-year span many veterinarians performed the neurological examination and subtle abnormalities may have been overlooked in some cases. However, neurological examinations were always performed by experienced clinicians or residents under strict supervision by ECVN diplomates, thus minimizing this situation. Due to the emergency conditions in which some cases are referred, many patients were examined following an epileptic seizure or status epilepticus. Therefore, the percentage of patients with SE and an abnormal neurological examination may have been overestimated. These dogs may have had a normal neurological examination if they had been examined at a time distant from the seizure episode. This limitation may negatively bias our percentage of dogs with a normal neurological examination despite SE, but emphasizes the need to perform advanced imaging in Boxers with a history of seizures. Other limitations of the study are the variable MRI protocols and different MRI scanners used, due to the long study period. The majority of the studies were performed with a low-field MRI scanner. Because of the lack of a histopathological confirmation in most cases, it cannot be excluded that inflammatory or vascular conditions could have been misdiagnosed for a low-grade, non-contrast-enhancing glioma in a few cases.

In conclusion, Boxer dogs experiencing seizures have a high probability of having intracranial neoplasia, regardless of their age and the result of the neurological examination. It is therefore always advisable to perform advanced imaging to better define the diagnosis and hence an adequate prognosis.

Data availability statement

The raw data supporting the conclusions of this article will be made available by the authors, without undue reservation.

Ethics statement

Ethical review and approval was not required for the animal study because this is a retrospective clinical study. Written informed consent for participation was not obtained from the owners because for the retrospective nature and for the long study period (14 years).

Author contributions

TL and FB were responsible for the study conception. TL collected the data. FB and MB supervised data analysis and manuscript editing. TL and MB wrote the manuscript. All authors contributed to the article and approved the submitted version.

Acknowledgments

The authors thank Jack Amey for the revision of the English language.

Conflict of interest

The authors declare that the research was conducted in the absence of any commercial or financial relationships that could be construed as a potential conflict of interest.

Publisher's note

All claims expressed in this article are solely those of the authors and do not necessarily represent those of their affiliated organizations, or those of the publisher, the editors and the reviewers. Any product that may be evaluated in this article, or claim that may be made by its manufacturer, is not guaranteed or endorsed by the publisher.

References

1. Berendt M, Farquhar RG, Mandigers PJJ, Pakozdy A, Bhatti SFM, De Risio L, et al. International veterinary epilepsy task force consensus report on epilepsy definition, classification and terminology in companion animals. *BMC Vet Res.* (2015) 11:464. doi: 10.1186/s12917-0150460-3

2. Hulsmeyer VI, Fischer A, Mandigers PJJ, De Risio L, Berendt M, Rusbridge, et al. International veterinary epilepsy task force's current understanding of idiopathic epilepsy of genetic or suspected genetic origin in purebred dogs. *BMC Vet Res.* (2015) 11:175. doi: 10.1186/s12917-015-0463-0

3. Viitmaa R, Cizinauskas S, Orro T, Niilo-Rämä M, Gordin E, Lohi H, et al. Phenotype, inherence characteristics, and risk factors for idiopathic epilepsy in Finnish Spitz dogs. *J Am Vet Med Assoc.* (2013) 243:1001–9. doi: 10.2460/javma.243.7.1001

4. Patterson EE, Armstrong PJ, O'Brien DP, Roberts MC, Johnson GS, Mickelson JR. Clinical description and mode of inheritance of idiopathic epilepsy in English springer spaniels. *J Am Vet Med Assoc.* (2005) 226:54–8. doi: 10.2460/javma.2005.226.54

5. Patterson EE, Mickelson JR, Da Y, Roberts MC, McVey AS, O'Brien DP, et al. Clinical characteristics and inheritance of idiopathic epilepsy in Vizslas. *J Vet Intern Med.* (2003) 17:319–25. doi: 10.1111/j.1939-1676.2003.tb02455.x

6. Oberbauer AM, Grossman DI, Irion DN, Schaffer AL, Eggleston ML, Famula TR. The genetics of epilepsy in the Belgian tervuren and sheepdog. *J Hered.* (2003) 94:57–63. doi: 10.1093/jhered/esg010

7. Kathmann I, Jaggy A, Busato A, Bärtschi M, Gaillard C. Clinical and genetic investigations of idiopathic epilepsy in the Bernese mountain dog. *J Small Anim Pract.* (1999) 40:319–25. doi: 10.1111/j.1748-5827.1999.tb03089.x

8. Jaggy A, Faissler D, Gaillard C, Srenk P, Graber H. Genetic aspects of idiopathic epilepsy in Labrador retrievers. *J Small Anim Pract.* (1998) 39:275–80. doi: 10.1111/j.1748-5827.1998.tb03650.x

9. Jokinen TS, Metsähonkala L, Bergamasco L, Viitmaa R, Syrjä P, Lohi H, et al. Benign familial juvenile epilepsy in Lagotto Romagnolo dogs. *J Vet Intern Med.* (2007) 21:464–71. doi: 10.1892/0891-6640 (2007) 21[464:bfjeil]2.0.co;2

10. Casal ML, Munuve RM, Janis MA, Werner P, Henthorn PS. Epilepsy in irish wolfhounds. *J Vet Intern Med.* (2006) 20:131–5. doi: 10.1892/0891-6640(2006)20[131:eiiw]2.0.co;2

11. Berendt M, Gredal H, Pedersen LG, Alban L, Alving J. A cross-sectional study of epilepsy in danish labrador retrievers: prevalence and selected risk factors. *J Vet Intern Med.* (2002) 16:262–8. doi: 10.1892/0891-6640(2002)016<0262:acsoei>2.3.co;2

12. Heynold Y, Faissler D, Steffen F, Jaggy A. Clinical, epidemiological and treatment results of idiopathic epilepsy in 54 labrador retrievers: a long-term study. *J Small Anim Pract.* (1997) 38:7–14. doi: 10.1111/j.1748-5827.1997.tb02977.x

13. Hülsmeyer V, Zimmermann R, Brauer C, Sauter-Louis C, Fischer A. Epilepsy in border collies: clinical manifestation, outcome, and mode of inheritance. *J Vet Intern Med.* (2010) 24:171–8. doi: 10.1111/j.1939-1676.2009.0438.x

14. Hall R, Labruyere J, Volk H, Cardy TJ. Estimation of the prevalence of idiopathic epilepsy and structural epilepsy in a general population of 900 dogs undergoing MRI for epileptic seizures. *Vet Rec.* (2020) 187:e89. doi: 10.1136/vr.105647

15. Pákozdy A, Leschnik M, Tichy AG, Thalhammer JG. Retrospective clinical comparison of idiopathic versus symptomatic epilepsy in 240 dogs with seizures. *Acta Vet Hung.* (2008) 56:471–83. doi: 10.1556/AVet.56.2008.4.5

16. Heske L, Nødtvedt A, Jäderlund KH, Berendt M, Egenvall A. A cohort study of epilepsy among 665,000 insured dogs: incidence, mortality and survival after diagnosis. *Vet J.* (2014) 202:471–6. doi: 10.1016/j.tvjl.2014.09.023

17. Erlen A, Potschka H, Volk HA, Sauter-Louis C, O'Neill DG. Seizures in dogs under primary veterinary care in the United Kingdom: etiology, diagnostic testing, and clinical management. *J Vet Intern Med.* (2020) 34:2525–35. doi: 10.1111/jvim.15911

18. Truvé K. Bioinformatics mining for disease causing mutations: using the dog genome as a model for human disease (Doctorial thesis). Swedish university of agricultural sciences, Uppsala. *Acta Univ Agric Sueciae.* (2012) 64:61–64.

19. Kishimoto TE, Uchida K, Chambers JK, Kok MK, Son NV, Shiga T, et al. A retrospective survey on canine intracranial tumors between 2007 and 2017. *J Vet Med Sci.* (2020) 82:77–83. doi: 10.1292/jvms.19-0486

20. Song RB, Vite CH, Bradley CW, Cross JR. Postmortem evaluation of 435 cases of intracranial neoplasia in dogs and relationship of neoplasm with breed, age, and body weight. *J Vet Intern Med.* (2013) 27:1143–52. doi: 10.1111/jvim.12136

21. Snyder JM, Shofer FS, Van Winkle TJ, Massicotte C. Canine intracranial primary neoplasia: 173 cases (1986-2003). *J Vet Intern Med.* (2006) 20:669–75. doi: 10.1892/0891-6640(2006)20[669:cipnc]2.0.co;2

22. Hayes HM, Priester WA Jr, Pendergrass TW. Occurrence of nervous-tissue tumors in cattle, horses, cats and dogs. *Int J Cancer.* (1975) 15:39–47. doi: 10.1002/ijc.2910150106

23. Parker RL, Du J, Shinn RL, Drury AG, Hsu FC, Roberston JL, et al. Incidence, risk factors, and outcomes for early postoperative seizures in dogs with rostrotentorial brain tumors after intracranial surgery. *J Vet Intern Med.* (2022) 36:694–701. doi: 10.1111/jvim.16391

24. Forward AK, Volk HA, Cherubini GB, Harcourt-Brown T, Plessas IN, Garosi L, et al. Clinical presentation, diagnostic findings and outcome of dogs undergoing surgical resection for intracranial meningioma: 101 dogs. *BMC Vet Res.* (2022) 18:88. doi: 10.1186/s12917-022-03182-y

25. Nielen AL, Janss LL, Knol BW. Heritability estimations for diseases, coat color, body weight, and height in a birth cohort of boxers. *Am J Vet Res.* (2001) 62:1198–206. doi: 10.2460/ajvr.2001.62.1198

26. Fluehmann G, Doherr MG, Jaggy A. Canine neurological diseases in a referral hospital population between 1989 and 2000 in Switzerland. *J Small Anim Pract.* (2006) 47:582–7. doi: 10.1111/j.1748-5827.2006.00106.x

27. Arrol L, Penderis J, Garosi L, Cripps P, Gutierrez-Quintana R, Gonçalves R. Aetiology and long-term outcome of juvenile epilepsy in 136 dogs. *Vet Rec.* (2012) 170:335. doi: 10.1136/vr.100316

28. Lavely JA. Pediatric seizure disorders in dogs and cats. *Vet Clin North Am Small Anim Pract.* (2014) 44:275–301. doi: 10.1016/j.cvsm.2013.10.004

29. Estey CM. Congenital hydrocephalus. *Vet Clin North Am Small Anim Pract.* (2016) 46:217–29. doi: 10.1016/j.cvsm.2015.10.003

30. Lazzerini K, Gutierrez-Quintana R, José-López R, McConnell F, Gonçalves R, McMurrough J, et al. Clinical features, imaging characteristics, and long-term outcome of dogs with cranial meningocele or meningoencephalocele. *J Vet Intern Med.* (2017) 31:505–12. doi: 10.1111/jvim.14638

31. Jeffery N. Ethmoidal encephalocoele associated with seizures in a puppy. *J Small Anim Pract.* (2005) 46:89–92. doi: 10.1111/j.1748-5827.2005.tb00299.x

32. Cornelis I, Van Ham L, Gielen I, De Decker S, Bhatti SFM. Clinical presentation, diagnostic findings, prognostic factors, treatment and outcome in dogs with meningoencephalomyelitis of unknown origin: a review. *Vet J.* (2019) 244:37–44. doi: 10.1016/j.tvjl.2018.12.007

33. Tipold A. Diagnosis of inflammatory and infectious diseases of the central nervous system in dogs: a retrospective study. *J Vet Intern Med.* (1995) 9:304–14. doi: 10.1111/j.1939-1676.1995.tb01089.x

34. Podell M, Fenner WR, Powers JD. Seizure classification in dogs from a nonreferral-based population. *J Am Vet Med Assoc.* (1995) 206:1721–8.

35. De Risio L, Bhatti S, Muñana K, Penderis J, Stein V, Tipold A, et al. International veterinary epilepsy task force consensus proposal: diagnostic approach to epilepsy in dogs. *BMC Vet Res.* (2015) 11:148. doi: 10.1186/s12917-015-0462-1

36. Ghormley TM, Feldman DG, Cook Jr JR. Epilepsy in dogs five years of age and older: 99 cases (2006-2011). *J Am Vet Med Assoc*. (2015) 246:447–50. doi: 10.2460/javma.246.4.447

37. Kaczmarska A, José-López R, Czopowicz M, Lazzerini K, Leblond G, Stalin C, et al. Postencephalitic epilepsy in dogs with meningoencephalitis of unknown origin: clinical features, risk factors, and long-term outcome. *J Vet Intern Med.* (2020) 34:808–20. doi: 10.1111/jvim.15687

38. Packer RM, Shihab NK, Torres BB, Volk HA. Clinical risk factors associated with anti-epileptic drug responsiveness in canine epilepsy. *PLoS ONE.* (2014) 9:e106026. doi: 10.1371/journal.pone.0106026

39. Blades Golubovic S, Rossmeisl Jr JH. Status epilepticus in dogs and cats, part 1: etiopathogenesis, epidemiology, and diagnosis. *J Vet Emerg Crit Care.* (2017) 27:278–87. doi: 10.1111/vec.12605

40. Bush WW, Barr CS, Darrin EW, Shofer FS, Vite CH, Steinberg SA. Results of cerebrospinal fluid analysis, neurologic examination findings, and age at the onset of seizures as predictors for results of magnetic resonance imaging of the brain in dogs examined because of seizures: 115 cases (1992-2000). *J Am Vet Med Assoc.* (2002) 220:781–4. doi: 10.2460/javma.2002.220.781

frontiers | Frontiers in Veterinary Science

TYPE Original Research
PUBLISHED 19 August 2022
DOI 10.3389/fvets.2022.957278

OPEN ACCESS

EDITED BY
Luisa De Risio,
Linnaeus Veterinary Limited,
United Kingdom

REVIEWED BY
Sam Long,
Veterinary Referral Hospital, Australia
Viktor Paluš,
Neurovet, Slovakia
Simon Platt,
University of Georgia, United States

*CORRESPONDENCE
Carlotta Remelli
carlotta.remelli@gmail.com

†These authors have contributed equally to this work and share first authorship

SPECIALTY SECTION
This article was submitted to Veterinary Neurology and Neurosurgery, a section of the journal Frontiers in Veterinary Science

RECEIVED 30 May 2022
ACCEPTED 02 August 2022
PUBLISHED 19 August 2022

CITATION
Remelli C, Martello A, Valentini A, Contiero B and Bernardini M (2022) Magnetic resonance imaging highlights the meningeal involvement in steroid responsive meningitis-arteritis and suggests the inflammation of the surrounding tissues (70 cases). *Front. Vet. Sci.* 9:957278. doi: 10.3389/fvets.2022.957278

Magnetic resonance imaging highlights the meningeal involvement in steroid responsive meningitis-arteritis and suggests the inflammation of the surrounding tissues (70 cases)

Carlotta Remelli[1*†], Alba Martello[1†], Alessia Valentini[1], Barbara Contiero[1] and Marco Bernardini[1,2]

[1]Department of Animal Medicine, Productions and Health, University of Padua, Legnaro, Italy, [2]Anicura I Portoni Rossi Veterinary Hospital, Zola Predosa, Bologna, Italy

Introduction: Steroid-responsive meningitis-arteritis (SRMA) is an immune-mediated disorder of young dogs for which there is no definitive ante-mortem diagnostic test. Magnetic Resonance Imaging (MRI) can be used to explore other differentials and extensive reports about its usefulness in the diagnosis of SRMA are lacking. The aims of this study were to retrospectively investigate the characteristics of MRI studies of the cervical spine of dogs diagnosed with SRMA and to compare the diagnostic capability of MRI obtained with low-field and high-field units.

Materials and methods: This is a double center, retrospective case series. Databases were searched between 2008 and 2021 for dogs with a diagnosis of SRMA. Dogs were included if the following criteria were fulfilled: a diagnosis of cervical SRMA, results of CSF analysis, and MRI of the cervical spine available for re-evaluation.

Results: Seventy cases were selected. MRI abnormalities were found in 69 cases (98.6%). Enhancement of the meninges, nerve roots, synovium of the articular facets and paravertebral muscles was present in 61 (87.1%), 10 (14.3%), 34 (48.6%), and 34 (48.6%) cases, respectively, when considering all MRI. In the low-field MRI, enhancement of these structures was present in 45 (90%), 4 (8%), 21 (42%) and 23 (46%) cases, respectively. In the high-field MRI, enhancement of these structures was present in 16 (80%), 6 (30%), 13 (65%) and 11 (55%) cases, respectively. Fat suppressed T1W images showed meningeal enhancement better than T1W images. When all the MRIs were considered, a significant increase in cell count of the cerebrospinal fluid was found between the three groups based on the meningeal MRI score ($p = 0.001$). In cases with no meningeal enhancement but enhancement of synovium of the articular facets and/or muscles a significantly lower cerebrospinal fluid cell count was present ($p = 0.043$), when considering all MRIs.

Conclusions: The most frequent detection on cervical MRI of dogs affected by SRMA is meningeal enhancement, often accompanied by enhancement of the synovium of the articular facets and/or muscular enhancement. Both low-field and high-field MRI have good diagnostic capability but the latter enables a more thorough investigation thanks to specific sequences. MRI is useful as a complementary tool to cerebrospinal fluid analysis.

KEYWORDS

steroid-responsive meningitis-arteritis (SRMA), dog, magnetic resonance imaging (MRI), cervical spine, polyarthritis, myositis, cerebrospinal fluid (CSF), central nervous system (CNS)

Introduction

Steroid-responsive meningitis-arteritis (SRMA) is an immune-mediated disorder commonly recognized in dogs (1). Even though SRMA typically affects dogs of 6–18 months of age (1, 2) SRMA is also described in older dogs (3–6). Any breed can be affected, with a prominent predisposition in Beagles, Bernese Mountain Dogs, Border Collies, Boxers, English Springer Spaniels, Jack Russell Terriers, Nova Scotia Duck Tolling Retrievers, Weimaraners and Whippets (1, 7–9). An acute form and a chronic form of SRMA may occur. The former is characterized by cervical pain and stiffness, often associated with stiff gait and fever, the latter by ataxia, paresis, and spinal nerve deficits as a consequence of disease progression to the spinal cord (1, 10). SRMA-affected dogs may also show myositis and polyarthritis (11–13).

There are no definitive ante-mortem diagnostic tests for SRMA (14). Nowadays the diagnosis is based on a patient's particular signalment, medical history, neurological examination, bloodwork and, above all, cerebrospinal fluid (CSF) analysis. In the acute form CSF commonly presents a neutrophilic pleocytosis often characterized by more than 500 cells/μl in addition to an elevated protein concentration, whereas in the chronic form CSF is usually characterized by a mixed, less severe pleocytosis with a normal or mildly elevated total protein concentration (1, 15). Magnetic resonance imaging (MRI) of the cervical spine of dogs suspected to be affected by SRMA may show features suggesting meningeal inflammation, such as meningeal enhancement in T1-weighted (T1W) images after intravenous injection of a gadolinium-based contrast agent (GBCAs) (1, 16). Furthermore, MRI may reveal muscular abnormalities, such as T2-weighted (T2W) and short tau inversion recovery (STIR) hyperintensity (13, 16), as well as contrast enhancement (16). T2W hyperintensity or contrast enhancement inside the spinal cord may signal lesion progression (16). MRI is mainly considered useful to explore other differentials (16). Nevertheless, extensive reports about the usefulness of MRI in the diagnosis of SRMA are lacking.

The aims of this retrospective study were (1) to investigate the characteristics of MRI studies of the cervical spine of dogs diagnosed to be affected by SRMA and (2) to compare the diagnostic capability of MRI obtained with low-field (LF) and high-field (HF) MRI units.

Abbreviations: SRMA, Steroid-responsive meningitis-arteritis; MRI, magnetic resonance imaging; CSF, cerebrospinal fluid; LF, low field; HF, high field; T1W, T1 weighted; T2W, T2 weighted; FAT SAT, fat saturation; STIR, Short tau inversion recovery.

Materials and methods

Case recruitment criteria

The medical records of dogs from 2 veterinary institutions (the Veterinary Teaching Hospital of the University of Padua and the AniCura Portoni Rossi Veterinary Hospital) were searched from August 2008 to November 2021 for dogs with a diagnosis of SRMA. Dogs were included if the following criteria were fulfilled: a diagnosis of cervical SRMA, results of CSF analysis, and MRI of the cervical spine available for re-evaluation. Eventual cases with a diagnosis of SRMA in spite of a normal CSF were excluded and discussed separately. For dogs that had a second presentation during the study period the relative medical record and cervical MRI were similarly reviewed.

Medical records review

Details regarding signalment (breed, sex and age) and history (duration of clinical signs and pharmacological treatments in a 10-day time span before referral) were recorded. The results of the neurological examinations were reviewed and the following parameters were considered: cervical pain and stiffness, stiff gait, paresis, ataxia, and cranial and spinal nerve deficits. When available, body temperature was reviewed considering a temperature higher than 39.5°C as pyrexia.

TABLE 1 Key to T1/T1 FAT-SAT contrast enhancement rating for each cervical structure analyzed in the study.

Score / Structure	0	1	2
Meninges	No contrast enhancement	Mild and incomplete enhancement of the meningeal ring	Marked and complete enhancement of the meningeal ring
Nerve roots	No contrast enhancement or periradicular blood vessels enhancement	Mild nerve roots enhancement	Marked nerve roots enhancement
Synovium of the articular facets	No contrast enhancement	Mild synovial enhancement	Marked synovial enhancement
Muscles	No contrast enhancement	Mild muscular enhancement	Marked muscular enhancement

Response to the treatment was also noticed, when the follow-up was available.

CSF analysis review

Cases with no CSF differential count were excluded. Cell count (White Blood Cells (WBC)/μL), neutrophil percentage and albumin concentration were assessed. The reference intervals for CSF parameters are reported elsewhere (15). Samples were divided in four classes based on the increased cell count (>500, 101–500, 31–100, 6–30 WBC/μL); four classes based on neutrophil percentage (>60, 31–60, 10–30, <10%) and four classes based on albumin concentration (>300, 101–300, 30–100, <30 mg/dL).

MR images review

MRI studies were performed under general anesthesia with a LF (0.22 Tesla) MRI scanner (MrVet, Paramed Medical Systems, Genoa, Italy) from August 2008 to March 2018 and with a HF (1.5 Tesla) MRI scanner (Vantage Elan, Canon Medical Systems Europe B.V., Netherlands) from April 2018 to November 2021. To be included in the study and considered for re-evaluation, MRI had to include at least pre- and post-administration of a GBCA T1W images, either with or without fat suppression (T1W FAT-SAT), acquired in transverse and sagittal planes, as well as T2W or STIR images in the transverse plane.

All MRI studies were reviewed by two veterinarians alongside a board-certified neurologist using a DICOM viewer (2020 Horos Project™). The post-processing subtraction technique was used on T1W images to highlight contrast agent uptake. Comparison between T1W and T1W FAT-SAT images, as well as between T2W and STIR images, was then made to highlight differences in post-contrast enhancement and muscular hyperintensity, respectively.

To evaluate the extent of the meningeal contrast agent uptake, MR images in both transverse and sagittal planes were evaluated. A thick and long (over more contiguous images) enhancement of the meninges was considered suggestive of meningeal inflammation. Contrast agent uptake of nerve roots, synovium of the articular facets and paravertebral muscles was only analyzed in the transverse plane. For each structure a subjective score from 0 to 2 was assigned by each observer at the level of both the vertebral body (from C1 to C7) and the intervertebral space (from C1-C2 to C6-C7), based on the degree of contrast enhancement (Table 1). A similar score was assigned at the same levels, based on T2/STIR muscle hyperintensity, with scores 0, 1 and 2 meaning absent, mild and marked muscular hyperintensity, respectively. Spinal cord parenchyma contrast enhancement was recorded, if present. Each MRI study was then labeled for each structure as 0 if no contrast enhancement was present, as 1 if contrast enhancement was present at least in one cervical level. Finally, MRIs were globally classified based on the distribution of T1 contrast enhancement as absent or involving one or more of the following cervical structures: meninges, synovium of the articular facets, and muscles.

All the observers were aware of all data available in the medical reports. Images were independently analyzed by each observer. At each level, for a given structure to be labeled as "enhancing," all the observers had to agree about the presence of the enhancement. Relatively to the entity of the enhancement, a discussion was carried on until a consensus between observers was reached.

A comparison of the above parameters between studies conducted with LF and HF MRI was then made to highlight possible differences due to the different magnetic strength.

Crossmatch between CSF and MR images

The degree of meningeal enhancement seen in MRI, as well as the distribution of enhancement among cervical structures, were matched with CSF cell count to determine any potential correlation, as a whole and then separately for each type of MRI.

Statistical analyses

Numerical variables are presented as median, interquartile range (IQR) and range. Categorical variables are summarized as

10.3389/fvets.2022.957278

TABLE 2 Breeds included in the study.

Breeds	Number (%)
Boxer	14 (20.6%)
Mixed breed dog	14 (20.6%)
Bernese mountain dog	10 (14.7%)
Weimaraner	6 (8.8%)
Beagle	4 (5.9%)
Golden retriever	3 (4.4%)
Dachshund, pitbull terrier	2 (2.9%)
Border collie, bull mastiff, dogo argentino, german shepherd dog, labrador retriever, maremma sheepdog, nova scotia duck tolling retriever, pembroke welsh corgi, pointer, poodle, schnauzer, spitz, whippet	1 (1.47%)

counts and percentages. Statistical analysis was performed with the statistical software MedCal® (Version 12.6.1.0, Software bvba). A p-value <0.05 was considered significant for all tests. A two proportion z-test for equality of two percentages was performed to (1) evaluate if a significant difference was present between LF and HF MRI in the detection of meningeal, nerve root, synovium of the articular facets, muscle, and spinal cord parenchyma enhancement; (2) evaluate if a significant difference was present between the incidence of synovium of the articular facets enhancement and muscular enhancement using LF and HF MRI and (3) estimate if the increased conspicuity of the meningeal contrast uptake shown through the subtraction technique with LF MRI was significantly different compared to that seen with HF MRI. A Kruskal-Wallis non-parametric test was performed to evaluate if significant differences were present between the CSF cell count in the three MRI groups based on the degree of meningeal enhancement (0 = absent, 1 = mild, 2 = marked), both on the total number of MRI and then on the LF and HF MRI individually. Cases were then grouped depending on the distribution of enhancement between cervical structures, and their CSF cell count distribution was studied with a Kruskal-Wallis non-parametric test, both on the total number of MRI and on LF and HF MRI separately. Three MRI patterns of enhancement were identified for this test: cases with meningeal and synovium of the articular facets and/or muscular enhancement (group 1), cases with meningeal enhancement alone (group 2), and cases with synovium of the articular facets and/or muscular enhancement but without meningeal enhancement (group 3).

A Fisher exact test was performed to analyze if meningeal enhancement on MRI was predictive of CSF abnormality (2 × 2 contingency table). In this test the cases with normal CSF were also included.

Results

Case recruitment criteria

Ninety-three cases were included after the first search based on a diagnosis of SRMA in the medical records. Of these, 4 cases were excluded because of the absence of a CSF differential cell count, and 17 cases because of an incomplete MRI protocol. Two cases had a normal CSF and were then excluded; they will however be separately discussed. Seventy cases were therefore included in the study. Two dogs fulfilling the inclusion criteria presented twice, therefore results for breed and sex represent a total of 68 dogs.

Medical records review

The most represented breeds were Boxers ($n = 14$; 20.6%), mixed breeds ($n = 14$; 20.6%), and Bernese Mountain Dogs ($n = 10$; 14.7%). Table 2 lists all the breeds included in the study. There were 34 males (50%) and 34 females (50%). Duration of the clinical signs was <4 days in 25 dogs, 4–10 days in 24 dogs, and more than 10 days in 21 dogs. Median duration of the clinical signs before referral was 6.5 days (IQR 11.75; range 1–60 days). Four cases were confirmed relapses based on the CSF analysis and 6 cases were suspected relapses based on the history. Median age at the first presentation was 10 months (IQR 5.5; range 3–67 months). In the 10 day period before referral, 53 dogs (75.7%) had received one or more drugs including glucocorticoids ($n = 9$), non-steroidal anti-inflammatory drugs (NSAIDs) ($n = 27$), opioids ($n = 24$) and antimicrobials ($n = 24$). At neurological examination, 50 dogs (71.4%) had both cervical pain and stiffness, 12 dogs (17.1%) manifested only cervical pain and 4 dogs (5.7%) had only cervical stiffness; in 4 dogs (5.7%) cervical pain or stiffness were not detected on the neurological examination but were reported in the history. Twelve dogs (17.1%) showed paresis and 14 dogs (20%) showed ataxia. Other deficits detected on the neurological examination were: spinal nerve reflex abnormalities ($n = 8$), proprioceptive deficits ($n = 6$), cranial nerve deficits ($n = 3$), and an abnormal menace response ($n = 3$). Body temperature data was available for 32 dogs, 24 of which (75%) were pyretic. Response to the treatment was documented in 57 cases (81.4%) and was reported to be good in all of them.

CSF analysis review

Sixty-three (90%) CSF samples were collected from the cerebellomedullary cistern and 7 (10%) from the lumbar subarachnoid space. Median cell count was 945 WBC/μL

(IQR 1623.75; range 7–6,133 WBC/μL). Forty-five (64.3%) CSF samples showed a very marked pleocytosis, with more than 500 WBC/μL and a median cell count of 1,504 WBC/μL (IQR 1515; range 509-6133 WBC/μL). In 65 (92.9%) samples, more than 60% of the cells were neutrophils, with a median neutrophil percentage of 81% (IQR 15, range 61–98%). The results of CSF analysis (grouped by cell count, neutrophil percentage and albumin concentration) are summarized in Table 3.

TABLE 3 CSF analysis results.

Parameters evaluated	Number (%)
Cell count	
>500 WBC/ μL	45 (64.3%)
101–500 WBC/μL	11 (15.7%)
31–100 WBC/μL	5 (7.1%)
6–30 WBC/μL	9 (12.9%)
Neutrophil percentage	
>60%	65 (92.9%)
31–60%	4 (5.7%)
10–30%	1 (1.4%)
<10%	0 (0.0%)
Albumin concentration	
>300 mg/dL	11 (15.7%)
101–300 mg/dL	9 (12.9%)
30–100 mg/dL	45 (64.3%)
<30 mg/dL	5 (7.1%)

MR images review

Sixty-nine (98.6%) MRI studies showed contrast enhancement of one or more structures. T1W post-contrast images demonstrated enhancement of meninges in 61 cases (87.1%), nerve roots in 10 (14.3%), synovium of the articular facets in 34 (48.6%) and paravertebral muscles in 34 (48.6%). Marked contrast enhancement (score 2) was present in 33 studies (45.8%) in at least one compartment, including meninges ($n = 15$), nerve roots ($n = 3$), synovium of the articular facets ($n = 11$) and paravertebral muscles ($n = 10$) (Figure 1). Moreover, spinal cord parenchymal contrast enhancement was present in 10 studies (14.3%) and was always associated with meningeal enhancement. Distribution of meningeal contrast enhancement in the cervical spine is summarized in Table 4. In the 8 MRI studies where both STIR and T2W sequences were available, muscular lesions were detected in both modalities in 5 cases, even easily detectable on STIR sequence, and were not seen in any in the remaining 3. The 34 cases demonstrating hyperintense muscular areas in either T2W or STIR sequences also showed T1W contrast enhancement of the same areas.

The post-processing subtraction technique increased the conspicuity of the enhancement at the meningeal level in 42 cases (60%) (Figure 2), in the synovium of the articular facets in 7 cases (10%) and in muscles in 1 case (1.4%). The incidence of contrast uptake was 48.6% for both the synovium of the articular facets and muscular structures. MRI patterns of alterations due to T1 contrast enhancement and their distribution between LF and HF MRI are summarized in Table 5.

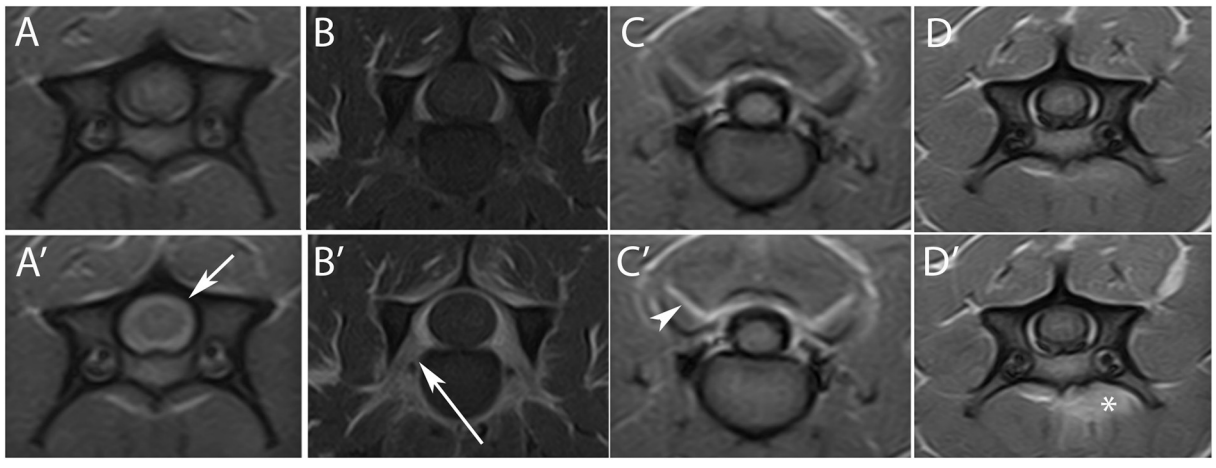

FIGURE 1
Transverse T1W images pre- (upper row) and post- (lower row) contrast agent administration, at level of C4 **(A,A′,D,D′)**, C5–C6 **(B–B′)**, and C2–C3 **(C–C′)**. A marked contrast enhancement is evident at the level of the meninges [**(A′)**—short arrow], nerve roots [**(B′)**—long arrow], synovium of the articular facets [**(C′)**—arrowhead], and muscles [**(D′)**—asterisk].

T1W post-contrast images evaluated separately from the LF (50 cases) and HF (20 cases) MRI demonstrated enhancement of meninges in 45 (90%) and 16 (80%) cases, respectively, nerve roots in 4 (8%) and 6 (30%), respectively, synovium of the articular facets in 21 (42%) and 13 (65%), respectively, paravertebral muscles in 23 (46%) and 11 (55%), respectively, and in the spinal cord parenchyma in 9 (18%) and 1 (5%), respectively. No significant difference was found between LF and HF MRI in the identification of meningeal ($p = 0.463$), synovium of the articular facets ($p = 0.140$), paravertebral muscles ($p = 0.677$), and spinal cord parenchyma ($p = 0.305$) enhancement. A mild significant difference in the identification of nerve root enhancement ($p = 0.046$) was found.

The subtraction technique increased the conspicuity of contrast agent uptake at the level of the meninges in 34 (68%) LF and 8 (40%) HF MRI. In 5 (10%) LF MRI and in 3 (15%) HF MRI, the diagnosis would have been missed without the use of the subtraction technique. However, no significant difference in the utility of the subtraction technique at the level of the meninges was found between LF and HF MRI ($p = 0.059$).

Incidence of contrast uptake in the synovium of the articular facets was 42 and 65% and incidence of muscular contrast uptake was 46 and 55% in LF and HF MRI, respectively. However, no significant difference was found between LF and HF MRI in enhancement detection at the level of either synovium of the articular facets or muscles ($p = 0.140$ and $p = 0.677$).

Seven HF MRI had both T1W and T1W FAT SAT sequences available. In 4 of 5 MRI (80%), in which meningeal enhancement was present, the contrast uptake was seen better on the T1W FAT SAT images. Particularly, in 3 of these 4 cases meningeal enhancement was only easily detectable on T1W images through the application of the subtraction technique, whereas on T1W FAT SAT this was never necessary (Figure 3). Enhancement of the synovium of the articular facets was present in 5 MRI and in 2 (40%) of these the contrast uptake was seen better on the T1W

TABLE 4 Distribution of meningeal contrast enhancement in the cervical spine.

Cervical level	Number (%)
C1	32/63 (50.8%)
C1–C2	36/68 (52.9%)
C2	43/69 (62.3%)
C2–C3	49/70 (70.0%)
C3	53/70 (75.7%)
C3–C4	53/70 (75.7%)
C4	50/70 (71.4%)
C4–C5	48/69 (69.6%)
C5	42/69 (60.9%)
C5–C6	40/69 (58.0%)
C6	38/69 (55.1%)
C6–C7	37/67 (55.2%)
C7	33/63 (52.4%)

For each cervical level, the percentage of cases with meningeal enhancement was calculated based on the number of images available at that level.

TABLE 5 MRI patterns of alterations based on T1 contrast enhancement distribution between cervical structures.

Enhancing structures	Total MRI	Low field MRI	High field MRI
None (normal MRI)	1	1	0
Meninges	16	12	4
Synovium of the articular facets	1	1	0
Muscles	3	2	1
Meninges and synovium of the articular facets	18	13	5
Meninges and muscles	16	14	2
Synovium of the articular facets and muscles	4	1	3
Meninges, synovium of the articular facets and muscles	11	6	5
Total number of cases	70	50	20

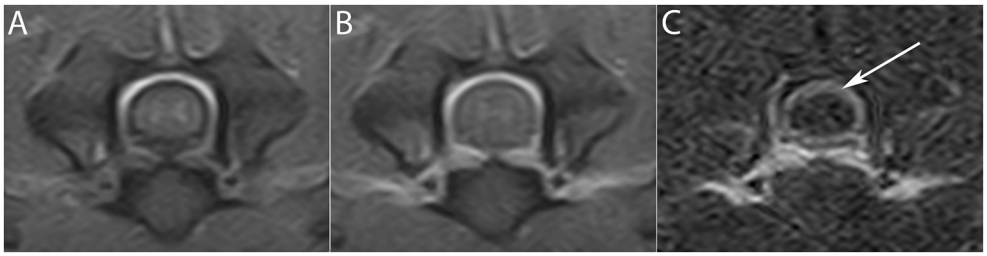

FIGURE 2
Subtraction technique in the detection of meningeal enhancement. **(A)** Pre- and **(B)** post-contrast transverse T1W image at the level of the C5–C6 intervertebral space. After subtraction **(C)**, a subtle meningeal enhancement not easily detectable in **(B)** is seen (arrow).

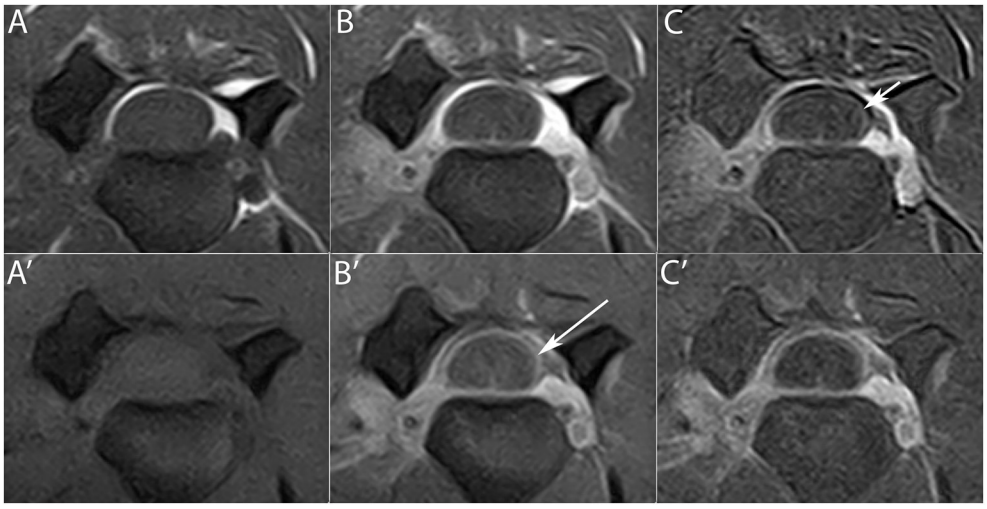

FIGURE 3
Transverse T1W (upper row) and T1 FAT SAT (lower row) images pre- **(A,A')** and post- **(B,B')** contrast administration at the level of the C3–C4 intervertebral space. Meningeal enhancement is visible on the T1W images only with the application of the subtraction technique **(C)** (short arrow), while it is easily detectable in T1W FAT SAT images **(B')** (long arrow). The subtraction technique in T1W FAT SAT images **(C')** is therefore not necessary.

FAT SAT images. In 1 (25%) of the 4 studies in which muscular enhancement was present, the contrast uptake was seen only on the T1W FAT SAT images.

Crossmatch between CSF and MR images

Median CSF cell count of the three groups based on the degree of MRI meningeal enhancement was 39 WBC/μL (IQR 581; range 7–2,341) in group 0, 757 WBC/μL (IQR 1435.8; range 16–6,133) in group 1, and 1,820 WBC/μL (IQR 1951.5; range 156–5,976) in group 2, when all the MRI were considered. When only the LF MRI were considered, median cell count was 111 WBC/μL (IQR 558; range 7–2,341) in group 0, 682 WBC/μL (IQR 1595.8; range 16–6,133) in group 1 and 1,896 WBC/μL (IQR 2,334; range 509–5,976) in group 2. When only the HF MRI were considered, median cell count was 19.5 WBC/μL (IQR 156.5; range 15–620) in group 0, 1206.5 WBC/μL (IQR 1,344; range 35–2,133) in group 1 and 988 WBC/μL (IQR 832; range 156–1,820) in group 2. A significant increase in CSF cell count was found between each of the three groups when all the MRI were considered ($p = 0.001$) (Figure 4A), and between groups 1 and 2 when only the LF MRI were considered ($p = 0.016$) (Figure 4B). No significant differences were found between the groups when only the HF MRI were considered ($p = 0.06$) (Figure 4C).

Median cell count of the three groups based on the MRI distribution of enhancement between cervical structures was 1,136 WBC/μL (IQR 1,554; range 16–6,133) in group 1, 1,262 WBC/μL (IQR 1,707; range 24–5,976) in group 2 and 75 WBC/μL (IQR 581.5; range 15–2,341) in group 3, when all the MRI were considered. When only the LF MRI were considered, median cell count was 1,136 WBC/μL (IQR 2,126; range 16–6,133) in group 1, 1,262 WBC/μL (IQR 1885.5; range 24–5,976) in group 2 and 354 WBC/μL (IQR 940; range 39–2,341) in group 3. When only the HF MRI were considered, median cell count was 1206.5 WBC/μL (IQR 1377.3; range 35–1,820) in group 1, 848 WBC/μL (IQR 1478.3; range 156–2,133) in group 2 and 19.5 WBC/μL (IQR 156.5; range 15–620) in group 3. One case had a normal MRI and was therefore not included in the analysis. A significant decrease in CSF cell count was found between group 1 and group 3, when all MRI were considered ($p = 0.043$) (Figure 5A). No significant differences were found between the groups when only LF (Figure 5B) or HF MRI (Figure 5C) were considered. MRI meningeal enhancement was not predictive of CSF abnormality ($p = 0.260$). MRI and CSF findings are summarized in Table 6.

Discussion

Due to the retrospective nature of this paper, encompassing a 13-year period, a common gold standard diagnostic test for SRMA was not available. The diagnosis of SRMA was made relying not on a single parameter, but on a combination of patient's medical history of cervical pain, neurological examination, MRI and CSF results. Anyway, the white cell differential played an important role: 60% or more neutrophils on CSF cell count were found in all cases but 4. Two of this 4 cases had a considerable neutrophilic pleocytosis (41 and 59%).

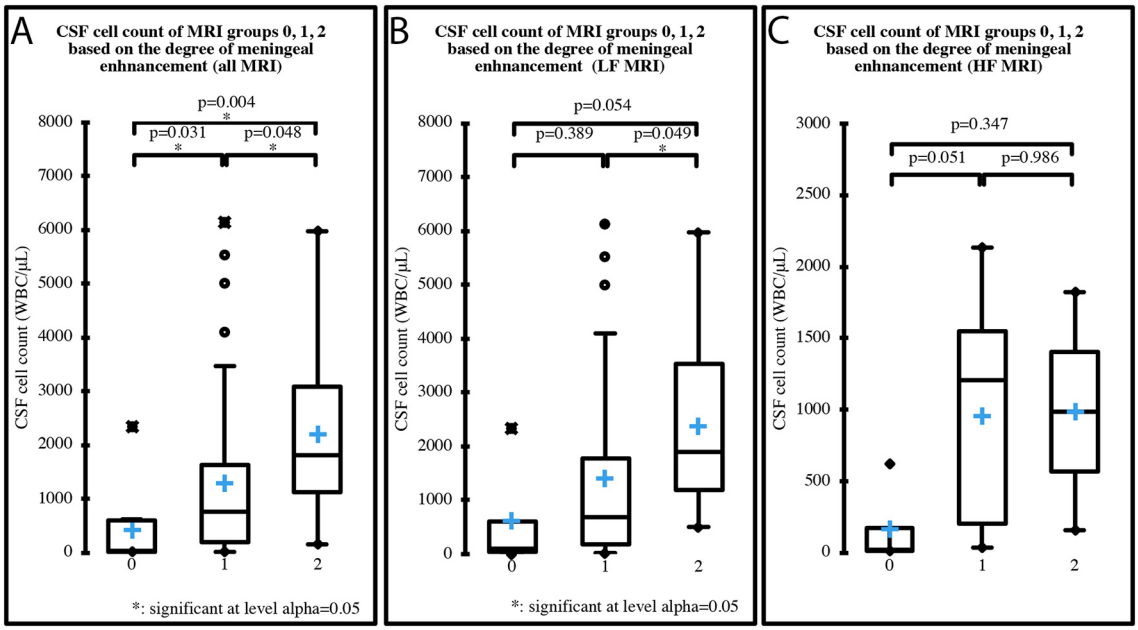

FIGURE 4
CSF cell count distribution in MRI groups based on the degree of meningeal enhancement (group 0 = absent, group 1 = mild, group 2 = marked), analyzing all 70 MRI **(A)**, the 50 LF MRI **(B)** and the 20 HF MRI **(C)**. Boxes contain values from 1st to 3rd quartile, lines inside boxes indicate median values, crosses inside boxes indicate mean values, endpoints of vertical lines are proportional to the interquartile-deviation and dots outside "whiskers" represents outlier values.

The remaining 2 cases had a mixed pleocytosis and a history compatible with the chronic form of the pathology, according to the history and in line with literature (1, 15). These two dogs were also the only ones where the CSF results might be affected by a pre-referral treatment, since a CSF analysis highly compatible with SRMA was found in all others pre-treated dogs. In our population, therefore, a pre-referral treatment did not constitute a diagnostic issue.

Breed distribution in our study reflects what has been previously described (1, 7, 8, 12). Multiple breeds were affected, however Boxers, mixed breed dogs, Bernese Mountain Dogs, Weimaraners and Beagles were overrepresented. Therefore, when clinically consistent, SRMA should be considered as a differential diagnosis regardless of breed. The median age (10 months), the range of age at first presentation (3–67 months), and the absence of a sex predisposition registered in our population reflect what has already been reported in the literature (1, 8). Twenty-five percent of dogs were not pyrexic, indicating that a normal temperature does not rule out SRMA as a differential diagnosis, as has previously been reported (16).

The first aim of our study was to investigate the MRI characteristics of the cervical spine in dogs diagnosed with SRMA. MRI showed abnormalities in 98.6% of cases, suggesting its considerable usefulness. Most of these cases had MRI features suggestive of meningeal inflammation (87.1%), with the cervical site most often affected being the tract between C2-C3 and C4. This finding could help during the acquisition of MRI of the cervical spine. The loss of signal intensity at the borders of the field of view in LF MRI could have biased this result, which therefore has to be considered cautiously. However, even in the studies conducted with HF MRI and characterized by a more homogeneous field of view, the aforementioned tract was the most typical area of contrast agent uptake.

Besides meningeal enhancement, spinal cord parenchymal enhancement was seen in 14.3% of our cases. Median duration of clinical signs before referral of these cases was 9.5 days (IQR 11.25; range 3–60 days) and most of them (8/10) showed deficits at neurological examination, consistent with the reported involvement of the motor and proprioceptive systems in the more chronic form of SRMA (1). However, no parenchymal contrast agent uptake was seen in the remaining 16 cases showing neurological deficits consistent with a cervical localization. Therefore, contrast agent uptake seems to be less useful in detecting parenchymal inflammation than meningeal inflammation, most likely for the less conspicuous vascularization of the parenchyma, which is provided by branches arising from the diffuse plexus present on the surface of the spinal cord (17). Moreover, we cannot exclude an overinterpretation of the neurological findings: sometimes large breed dogs with severe cervical pain show, due to the pain itself, an abnormal gait, that may be misinterpreted as ataxic or paretic.

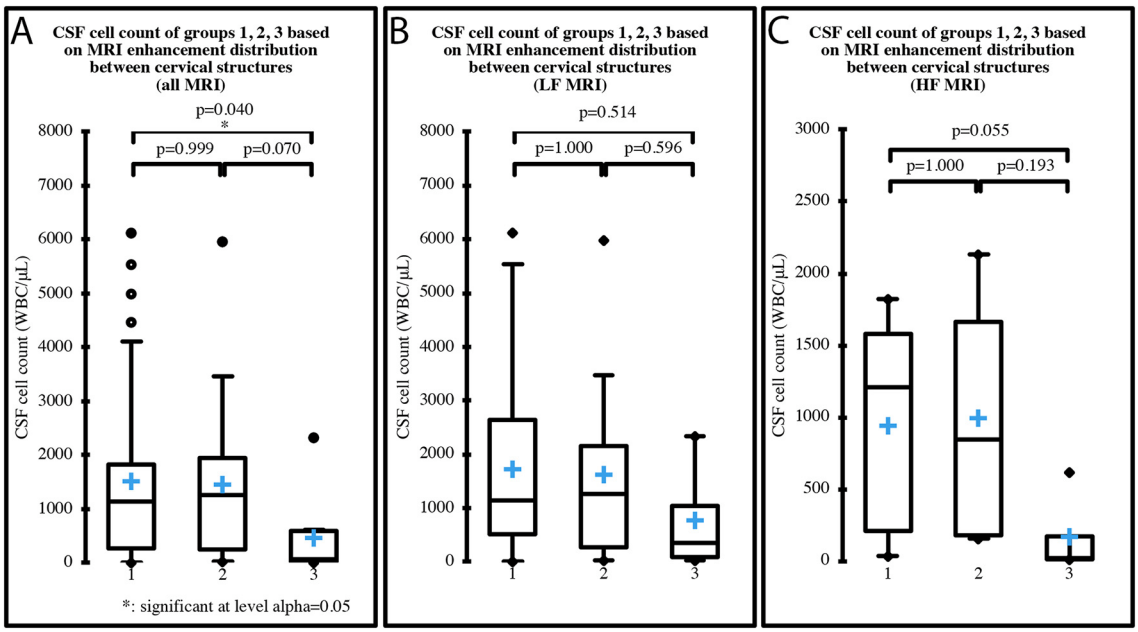

FIGURE 5
CSF cell count distribution in MRI groups based on the distribution of enhancement among cervical structures (group 1 = meningeal enhancement concurrently with synovium of the articular facets and/or muscular enhancement, group 2 = meningeal enhancement alone, group 3 = synovium of the articular facets and/or muscular enhancement). One case had normal MRI and was therefore not included in the analysis, which was performed on all 69 MRI **(A)**, on the 49 LF MRI **(B)** and on the 20 HF MRI **(C)**. Boxes contain values from 1st to 3rd quartile, lines inside boxes indicate median values, crosses inside boxes indicate mean values, endpoints of vertical lines are proportional to the interquartile-deviation and dots outside "whiskers" represents outlier values.

TABLE 6 Crossmatch between MRI findings (columns) and CSF findings (rows).

CSF \ MRI (contrast enhancing structures)	None (normal MRI)	Meninges	Synovium of the articular facets	Muscles	Meninges and synovium of the articular facets	Meninges and muscles	Synovium of the articular facets and muscles	Meninges, synovium of the articular facets and muscles
Cell count								
>500 WBC/µL	0	10	1	0	12	15	2	5
101–500 WBC/µL	0	4	0	1	3	0	0	3
31–100 WBC/µL	0	1	0	1	2	0	0	1
6–30 WBC/µL	1	1	0	1	1	1	2	2
Neutrophil %								
>60%	1	16	1	1	17	15	4	10
31–60%	0	0	0	1	1	1	0	1
10–30%	0	0	0	1	0	0	0	0
<10%	0	0	0	0	0	0	0	0
Albumin concentration								
>300 mg/dL	0	3	0	0	6	2	0	0
101–300 mg/dL	0	2	0	0	2	5	0	0
30–100 mg/dL	1	9	1	3	10	8	4	9
<30 mg/dL	0	2	0	0	0	1	0	2

For each match, the number of cases is reported.

The prevalence of enhancement of the synovium of the articular facets and of the paravertebral muscles in this study was the same for both conditions (48.6%). In veterinary literature SRMA and concomitant immune-mediated polyarthritis or immune-mediated myositis have been reported (11, 12). In one study, 46% of dogs with immune-mediated polyarthritis (IMPA) and spinal hyperesthesia had a CSF analysis consistent with SRMA (12). In that study, none of the dogs with concurrent SRMA and IMPA presented swelling of the appendicular joints or lameness, but inflammation was observed in synovial fluid analysis in 25–100% of the joints evaluated in each dog. As such, synovial fluid analysis has been suggested as a routine procedure in dogs with SRMA (12). The high incidence of enhancement of the synovium of the cervical articular facets detected on MRI in our study reinforces the supposition that polyarthritis could be more frequent than clinically expected.

It has been hypothesized that the pathogenesis of myositis in SRMA may include extension of the meningeal inflammation to the paraspinal muscles through spinal nerve roots (13). All but 4 cases with radicular enhancement in our study had muscular enhancement too, in agreement with this hypothesis. On the other hand, the majority of cases with muscular enhancement did not present a concomitant radicular contrast uptake and so the spread of inflammation through arteries could be hypothesized, which in addition would explain the presence of enhancement in the synovium of the articular facets, and hence the presumed cervical arthritis. In support of this hypothesis, arteritis of variable extent was found in several organs, including muscles, in a histopathologic study of SRMA (11).

In a previous report on inflammatory spinal cord diseases, muscular hyperintensity was seen in most of the cases and was detected better in STIR than in T2W images (13). The suppression of the signal of the adipose tissue ventral to the vertebrae in STIR sequences allows easier identification of muscular inflammation (13). We have seen a similar feature in our population, supporting the inclusion of STIR sequences in the MRI protocol in cases with suspected SRMA to highlight a potential muscular extension of the inflammation.

Contrast enhanced T1W images did not seem to provide more information than T2W images in the detection of idiopathic inflammatory myopathies in humans and dogs (18, 19). Our study identified a similar pattern; the administration of contrast agent always resulted in an enhancement in the T1W sequences in the areas of muscle showing T2W/STIR hyperintensity and never enabled the identification of further areas of putative muscular inflammation. However, other conditions, such as myonecrosis, fatty infiltration, rhabdomyolysis or soft tissue tumors with central necrosis, are associated with increased signal intensity on T2W images and can therefore resemble myositis (19, 20). Consequently, the acquisition of post-contrast T1W images remains essential in the MR investigations of presumed myositis.

Denervated muscles may present T1W contrast enhancement too (21). MRI can help in differentiating myositis from denervation as the former often results in multifocal changes while the latter causes diffuse changes affecting the entire muscle (19). We presume that our findings are consistent with myositis as the majority of cases had multifocal muscular enhancement and, when focal enhancement was found, it never affected the entire muscle.

The post-processing subtraction technique was a considerable aid in detecting subtle meningeal contrast enhancement. The utility of this technique at the spinal level is reported, especially for areas of contrast enhancement that are close to fat, whose bright signal tends to hide pathologic lesions (22, 23). Our findings fully support its application; we would recommend the use of subtraction on MRI of suspected SRMA cases, as the meninges are contiguous to the epidural fat.

The second aim of the present study was to compare the diagnostic capabilities of LF and HF MRI. We did not find any statistical difference between LF and HF MRI regarding the conspicuity of contrast enhancement in the meninges, synovium of the articular facet, muscles or spinal cord parenchyma. It would therefore appear that LF MRI can be used during the work up of cases of SRMA, because the greater spatial resolution of HF MRI is not required for these tissues. LF MRI underperformed in the detection of nerve root inflammation, since the percentage of cases with nerve root enhancement seen in LF MRI was significantly lower than those seen with HF MRI ($p = 0.046$). The conspicuity of contrast media uptake decreases with decreasing field strength (24). This could explain why LF MRI is less useful for detecting enhancement in small structures such as nerve roots.

The acquisition of T1W FAT SAT sequences is generally performed only with HF MRI, because the chemical shift between fat and water is too small in LF MRI to achieve a selective chemical saturation of fat without also producing water saturation (25). Acquisition of these sequences is possible after administration of a contrast agent. The hyperintense signal of the contrast agent is then not confused with the hyperintense signal of the adipose tissue. Thanks to the suppression of the epidural fat, the contrast-enhancing meninges are easily detected when an inflammatory process is present (26). Spectral fat saturation substantially improves the visualization of muscle inflammation as well (19). In this, our findings are consistent with previous studies and benefited from this technique.

In some of our cases, meningeal enhancement was only easily detectable on standard T1W images through the application of the subtraction technique. In the subtraction process the magnetic resonance signal is removed from the final image so that the densities recorded are dependent upon the vascularity of the tissue (27). Since adipose tissue has a low vascularity, fat signal is effectively suppressed with this technique (27), explaining the improved detection of meningeal enhancement.

For satisfactory subtraction studies, the post-contrast T1W sequence should reproduce exactly the cross-sections of tissue shown on the initial unenhanced sequence. A perfect subtraction study is unachievable when any minor movement between pre- and post-contrast scans takes place (27). Minimizing the deleterious effects that movements (respiratory and cardiac) of the anesthetized patient have on images is then an essential issue in the acquisition of MRI (23). To reduce the effects of motion artifact, some studies may require dedicated scanning hardware or software. These are generally present in HF scanners used in veterinary medicine as they are made for the human medical market, but may not be present in LF systems which are typically designed for human extremities, in which motion artifacts are hardly an issue (28). Moreover, the prominence of signal due to motion is reduced by increasing the signal to noise ratio (SNR) which is lower in LF compared to HF MRI (23). Nevertheless, these LF MRI features seem not to have affected the usefulness of subtraction in our study, as this was more frequently useful in LF than in HF MRI. On the contrary, it can be hypothesized that the lower utility of subtraction in HF MRI could be due to the higher spatial resolution (23) and to the higher conspicuity of contrast agent uptake in a higher field strength (24). Anyway, no significant difference was found between the utility of subtraction in LF and HF MRI ($p = 0.059$), therefore its application is always recommended, regardless of the field used.

Comparisons between LF and HF MRI must be interpreted cautiously due to the difference in the number of cases. An overall greater number of cases would have led to a more powerful statistical analysis.

A crossmatch between MRI findings and CSF results was applied in an attempt to establish a possible correlation between the severity of the inflammation detected through CSF analysis and the features of the contrast uptake on MRI.

Meningeal enhancement was not predictive of an abnormal CSF ($p = 0.260$). Since the number of cases with normal CSF was very low ($n = 2$), future studies with a greater number of cases could re-assess this finding.

When only the LF MRI were considered, CSF cell count significantly increased between the group with MRI meningeal score 1 and the group with MRI meningeal score 2; yet when only HF MRI was considered no significant increase was found. Thus, with a LF scanner the more the meninges are inflamed the more the enhancement is visible, while a HF scanner permits identification of the enhancement regardless of the degree of inflammation shown by the CSF analysis. Once again, a possible explanation for this trend could be the higher spatial resolution of HF MRI (23). Moreover, when pooling all the cases from the different types of MRI, CSF cell count significantly increased between all three groups. Then, stronger was the degree of contrast agent uptake in MRI and significantly higher was the cell count at the CSF analysis (Figure 4A). This finding highlights a possible correlation between the degree of meningeal inflammation seen on CSF and on MRI, probably because the increased vascular permeability due to the arteritis can explain both contrast agent leakage and cellular migration from the vascular compartment. Glucocorticoids could reduce the WBC count in CSF by reducing the degree of inflammatory response (15, 29) and a similar effect can be hypothesized for NSAIDs. Cases that received these drugs in our study were split almost proportionally among the three groups based on MRI meningeal score and the majority received a single dose. We therefore believe that it is very unlikely that the statistical results were affected by prior treatments.

In 9 (12.8%) cases there was no meningeal enhancement in spite of an abnormal CSF. The lack of contrast enhancement in inflammatory conditions is well-described in the literature (30–34). It has been supposed there may be a threshold of inflammation above which the disruption of the blood-meningeal barrier is enough to permit the visualization of the contrast enhancement when meningitis is present (35). It is possible that in our 9 cases this threshold was not reached. Indeed, 2 of our dogs received NSAID treatments before referral, 1 received glucocorticoid treatment, and 1 received both. These treatments could have lowered the degree of inflammation below the threshold and justify the lack of contrast enhancement.

Eight of the 9 cases that showed no meningeal enhancement in spite of an abnormal CSF also had concomitant enhancement of the synovium of the articular facets and/or muscular enhancement. The CSF cell count of these dogs was significantly lower than the CSF cell count of cases with synovium of the articular facets and/or muscular enhancement as well as concurrent meningeal enhancement ($p = 0.040$) (Figure 5A), despite a greater percentage of cases belonging to the latter group received glucocorticoid and/or NSAID treatments before referral. Due to these results, we may speculate the existence of cases of SRMA in which the aberrant immune-mediated response is directed more toward non-neurological structures. Different forms of SRMA or, at least, different stages with different tissular targets could therefore exist and future studies are needed to investigate this hypothesis.

According to the initial search of the database, 2 dogs had a diagnosis of SRMA in spite of a normal CSF analysis. Case number 1 was a 22-month-old, female Bernese Mountain Dog, with a previous diagnosis of SRMA 15 months earlier, a neurologic examination suggestive of cervical pain, and meningeal enhancement on MRI. Chronic/relapsing cases may have normal CSF (7, 10, 36), so we believe that this dog was likely affected by a second episode of SRMA, according to the MRI findings.

Case number 2 was a 4-month-old, male Boxer with a history of cervical pain in the absence of deficits at neurological examination, consistent with SRMA. MRI showed enhancement of the synovium of two pairs of articular facets. This dog could then be affected by a primary polyarthritis with cervical involvement (12). Since a concurrent inflammation of the synovium of the articular facets has been observed in 48.6% of

the cases of SRMA in our study, and since CSF analysis can be normal in SRMA (2, 36), we hypothesized that this dog might be affected by a form of SRMA with a concurrent polyarthritis in a stage in which the aberrant immune-mediated response currently does not involve neurological structures.

This study has several limitations, mainly related to its retrospective nature.

The main limitation of the present study is the lack of a common gold standard diagnostic test, mostly due to the long duration of the study, encompassing a 13-year period. The diagnosis of SRMA was made on the basis of a combination of clinical and diagnostic information. The risk that a few cases with other diseases mimicking SRMA were included does exist.

MRI protocols varied through the years and post-contrast transverse images at one or more cervical levels were absent in many studies. This situation might have underestimated the real involvement of the meninges and extra-neural tissue, which could then be greater than we have reported. However, our results are based on the intensity of the contrast enhancement rather than on its extent along the cervical spine, therefore they should not have been altered by incompleteness of the imaging studies. Regarding the interpretation of the images, further limitations of the present study were the lack of a control group and that the observers were not blinded about neurological examination and the results of the clinical-pathological investigations.

A histopathological confirmation of the inflammation is lacking for both neural and extra-neural tissues and the diagnosis of polyarthritis and myositis is always presumed. However, in human beings it is reported that enhancement of the facets' joint rim after contrast agent administration will establish a diagnosis of synovitis (37). Moreover, although a histopathological diagnosis remains the gold standard for the diagnosis of human dermatomyositis, in recent decades the extensive use of MRI has restricted the number of biopsies carried out (38, 39).

Conclusions

Meningeal enhancement is the most frequent diagnostic imaging finding in dogs affected by SRMA, often accompanied by enhancement of the synovium of the articular facets or muscular enhancement. When meningeal enhancement is absent, less marked CSF abnormalities are usually present. Low-field and HF MRI both have a good diagnostic overall capability, although HF MRI enables a more thorough investigation thanks to specific sequences, particularly T1W FAT-SAT, which can readily show meningeal enhancement.

In conclusion, this study highlights the usefulness of MRI as a complementary tool to CSF analysis in the diagnostic work up of SRMA. Furthermore, this study suggests MRI could have a diagnostic role in cases with a normal CSF but a clinical presentation suggestive of this condition. Further prospective studies are needed to complete the description of MRI patterns in SRMA and to more reliably compare LF and HF MRI.

Data availability statement

The original contributions presented in the study are included in the article/supplementary material, further inquiries can be directed to the corresponding author/s.

Ethics statement

Ethical review and approval was not required for the animal study because retrospective study. Written informed consent for participation was not obtained from the owners because retrospective study on routine clinical work-up.

Author contributions

MB designed the study and supervised the study. AV and MB contributed the cases and finalized the manuscript. CR and AM selected and analyzed the cases and wrote the first draft. BC provided the statistical analysis. All authors provided input into the final version of the manuscript, contributed to the article, and approved the submitted version.

Acknowledgments

We would like to thank Jack Amey for revising the English language.

Conflict of interest

The authors declare that the research was conducted in the absence of any commercial or financial relationships that could be construed as a potential conflict of interest.

Publisher's note

References

1. Tipold A, Schatzberg SJ. An update on steroid responsive meningitis arteritis. *J Small Anim Pract.* (2010) 51:150–4. doi: 10.1111/j.1748-5827.2009.00848.x

2. Cizinauskas S, Jaggy A, Tipold A. Long-term treatment of dogs with steroid-responsive meningitis-arteritis: clinical, laboratory and therapeutic results. *J Small Anim Pract.* (2000) 41:295–301. doi: 10.1111/j.1748-5827.2000.tb03205.x

3. Maiolini A, Carlson R, Schwartz M, Gandini G, Tipold A. Determination of immunoglobulin A concentrations in the serum and cerebrospinal fluid of dogs: an estimation of its diagnostic value in canine steroid-responsive meningitis-arteritis. *Vet J.* (2012) 191:219–24. doi: 10.1016/j.tvjl.2010.12.018

4. Biedermann E, Tipold A, Flegel T. Relapses in dogs with steroid-responsive meningitis-arteritis. *J Small Anim Pract.* (2016) 57:91–5. doi: 10.1111/jsap.12418

5. Freundt-Revilla J, Maiolini A, Carlson R, Beyerbach M, Rentmeister K, Flegel T, et al. Th17-skewed immune response and cluster of differentiation 40 ligand expression in canine steroid-responsive meningitis-arteritis, a large animal model for neutrophilic meningitis. *J Neuroinflamm.* (2017) 14:20. doi: 10.1186/s12974-016-0784-3

6. Carletti BE, De Decker S, Rose J, Sanchez-Masian D, Bersan E, Cooper C, et al. Evaluation of concurrent analysis of cerebrospinal fluid samples collected from the cerebellomedullary cistern and lumbar subarachnoid space for the diagnosis of steroid-responsive meningitis arteritis in dogs. *J Am Vet Med Assoc.* (2019) 255:1035–8. doi: 10.2460/javma.255.9.1035

7. Lowrie M, Penderis J, McLaughlin M, Eckersall PD, Anderson TJ. Steroid responsive meningitis-arteritis: a prospective study of potential disease markers, prednisolone treatment, and long-term outcome in 20 dogs (2006–2008). *J Vet Intern Med.* (2009) 23:862–70. doi: 10.1111/j.1939-1676.2009.0337.x

8. Rose JH, Kwiatkowska M, Henderson ER, Granger N, Murray JK, Harcourt-Brown TR. The impact of demographic, social, and environmental factors on the development of steroid-responsive meningitis-arteritis (SRMA) in the United Kingdom. *J Vet Intern Med.* (2014) 28:1199–202. doi: 10.1111/jvim.12360

9. Hansson-Hamlin H, Lilliehook I. Steroid-responsive meningitis arteritis in Nova Scotia duck tolling retrievers. *Vet Rec.* (2013) 173:527. doi: 10.1136/vr.101847

10. Tipold A, Jaggy A. Steroid responsive meningitis-arteritis in dogs: long-term study of 32 cases. *J Small Anim Pract.* (1994) 35:311–6. doi: 10.1111/j.1748-5827.1994.tb03293.x

11. Hayes TJ, Roberts GK, Halliwell WH. An idiopathic febrile necrotizing arteritis syndrome in the dog: beagle pain syndrome. *Toxicol Pathol.* (1989) 17:129–37. doi: 10.1177/019262338901700109

12. Webb AA, Taylor SM, Muir GD. Steroid-responsive meningitis-arteritis in dogs with noninfectious, nonerosive, idiopathic, immune-mediated polyarthritis. *J Vet Intern Med.* (2002) 16:269–73. doi: 10.1111/j.1939-1676.2002.tb02368.x

13. Eminaga S, Cherubini GB, Villiers E, Targett M, Caine A. STIR muscle hyperintensity in the cervical muscles associated with inflammatory spinal cord disease of unknown origin. *J Small Anim Pract.* (2013) 54:137–42. doi: 10.1111/jsap.12035

14. Günther C, Steffen F, Alder DS, Beatrice L, Geigy C, Beckmann K. Evaluating the use of cytosine arabinoside for treatment for recurrent canine steroid-responsive meningitis-arteritis. *Vet Rec.* (2020) 187:e7. doi: 10.1136/vr.105683

15. Di Terlizzi R, Platt SR. The function, composition and analysis of cerebrospinal fluid in companion animals: part II—analysis. *Vet J.* (2009) 180:15–32. doi: 10.1016/j.tvjl.2007.11.024

16. Lau J, Nettifee JA, Early PJ, Mariani CL, Olby NJ, Muñana KR. Clinical characteristics, breed differences, and quality of life in North American dogs with acute steroid-responsive meningitis-arteritis. *J Vet Intern Med.* (2019) 33:1719–27. doi: 10.1111/jvim.15543

17. De Lahunta A, Glass E, Kent M. *Veterinary Neuroanatomy and Clinical Neurology*. 5th ed. Philadelphia: Elsevier (2021).

18. Reimers CD, Schedel H, Fleckenstein JL, Nägele M, Witt TN, Pongratz DE, et al. Magnetic resonance imaging of skeletal muscles in idiopathic inflammatory myopathies of adults. *J Neurol.* (1994) 241:306–14. doi: 10.1007/BF00868438

19. Platt SR, McConnell JF, Garosi LS, Ladlow J, de Stefani A, Shelton GD. Magnetic resonance imaging in the diagnosis of canine inflammatory myopathies in three dogs. *Vet Radiol Ultrasound.* (2006) 47:532–7. doi: 10.1111/j.1740-8261.2006.00181.x

20. Kattapuram TM, Suri R, Rosol MS, Rosenberg AE, Kattapuram SV. Idiopathic and diabetic skeletal muscle necrosis: evaluation by magnetic resonance imaging. *Skeletal Radiol.* (2005) 34:203–9. doi: 10.1007/s00256-004-0881-8

21. Koltzenburg M, Bendszus M. Imaging of peripheral nerve lesions. *Curr Opin Neurol.* (2004) 17:621–6. doi: 10.1097/00019052-200410000-00013

22. Dennis R. Optimal magnetic resonance imaging of the spine. *Vet Radiol Ultrasound.* (2011) 52:72–80. doi: 10.1111/j.1740-8261.2010.01787.x

23. Mai W. *Diagnostic MRI in Dogs and Cats*. Boca Raton: CPC Press Taylor & Francis Group. (2018). doi: 10.1201/9781315121055

24. Lindsey RO, Yetkin FZ, Prost R, Haughton VM. Effect of dose and field strength on enhancement with paramagnetic contrast media. *AJNR Am J Neuroradiol.* (1994) 15:1849–52.

25. Delfaut EM, Beltran J, Johnson G, Rousseau J, Marchandise X, Cotten A. Fat suppression in MR imaging: techniques and pitfalls. *Radiographics.* (1999) 19:373–82. doi: 10.1148/radiographics.19.2.g99mr03373

26. D'Anjou MA, Carmel EN, Tidwell AS. Value of fat suppression in gadolinium-enhanced magnetic resonance neuroimaging. *Vet Radiol Ultrasound.* (2011) 52(1 Suppl 1):S85–90. doi: 10.1111/j.1740-8261.2010.01789.x

27. Lloyd GA, Barker PG, Phelps PD. Subtraction gadolinium enhanced magnetic resonance for head and neck imaging. *Br J Radiol.* (1993) 66:12–6. doi: 10.1259/0007-1285-66-781-12

28. Elliott I, Skerritt GC. *Handbook of Small Animal MRI*. 1st ed. Ames: Wiley-Blackwell (2010).

29. Dewey CW, da Costa RC. *Canine and Feline Neurology*. 3rd ed. Ames: John Wiley & Sons (2016).

30. Cherubini GB, Platt SR, Anderson TJ, Rusbridge C, Lorenzo V, Mantis P, et al. Characteristics of magnetic resonance images of granulomatous meningoencephalomyelitis in 11 dogs. *Vet Rec.* (2006) 159:110–5. doi: 10.1136/vr.159.4.110

31. Granger N, Smith PM, Jeffery ND. Clinical findings and treatment of non-infectious meningoencephalomyelitis in dogs: a systematic review of 457 published cases from 1962 to 2008. *Vet J.* (2010) 184:290–7. doi: 10.1016/j.tvjl.2009.03.031

32. Lowrie M, Smith PM, Garosi L. Meningoencephalitis of unknown origin: investigation of prognostic factors and outcome using a standard treatment protocol. *Vet Rec.* (2013) 172:527. doi: 10.1136/vr.101431

33. Paušová TK, Tomek A, Šrenk P, Belašková S. Clinical presentation, diagnostic findings, and long-term survival time in 182 dogs with meningoencephalitis of unknown origin from central europe that were administered glucocorticosteroid monotherapy. *Top Companion Anim Med.* (2021) 44:100539. doi: 10.1016/j.tcam.2021.100539

34. Coates JR, Jeffery ND. Perspectives on meningoencephalomyelitis of unknown origin. *Vet Clin North Am Small Anim Pract.* (2014) 44:1157–85. doi: 10.1016/j.cvsm.2014.07.009

35. Mathews VP, Kuharik MA, Edwards MK, D'Amour PG, Azzarelli B, Dreesen RG. Dyke award. Gd-DTPA-enhanced MR imaging of experimental bacterial meningitis: evaluation and comparison with CT. *AJR Am J Roentgenol.* (1989) 152:131–6. doi: 10.2214/ajr.152.1.131

36. Lowrie M, Penderis J, Eckersall PD, McLaughlin M, Mellor D, Anderson TJ. The role of acute phase proteins in diagnosis and management of steroid-responsive meningitis arteritis in dogs. *Vet J.* (2009) 182:125–30. doi: 10.1016/j.tvjl.2008.05.001

37. Perolat R, Kastler A, Nicot B, Pellat JM, Tahon F, Attye A, et al. Facet joint syndrome: from diagnosis to interventional management. *Insights Imag.* (2018) 9:773–89. doi: 10.1007/s13244-018-0638-x

38. Maurer B, Walker UA. Role of MRI in diagnosis and management of idiopathic inflammatory myopathies. *Curr Rheumatol Rep.* (2015) 17:67. doi: 10.1007/s11926-015-0544-x

39. Gowdie PJ, Allen RC, Kornberg AJ, Akikusa JD. Clinical features and disease course of patients with juvenile dermatomyositis. *Int J Rheum Dis.* (2013) 16:561–7. doi: 10.1111/1756-185X.12107

frontiers | Frontiers in Veterinary Science

TYPE Case Report
PUBLISHED 14 September 2022
DOI 10.3389/fvets.2022.955758

OPEN ACCESS

EDITED BY
Luisa De Risio,
Linnaeus Veterinary Limited,
United Kingdom

REVIEWED BY
Shinji Tamura,
Tamura Animal Clinic, Japan
Miyoko Saito,
Azabu University, Japan

*CORRESPONDENCE
Federica Tirrito
federica.tirrito@yahoo.it

†These authors share senior authorship

SPECIALTY SECTION
This article was submitted to Veterinary Neurology and Neurosurgery, a section of the journal Frontiers in Veterinary Science

RECEIVED 29 May 2022
ACCEPTED 16 August 2022
PUBLISHED 14 September 2022

CITATION
Di Tosto M, Callegari C, Matiasek K, Lacava G, Salvatore G, Muñoz Declara S, Betti B and Tirrito F (2022) Case report: Atypical and chronic masticatory muscle myositis in a 5-month old Cavalier King Charles Spaniel. Clinical and diagnostic findings, treatment and successful outcome. *Front. Vet. Sci.* 9:955758. doi: 10.3389/fvets.2022.955758

Case report: Atypical and chronic masticatory muscle myositis in a 5-month old Cavalier King Charles Spaniel. Clinical and diagnostic findings, treatment and successful outcome

Martin Di Tosto[1], Carolina Callegari[1†], Kaspar Matiasek[2], Giuseppe Lacava[1], Giovanna Salvatore[1], Sara Muñoz Declara[1], Barbara Betti[1] and Federica Tirrito[1,3*†]

[1]AniCura Istituto Veterinario Novara, Granozzo con Monticello, Novara, Italy, [2]Section of Clinical & Comparative Neuropathology, Ludwig Maximilian University of Munich, Munich, Germany, [3]Studio Veterinario Associato Vet2Vet di Ferri e Porporato, Orbassano, Torino, Italy

Masticatory muscle myositis (MMM) is the second most common inflammatory myopathy diagnosed in dogs, but it is rarely described in puppies. The disease is characterized by the production of autoantibodies against 2M myofibers contained in masticatory muscle, although the cause of this production is still unclear. The aim of the present case report was to describe the clinical presentation, diagnostic findings, treatment, and follow-up of an atypical case of chronic masticatory muscle myositis in a very young dog. A 5-month old Cavalier king Charles Spaniel (CKCS) was presented to the AniCura Istituto Veterinario Novara with a two weeks, progressive history of lethargy and difficulty in food prehension. Neurological examination revealed bilateral masticatory muscle atrophy, mandibular ptosis with the jaw kept open, inability to close the mouth without manual assistance, jaw pain, and bilateral reduction of palpebral reflex and menace reaction; vision was maintained. A myopathy was suspected. Computed tomography (CT), magnetic resonance imaging (MRI), enzyme-linked immunosorbent assay test for 2M antibodies, and histopathological examination of masticatory muscle biopsy confirmed the diagnosis of MMM. Glucocorticoids treatment was started and clinical signs promptly improved. To the authors' knowledge, this is the first case describing mandibular ptosis in a dog affected by chronic MMM, successfully managed with medical treatment and the first report describing the CT and MRI findings in a young CKCS affected by MMM.

KEYWORDS

CKCS, CT, dog, masticatory muscle myositis, MRI

Introduction

Masticatory and limb muscles have the same embryonic precursor and are composed by type 1 and type 2 myofibers (1). One feature of masticatory muscle is the presence of type 2M fibers and a type 1 fiber variant (1–6). However, the masticatory muscle formed by type 2M fibers and a type 1 fiber variant are the temporalis muscle, masseter muscle and pterygoid (lateral and medial) muscles; interestingly, digastricus muscle is the only masticatory muscle that does not have type 2M fibers and a type 1 fiber variant (4, 5, 7). Masticatory muscle myositis (MMM) is one of the most common inflammatory myopathy of the dog (3, 8). MMM have an immune-mediated origin in which autoantibodies against the type 2M fibers are produced. The etiology of this myopathy is still unknown, and one hypothesis is based on molecular mimicry with autoantibodies produced in response to an infectious agent that cross react with self-antigens of 2M myofibers (5). Dogs affected by MMM can be presented for lethargy, jaw pain, hyporexia or anorexia, fever, trismus (jaw muscles spasm with restriction in mouth opening), enophtalmos or exophthalmos, swelling or atrophy of the face (4, 5, 9). Swelling and pain of masticatory muscle are typical of the acute phase, whereas in the chronic phase muscle atrophy is prevalent and masticatory muscle are replaced by fibrous tissue (4). MMM can affect any dog, but a predilection for large breed dogs has been observed and in particular German shepherds, Golden retriever, Labrador retrievers, Doberman pinschers, and Cavalier King Charles Spaniels (CKCS) (4, 5).

The MMM has not an age predisposition (4); however, most dogs with MMM are young adults and the median age of onset is 3 years, but diagnosis of MMM has also been reported in CKCS puppies as young as 4-months (4, 5, 10). The serological test for 2M antibodies has a high sensitivity (80–90%) and specificity (100%) for diagnosis of masticatory muscle myositis and is the preferred diagnostic test (5). Diagnostic imaging with computed tomography (CT) and magnetic resonance imaging (MRI) may aid in diagnosis of MMM, revealing swelling in acute phase or atrophy in chronic phase of masticatory muscle, areas of masticatory muscle that present signal changes, and contrast enhancement (4, 11). Histological evaluation of masticatory muscle biopsy is another procedure that may aid in the diagnosis of MMM and, at the same time, is useful in providing information about prognosis (5). In the acute phase, muscle biopsy reveals mixed inflammatory infiltrates associated with myofiber necrosis and phagocytosis, while in the chronic phase muscle biopsies are characterized by fibrous tissue and low cellular infiltration (5, 12). Treatment of MMM is based on the use of immunosuppressive drugs and glucocorticoids are usually the first choice (5, 13). A positive outcome in MMM necessitates early diagnosis and appropriate treatment. In fact, patients treated in the chronic phase of the disease are affected by muscle fibrosis and may carry a worse prognosis, compared to acute phase, for improvement of clinical signs (5). The aims of this study were to report the clinical presentation of a 5-month old CKCS affected by an atypical and chronic form of MMM and to describe CT and MRI abnormalities and follow-up of this unusual case in order to better understand clinical and diagnostic alterations that may be found.

Case description

A 5-month old, intact male CKCS was referred for a two weeks progressive history of lethargy, inability to close the jaw, and difficulty in food prehension. No information on littermates' health was available. Clinical examination revealed lethargy, and mandibular and retropharyngeal lymphadenopathy; no ocular abnormality (e. g. conjunctivitis, enophthalmos or exophthalmos) was present. Neurological examination revealed inability to close the mouth without assistance and concurrent inability to adequately open the jaw (trismus), jaw pain, bilateral reduction of palpebral reflex and menace reaction with incomplete closure of the eyelids; bilateral atrophy of temporal and masseter muscles was also present (Supplementary Video 1). The neurolocalization was neuromuscular; a myopathy was suspected but facial or trigeminal neuropathies could not be excluded because of the incomplete closure of the eyelids and the mandibular ptosis. Blood analysis, serology for infectious diseases (*Dirofilaria immitis, Ehrlichia canis, Leishmania infantum, Borrelia* spp., *Anaplasma phagocytophilum, Babesia canis, Hepatozoon canis, Toxoplasma gondii,* and *Neospora caninum*), fine needle aspiration of lymph nodes, 2M antibodies assay ELISA, CT and MRI of the head and biopsies of temporalis and masseter muscles were performed.

Diagnostic assessment, therapeutic intervention, follow-up and outcome

Hematology and biochemistry evaluation revealed mild anemia (29.1% hematocrit, range 38.3–56.5%), moderate leucocytosis (33.4 K/μL, range 4.9–17.6 K/μL) with mature neutrophilia (28.1 K/μL segmented neutrophils, range 2.94–12.67 K/μL), mild hyperglobulinemia (4.9 g/dL, range 2.4–4.3 g/dL) and hypoalbuminemia (2.3 g/dL, range 2.8–4.3 g/dL), mild elevation of creatine kinase (2126 U/L, range 41–378 U/L), mild increase of aspartate aminotransferase (237 U/L, range 14–159 U/L), and mild elevation of C reactive protein (61.7 mg/L, range 0–10.7 mg/L). Trismus was confirmed because it was not possible to open the dog's mouth during general anesthesia. Lymph node cytology revealed reactive lymphadenopathy. Diagnostic imaging was performed and CT study (64 slices, Optima 660, General

Electric, Milan, Italy) of the head highlighted symmetrical reduction in volume of masseter, temporalis, and pterygoid muscles with moderate contrast enhancement (Figure 1); mandibular and retropharyngeal lymphadenomegaly was also reported. Magnetic resonance imaging study (1.5 Tesla, SIGNA Creator, General Electric, Milan, Italy) of the head revealed symmetric and severe masticatory muscle atrophy. Temporalis, masseter, and pterygoid muscles showed diffuse, bilateral and heterogeneous hyperintensity on T2-weighted, fluid attenuated inversion recovery (FLAIR) and short tau inversion recovery (STIR) images; these muscles appeared isointense on T1-weighted sequences compared to the signal of normal muscles (Figure 2). A strong and diffuse contrast enhancement of the masticatory muscle (with the exception of the digastricus muscle) was present after contrast administration (Figure 2), no signal changes, contrast enhancement or swelling of extraocular muscle were identified (Figure 3); regional lymph nodes appeared enlarged. ELISA test for 2M antibodies was 1:1000 (reference range < 1:100). Serology for infectious diseases was negative with exception of mild positivity for *B. canis* (15.8 U, reference range < 14 U); serology for *B. canis* was repeated two weeks later and ruled out an acute infection. Temporalis and masseter muscle histopathology revealed multifocal, mixed cellular, chronic, moderate to marked myofascitis with myofibrosis and muscle atrophy (Figure 4). Based on clinical signs, imaging and histopathological findings, a diagnosis of an atypical and chronic form of juvenile MMM was made. Prednisolone was started with a dose of 1 mg/kg every 12 h. After two weeks of therapy the dog developed intense glucocorticoids associated side effects (i.e., gastrointestinal signs and severe neutrophilic leucocytosis); for this reason, glucocorticoids were rapidly tapered to 0.5 mg/kg every 24 h and this dose was continued for 3 weeks. At follow-up evaluations, clinical signs of MMM and blood analysis improved: dropped mandible and trismus were no longer present, food prehension was normal, masticatory muscle atrophy improved, and creatine kinase and c-reactive protein levels in serum were within reference range. The dose of prednisolone was further gradually tapered in three months. At three months follow-up, the dog was clinically stable and treatment with glucocorticoids was interrupted. Three months after treatment, the dog showed a mild relapse of clinical signs with reluctance to play with a ball due to difficulty in opening the mouth and mild inappetence; a course of prednisolone (0.5 mg/kg every 24 h) of one month duration was effective in complete resolution of clinical signs. Two months after the last administration of glucocorticoids, the dog did not present any signs of jaw pain or difficulty in food prehension, complete blood exams were unremarkable, and neurological examination was normal with the exception of moderate masticatory muscles atrophy (Supplementary Video 2). ELISA test for 2M antibodies was repeated and the result was negative (test result < 1:100, reference range < 1:100).

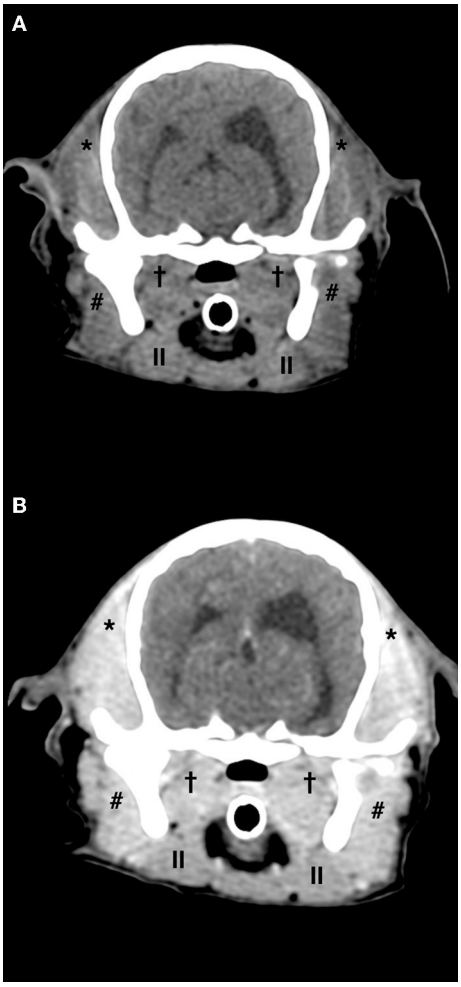

FIGURE 1
Computed tomography pre-contrast **(A)** and post-contrast **(B)** images of the head of a 5-month old Cavalier King Charles Spaniel affected by masticatory muscle myositis. Note the severe, diffuse, and bilateral atrophy of temporalis, masseter, and pterygoid muscles and contrast enhancement of the masticatory muscle in post-contrast image (* temporalis muscle, # masseter muscle, † pterygoid muscle, ‖ digastricus muscle).

Discussion

Masticatory muscle myositis in juvenile CKCS is a rare immune-mediated disorder for which a genetic predisposition has been hypothesized and the classical clinical signs of MMM are trismus, jaw pain and swelling or masticatory muscle atrophy (5). In our case, no information about littermates was known and in addition to the classical clinical signs, a reduction of palpebral reflex and menace reaction, and mandibular ptosis were also encountered. Deficit of palpebral reflex and menace reaction may be the result of orbicularis oculi muscle myopathy or facial neuropathy, anatomical structures that are generally spared in cases of MMM (10, 14). A previous case report of

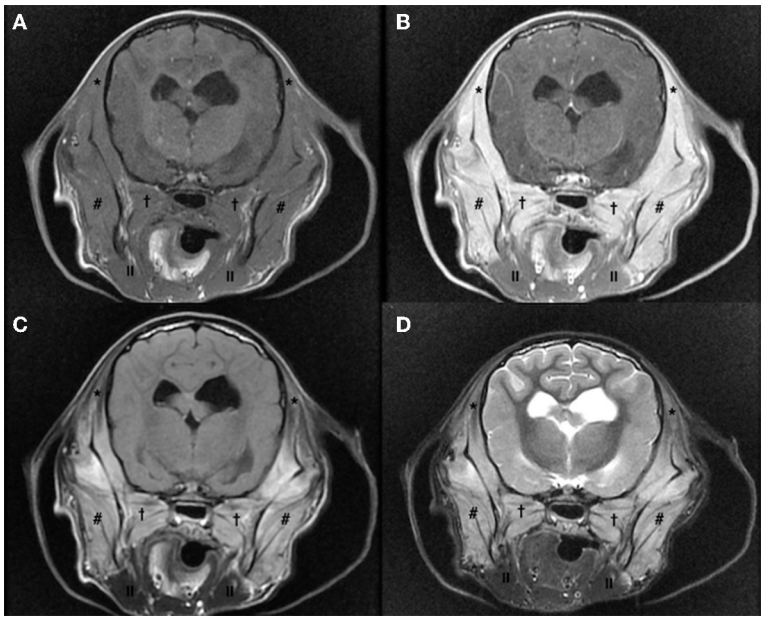

FIGURE 2
Magnetic resonance imaging study of the head of a 5-month old Cavalier King Charles Spaniel affected by masticatory muscle myositis; pre-contrast T1-W image **(A)**, post-contrast T1-W image **(B)**, fluid attenuated inversion recovery (FLAIR) **(C)** and short tau inversion recovery (STIR) **(D)** images. Note the severe, diffuse, and bilateral atrophy of temporalis, masseter, and pterygoid muscles that appear isointense on T1-W images pre-contrast **(A)** and showing a strong contrast enhancement **(B)**; these muscles appear hyperintense on FLAIR **(C)** and STIR **(D)** images, compared to the signal in normal muscles (* temporalis muscle, #masseter muscle, †pterygoid muscle, ||digastricus muscle).

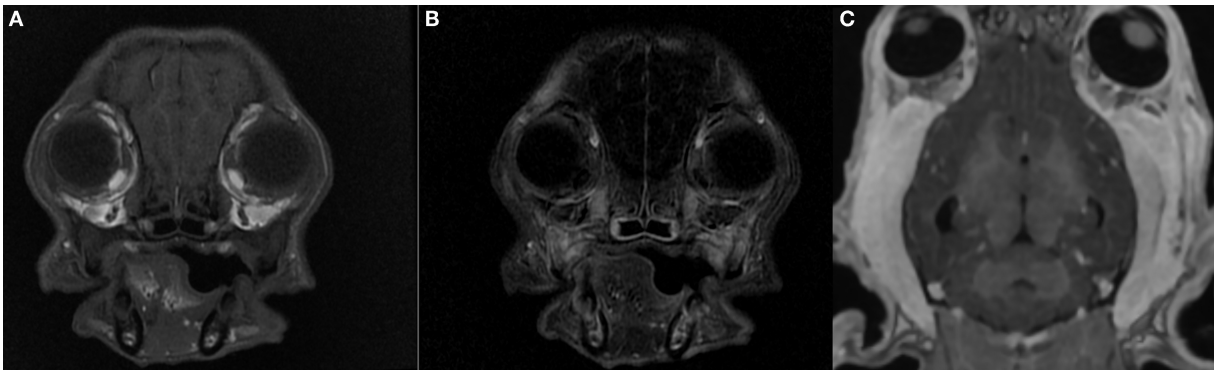

FIGURE 3
Magnetic resonance imaging study of the head of a 5-month old Cavalier King Charles Spaniel affected by masticatory muscle myositis; pre-contrast T1-W image **(A)**, post-contrast T1-W subtraction image **(B)**, pre contrast 3D T1-W image **(C)**. Note the absence of extraocular muscle swelling and contrast enhancement; no evidence of exophthalmos.

CKCS dogs affected by an atypical form of MMM reported the loss of palpebral reflex and menace reaction but MRI study was not performed and the etiology of those clinical signs remained unclear. Ocular signs have also been reported in 44% of dogs affected by MMM; it is because, in the acute phase, the swelling of pterygoid muscle may cause exophthalmos (5). In the present case the dog was affected by a chronic form of MMM and MRI study did not reveal swelling of pterygoid muscle or any abnormalities or signal changes of orbicularis oculi muscle (Figure 3). An electrodiagnostic investigation, not performed in our case, might have helped in clarifying the cause of these clinical signs.

Part of the uncommon clinical presentation of the dog was the concurrent trismus and inability to raise the mandible. Trismus refers to a masticatory muscle spasm causing a reduction in jaw movement (15) and is reported in 41% of

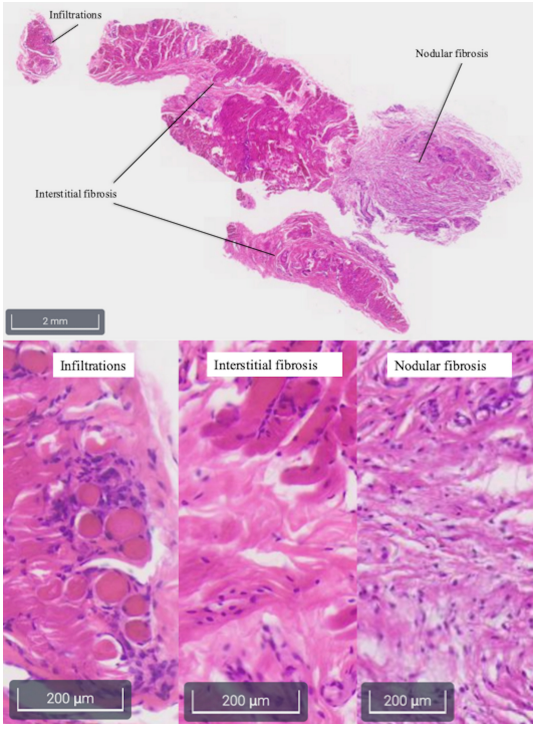

FIGURE 4
Photomicrograph of histological, hematoxylin and eosin stained, section of a temporalis muscle of a 5-month old Cavalier King Charles Spaniel affected by masticatory muscle myositis. Note the inflammatory infiltration and the interstitial and nodular fibrosis of the temporalis muscle.

dogs with MMM, representing one of the main clinical signs in this disease (9). In contrast, the inability to close the mouth without manual assistance has been previously reported only in one dog allegedly affected by MMM; specifically, the dog showed an acute form of masticatory muscle compartmental syndrome due to histiocytic and neutrophilic temporalis muscle myositis with myofiber degeneration and necrosis that caused masticatory muscle dysfunction and inability to close the mouth (16). The authors hypothesized that the compartmental syndrome was the consequence of the masticatory muscle myositis but the diagnosis of MMM was not confirmed since the ELISA test for 2M antibodies was negative (16). Therefore, to the authors' knowledge, this is the first report describing a dropped mandible in a case of confirmed MMM. A possible explanation for this peculiar clinical sign might be a bilateral neuropathy of the trigeminal nerve due to an extension of the disease from the masticatory muscle to the fifth nerve (10). However, this hypothesis was considered unlikely because of the absence of any other fitting clinical signs, besides from the dropped mandible, or of alterations of the trigeminal nerve and trigeminal nucleus reported at the neurological examination and CT and MRI studies, respectively. Another justification for the inability to close the jaw might be the reduced functionality of temporalis, masseter, and pterygoid muscles, whose main task is to close the mouth (17), as a consequence of their inflammation, atrophy, and fibrosis.

MMM has been scantly described in CKCS puppies (10) and previous reports describing CT and MRI findings in dogs affected by MMM have been mainly conducted in other breeds (11, 18, 19); in particular on CT scan, all masticatory muscle besides from digastricus muscle may appear reduced in volume as a consequence of muscle atrophy, and hypoattenuating in pre-contrast scans with inhomogeneous contrast enhancement; regional lymph nodes may appear enlarged with homogenous contrast enhancement (18). MRI however is considered the best imaging modality to identify MMM in dogs, allowing an early detection of the affected muscles (11, 20, 21). MRI findings include iso-hypointense signal of masticatory muscles on T1-weighted images and hyperintense signal of these structures on T2-weighted, FLAIR, and STIR images, compared to the signal of other muscles, contrast enhancement of masticatory muscle is often present (11, 16). CT and MRI findings of our case are similar to those described in the previous literature.

In the present case, glucocorticoids treatment allowed a significant clinical improvement, despite the signs of chronic inflammation. The dog was able to completely open its mouth and most of the masticatory muscle trophism recovered.

Chronic forms of MMM have generally a poor prognosis, based on muscle fibrosis and atrophy; however, restoration of masticatory muscle function has been reported (4, 22). In particular, few reports described young dogs affected by MMM with histopathological evidence of muscle fibrosis and atrophy that regained jaw mobility and masticatory muscle trophism after glucocorticoids treatment (10, 22). An hypothesis for the relevant improvement of clinical signs in young dogs affected by chronic MMM might be that the skeletal muscle resident stem cells have a regenerative capacity and are therefore able to respond to tissue injury, this regenerative capacity may decline with aging (23, 24). However, the relationship between histopathological findings and recovery of masticatory muscle function in younger compared to older dogs needs further investigation. A previous study on juvenile CKCSs affected by an atypical form of MMM also reported progressive clinical improvement and normalization of facial appearance with glucocorticoids; nevertheless, in that study dogs were presented for examination earlier in the course of the disease than the dog of this report (10).

This report described a case of CKCS puppy affected by an atypical form of MMM that showed trismus and concurrent mandibular ptosis and it is interesting to speculate that CKCS puppies may be affected by a breed-specific variant of MMM. To the authors' knowledge, there are no previous reports describing CT and MRI findings of juvenile chronic form of MMM in

CKCS dogs and, based on the present case, it is possible that this form has a similar MRI appearance to the previously reported adult forms of MMM. Young CKCSs with MMM might have a good prognosis with rapid and marked improvement with glucocorticoid treatment, even if presented with signs of chronicity.

Data availability statement

The original contributions presented in the study are included in the article/Supplementary material, further inquiries can be directed to the corresponding author/s.

Ethics statement

Ethical review and approval was not required for the animal study because the authors presented the case of a dog that underwent standard clinical and diagnostic investigations (blood exams, CT and MRI studies of the head, muscle biopsy) approved by the owner and did not perform any experimental treatment. Written informed consent was obtained from the owners for the participation of the animal in this study.

Author contributions

MD, CC, KM, GL, GS, SM, BB, and FT contributed to the conception and design of the study. CC and FT followed all of the clinical aspects of the case. MD and FT wrote the first draft of the manuscript. CC, KM, GL, GS, SM, and BB wrote sections of the manuscript. All authors contributed to the article and approved the submitted version.

Acknowledgments

Presented in part as an oral presentation at the VIII NEUROLATINVET Congress, 2021.

Conflict of interest

The authors declare that the research was conducted in the absence of any commercial or financial relationships that could be construed as a potential conflict of interest.

Publisher's note

Supplementary material

The Supplementary Material for this article can be found online at: https://www.frontiersin.org/articles/10.3389/fvets.2022.955758/full#supplementary-material

References

1. Shelton GD, Cardinet GH. Bandman E. Expression of fiber type specific proteins during ontogeny of canine temporalis muscle. *Muscle Nerve.* (1988) 11:124–32. doi: 10.1002/mus.880110207

2. Shelton GD, Cardinet GH, Bandman E. Canine masticatory muscle disorders: a study of 29 cases. *Muscle Nerve.* (1987) 10:753–66. doi: 10.1002/mus.880100812

3. Evans J, Levesque D, Shelton GD. Canine inflammatory myopathies: a clinicopathologic review of 200 cases. *J Vet Intern Med.* (2004) 18:679–91. doi: 10.1111/j.1939-1676.2004.tb02606.x

4. Castejon-Gonzalez AC, Soltero-Rivera M, Brown DC, Reiter AM. Treatment outcome of 22 dogs with masticatory muscle myositis (1999–2015). *J Vet Dent.* (2018) 35:281–9. doi: 10.1177/0898756418813536

5. Melmed C, Shelton GD, Bergman R, Barton C. Masticatory muscle myositis: pathogenesis, diagnosis, and treatment. *Compendium Continuing Edu Practis Vet North Am Ed.* (2004) 26:590–605.

6. Orvis J, Cardinet III GH. Canine muscle fiber types and susceptibility of masticatory muscles to myositis. *Muscle Nerve.* (1981) 4:354–9. doi: 10.1002/mus.880040411

7. Bubb WJ, Sims MH. Fiber type composition of rostral and caudal portions of the digastric muscle in the dog. *Am J Vet Res.* (1986) 47:1834–42.

8. Shelton GD. From dog to man: the broad spectrum of inflammatory myopathies. *Neuromuscul Disord.* (2007) 17:663–70. doi: 10.1016/j.nmd.2007.06.466

9. Gatineau M, El-Warrak AO, Marretta SM, Kamiya D, Moreau M. Locked jaw syndrome in dogs and cats: 37 cases (1998–2005). *J Vet Dent.* (2008) 25:16–22. doi: 10.1177/089875640802500106

10. Pitcher GD, Hahn CN. Atypical masticatory muscle myositis in three cavalier King Charles spaniel littermates. *J Small Anim Pract.* (2007) 48:226–8. doi: 10.1111/j.1748-5827.2006.00242.x

11. Cauduro A, Paolo F, Asperio RM, Rossini V, Dondi M, Simonetto LA, et al. Use of MRI for the early diagnosis of masticatory muscle myositis. *J Am Anim Hosp Assoc.* (2013) 49:347–52. doi: 10.5326/JAAHA-MS-5915

12. Paciello O, Shelton GD, Papparella S. Expression of major histocompatibility complex class I and class II antigens in canine masticatory muscle myositis. *Neuromuscul Disord.* (2007) 17:313–20. doi: 10.1016/j.nmd.2007.01.012

13. Podell M. Inflammatory myopathies. *Vet Clin North Am Small Anim Pract.* (2002) 32:147–67. doi: 10.1016/S0195-5616(03)00083-4

14. De Lahunta A, Glass E, Kent M. *Veterinary Neuroanatomy and Clinical Neurology 4th Edition*. St. Louis: Elsevier Editor (2015). Chapter 6, p. 162–196.

15. Tveterås K, Kristensen S. The aetiology and pathogenesis of trismus. *Clin Otolaryngol Allied Sci.* (1986) 11:383–7. doi: 10.1111/j.1365-2273.1986.tb00141.x

16. Cray MT, Spector DI, West CL. Acute masticatory muscle compartmental syndrome in a dog. *J Am Vet Med Assoc.* (2018) 253:606–10. doi: 10.2460/javma.253.5.606

17. Hermanson JW. The Muscular System. In: Evans HE, De Lahunta A, editors. *Miller's Anatomy of the Dog 4th Edition*. St. Louis: Elsevier Editor (2013). p. 185–280.

18. Reiter AM, Schwarz T. Computed tomographic appearance of masticatory myositis in dogs: 7 cases (1999–2006). *J Am Vet Med Assoc.* (2007) 231:924–30. doi: 10.2460/javma.231.6.924

19. Bishop TM, Glass EN, De Lahunta A, Shelton GD. Imaging diagnosis—masticatory muscle myositis in a young dog. *Vet Radiol Ultrasound.* (2008) 49:270–2. doi: 10.1111/j.1740-8261.2008.00364.x

20. Platt SR, McConnell JF, Garosi LS, Ladlow J, de Stefani A, Shelton GD. Magnetic resonance imaging in the diagnosis of canine inflammatory myopathies in three dogs. *Vet Radiol Ultrasound.* (2006) 47:532–7. doi: 10.1111/j.1740-8261.2006.00181.x

21. Schulze M, Kötter I, Ernemann U, Fenchel M, Tzaribatchev N, Claussen CD, et al. findings in inflammatory muscle diseases and their noninflammatory mimics. *AJR Am J Roentgenol.* (2009) 192:1708–16. doi: 10.2214/AJR.08.1764

22. Nanai B, Phillips L, Christiansen J, Shelton GD. Life threatening complication associated with anesthesia in a dog with masticatory muscle myositis. *Vet Surg.* (2009) 38:645–9. doi: 10.1111/j.1532-950X.2009.00515.x

23. Lei H, Yu B, Huang Z, Yang X, Liu Z, Mao X, et al. Comparative analysis of mesenchymal stem cells from adult mouse adipose, muscle, and fetal muscle. *Mol Biol Rep.* (2013) 40:885–92. doi: 10.1007/s11033-012-2129-3

24. Sousa-Victor P, García-Prat L, Serrano AL, Perdiguero E, Muñoz-Cánoves P. Muscle stem cell aging: regulation and rejuvenation. *Trends Endocrinol Metab.* (2015) 26:287–96. doi: 10.1016/j.tem.2015.03.006

frontiers | Frontiers in Veterinary Science

TYPE Case Report
PUBLISHED 06 October 2022
DOI 10.3389/fvets.2022.958390

OPEN ACCESS

EDITED BY
Andrea Tipold,
University of Veterinary Medicine Hannover, Germany

REVIEWED BY
Andrea Fischer,
Ludwig Maximilian University of Munich, Germany
Fabio Stabile,
Southfields Veterinary Specialists, United Kingdom

*CORRESPONDENCE
Devon W. Hague
hague@illinois.edu

SPECIALTY SECTION
This article was submitted to Veterinary Neurology and Neurosurgery, a section of the journal Frontiers in Veterinary Science

RECEIVED 31 May 2022
ACCEPTED 29 August 2022
PUBLISHED 06 October 2022

CITATION
Graham LT, Vitale SN, Foss KD, Hague DW, Anderson KM and Maddox CW (2022) Canine brucellosis in three littermates, case report. *Front. Vet. Sci.* 9:958390. doi: 10.3389/fvets.2022.958390

Canine brucellosis in three littermates, case report

Lindsey T. Graham[1], Samantha N. Vitale[1], Kari D. Foss[1], Devon W. Hague[1]*, Kimberly M. Anderson[2] and Carol W. Maddox[3]

[1]Department of Veterinary Clinical Medicine, College of Veterinary Medicine, University of Illinois Urbana-Champaign, Urbana, IL, United States, [2]Department of Small Animal Clinical Sciences, College of Veterinary Medicine, University of Tennessee, Knoxville, TN, United States, [3]Department of Pathobiology, College of Veterinary Medicine, University of Illinois Urbana-Champaign, Urbana, IL, United States

Three adult littermates were diagnosed with *Brucella canis, two* of which were diagnosed with discospondylitis. The first littermate, a 2-year-old spayed-female Labrador Retriever, was evaluated for progressive episodes of cervical pain, lethargy, reported circling to the right, and a right-sided head tilt. Magnetic resonance imaging (MRI) of the cervical spine revealed changes consistent with discospondylitis at C6-C7. MRI of the brain was unremarkable and cerebrospinal fluid analysis was declined. *Brucella* spp. was isolated from aerobic and Brucella blood cultures. PCR performed on the isolate identified *Brucella canis* and indirect fluorescent antibody (IFA) testing for *Brucella canis* also confirmed the species. Patient #1 was treated with doxycycline and marbofloxacin for 1 year. Clinical signs returned 2-years after diagnosis. Following the diagnosis of patient #1, a known littermate (patient #2) was tested for *Brucella canis*. Patient #2 was 2 years old and asymptomatic at the time of diagnosis. Aerobic and *Brucella* spp. cultures, PCR, and IFA were obtained and were diagnostic for *Brucella canis.* A 6-month course of marbofloxacin and doxycycline was implemented. The patient remained PCR positive following 4 months of treatment and repeat cultures were planned following 6 months of treatment; however, the patient was lost to follow-up. A third littermate (patient #3) was identified by the family of patient #1. Patient #3 was evaluated at 18 months of age for a 6-month history of progressive lumbosacral pain. Spinal radiographs revealed discospondylitis of the C3-C4, T12-T13, and L7-S1 vertebral endplates. Computed tomography (CT) of the lumbosacral spine was also consistent with discospondylitis at L7-S1. *Brucella canis* serologic testing consisting of rapid slide agglutination test, 2ME-rapid slide agglutination test, and cytoplasmic agar gel immunodiffusion was positive. Enrofloxacin was administered for 7 months and was discontinued thereafter based on radiographic evidence of healing and resolution of clinical signs. Although *Brucella canis* is not a rare disease in dogs, the documentation of two out of three adult littermates with associated discospondylitis is an interesting feature. In addition, this report highlights available diagnostic and treatment options, as each patient was managed differently based on clinical signs and the preference of the managing clinician.

KEYWORDS

***Brucella canis*, discospondylitis, marbofloxacin, rapid slide agglutination test, magnetic resonance imaging, case report**

Introduction

Discospondylitis is a primary infection of the vertebral endplates with secondary extension into the intervertebral disc space (1–3). A majority of cases develop when an infectious organism spreads hematogenously to a vertebral endplate; however, in rare instances, the infection may start within the intervertebral disc and spread to the adjacent endplates (1). The most common bacterial species isolated is *Staphylococcus*; however, *Streptococcus*, *E. coli*, and *Brucella canis* have been identified as causative agents, among others (1–3). In any patient diagnosed with discospondylitis, blood and urine cultures are recommended; however, combined blood and urine culture yield a variable success rate in isolating the causative agent, ranging from 30 to 78% (2). Fluoroscopically guided percutaneous intervertebral disc aspiration has shown to be a valuable method of obtaining culture samples in patients with discospondylitis, especially in dogs with negative blood and urine cultures (4). Although known to be a cause of discospondylitis, *Brucella canis* is an uncommon bacterial isolate. In a retrospective study evaluating 135 dogs with discospondylitis, *Brucella canis* was deemed to be the causative agent in 14 dogs (5); although due to the difficulty in isolating the organism, this may have been an underestimation (6, 7). Serologic testing consisting of rapid slide agglutination test (RSAT), 2-mercaptoethanol rapid slide agglutination test (2ME-RSAT), and cytoplasmic agar gel immunodiffusion (AGID-cp) is a commonly utilized diagnostic method. RSAT is considered the most sensitive serologic test but may yield false positives (6). When RSAT is positive, a more specific 2ME-RSAT is recommended. AGID is the preferred confirmatory test when RSAT and 2ME-RSAT are positive (5–7). Tube agglutination testing (TAT), microagglutination testing (MAT), indirect fluorescent antibody (IFA) testing, and enzyme-linked immunosorbent assay (ELISA) are additional serologic tests that have also been performed for the diagnosis of *Brucella canis* (7).

To our knowledge, this is the first report of *Brucella canis* being isolated from multiple adult littermates, two of which were diagnosed with discospondylitis. While there is another case report documenting *Brucella canis* in two littermate puppies, both puppies were subclinical (8). Outbreaks of *Brucella canis* have also been documented within breeding kennels in various countries, though affected littermates were not specifically identified (9–11). This case report describes the diagnostic and treatment methods used in three adult littermates with *Brucella canis*, and the challenges to eliminate the infection. Out of the three littermates, two were diagnosed with discospondylitis, which serves as a reminder to consider *Brucella canis* in any dog with discospondylitis, regardless of age or neuter status.

Case descriptions, diagnostic interpretation, and therapeutic intervention

Patient #1

Patient #1, a 2-year-old spayed female Labrador Retriever, presented to the University of Illinois Veterinary Teaching Hospital for episodes of cervical pain and lethargy, which were first noted at 7 months of age. The episodes progressed to include circling to the right and a right-sided head tilt. Each episode lasted a few days in duration followed by complete resolution. Clinical signs were initially managed with carprofen (Rimadyl®; Zoetis, Kalamazoo, MI) at 1.6 mg/kg PO q12h and methocarbamol (Robaxin®; Zoetis, Kalamazoo, MI) at 16 mg/kg PO q12h. Approximately 3 months before the initial neurologic evaluation, the patient experienced another episode, during which a brief period of presumptive nystagmus was noted. Due to concerns of increased discomfort, gabapentin (10 mg/kg PO q8h) was prescribed. Video evidence of the nystagmus and circling episodes was unavailable. Due to the increase in severity and duration of clinical signs, the patient was referred for further evaluation. Upon presentation, the patient's physical and neurologic examinations were unremarkable. To yield the most useful diagnostic information, all medications were discontinued and the clients were instructed to return during the next episode for further evaluation and neurodiagnostic workup. The patient represented 6 weeks later as the signs returned and had been present for 10 days in duration. At this time, the neurologic exam revealed a slight right-sided head tilt (estimated 10–15 degrees), neck guarding with muscle fasciculations, and decreased range of motion in the dorsal direction. The remainder of the neurologic exam was unremarkable. Positional nystagmus was not appreciated during either of the examinations. Based on the examination findings, a problem affecting the cervical spine was considered. This could include pathology of the bones and/or soft tissues surrounding the cervical spine, pain from meningitis, or compressive spinal cord disease. While the patient did not demonstrate changes to support myelopathy, one consideration for the reported episode of nystagmus was pathology along the medial vestibulospinal tract within the parenchyma of the cervical spinal cord. An alternative consideration was an additional lesion in the central or peripheral vestibular system, though no other vestibular signs other than the head tilt, which can manifest in patients with cervical discomfort or vestibular dysfunction, were observed.

Based on this patient's examination findings and history, magnetic resonance imaging (MRI) of the brain and cervical spine was recommended. Before MRI, a venous blood gas, packed cell volume, and total solids were performed and were unremarkable. MRI of the cervical spine and brain was performed using a 3.0 Tesla magnet (MAGNETOM®

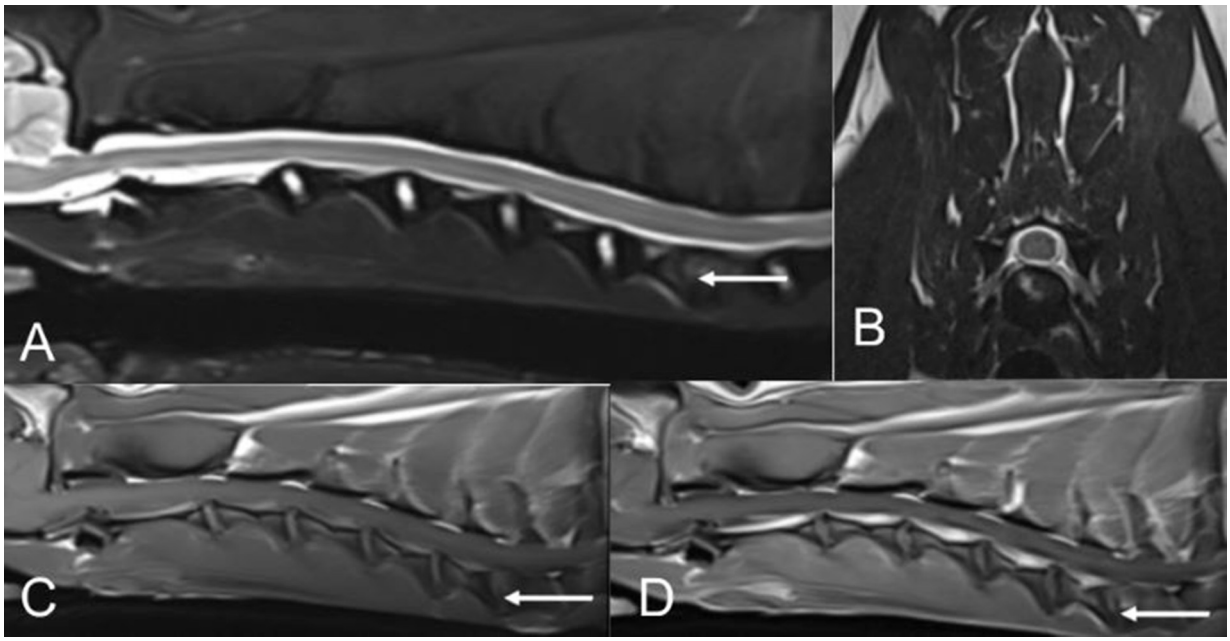

FIGURE 1
MR images of the cervical spine from patient #1. **(A,B)** T2W sagittal and T2W transverse (at the level of the C6-C7 intervertebral disc space). **(C)** T1W sagittal pre-contrast. **(D)** T1W sagittal post-contrast.

Skyra, Siemens. Munich, Germany). Results of the cervical MRI revealed T2W hyperintensity, T1W mixed hypo-iso-intensity, and T1W post-contrast enhancement of the endplates of the caudal C6 and cranial C7 vertebral bodies with irregularity in the structure of the dorsal aspects of the endplates and the corresponding intervertebral disc (Figure 1). These findings were consistent with discospondylitis of the C6-C7 intervertebral disc space and associated vertebral bodies. The brain appeared unremarkable. A cause for the patient's head tilt, reported circling, and nystagmus was not determined based on these findings. Cerebrospinal fluid (CSF) analysis would have been beneficial and was recommended to evaluate for meningoencephalomyelitis, but the patient's family declined.

A blood sample was aseptically collected and submitted for aerobic, anaerobic, and *Brucella* spp. bacterial cultures. A urine sample was obtained *via* cystocentesis for culture. Pending culture and susceptibility results, generic cephalexin (Aurobindo Pharma, East Windsor, NJ) was prescribed (25 mg/kg PO q12h). Shortly after beginning treatment, the patient became increasingly painful, prompting the addition of enrofloxacin (Baytril®; Elanco, Shawnee, KS) at 4.5 mg/kg PO q12h to increase the spectrum of coverage. The patient's clinical signs improved 3 days following this addition.

Aerobic and *Brucella* spp. blood cultures yielded *Brucella* spp. growth. A specific Brucella blood culture, consisting of plating on Brucella agar with 5% sheep blood, in addition to routine blood culture was performed. Polymerase chain reaction (PCR) of the isolate and indirect fluorescent antibody (IFA) testing for *Brucella canis* was used to identify the species. All tests were performed at the Veterinary Diagnostic Lab at the University of Illinois College of Veterinary Medicine and were performed by one of the authors (CM). Due to zoonotic potential and state reporting requirements, the state veterinarian was contacted. Following the diagnosis of *Brucella canis*, cephalexin was discontinued and doxycycline (5 mg/kg PO q12h) was administered concurrently with enrofloxacin, pending results of a susceptibility panel. The results of the panel showed that the *Brucella canis* organism was susceptible to marbofloxacin and had intermediate sensitivity to enrofloxacin; therefore, enrofloxacin was discontinued and marbofloxacin (Zeniquin®; Zoetis, Kalamazoo, MI) was prescribed (3.3 mg/kg PO q24h). The panel also showed susceptibility to doxycycline. Based on the favorable response to treatment and susceptibility results, this patient was treated with doxycycline and marbofloxacin for 12 months, and whole blood cultures obtained 6, 12, and 18 months following diagnosis were negative. The patient remained subclinical until ∼26 months following diagnosis, at which time she exhibited similar signs as before diagnosis. IFA for *Brucella canis* was submitted and was positive. Doxycycline and marbofloxacin were restarted, and the patient was lost to follow-up thereafter.

Patient #2

Following the diagnosis of patient #1, the family of patient #2 (who were acquainted with the family of patient #1) was notified and instructed to have patient #2 tested for *Brucella canis*. Patient #2 was not examined by the authors, though was examined by two other services at the same institution within 1 year of diagnosis. Patient #2 had a previous 10-month history of intermittent lumbar and coxofemoral joint pain. Radiographs of the lumbar spine were performed at the onset of signs and were unremarkable. Orthopedic evaluation attributed the joint pain to bilateral hip dysplasia, and no overt neurologic abnormalities were appreciated. In addition to intermittent lumbar and joint pain, this patient developed exophthalmia and a fever 6 months before being diagnosed with *Brucella canis*. A computed tomography (CT) of the head and culture of fluid from the retrobulbar space were consistent with an abscess. *Enterococcus* spp., *Pasturella canis*, and *Actinomyces* spp. were isolated and the abscess resolved following treatment with broad-spectrum antibiotics. After notification of patient #1's diagnosis, blood from patient #2 was submitted for aerobic and *Brucella spp*. cultures, PCR, and IFA. All submitted tests were positive for *Brucella canis* and the state veterinarian was notified. Anaerobic testing was not submitted due to the low clinical suspicion. Patient #2 was asymptomatic at the time of diagnosis. Susceptibility results were similar to those of patient #1; therefore, a 6-month course of marbofloxacin and doxycycline was prescribed. The patient remained PCR positive following 4 months of treatment and repeat cultures were planned following a total of 6 months of treatment. This patient was lost to follow-up before the culture recheck.

Patient #3

A third littermate (patient #3) was identified with the assistance of patient #1's family. Similar to patient #1, patient #3 was diagnosed with *Brucella canis*-associated discospondylitis. Patient #3 was not examined by the authors, though was evaluated and diagnosed at the institution of one of the authors (KA), making records and imaging results accessible. Patient #3 presented to the University of Tennessee College of Veterinary Medicine at ∼18 months of age for a 6-month history of progressive lower back pain when squatting or jumping. Initial neurologic examination revealed hyperesthesia upon lumbosacral palpation and was otherwise unremarkable. In the absence of any other neurologic deficits, a precise neurolocalization was not possible, and a disorder of the lumbosacral region was suspected. Similar to patient #1, an alternative consideration was pathology in the bones, joints, or soft tissues surrounding the lumbosacral spine. Differential diagnoses for this patient included inflammatory disease,

FIGURE 2
Radiographs from of the cervical, thoracolumbar, and lumbosacral spine, and CT of the lumbosacral spine (top to bottom) from patient #3.

congenital malformation, unwitnessed traumatic injury, and less likely neoplasia.

Following patient #3's examination, radiographs of the cervical, lumbar, and thoracic spine were performed and revealed lysis of the vertebral endplates of C3-C4, T12-T13, and L7-S1, consistent with discospondylitis (Figure 2). A CT of the lumbosacral spine was performed. The reason for performing CT only of the lumbosacral spine was unclear upon review of available medical records. The CT scan showed lysis and irregularity within the vertebral endplates at L7-S1, further supporting the diagnosis of discospondylitis (Figure 2). The patient was initially prescribed amoxicillin/clavulanic acid (Clavamox®; Zoetis, Parsippany, NJ) at 23 mg/kg PO q12h. Aerobic and anaerobic whole blood and urine (collected *via* cystocentesis) cultures were submitted in addition to *Brucella canis* serologic testing consisting of RSAT, 2ME-RSAT, and AGID-cp. While no growth was present on blood and urine cultures, all submitted serologic tests were positive for *Brucella canis*. Due to the positive serologic results and low clinical suspicion, fungal testing was not performed. Amoxicillin/clavulanic acid was discontinued in favor of enrofloxacin (5.5 mg/kg PO q24h). Spinal radiographs obtained 3 and 6 months following diagnosis showed evidence of osteoproliferation of the endplates at C3-C4 and L7-S1, while the lesion at T12-T13 remained static. In addition, no new lesions were observed and the patient was reportedly free of clinical signs. Enrofloxacin was administered at the initial dosage for a total of 7 months and was discontinued thereafter. At the time of discontinuation, the patient was asymptomatic and was lost to follow-up thereafter.

Discussion

In this case report, we presented three adult canine littermates who tested positive for *Brucella canis,* two of which were diagnosed with discospondylitis. While a variety of diagnostic tests have been utilized for the detection of *Brucella canis*, it is often difficult to diagnose due to the low and variable number of infected leukocytes in circulation and the organism's tendency to reside in tissues (6, 7). Definitive diagnosis relies on isolating the organism from whole blood or other infected tissues and fluids; however, *Brucella canis* tends to grow slowly and is fastidious for culture (6, 7). In patients #1 and #2, blood cultures were not positive until 5 days of incubation. Based on author (a PhD microbiologist, CM) experience and available literature, Brucella agar and incubation in a 5% CO_2 environment may also be required to encourage growth (12). Due to these diagnostic challenges, a single negative culture may not rule out *Brucella canis* (6, 7, 13) and some authors recommend submitting a series of three blood cultures collected at least 24 h apart before a negative result is confirmed (6). Serology and PCR are additional diagnostic options (7). Some of the most commonly utilized serologic tests include MAT, RSAT, 2-ME RSAT, and AGID. Sensitivity and specificity for MAT, respectively, are 66.7–88.9% and 100% (14, 15). The reported sensitivity and specificity for RSAT are 70.6% and 83.34%. For 2-ME RSAT and AGID, the sensitivity and specificity are 31.8% and 100%, and 52.9% and 100%, respectively (16). IFA is typically used as a screening test due to its high sensitivity, making RSAT the reference test to confirm or rule out positive IFA samples. ELISA has been utilized and sensitivity and specificity vary based on the antigen used (17, 18). While specific PCRs for *Brucella canis* have been developed, the sensitivity and specificity of PCR for *Brucella canis* have not been determined in canine populations (17, 19–21). Furthermore, PCR results may depend on whether patients are bacteremic at the time of sampling, have been treated with recent antibiotics, and whether PCR inhibitors are present in the sample (14, 18). Therefore, serology may be preferred as it can provide more rapid results and is more widely available over PCR.

Discospondylitis generally requires up to a year of antimicrobial treatment, with a reported mean duration of 53.7 ± 45.4 weeks (2) regardless of the etiologic agent. *Brucella canis*-associated discospondylitis tends to be even more challenging to treat as the organism may be harbored in tissues for extended periods of time and despite long-term treatment, and the patient may never clear the infection even after the resolution of clinical signs (5) and seronegative conversion (7). The organism's tendency to recrudesce was exemplified in patient #1 when signs returned over 2 years following initial diagnosis despite chronic treatment with doxycycline and marbofloxacin. *Brucella canis*-associated discospondylitis often requires multiple classes of antibiotics, and historically a combination of tetracyclines and aminoglycosides has been effective in the resolution of clinical signs (1, 5). Combination therapy with doxycycline and rifampicin combined with surgical resection of infected tissues is effective in treating *Brucella suis* in dogs (22). Current World Health Organization recommendations for human brucellosis are combination therapy with either doxycycline and rifampicin or doxycycline and streptomycin (23). As an alternative to combination therapy in dogs, monotherapy with enrofloxacin has demonstrated similar efficacy for *Brucella canis*, preserved fertility, and prevented bacterial dissemination in a group of dogs following a kennel outbreak (9). Based on susceptibility results, marbofloxacin was used in place of enrofloxacin, in patients #1 and #2, who were also treated with doxycycline. Patient #3 was treated with enrofloxacin alone. While treatment with fluoroquinolones has shown some success in managing clinical signs in dogs, judicious use is imperative due to the growing resistance to fluoroquinolones (24, 25). It should be noted that fluoroquinolones were unable to achieve long-term control in our patients as one patient remained bacteremic during treatment and another patient relapsed a year after discontinuation of treatment.

The patients presented in this case report varied from the common presentation of discospondylitis from other causes, being female, and ≤2 years of age at the time of diagnosis.

Males are at least two times as likely as females to be diagnosed with discospondylitis (2, 5), and most patients are middle-aged or older, with a mean age of 6.8 years reported in one study (26) and an odd's ratio highest in dogs over 10 years in another (2). The two patients with discospondylitis in this report were noted to have lesions in the cervical spine (C6-C7 for patient #1 and C3-C4 for patient #3), which is typically the least common section of the spinal cord to be affected. Patient #3 also had lesions in the more commonly affected thoracic and lumbosacral regions. Thoracolumbar imaging was not performed in patient #1, therefore undiagnosed lesions may have been possible. In a retrospective study of 513 dogs diagnosed with discospondylitis, a majority of lesions were located in the thoracic and lumbar vertebral bodies with the L7-S1 segment being the most commonly affected site. Cervical vertebrae were affected in only 13.8% of the dogs in this study (2). In another study, lesions of the thoracic and lumbar spine were also more commonly reported than those in the cervical spine (26). Interestingly, a paper by Buhmann et al. also reported brucella-associated discospondylitis in 4 young females, ranging from 7 months to 2.5 years of age, and 3 of the 4 had lesions in the cervical spine (27).

We have documented three adult littermates who were diagnosed with *Brucella canis*, two of which developed discospondylitis. Despite its diagnostic challenges, *Brucella canis* was identified in all three littermates using various diagnostic methods (including blood culture, PCR, and multiple serologic tests). When dogs are diagnosed with *Brucella canis,* treatment can be challenging and requires chronic, and potentially life-long, antibiotic administration without guarantee of clearance of the organism. The need for a reliable and consistent diagnostic protocol for *Brucella canis* remains, and could prove beneficial for veterinarians should the need for testing one or multiple patients arise.

Data availability statement

The original contributions presented in the study are included in the article/supplementary material, further inquiries can be directed to the corresponding author/s.

Author contributions

LG was responsible for drafting the manuscript. All authors read and approved the final version of the manuscript.

Acknowledgments

The authors acknowledge Dr. Matt Bussan, Dr. Mark Ernst, Dr. Connie Austin, Dr. Kimberly Burks, and Denise Weber, CVT for their assistance in the management and care of patients #1 and #2.

Conflict of interest

The authors declare that the research was conducted in the absence of any commercial or financial relationships that could be construed as a potential conflict of interest.

Publisher's note

References

1. Thomas W. Diskospondylitis and other vertebral infections. *Vet Clin North Am Small Anim Pract*. (2000) 30:169–82. doi: 10.1016/S0195-5616(00)50008-4

2. Burkert BA, Kerwin SC, Hosgood GL, Pechman RD, Fontenelle JP. Signalment and clinical features of diskospondylitis in dogs: 513 cases (1980-2001). *J Am Vet Med Assoc*. (2005) 227:268–75. doi: 10.2460/javma.2005.227.268

3. Ruoff CM, Kerwin SC, Taylor AR. Diagnostic imaging of discospondylitis. *Vet Clin North Am Small Anim Pract*. (2018) 48:85–94. doi: 10.1016/j.cvsm.2017.08.007

4. Fischer A, Mahaffey MB, Oliver JE. Fluoroscopically guided percutaneous disk aspiration in 10 dogs with diskospondylitis. *J Vet Intern Med*. (1997) 11:284–7. doi: 10.1111/j.1939-1676.1997.tb00466.x

5. Kerwin SC, Lewis DD, Hribernik TN, Partington B, Hosgood GL, Eilts BE. Diskospondylitis associated with *Brucella canis* infection in dogs: 14 cases (1980-1991). *J Am Vet Med Assoc*. (1992) 201:1253–7.

6. Hollett RB. Canine brucellosis: outbreaks and compliance. *Theriogenology*. (2006) 66:575–87. doi: 10.1016/j.theriogenology.2006.04.011

7. Makloski CL. Canine brucellosis management. *Vet Clin North Am Small Anim Pract*. (2011) 41:1209–19. doi: 10.1016/j.cvsm.2011.08.001

8. Dentinger CM, Jacob K, Lee LV, Mendez HA, Chotikanatis K, McDonough PL, et al. Human *Brucella canis* infection and subsequent laboratory exposures associated with a puppy, New York City, 2012. *Zoonoses Public Health*. (2015) 62:407–14. doi: 10.1111/zph.12163

9. Wanke MM, Delpino MV, Baldi PC. Use of enrofloxacin in the treatment of canine brucellosis in a dog kennel (clinical trial). *Theriogenology*. (2006) 66:1573–8. doi: 10.1016/j.theriogenology.2006.01.034

10. Weese JS, Hrinivich K, Anderson MEC. *Brucella canis* in commercial dog breeding kennels, Ontario, Canada. *Emerg Infect Dis*. (2020) 26:3079–80. doi: 10.3201/eid2612.201144

11. Keid LB, Chiebao DP, Batinga MCA, Faita T, Diniz JA, Oliveira TMF de S, et al. Brucella canis infection in dogs from commercial breeding kennels in Brazil. *Transbound Emerg Dis*. (2017) 64:691–7. doi: 10.1111/tbed.12632

12. Theron J, Cloete T. Brucella characteristics. In: *Encyclopedia of Food Microbiology*. Cambridge, MA: Academic Press (1999). p. 319–24. doi: 10.1006/rwfm.1999.0255

13. Wanke MM. Canine brucellosis. *Anim Reprod Sci*. (2004) 82–83:195–207. doi: 10.1016/j.anireprosci.2004.05.005

14. Mol JPS, Guedes ACB, Eckstein C, Quintal APN, Souza TD, Mathias LA, et al. Diagnosis of canine brucellosis: comparison of various serologic tests and PCR. *J Vet Diagn Invest*. (2020) 32:77–86. doi: 10.1177/1040638719891083

15. Castillo Y, Tachibana M, Kimura Y, Kim S, Ichikawa Y, Endo Y, et al. Microplate agglutination test for canine brucellosis using recombinant antigen-coated beads. *Int Scholarly Res Notices*. (2014) 2014:1–4. doi: 10.1155/2014/348529

16. Keid LB, Soares RM, Vasconcellos SA, Megid J, Salgado VR, Richtzenhain LJ. Comparison of agar gel immunodiffusion test, rapid slide agglutination test, microbiological culture and PCR for the diagnosis of canine brucellosis. *Res Vet Sci*. (2009) 86:22–6. doi: 10.1016/j.rvsc.2008.05.012

17. Cosford KL. Brucella canis: An update on research and clinical management. *Can Vet J*. (2018) 59:74–81.

18. Santos RL, Souza TD, Mol JPS, Eckstein C, Paíxão TA. Canine brucellosis: an update. *Front Vet Sci*. (2021) 8:594291. doi: 10.3389/fvets.2021.594291

19. Kaden R, Ågren J, Båverud V, Hallgren G, Ferrari S, Börjesson J, et al. Brucellosis outbreak in a Swedish kennel in 2013: determination of genetic markers for source tracing. *Vet Microbiol*. (2014) 174:523–30. doi: 10.1016/j.vetmic.2014.10.015

20. Kang SI, Lee SE, Kim JY, Lee K, Kim JW, Lee HK, et al. A new Brucella canis species-specific PCR assay for the diagnosis of canine brucellosis. *Compar Immunol Microbiol Infect Dis*. (2014) 37:237–41. doi: 10.1016/j.cimid.2014.07.003

21. Kauffman LK, Bjork JK, Gallup JM, Boggiatto PM, Bellaire BH, Petersen CA. Early detection of brucella canis via quantitative polymerase chain reaction analysis. *Zoonoses Public Health*. (2014) 61:48–54. doi: 10.1111/zph.12041

22. James D, Golovsky G, Thornton J, Goodchild L, Havlicek M, Martin P, et al. Clinical management of Brucella suis infection in dogs and implications for public health. *Aust Vet J*. (2017) 95:19–25. doi: 10.1111/avj.12550

23. *Brucellosis*. World Health Organization (2020). Available online at: https://www.who.int/news-room/fact-sheets/detail/brucellosis (accessed August 6, 2022).

24. Hooper DC, Jacoby GA. Topoisomerase inhibitors: fluoroquinolone mechanisms of action and resistance. *Cold Spring Harb Perspect Med*. (2016) 6:1–21. doi: 10.1101/cshperspect.a025320

25. Redgrave LS, Sutton SB, Webber MA, Piddock LJV. Fluoroquinolone resistance: mechanisms, impact on bacteria, and role in evolutionary success. *Trends Microbiol*. (2014) 22:438–45. doi: 10.1016/j.tim.2014.04.007

26. Harris JM, Chen AV, Tucker RL, Mattoon JS. Clinical features and magnetic resonance imaging characteristics of diskospondylitis in dogs: 23 cases (1997–2010). *J Am Vet Med Assoc*. (2013) 242:359–65. doi: 10.2460/javma.242.3.359

27. Buhmann G, Paul F, Herbst W, Melzer F, Wolf G, Hartmann K, et al. Canine brucellosis: insights into the epidemiologic situation in Europe. *Front Vet Sci*. (2019) 6:151. doi: 10.3389/fvets.2019.00151

frontiers | Frontiers in Veterinary Science

TYPE Original Research
PUBLISHED 20 October 2022
DOI 10.3389/fvets.2022.982560

OPEN ACCESS

EDITED BY
Andrea Tipold,
University of Veterinary Medicine Hannover, Germany

REVIEWED BY
Karolin Campbell,
Radiovet, Switzerland
Andrea Meyer-Lindenberg,
Ludwig Maximilian University of Munich, Germany

*CORRESPONDENCE
Bianca F. Hettlich
bhettlich@gmail.com

SPECIALTY SECTION
This article was submitted to Veterinary Neurology and Neurosurgery, a section of the journal Frontiers in Veterinary Science

RECEIVED 30 June 2022
ACCEPTED 29 September 2022
PUBLISHED 20 October 2022

CITATION
Goffart LM, Precht C, Fosgate GT, Maiolini A and Hettlich BF (2022) Accuracy of end-on fluoroscopy in predicting implant position in relation to the vertebral canal in dogs. *Front. Vet. Sci.* 9:982560. doi: 10.3389/fvets.2022.982560

Accuracy of end-on fluoroscopy in predicting implant position in relation to the vertebral canal in dogs

Laura M. Goffart[1], Christina Precht[1], Geoffrey T. Fosgate[2], Arianna Maiolini[1] and Bianca F. Hettlich[1]*

[1]Department of Clinical Veterinary Medicine, Vetsuisse Faculty, University of Bern, Bern, Switzerland, [2]Department of Production Animal Studies, University of Pretoria, Onderstepoort, Pretoria, South Africa

Objective: To evaluate the accuracy of end-on fluoroscopy in predicting implant position in relation to the vertebral canal in the canine thoracolumbar vertebral column.

Study design: *In vitro* imaging and anatomic study.

Animals: Canine cadaveric thoracolumbar vertebral columns ($n = 5$).

Methods: Smooth Steinmann pins were inserted bicortically into the thoracolumbar vertebral columns between T10 and L7 using recommended insertion angles. Penetration of the spinal canal was not strictly avoided. After pin placement, end-on fluoroscopy images were obtained of each pin. Pin position was subsequently assessed by four evaluators and determined to either being out of the vertebral canal or in, with the latter being additionally divided into partially or completely penetrating the canal. To assess potential differences in modalities, fluoroscopy images were gray-scale inverted and evaluated again later by the same four individuals. Correct identification of pin position in relationship to the vertebral canal was assessed for both fluoroscopy images. Anatomic preparation of the spines was used for verification of pin position in relation to the spinal canal. Some data from this study were compared with historical data on accuracy using orthogonal radiography and computed tomography (CT).

Results: Overall sensitivity and specificity of F to detect vertebral canal penetration was 98.8 % (95% confidence interval (CI), 96.0–99.6) and 98.0% (95% CI, 77.0–99.9), respectively. For Fi, sensitivity and specificity were 97.0% (95% CI, 91.5–99.0) and 98.5% (95% CI, 81.5–99.9) respectively. F exceeded Fi for the sensitivity of detecting pin penetration into the vertebral canal ($p = 0.039$) but specificities were not different ($p = 0.585$). When comparing to historical data, the overall accuracy of end-on fluoroscopy (F) and inverted fluoroscopy (Fi) was statistical better than conventional radiographic assessment ($p < 0.001$).

Conclusion: End-on fluoroscopy is a highly accurate method for the assessment of pin position in relationship to the thoracolumbar spinal canal in cadaveric dogs.

Clinical significance: End-on fluoroscopy, with or without inversion, is accurate in identifying vertebral canal violation by bicortically placed Steinmann pins. When CT is not available, end-on fluoroscopy might be a valuable imaging modality to determine pin position in the canine vertebral column.

KEYWORDS

vertebral column, canine, bicortical pins, accuracy, fluoroscopy, end-on, gray-scale inversion

Introduction

Vertebral column stabilization in companion animals is performed for a variety of diseases potentially causing instability such as fractures and luxations (1), congenital deformities (2), diskospondylitis (3) or neoplasia (4). Various techniques for stabilization of the spinal column have been described in dogs, such as the use of pins or screws and polymethylmethacrylate (PMMA) (2, 5, 6), locking bone plates (7), clamp rod internal fixator (8), and external skeletal spinal fixation (9). Reliable postoperative evaluation of whether or not implants violate the vertebral canal is required for safe and successful treatment of patients with vertebral column disorders. Penetration into the vertebral canal can lead to iatrogenic injury of neural and vascular structures and might cause deterioration of the patient and prolonged patient recovery (10). Corridors and angles for implant positioning have been recommended for the entire spine (11), nevertheless, correct implant positioning must still be evaluated after surgery.

Conventional radiography is the most widely used imaging modality to assess the general position of spinal implants. However, standard radiography is not accurate enough to determine implant position in relation to the vertebral canal in dogs and sensitivity to detect vertebral canal violation was poor at only 50.7% (12). By contrast, computed tomography (CT) reached an accuracy of 100% for the identification of pins that were fully in or out of the vertebral canal, with overall sensitivity to evaluate spinal canal violation amounting to 93.4% (12). An important disadvantage of CT assessment of spinal implants in veterinary medicine is that it is usually performed after surgery is completed. If canal violation is detected at this point, it is after the fact that an injury might have occurred already and the animal has left the operating room. The ideal would be to not only have an accurate pre- and postoperative imaging modality to plan and assess implant placement in relation to the vertebral canal, but also one that can be used intraoperatively to assess implant position immediately and ideally even guide implant placement. This would increase patient safety, potentially save overall anesthesia time and thus reduce the patient's risk of infection (13). Since the 1990s, navigated spinal surgery has been introduced in human medicine to improve accuracy when placing implants such as pedicle screws (14). Recently, even more elaborated techniques, like robotic spinal surgery, have been introduced (15). However, due to limited availability and cost, these techniques are not regularly used in veterinary medicine.

Fluoroscopy is an imaging modality that also uses x-rays. It combines radiographic capabilities with the possibility to produce real-time moving images. In veterinary medicine, fluoroscopy is often used with a C-arm, where x-ray source and x-ray detector are connected *via* a movable c-shaped arm. This design allows capturing of intraoperative images from different angles. In veterinary spinal surgery, fluoroscopy is for instance used for better orientation during vertebral body pinning (9), closed positioning of spinal external skeletal fixators (16), percutaneous injections into canine intervertebral discs (17) and guided percutaneous discectomy (18). In human medicine, fluoroscopy has been outperformed by robot-assisted spinal surgery (19, 20). However, fluoroscopy remains an option if robot-assisted surgery is not available (21).

While radiographs are usually taken in two orthogonal views, fluoroscopy enables imaging from different angles. This might be an advantage in assessment of implant position in relation to the vertebral canal. While accuracy of standard radiographic projection is poor in determining location of diagonally placed bicortical pins, obtaining fluoroscopic images in line with the implant (end-on) might provide higher accuracy. A search of various publication databases (google scholar, PubMed) has revealed no veterinary studies assessing the accuracy of fluoroscopy for determining implant position in relation to the spinal canal in dogs or other species.

The goal of this study was to assess the accuracy of end-on fluoroscopy to determine position of bicortically placed pins in the canine cadaveric thoracolumbar spine. Both standard fluoroscopy and gray-scale inverted fluoroscopy images were assessed. Overall accuracy of both fluoroscopy modalities were also compared to historical data of conventional orthogonal radiography and CT to predict vertebral implant position. Our hypothesis was that end-on fluoroscopy would be an accurate

method for the assessment of pin position and that there would be no difference between standard and inverted fluoroscopy.

Materials and methods

This study was a canine cadaveric imaging and anatomic study. Dogs were client-owned and euthanized for reasons unrelated to the study. Use of the cadavers for the study was approved *via* written owner consent. Ethical approval by an institutional entity was not necessary as per local federal regulations. Vertebral columns from T9-L7 of 5 adult medium to large breed dogs were collected, frozen (−20°C), and thawed to room temperature before implant placement. For visualization of anatomic landmarks and pin placement, paraspinal musculature was removed. Subsequently, orthogonal laterolateral and dorsoventral radiographs of the thoracolumbar vertebral columns were obtained to exclude obvious pathological bony changes.

Insertion of pins

Vertebral bodies of T10-L7 were bilaterally implanted based on vertebral size with smooth 2.5 mm or 3 mm diameter Steinmann pins (Johnson & Johnson, DePuy Synthes, Oberdorf, Switzerland). All pins were inserted by the last author (BH). Either 1 or 2 pins were inserted on each side of the vertebral body, depending on the size of the vertebra. In the thoracic spine, the base of the accessory process and the tubercle of the ribs served as orientation points, while in the lumbar spine, the junction between the pedicle and the transverse processes was used. While published corridors and angles for pin insertion were considered (9, 11), insertion points and angles varied purposefully within a certain range. Penetration into the vertebral canal was not strictly avoided as the study required pins to be placed within and out of the vertebral canal. Orthogonal radiographs of the vertebral columns were again obtained after implantation to document general pin position within each vertebra; however, these radiographs were not used for implant evaluation (Figure 1).

Fluoroscopy

Each Steinmann pin of each vertebral column was labeled for identification on orthogonal radiographs. Subsequently, each pin was imaged fluoroscopically using a C-arm (OrthoScan FD-OR Mini C-arm, Scottsdale, Arizona, USA). To obtain an end-on view of each pin, the cadaveric spines were manually positioned until the navigation beam of the fluoroscope was perfectly aligned with each pin (Figure 2). Images were immediately assessed on the integrated screen of the fluoroscope

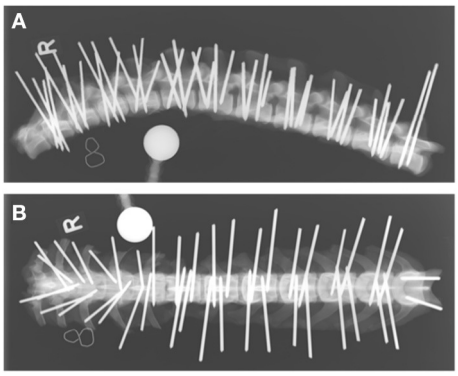

FIGURE 1
Laterolateral **(A)** and dorsoventral **(B)** radiographs of a cadaveric canine thoracolumbar vertebral column after bicortical pin placement. The "R" indicates right lateral recumbency **(A)** and the right side of the vertebral column **(B)**.

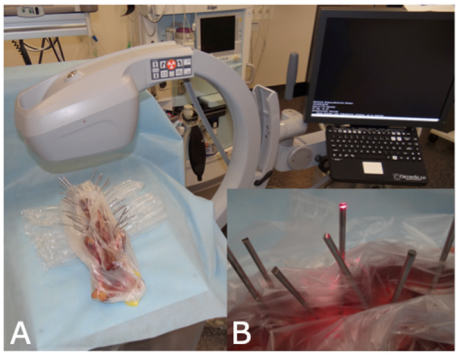

FIGURE 2
C-arm set-up for obtaining end-on fluoroscopy images. **(A)** Set-up of the C-arm and the cadaveric spine. During image generation the spine was manually positioned to achieve perpendicular projection. **(B)** The red laser beam of the C-arm was used as an optical guide to achieve perpendicular projection.

to assure that each pin was perfectly imaged end-on, creating a perfect circle of metal. The integrated fluoroscope screen allowed rotation and magnification of images but no digital enhancement. Each fluoroscopic image was labeled according to the identification number of that particular pin.

Fluoroscopic image evaluation

One small animal surgeon, 1 small animal surgery resident, 1 radiologist, and 1 neurologist evaluated the fluoroscopy images. All participants with the exception of the resident were board-certified in their specialty. Evaluation occurred >2 weeks after pin insertion and none of the participants were aware of the true

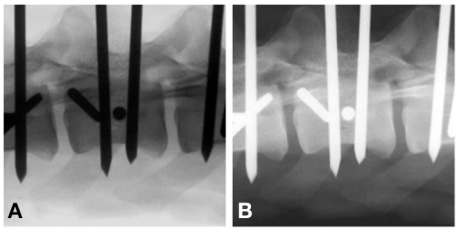

FIGURE 3
Standard **(A)** vs. gray-scale inverted **(B)** end-on fluoroscopy image of a bicortically placed pin lumbar vertebra 3. To be considered end-on, the pin had to present as a perfect circle (arrow).

pin position. The evaluators had to answer 3 questions for every pin assessed: (1) Does the implant penetrate the spinal canal? Answer: Yes or No. (2) If Yes: Is all or only part of the diameter of the implant violating the canal? (3) What is your confidence level for question (1)? Confidence level could be chosen between 50 % (completely unsure) to 100 % (certain). The definition of whether or not an implant penetrated the vertebral canal was adopted from a previous study (12). Pins that penetrated the spinal canal fully or partially were defined as "in," all other pins were defined as "out."

Fluoroscopic images (F) were adjusted using gray-scale inversion (Fi), and all images were evaluated again by the same evaluators using the same 3 questions (Figure 3). To reduce the chance of recognition, the second assessment of Fi was performed >1 week after the first and the order of pins to be assessed was haphazardly changed.

Anatomical preparation

Remaining soft tissues were removed using an enzymatic solution (BIOZYM SE, Spinnrad GmbH, Bad Segeberg, Germany). Direct visual inspection served as gold standard to assess pin position and presence and degree of vertebral canal violation (Figure 4).

Historical data of radiography and computed tomography

Overall accuracy data from the current study of both fluoroscopy modalities were compared to historical data of radiography and CT from Hettlich et al. (12), after which the current study was modeled. The 2010 study compared the accuracy of orthogonal radiography and cross-sectional imaging by computed tomography to predict Steinmann pin position in relation to the vertebral canal in canine cadavers. Cadaveric dogs of similar size and weight were used and evaluators included

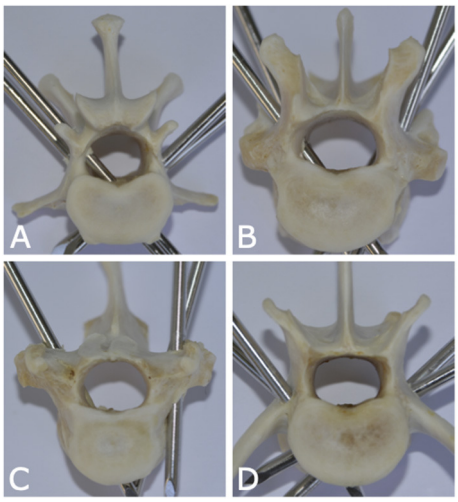

FIGURE 4
Photographs of anatomic canine vertebral specimens of dogs from this study illustrating various pin positions in relation to the vertebral canal. **(A)** Pin is fully penetrating the vertebral canal (left caudal pin of lumbar vertebra 1). **(B)** Pin is partially penetrating the vertebral canal (right cranial pin of thoracic vertebra 12). **(C)** Pin is partially penetrating with only cortical lift (right pin of thoracic vertebra 10). **(D)** None of the pins are penetrating the vertebral canal (lumbar vertebra 6).

specialists of surgery, neurology and diagnostic imaging. Results of that study demonstrated poor accuracy for orthogonal radiographs (sensitivity: 50.7%; specificity: 82.9%) and very good to excellent accuracy for CT (sensitivity: 93.4%; specificity: 86.4%). These historical data of overall accuracy were statistically compared to the results of the current study.

Statistical analysis

Sensitivity (Se) was defined as the proportion of spinal pins truly penetrating the spinal canal correctly identified as penetrating by the image evaluator. Specificity (Sp) was defined as the proportion of non-penetrating pins correctly identified by the evaluator. Overall accuracy was calculated as the proportion of all spinal pins correctly identified as penetrating or non-penetrating by the evaluator. Accuracy data were described using point and whisker plots created within the ggplot2 package (19) of R (20). Inter-rater agreement (kappa) and 95% confidence intervals (CI) were calculated for data collected from the four evaluators using standard formulas (21) entered into a commercial spreadsheet program (Excel, Microsoft Office Professional 2016, Redmond, WA, USA). Sensitivity and specificity were estimated using a generalized linear model assuming a binomial error distribution and included random effect terms for individual spinal pins, cadavers, and evaluators to account for the repeated observations on

the same pins within a small number of specimens. The primary variable of interest was imaging modality and the effects of this variable and other covariates on estimates of sensitivity and specificity were evaluated using univariate analyses. All variables were subsequently evaluated using a multivariable approach. Multivariable models were fit using a manual backwards stepwise approach in which variables were removed on-by-one until the Student t statistic for all remaining variables was $P < 0.05$. Commercial software was used for statistical modeling (IBM SPSS Statistics Version 25, International Business Machines Corp., Armonk, NY, USA) and results were interpreted at the 5% level of significance.

Results

Five canine cadavers of the following breeds were used for the study: Dalmatian ($n = 1$), Australian Shepherd ($n = 1$), German spitz ($n = 1$) and mongrel ($n = 2$). Mean bodyweight was 23.7 kg (range: 20.4–26.1 kg), mean age was 8.6 years (range: 3–12 years), and there were three male and two female dogs. None of the vertebral columns had radiographic evidence of bony changes.

A total of 193 pins were evaluated: T10 = 14 pins [7 penetrating the canal (in); 7 not penetrating the canal (out)], T11 = 17 pins (7 in; 10 out), T12 = 17 pins (10 in; 7 out), T13 = 18 pins (12 in; 6 out), L1 = 20 pins (12 in; 8 out), L2 = 20 pins (12 in; 8 out), L3 = 19 pins (11 in; 8 out), L4 = 20 pins (13 in; 7 out), L5 = 19 pins (8 in; 11 out), L6 = 19 pins (12 in; 7 out) and L7 = 10 pins (5 in; 5 out). There were a total of 95 left (57 in; 38 out) and 98 right pins (52 in; 46 out). In the caudal thoracic spine, insertion angles ranged from approximately 20 to 40 degrees; in the lumbar spine, from 40 to 60 degrees; in L7, angles ranged from 0 to 15 degrees.

The overall sensitivity in predicting spinal canal violation was 98.8% for F and 97.0% for Fi, this difference was statistically significant (Table 1; $p = 0.039$). Overall specificity for F and Fi was 98.0 and 98.5%, respectively ($p = 0.585$). While sensitivity of both F and Fi was 100% for complete penetration of the spinal canal, sensitivity of F was significantly higher for recognition of partial pin penetration compared to Fi [98.2 and 95.6%, respectively ($p = 0.038$)].

When comparing current to historical data, accuracy of F and Fi (just as CT) was significantly better than orthogonal radiographic projections in predicting implant position in relation to the vertebral canal (Table 2) (12). Sensitivity of the three modalities (F, Fi, CT) outperformed orthogonal radiographic projections. Only regarding specificity, significance was not reached ($p = 0.065$).

There was excellent agreement between the four evaluators, with an overall kappa agreement of 0.931 for F and 0.904 for Fi (Table 3). High evaluator confidence (i.e., 100% confidence) was associated with improved sensitivity and specificity of predicting spinal canal violation in our study (Supplementary Tables S4–S7).

Discussion

End-on fluoroscopy (F) and inverted fluoroscopy (Fi) could accurately assess pin position in relation to the vertebral canal in this canine cadaveric model, with high sensitivity and specificity for both. While both settings had high accuracy, sensitivity of F was higher than of Fi when assessing partially penetrating pins. Both F and Fi were significantly more accurate when compared to standard orthogonal radiography (historical data).

Accuracy of end-on fluoroscopy to predict implant position in relation to the canine vertebral canal has not been published before, nor have F and Fi been compared to other imaging modalities. This study presents valuable baseline data, demonstrating the potential for end-on fluoroscopy to assess spinal implants, which can be used for further clinical studies. The current veterinary literature only contains limited information regarding the clinical use of fluoroscopy during spinal implant positioning (9), without published data about the accuracy of fluoroscopy to assess spinal canal violation. Our study demonstrated high accuracy for fluoroscopy in this regard, which would support its use for clinical patients.

Gray-scale inversion can be used with any digital images using x-rays such as standard radiography, fluoroscopy and CT. While most clinicians are likely used to assessing x-ray-based images in their "native" state (dense structures being white), this apparently does not improve accuracy when it comes to assessment of pins in this study. Accuracy of both F and Fi was excellent in this study; however, our study did not find an advantage of inverted fluoroscopy over standard, with accuracy of F exceeding Fi when assessing partial violation of the vertebral canal. The value of gray-scale inversion has been controversially discussed in human medicine. While it improved nodule detection on chest radiography (22) and increased the sensitivity when assessing post-operative spinal orthopedic implants and osseous fusion on CT (23), it did not improve accuracy of dental calculus detection (24). The current literature suggests its use as an easy and useful adjunct when combined with conventional images (25). To the authors' knowledge, this is the first veterinary study evaluating the effect of gray-scale inversion on the accuracy of fluoroscopy to detect spinal canal violation. Based on results of this study, fluoroscopic images of spinal implants such as within this study should be assessed in their standard format (dense structures being black) and inversion should only be considered as an additional tool.

One critical aspect to consider with the use of fluoroscopy is radiation safety, including the use of proper personal protective gear and providing educational training (26). Especially in spinal surgery, active fluoroscopy might be needed for a longer period to adjust image position over each implant

TABLE 1 Agreement as estimated by the kappa statistic (95% confidence interval) for pin determination as penetrating or not penetrating the spinal canal using five cadaver dogs examined by four evaluators with two imaging modalities.

	Fluoroscopy			Inverted fluoroscopy		
Pin population	**"In" pins**	**"Out" pins**	**All pins**	**"In" pins**	**"Out" pins**	**All pins**
Spine location						
Thoracic	0.206 (0.072, 0.339)	ND	0.964 (0.866, 1.0)	0.304 (0.171, 0.438)	ND	0.939 (0.841, 1.0)
Lumbar	0.206 (0.112, 0.300)	0.636 (0.427, 0.745)	0.913 (0.842, 0.984)	0.329 (0.235, 0.423)	0.595 (0.486, 0.704)	0.884 (0.813, 0.955)
All	0.206 (0.129, 0.282)	0.648 (0.560, 0.735)	0.931 (0.873, 0.989)	0.321 (0.245, 0.398)	0.606 (0.519, 0.694)	0.904 (0.846, 0.961)
Pin location						
Cranial	−0.006 (−0.128, 116)	0.710 (0.594, 0.827)	0.956 (0.871, 1.0)	−0.012 (−0.134, 0.110)	0.710 (0.594, 0.827)	0.944 (0.860, 1.0)
Caudal	0.150 (0.039, 0.261)	0.658 (0.515, 0.802)	0.944 (0.857, 1.0)	0.351 (0.241, 0.462)	−0.008 (−0.152, 0.136)	0.896 (0.808, 0.984)
Left	0.327 (0.221, 0.433)	0.380 (0.250, 0.509)	0.952 (0.870, 1.0)	−0.022 (−0.128, 0.084)	0.380 (0.250, 0.509)	0.912 (0.830, 0.994)
Right	0.162 (0.051, 0.273)	0.752 (0.634, 0.870)	0.911 (0.830, 0.992)	0.438 (0.327, 0.549)	0.710 (0.592, 0.828)	0.894 (0.814, 0.975)
Canal entry						
Complete	ND	NA	NA	ND	NA	NA
Partial	0.198 (0.106, 0.291)	NA	NA	0.307 (0.215, 0.399)	NA	NA

NA, not applicable; ND, no data due to perfect agreement.

TABLE 2 Mixed–effects logistic regression comparing the accuracy of different modalities including retrospective data previously published (12).

Variable	Modality	Parameter estimate (β)	Odds ratio (95% CI)	*P*-value
Overall accuracy				
	Fluoroscopy	3.346	28.4 (14.1, 57.3)	<0.001
	Inverted fluoroscopy	3.027	20.6 (10.5, 40.4)	<0.001
	Computed tomography	2.308	10.1 (8.5, 11.9)	<0.001
	Radiology	Referent		
Sensitivity				
	Fluoroscopy	4.445	85.2 (24.8, 293)	<0.001
	Inverted fluoroscopy	3.580	35.9 (11.6, 110)	<0.001
	Computed tomography	3.594	36.4 (27.7, 47.7)	<0.001
	Radiology	Referent		
Specificity				
	Fluoroscopy	1.293	3.6 (0.9, 14.4)	0.065
	Inverted fluoroscopy	1.477	4.4 (1.1, 17.6)	0.037
	Computed tomography	0.302	1.4 (1.0, 1.8)	0.043
	Radiology	Referent		

CI, confidence interval; Sensitivity, probability of correctly detecting a pin that is penetrating the spinal canal; Specificity, probability of correctly detecting a pin that is not penetrating the spinal canal.
Data for fluoroscopy and inverted fluoroscopy were collected from the present study that included 5 canine cadaveric vertebral columns whereas historical data for computed tomography and radiograph were collected from 12 cadaveric vertebral columns. Comparisons performed using mixed–effects logistic regression including random effects for evaluator, spine, and individual pin identification.

with bilateral bicortical pins of different insertion angles. Hence, exposure time and number of people exposed need to always be minimized to follow the ALARA rules (27). Riley stated that when well-maintained machines are used appropriately during orthopedic surgeries, radiation exposure from fluoroscopy can be considered low (28). Additionally, exposure can be minimized using properly fitted protective garments and protective devices to block scatter radiation (29).

TABLE 3 Mixed–effects logistic regression comparing the sensitivity and specificity of fluoroscopy and inverted fluoroscopy while adjusting for the dependency among observations by including random effects for evaluator, spine, and individual pin identification. Study performed using five cadaver dogs examined by four evaluators with two imaging modalities.

	Sensitivity			Specificity		
	Fluoroscopy	Inverted fluoroscopy		Fluoroscopy	Inverted fluoroscopy	
Pin population	Percentage (95% CI)	Percentage (95% CI)	*P*–value*	Percentage (95% CI)	Percentage (95% CI)	*P*–value*
All	98.8 (96.0, 99.6)	97.0 (91.5, 99.0)	0.039	98.0 (77.0, 99.9)	98.5 (81.5, 99.9)	0.585
Location						
Thoracic	98.7 (93.4, 99.8)	97.1 (88.7, 99.3)	0.267	100†	100†	1.0
Lumbar	98.8 (95.6, 99.7)	97.0 (90.7, 99.1)	0.079	95.9 (47.1, 99.8)	97.0 (54.8, 99.9)	0.567
Confidence						
100%	99.3 (96.3, 99.9)	99.0 (95.5, 99.8)	0.896	99.3 (87.9, 100)	99.5 (91.4, 100)	0.762
<100%	97.5 (91.3, 99.3)	92.8 (80.4, 97.6)	0.054	94.5 (53.2, 99.6)	94.1 (49.8, 99.6)	0.852
Canal entry						
Complete	100†	100†	1.0	NA	NA	NA
Partial	98.2 (94.4, 99.5)	95.6 (88.3, 98.4)	0.038	NA	NA	NA

CI, confidence interval; N, not applicable.
*Comparing estimates between the two imaging modalities.
†No incorrect classifications and model unable to estimate confidence interval.

Furthermore, the use of a mini C-arm reduces radiation in comparison to its larger counterpart (30).

Fluoroscopy can be carried out using different types of machinery such as mobile fluoroscopy units (C-arm, mini C-arm) or larger, stationary fluoroscopy systems. Recently, C-arm cone-beam computed tomography (CBCT) has become available as a new imaging technology. It can provide fluoroscopic two-dimensional imaging for planning, fluoroscopic real-time intervention guidance and immediate multiplanar and three-dimensional (3D) post-treatment assessment (31). However, this technique is not yet widely available in veterinary medicine.

For this study, a mini C-arm was used, which served the needs of this study very well. Positioning and manipulation of the dissected specimen used in our study was easy due to their size. However, a larger C-arm with a larger bore diameter might be needed to adapt to patient size and to enable patient manipulation for implant positioning. For future clinical studies, a larger C-arm bore diameter might also be needed to allow handling of power equipment to insert implants, with the goal to reduce moving the C-arm or the patient. Use of a larger C-arm should to be based on patient size and be weighed against radiation safety aspects.

In human medicine, ultralow-dose CT-fluoroscopy-guidance can even further reduce radiation dose compared to fluoroscopy alone when used during lumbar spine epidural injections (32). However, to the authors' knowledge this technique is currently not used in veterinary medicine.

In clinical cases, normally a limited number of implants (< 10) need to be positioned in the canine spine (2, 5, 6, 9, 16). Therefore, strategies could be employed to reduce radiation exposure and follow adequate radiation safety guidelines.

Evaluator agreement and evaluator confidence were evaluated in our study. Agreement between the four evaluators was excellent, despite the differing specialization and different levels of clinical experience. This supports the clinical value of end-on fluoroscopy when evaluating these types of spinal implants, regardless of specific radiographic training or surgical experience. Evaluator confidence in this study was very high. This alone is not unusual; however, high confidence was linked to correct assessment in this study, meaning that evaluators were self-aware of their capability to correctly assess implant position. The more confident evaluators felt with their assessment, the more correct they were. This is in great contrast to the earlier study, where a display of high confidence was linked to incorrect assessment, especially with specialized evaluators (12). The reason for this positive connection between confidence and correct implant position in the current study is unknown but could be a function of the individuals participating in the study.

Given the *ex vivo* design, our study has several limitations. The number of specimens evaluated was limited to 5 medium to large breed dogs and data might be different for smaller breed dogs or cats. Additionally, soft tissue dissection of the spines was performed, which minimized superimposition of

tissue and might increase bony detail on fluoroscopy. The end-on pin position for fluoroscopy was achieved by manually repositioning and rotating the dissected vertebral column or each pin, while in a clinical setting, consideration has to be given to the entire animal and possible presence of spinal instability. Therefore, a more realistic method would be to move the C-arm around the patient, which might be inhibited by the animal itself, the surgical table and other instruments in the field.

Another limitation of the study is the environment during image evaluation. Evaluators assessed images on high resolution computer screens in a darkened room at their own pace. In clinical cases, the surgeon would examine the generated images on a screen that is integrated in the fluoroscopic machinery. Although some adjustment and inversion of images is usually possible with modern fluoroscopes, the attached screens will not reach the image quality of a diagnostic imaging monitor. Further studies will be needed to evaluate the impact of monitor-quality and stressed decision-making on accuracy of the detection of spinal canal violation in clinical cases.

Additionally, results of our study comparing current to historical data must be interpreted cautiously since the two studies are based on different populations of dogs and radiographic and CT assessment were not repeated in the current population. However, dog population and set-up of the current study was kept as consistent as possible in comparison to the previous study. Also, statistical models included random effect terms for cadavers and this will adjust for individual variability in effort to provide an unbiased comparison.

In conclusion, end-on fluoroscopy, both standard and inverted, can be used to assess pin positioning in relation to the vertebral canal of the thoracolumbar spine in medium to large breed dogs. Accuracy also outperformed radiography for the evaluation of pin position when compared to historical data. More studies are warranted to assess the use of fluoroscopy in clinical patients, not just after implantation, but also to guide safe implant insertion.

Data availability statement

The raw data supporting the conclusions of this article will be made available by the authors, without undue reservation.

Ethics statement

Ethical review and approval was not required for the animal study because in Switzerland it is not required to undergo Ethical Review/approval for studies undertaken on canine cadavers provided that owner consent was given to use these cadavers. The latter was the case in this study. Written informed consent was obtained from the owners for the participation of their animals in this study.

Author contributions

BH conceptualized the work and revised the manuscript. LG and BH prepared the specimen and obtained fluoroscopy images. LG, BH, CP, and AM evaluated implant position on imaging. GF conducted the statistical analysis. LG prepared the manuscript. GF, CP, and AM supported manuscript revision. All authors contributed to the article and approved the submitted version.

Conflict of interest

The authors declare that the research was conducted in the absence of any commercial or financial relationships that could be construed as a potential conflict of interest.

Publisher's note

All claims expressed in this article are solely those of the authors and do not necessarily represent those of their affiliated organizations, or those of the publisher, the editors and the reviewers. Any product that may be evaluated in this article, or claim that may be made by its manufacturer, is not guaranteed or endorsed by the publisher.

Supplementary material

The Supplementary Material for this article can be found online at: https://www.frontiersin.org/articles/10.3389/fvets.2022.982560/full#supplementary-material

References

1. Selcer R, Bubb W, Walker T. Management of vertebral column fractures in dogs and cats: 211 cases (1977–1985). *J Am Vet Med.* (1991) 198:1965.

2. Aikawa T, Kanazono S, Yoshigae Y, Sharp NJH, Munana KR. Vertebral stabilization using positively threaded profile pins and polymethylmethacrylate, with or without laminectomy, for spinal canal stenosis and vertebral instability caused by congenital thoracic vertebral anomalies. *Vet Surg.* (2007) 36:432–41. doi: 10.1111/j.1532-950X.2007.00289.x

3. Cabassu J, Moissonnier P. Surgical treatment of a vertebral fracture associated with a haematogenous osteomyelitis in a dog. *Vet Comp Orthop Traumatol.* (2007) 20:227–30. doi: 10.1160/VCOT-06-11-0089

4. Dernell WS, Van Vechten BJ, Straw RC, LaRue SM, Powers E, Withrow SJ. Outcome following treatment of vertebral tumors in 20 dogs (1986-1995). *J Am Anim Hosp Assoc.* (2000) 36:245–51. doi: 10.5326/15473317-36-3-245

5. Garcia JNP, MilthorpeI BK, Russell D, Johnson KA. Biomechanical study of canine spinal fracture fixation using pins or bone screws with polymethylmethacrylate. *Vet Surg.* (1994) 23:322–9. doi: 10.1111/j.1532-950X.1994.tb00491.x

6. Blass CE, Seim Ill HB. Spinal fixation in dogs using Steinmann pins and methylmethacrylate. *Vet Surg.* (1984) 13:203–10. doi: 10.1111/j.1532-950X.1984.tb00790.x

7. McKee W, Downes C. Vertebral stabilisation and selective decompression for the management of triple thoracolumbar disc protrusions. *J Small Anim Pract.* (2008) 49:536–9. doi: 10.1111/j.1748-5827.2008.00582.x

8. Zahn K, Matis U. The clamp rod internal fixator-application and results in 120 small animal fracture patients. *Vet Comp Orthop Traumatol.* (2004) 17:110–20. doi: 10.1055/s-0038-1632808

9. Wheeler JL, Cross AR, Rapoff AJ. A comparison of the accuracy and safety of vertebral body pin placement using a fluoroscopically guided versus an open surgical approach: an in vitro study. *Vet Surg.* (2002) 31:468–74. doi: 10.1053/jvet.2002.33616

10. Garreau de. Loubresse C. Neurological risks in scheduled spinal surgery. *Orthop Traumatol: Surg Res.* (2014) 100:S85–90. doi: 10.1016/j.otsr.2013.11.001

11. Watine S, Cabassu J, Catheland S, Brochier L, Ivanoff S. Computed tomography study of implantation corridors in canine vertebrae. *J Small Anim Pract.* (2006) 47:651–7. doi: 10.1111/j.1748-5827.2006.00070.x

12. Hettlich BF, Fosgate GT, Levine JM, Young BD, Kerwin SC, Walker M, et al. Accuracy of conventional radiography and computed tomography in predicting implant position in relation to the vertebral canal in dogs. *Vet Surg.* (2010) 39:680–7. doi: 10.1111/j.1532-950X.2010.00697.x

13. Eugster S, Schawalder P, Gaschen F, Boerlin P. A prospective study of postoperative surgical site infections in dogs and cats. *Vet Surg.* (2004) 33:542–50. doi: 10.1111/j.1532-950X.2004.04076.x

14. Nolte L, Zamorano L, Visarius H, Berlemann U, Langlotz F, Arm E, et al. Clinical evaluation of a system for precision enhancement in spine surgery. *Clin Biomech.* (1995) 10:293–303. doi: 10.1016/0268-0033(95)00004-5

15. Huang M, Tetreault TA, Vaishnav A, York PJ, Staub BN. The current state of navigation in robotic spine surgery. *Ann Transl Med.* (2021) 9:7. doi: 10.21037/atm-2020-ioi-07

16. Wheeler JL, Lewis DD, Cross AR, Sereda CW. Closed fluoroscopic-assisted spinal arch external skeletal fixation for the stabilization of vertebral column injuries in five dogs. *Vet Surg.* (2007) 36:442–8. doi: 10.1111/j.1532-950X.2007.00290.x

17. MacKenzie SD, Caswell JL, Brisson BA, Gaitero L, Chalmers HJ. Comparison between computed tomography, fluoroscopy, and ultrasonpgraphy for guiding percutaneous injection of the canine intervertebral disc. *Vet Radiol Ultrasound.* (2014) 55:571–81. doi: 10.1111/vru.12155

18. Kinzel S, Koch J, Stopinski T, Afify M, Kupper W, Buecker A, et al. Treatment of 10 dogs with discospondylitis by fluoroscopy-guided percutaneous discectomy. *Vet Rec.* (2005) 156:78–81. doi: 10.1136/vr.156.3.78

19. Han X, Tian W, Liu Y, Liu B, He D, Sun Y, et al. Safety and accuracy of robot-assisted versus fluoroscopy-assisted pedicle screw insertion in thoracolumbar spinal surgery: a prospective randomized controlled trial. *J Neurosurg Spine.* (2019) 30:615–22. doi: 10.3171/2018.10.SPINE18487

20. Fan Y, Du JP, Liu JJ, Zhang JN, Qiao HH, Liu SC, et al. Accuracy of pedicle screw placement comparing robot-assisted technology and the free-hand with fluoroscopy-guided method in spine surgery: an updated meta-analysis. *Medicine.* (2018) 97:10970. doi: 10.1097/MD.0000000000010970

21. Wu M-H, Dubey NK Li Y-Y, Lee C-Y, Cheng C-C, Shi C-S, et al. Comparison of minimally invasive spine surgery using intraoperative computed tomography integrated navigation, fluoroscopy, and conventional open surgery for lumbar spondylolisthesis: a prospective registry-based cohort study. *Spine J.* (2017) 17:1082–90. doi: 10.1016/j.spinee.2017.04.002

22. Lungren MP, Samei E, Barnhart H, McAdams HP, Leder RA, Christensen JD, et al. Gray-scale inversion radiographic display for the detection of pulmonary nodules on chest radiographs. *Clin Imaging.* (2012) 36:515–21. doi: 10.1016/j.clinimag.2012.01.009

23. Patel A, Haleem S, Rajakulasingam R, James SL, Davies AM, Botchu R. Comparison between conventional CT and grayscale inversion CT images in the assessment of the post-operative spinal orthopaedic implants. *J Clin Orthop Trauma.* (2021) 21:101567. doi: 10.1016/j.jcot.2021.101567

24. Hyer JC, Deas DE, Palaiologou AA, Noujeim ME, Mader MJ, Mealey BL. Accuracy of dental calculus detection using digital radiography and image manipulation. *J Periodontol.* (2021) 92:419–27. doi: 10.1002/JPER.19-0669

25. Shah A, Iyengar K, Botchu R. Gray scale inversion imaging (GSI) in Trauma and Orthopaedics. *J Ortho.* (2022) 30:62–5. doi: 10.1016/j.jor.2022.02.013

26. de Paula Freitas F. *Radiation Safety Behaviours Among Small Animal Veterinary Radiography and Fluoroscopy Workers*. Saskatoon: University of Saskatchewan. (2020).

27. Hendee WR, Edwards FM. ALARA and an integrated approach to radiation protection. *Semin Nucl Med.* (1986) 16:142–50. doi: 10.1016/S0001-2998(86)80027-7

28. Riley SA. Radiation exposure from fluoroscopy during orthopedic surgical procedures. *Clin Orthop Rel Res.* (1989) 248:257–60. doi: 10.1097/00003086-198911000-00041

29. Meisinger QC, Stahl CM, Andre MP, Kinney TB, Newton IG. Radiation protection for the fluoroscopy operator and staff. *Am J Roentgenol.* (2016) 207:745–54. doi: 10.2214/AJR.16.16556

30. Giordano BD, Baumhauer JF, Morgan TL, Rechtine GR. Patient and surgeon radiation exposure: comparison of standard and mini-C-arm fluoroscopy. *J Bone Joint Surg.* (2009) 91:297–304. doi: 10.2106/JBJS.H.00407

31. Wieschhoff GG, Miskin NP, Kim JS, Hamberg LM, Mandell JC. Radiation dose of fluoroscopy-guided versus ultralow-dose CT-fluoroscopy-guided lumbar spine epidural steroid injections. *Skelet Radiol.* (2022) 51:1055–62. doi: 10.1007/s00256-021-03920-7

32. Wallace MJ, Kuo MD, Glaiberman C, Binkert CA, Orth RC, Soulez G, et al. Three-dimensional C-arm cone-beam CT: applications in the interventional suite. *J Vasc Interv Radiol.* (2008) 19:799–813.

frontiers | Frontiers in Veterinary Science

TYPE Original Research
PUBLISHED 07 November 2022
DOI 10.3389/fvets.2022.1008447

OPEN ACCESS

EDITED BY
Luisa De Risio,
Linnaeus Veterinary Limited,
United Kingdom

REVIEWED BY
Daisuke Hasegawa,
Nippon Veterinary and Life Science University, Japan
Sam Long,
Veterinary Referral Hospital, Australia

*CORRESPONDENCE
Elizabeth Boudreau
bboudreau@cvm.tamu.edu

SPECIALTY SECTION
This article was submitted to Veterinary Neurology and Neurosurgery, a section of the journal Frontiers in Veterinary Science

RECEIVED 31 July 2022
ACCEPTED 20 October 2022
PUBLISHED 07 November 2022

CITATION
Boudreau E, Kerwin SC, DuPont EB, Levine JM and Griffin JF IV (2022) Temporal and sequence-related variability in diffusion-weighted imaging of presumed cerebrovascular accidents in the dog brain. *Front. Vet. Sci.* 9:1008447. doi: 10.3389/fvets.2022.1008447

Temporal and sequence-related variability in diffusion-weighted imaging of presumed cerebrovascular accidents in the dog brain

Elizabeth Boudreau[1]*, Sharon C. Kerwin[1], Emily B. DuPont[1], Jonathan M. Levine[1] and John F. Griffin IV[2]

[1]Department of Small Animal Clinical Sciences, School of Veterinary Medicine and Biomedical Sciences, Texas A&M University, College Station, TX, United States, [2]Department of Large Animal Clinical Sciences, School of Veterinary Medicine and Biomedical Sciences, Texas A&M University, College Station, TX, United States

Diffusion-weighted MRI (DWI) is often used to guide clinical interpretation of intraparenchymal brain lesions when there is suspicion for a cerebrovascular accident (CVA). Despite widespread evidence that imaging and patient parameters can influence diffusion-weighted measurements, such as apparent diffusion coefficient (ADC), there is little published data on such measurements for naturally occurring CVA in clinical cases in dogs. We describe a series of 22 presumed and confirmed spontaneous canine CVA with known time of clinical onset imaged on a single 3T magnet between 2011 and 2021. Median ADC values of $< 1.0x10^{-3}$ mm^2/s were seen in normal control tissues as well as within CVAs. Absolute and relative ADC values in CVAs were well-correlated ($R^2 = 0.82$). Absolute ADC values $< 1.0x10^{-3}$ mm^2/s prevailed within ischemic CVAs, though there were exceptions, including some lesions of < 5 days age. Some lesions showed reduced absolute but not relative ADC values when compared to matched normal contralateral tissue. CVAs with large hemorrhagic components did not show restricted diffusion. Variation in the DWI sequence used impacted the ADC values obtained. Failure to identify a region of ADC $< 1.0x10^{-3}$ mm^2/s should not exclude CVA from the differential list when clinical suspicion is high.

KEYWORDS

diffusion, ADC, ischemia, stroke, canine, MRI

Introduction

The assessment of restricted diffusion in brain tissue *via* MRI is used routinely for evaluation of suspected cerebrovascular accidents (CVA) in human neuroimaging (1, 2). While restricted diffusion is not pathognomonic for CVAs, it can be used to evaluate the extent of injury (3, 4), including identification of clinically silent regions of injury (5, 6), and to track the fate of injured tissue (7, 8). It is well-established that the diffusion-weighted imaging (DWI) characteristics in human CVA change over time (9–13).

Although certain diffusion-weighted characteristics [i.e., median apparent diffusion coefficient (ADC)] have been reported for a small number of CVAs in dogs (14–16), most clinical canine DWI studies have focused on neoplastic (17, 18) or inflammatory lesions (19, 20), or on diffusion tensor tractography (21–24).

The relationship between lesion age and MRI appearance of CVA in the dog brain has been described in experimental studies with induced lesions, including the temporal evolution of their appearance on DWI (24–30), but these have rarely focused on the acute to early subacute (24 h—7 d) phases of injury during which most veterinary patients with suspected CVA would be expected to have MRI performed. Also, it is not known if induced lesions are representative of the changes seen after naturally occurring CVA.

Temporal evolution of the DWI appearance of CVA is different between species (4, 9, 31). Therefore, it is not sufficient to assume that the diffusion-weighted appearance of naturally occurring canine CVA will be the same as that in humans or rodents, for whom more robust data sets are already available.

Expected changes in diffusion-weighted signal may be affected by the presence of blood, especially with echoplanar (EPI) DWI techniques that are more sensitive to susceptibility artifact. Since hemorrhagic transformation of infarction is a well-known complication in human CVA (32, 33) and is thought to occur in dogs (34, 35), understanding of the DWI appearance of both hemorrhagic and ischemic CVA is necessary for correct interpretation in a veterinary clinical setting.

We report on the DWI characteristics of presumptive spontaneous canine CVA as they relate to the age of the insult, the type of DWI (EPI vs. non-EPI) and the presence or absence of a hemorrhagic component of the lesion for a series of cases imaged at a single institution on a single 3T magnet between 2011 and 2021.

Materials and methods

Case identification

A single institution's medical record database was reviewed for cases meeting the predetermined inclusion criteria. To be included, dogs must have had a complete standard brain imaging series, including T2-weighted fluid attenuated inversion recovery (T2-FLAIR) imaging, T2*-weighted imaging, and DWI in the transverse plane, performed on a single 3T magnet (Siemens Verio). Sequence parameters for the standard brain imaging series are included in Supplementary Table S1. Eligible cases had MRI performed between July 2011 and December 2021. Identified cases were imaged using either an EPI (Siemens proprietary RESOLVE) or a non-EPI (Siemens proprietary BLADE) DWI sequence. Supplementary Table S1 contains details of these sequences for our institution. The b-values for the two sequences were selected based on visual optimization on past clinical case data by radiology faculty and technical staff and were not adjusted during the collection of the cases in this report. Also see the Discussion for further comparison of the two sequences.

Included cases were further required to meet the following requirements: 1) a solitary intra-axial lesion identified at the time of original MRI interpretation with CVA listed as a possible differential diagnosis (regardless of its position on the prioritized differential list); 2) no confirmed alternative diagnosis nor definitive treatment for another presumed diagnosis (i.e., immunosuppression, radiation therapy, chemotherapy, or surgery). All identified cases also had 3D pre- and post-Gadolinium T1-weighted sequences performed, though these were not required for inclusion nor analyzed in this report.

To be retained, cases were required to have at least one of the following: $\geq$5 months clinical follow-up with no progression of signs; histopathological confirmation of the nature of the lesion; or repeat MRI showing a static to resolving lesion with no progression of clinical signs in the interim. Additionally, cases were excluded if the lesion was $<$ 5 mm in its largest dimension due to resolution limitations on the diffusion-weighted images.

The onset of signs was required to be acute ($<$ 48 h from normal to affected). The ages of the lesions were measured as the time between onset of signs documented in the electronic medical record and time of MRI.

Definition of DWI and ADC region of interest (ROI)

A freehand ROI tool was used to outline the volume of the region hyperintense to contralateral parenchyma on T2-FLAIR transverse images for all lesions and the volume of the region hypointense to contralateral parenchyma on T2*-weighted transverse images for hemorrhagic lesions. These volumetric ROIs were then copied to the corresponding DWI and ADC images. For comparison, an ellipsoidal volume in a corresponding contralateral parenchymal region was similarly selected (OsiriX version 12.5.2). The individual pixel values within the regions of interest were extracted for descriptive statistical analysis (Matlab Mac R2022a). Both raw ADC values and the ratio of ADC values to the median value of the contralateral control region are reported. Regions of interest were drawn on anonymized images by a single boarded neurologist/radiology resident (EBM) blinded to all clinical information.

Due to the small number of cases and numerous sources of variability in this retrospective case series, formal statistical analysis of these data was deemed inappropriate.

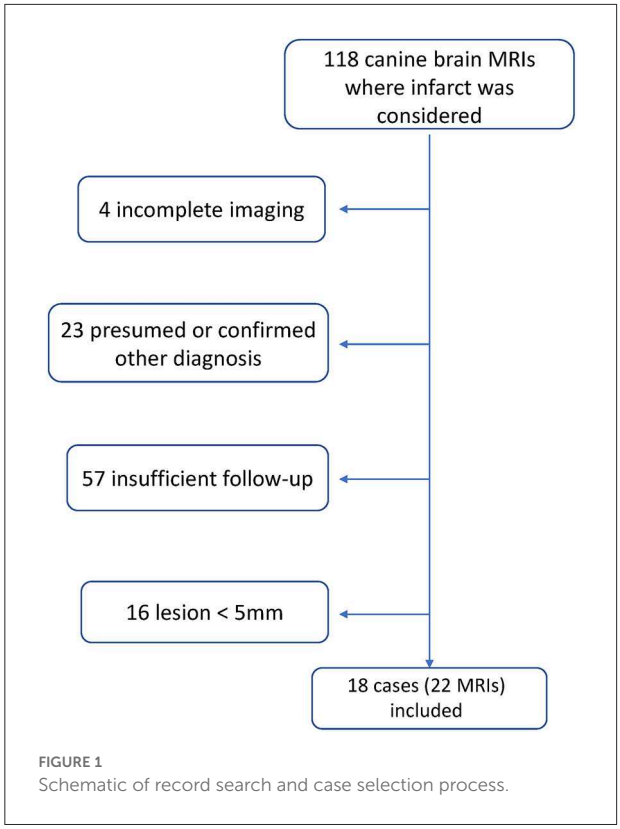

FIGURE 1
Schematic of record search and case selection process.

Results

Case selection

During the specified interval 1,546 canine brain MRIs were performed at the institution on 1,391 patients. Figure 1 shows the process of case identification. After sequential application of the parameters listed in the Methods, there remained 18 cases that met all inclusion criteria.

Of these, eight were presumed or confirmed ischemic CVA and ten were presumed or confirmed hemorrhagic CVA. Six of the ischemic CVA met the criterion of $\geq$ 5 months of clinical follow-up without progression of signs; two had histopathological confirmation. Five hemorrhagic CVA had $\geq$ 5 months of clinical follow-up without progression of signs; one had histopathological confirmation; and four had repeat MRI showing a static to resolving lesion, yielding a total of 22 image sets for analysis.

Clinical data

No cases were excluded due to gradual onset of signs. Table 1 shows the signalment and time elapsed between onset of signs and MRI; with cases having repeat MRI represented twice. Ischemic lesion ages ranged from 0–5 days. Hemorrhagic lesion ages ranged from 0–132 days. Eight of the hemorrhagic CVA image sets had T2-FLAIR hyperintensity exclusive of the region of T2* hypointensity. All of these had a lesion age of $\leq$ 14 days. Six hemorrhagic CVA image sets did not have T2-FLAIR hyperintensity beyond the bounds of the region of T2* hypointensity; five of these had a lesion age of $\geq$21 days.

Median ADC values of normal control regions

Table 1 shows the location of each lesion and median ADC value of the contralateral matched parenchyma. Ischemic CVAs occurred in the brainstem and cerebellar gray matter. Hemorrhagic CVAs occurred in the forebrain, and the associated T2-FLAIR hyperintensity was seen predominantly in subcortical white matter. Normal control median ADC values were in general $< 1.0\text{x}10^{-3}$ mm^2/s (see Discussion), with lower values for brainstem structures and subcortical white matter, and slightly higher values for cerebellar gray matter and cortical tissue.

DWI of T2-flair hyperintense regions

Figure 2 shows selected transverse images demonstrating a ROI and the corresponding contralateral normal control region superimposed on the DWI and ADC series for a representative ischemic CVA. The probability histogram for pixel values within the ROI, with the median value of the contralateral normal control region also indicated, are shown for this example.

Figure 3 shows the relationship between median absolute and relative (normalized to the median value of the contralateral normal control region) ADC values for the eight ischemic and eight hemorrhagic CVAs that exhibited T2-FLAIR hyperintensity outside of the region of T2* hypointensity (see Materials and Methods). The best fit regression line is represented by $ADC_{relative} = 1.79 * ADC_{raw}\text{-}0.2$.

Figure 4 shows the probability histograms for the absolute and relative pixel values on ADC series for the eight ischemic CVA in our data set, arranged by lesion age. The median absolute and relative ADC value for each scan is shown in Table 1. The median absolute ADC values were lowest for the two ischemic CVA that were imaged within 24 h of the onset of signs.

For the corresponding analysis of hemorrhagic CVA, ADC values associated with regions of T2-FLAIR hyperintensity were defined to exclude pixels that were also within the region of T2* hypointensity. Figure 5 shows an example of the process for generating the probability histogram for an example hemorrhagic CVA. Figure 6 shows the probability histograms for the T2-FLAIR hyperintense regions of the eight hemorrhagic CVA that had such regions, arranged by lesion age, analogous to Figure 4. The median absolute and relative ADC value, and

TABLE 1 Clinical data for 22 image sets included in this report.

Age (yrs)	Breed	Sex/Neuter status	Duration of signs (days)	T2* signal void	EPI	Lesion location	Median ADC contralateral control (x10^{-3} mm^2/s)	Median ADC T2-FLAIR ROI (x10^{-3} mm^2/s)	Median relative ADC T2-FLAIR ROI
12	Mixed breed	FI	0	N	N	medulla	0.631	0.300	0.475
13	Yorkshire terrier	MN	0	N	Y	cerebellum	0.765	0.399	0.522
12	Greyhound	FN	1	N	N	thalamus + midbrain	0.580	0.888	1.53
1	Labrador retriever	FI	2	N	N	internal capsule	0.757	0.757	1.00
12	Shih Tzu	FN	2	N	Y	midbrain	0.739	0.436	0.590
16	Bichon Frise	MN	3	N	Y	cerebellum	0.944	0.729	0.791
14	Chihuahua	MN	3	N	N	midbrain + cerebellum	0.633	0.582	0.919
5	Cavalier King Charles spaniel	FN	4	N	N	cerebellum	0.677	0.676	0.999
3	Pit bull terrier	M	0	Y	N	subcortical white matter	0.448	0.990	2.21
11	Mixed breed	MN	2	Y	N	subcortical white matter	0.672	1.27	1.88
6	Boston terrier	MN	2	Y	Y	subcortical white matter	0.485	1.31	2.69
4	Pit bull terrier	FN	3	Y	Y	subcortical white matter	0.706	0.933	1.32
12	Mixed breed	FN	3	Y	Y	subcortical white matter	0.699	1.27	1.81
15	Cardigan Welsh Corgi	FN	5	Y	N	frontal cortex	0.756	n/a	n/a
11	Yorkshire terrier	FN	5	Y	N	subcortical white matter	0.673	1.23	1.83
	2nd MRI		32	Y	N	subcortical white matter	0.641	n/a	n/a
9	Golden retriever	MN	11	Y	Y	subcortical white matter	0.721	0.857	1.19
	2nd MRI		65	Y	Y	subcortical white matter	0.754	n/a	n/a
11	Australian cattle dog	FN	14	Y	N	subcortical white matter	0.684	1.11	1.62
	2nd MRI		132	Y	N	subcortical white matter	0.692	n/a	n/a
13	Australian shepherd	FN	27	Y	N	occipital cortex	0.885	n/a	n/a
	2nd MRI		132	Y	N	occipital cortex	1.14	n/a	n/a

Column labeled $T2^*$ signal indicates hemorrhagic (Y) or ischemic (N) presumed CVA. Column labeled EPI indicates if echo planar (Y) or non-echo planar (N) diffusion-weighted imaging was used. Duration of clinical signs is the number of days elapsed between the onset of neurological signs and MRI. Because ADC values were only analyzed for those image sets that had T2-FLAIR hyperintensity on MRI, hemorrhagic presumed CVAs with no T2-FLAIR hyperintensity do not have ADC values.

10.3389/fvets.2022.1008447

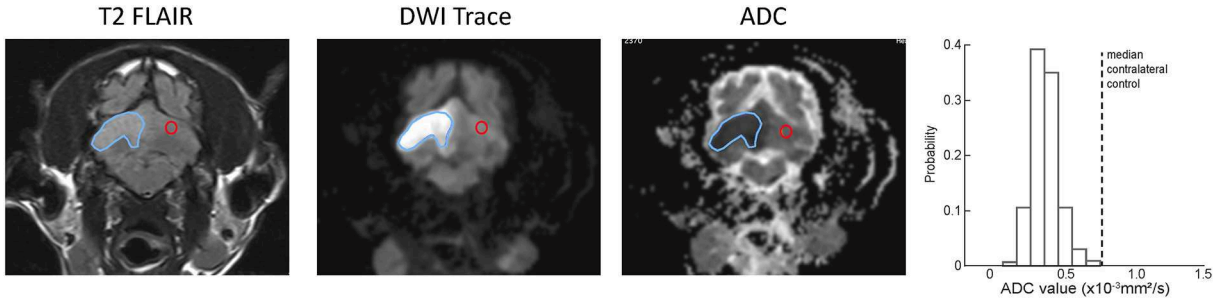

FIGURE 2
Examples of ROI (blue outline) and contralateral normal control (red outline) region selection for a single slice from representative example ischemic CVA. A region was selected for every slice on the T2-FLAIR transverse images and copied to the corresponding slice for the DWI and ADC series. The histogram at the right shows the ADC values within the ROI, as well as the median ADC value within the contralateral control region (dotted line).

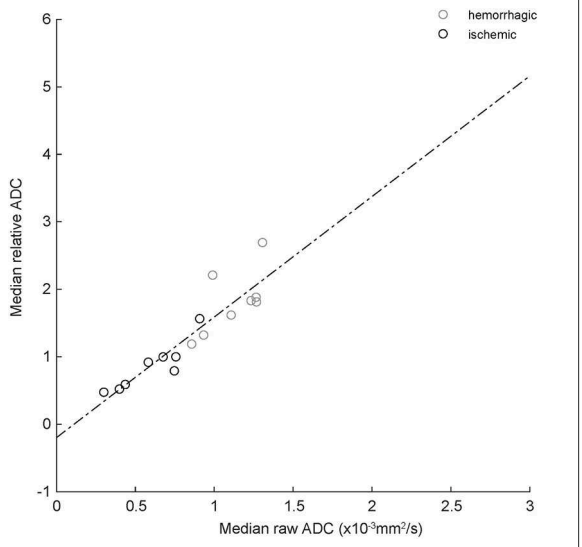

FIGURE 3
Correlation between absolute and relative median ADC values for ischemic (black circles) and hemorrhagic (gray circles) CVAs. The dashed line is best-fit linear regression (equation in text). $R^2 = 0.82$, indicating good correlation.

corresponding median control ADC value, for each scan is shown in Table 1. The median absolute ADC values for these lesions were generally greater than the median ADC value of the contralateral control region, and $>1.0x10^{-3}$ mm^2/s, for all lesion ages.

DWI of T2* hypointense regions

Five of the hemorrhagic CVA image sets were generated using proprietary EPI DWI (RESOLVE), with b = 1000s/mm^2. Nine of the hemorrhagic CVA image sets were generated using proprietary non-EPI DWI (BLADE), with b = 800s/mm^2. See Figure 5 for an example of selected transverse images demonstrating a ROI, identified on T2* transverse images, superimposed on the (EPI) DWI and ADC series for a representative hemorrhagic CVA.

It has been suggested that the greater susceptibility artifact in EPI DWI may artificially lower ADC values near paramagnetic regions (such as areas of hemorrhage). To determine if EPI vs. non-EPI DWI had a systematic impact on ADC values calculated within a hemorrhagic region, we evaluated the distribution of pixel values that lay within the bounds of the hypointense region defined on corresponding T2* series for the 14 hemorrhagic CVA image sets, segregated by method of image generation. Pixels within the T2* hypointense region were more likely to have a value of ADC=0 on non-EPI DWI sets (25.8% vs. 13.6%). ADC value is calculated as

$$ADC = -\ln(SI_{b0}/SI_{b1})/(b0 - b1) \quad (1)$$

Where, SI_{b0} is the pixel intensity value at $b0$, SI_{b1} is the pixel intensity at $b1$, $b0$ = 0s/ mm^2, and $b1$ = 800s/mm^2 for non-EPI and $b1$ = 1000s/mm^2 for EPI (see Materials and Methods for additional sequence details). The proportion of very low pixel values was greater for non-EPI DWI at both $b0$ and $b1$ (Figure 7).

Discussion

DWI MRI characteristics are known to vary with hardware (36, 37) and software (37–39) properties and are subject to interobserver variability in measurement (40, 41). Nonetheless, they are included in many standard brain MRI series and are regularly interpreted by neuroradiologists and neurologists. In human neuroimaging, DWI is used to detect and characterize alterations in water diffusion as distinct from pathological processes that increase water content, and therefore T2-weighted signal intensity, without restricting diffusion. Major

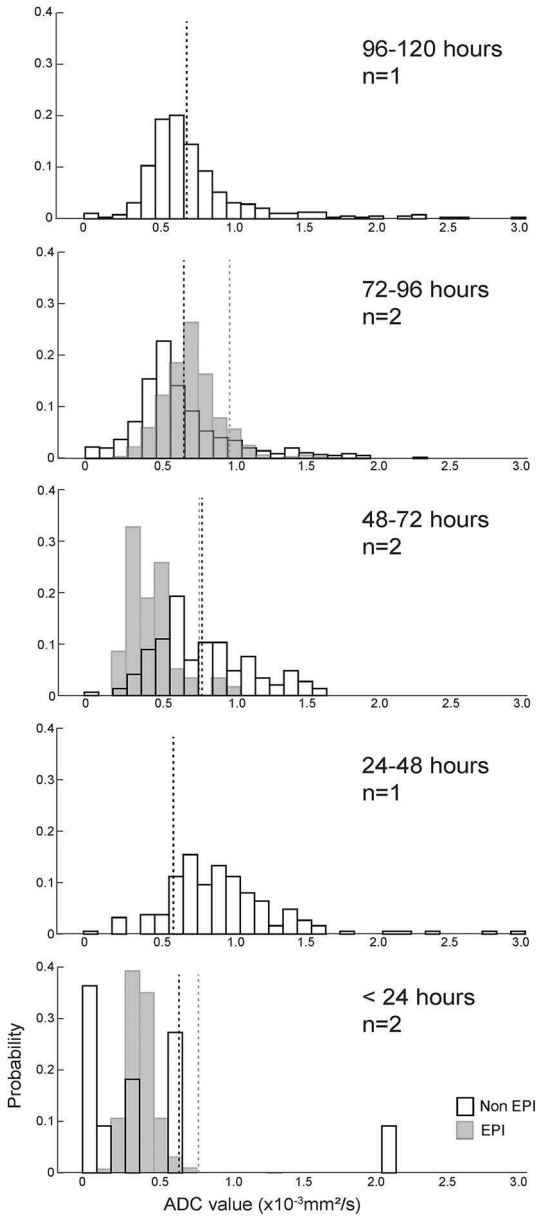

FIGURE 4
ADC value histograms for eight ischemic CVAs, arranged by duration of clinical signs (more recent events below older events). Black outline bars indicate non-EPI DWI, and light gray bars indicate EPI DWI. The dotted lines show median ADC values for the control regions for each histogram, with black dotted lines corresponding to non-EPI DWI, and gray dotted lines corresponding to EPI DWI. Median absolute and relative ADC values for the T2-FLAIR ROIs, median absolute ADC values for the contralateral control regions, and anatomical locations of the lesions/control selections are listed in Table 1. For most cases, the ROIs had median absolute ADC values $< 1.0x10^{-3}$ mm^2/s and median relative ADC values < 1. The CVAs with the shortest duration had the lowest ADC values.

applications of this technique include improving sensitivity for detection, determination of onset, and estimation of lesion extent in CVAs (42–45). There are little existing published data on the DWI characteristics of spontaneous CVAs in dogs to inform appropriate clinical interpretation of these sequences.

Absolute vs. relative ADC values

Consistent with previous reports (46, 47), we found that median ADC values for normal tissues in our sample population were generally $< 1.0x10^{-3}$ mm^2/s, indicating that identification of values below that cutoff within an ROI cannot be used in isolation to confirm pathologically restricted diffusion. A previous publication has demonstrated that absolute ADC values vary with anatomical location in normal dog brain (46), suggesting that relative ADC values may be a better tool for identification of abnormal parenchyma.

Ischemic CVAs

Previous investigations of an experimental ischemic stroke model using induced middle cerebral artery occlusion in healthy dogs showed relatively low ADC within the injured area at 3 days compared to 10 days (25) and high ADC values at 8 and 35 days (48). Because ADC for a given pixel is calculated based on the relationship between the SI_{b0} and SI_{b1} value (see Equation 1 in *Results*), an increase in ADC may occur due to a decrease in SI_{b1}, and increase in SI_{b0}, or both. In both referenced studies, the increase in ADC over time was shown to correlate with a decline in SI_{b1} pixel values within the injured region, with little change in T2-weighted SI_{b0} or T2-FLAIR signal within the region over the same timepoints.

In humans, ADC values have been reported to remain reduced relative to normal values in ischemic stroke for ≥ 1 week (10, 12), with a transition period between 8 and 14 days (10), and increased ADC values after 14 days (10) and at 30 days (12). Others have demonstrated that the time course of evolution of ADC values after ischemic stroke in humans can be affected by recovery of perfusion (49), further complicating interpretation in lesions for which the exact time of onset is unknown.

Reports of ADC values in spontaneous canine CVAs are sparse, especially those using within-patient control values. One case series identified two ischemic CVAs with estimated age of 24–48 h and absolute median ADC values of 0.67 and 0.68 x 10^{-3} mm^2/s, and one ischemic CVA with estimated age of 10–14 days with absolute median ADC value of $1.10x10^{-3}$ mm^2/s (14). Others indicate that the majority of presumed ischemic CVAs imaged 1–5 days after onset of signs had low ADC values (15, 16), though methods of calculation, values, and specific lesion ages were not reported.

Rodent ischemic CVA DWI abnormalities resolve faster than those observed in humans (4, 9, 31, 50). Dogs and primates are more gyrencephalic, have more gray matter volume, and have a

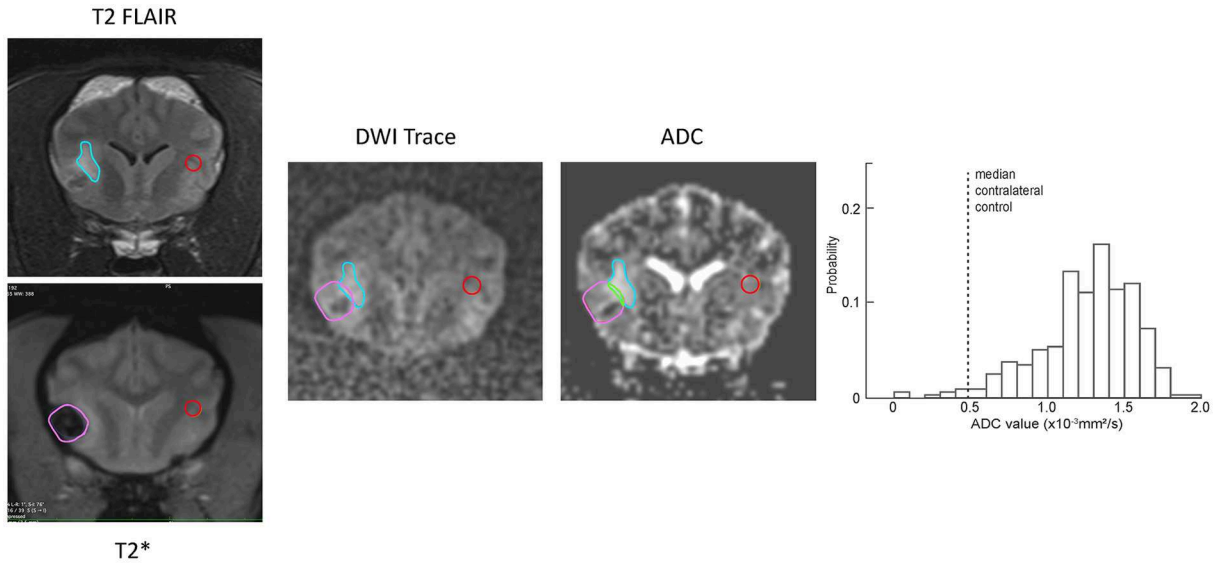

FIGURE 5
Examples of ROI (blue outline) and contralateral normal control (red outline) region selection for a representative example hemorrhagic CVA. The regions were selected on the T2-FLAIR transverse images and copied to the DWI and ADC series. The region of T2* hypointensity was defined on the corresponding T2* transverse image (lavender outline). Pixels that were within both the T2-FLAIR hyperintense region and the T2* hypointense region (green outline) were excluded from the resulting probability histogram (right). The histogram shows the ADC values of non-excluded pixels within the ROI, as well as the median ADC value within the contralateral control region (dotted line).

larger proportion of subcortical white matter affected by induced stroke, as compared to rodents (50). Consistent with previous reports, we show examples of presumed canine CVAs with reduced ADC values up to 5 days after the onset of signs. The most profound reduction in ADC values was observed in the cases with the shortest duration of clinical signs, as expected by analogy to the evolution of ADC map changes in human CVAs.

Hemorrhagic CVAs

The MRI appearances of presumed or confirmed naturally occurring intraparenchymal hemorrhage in dogs (51, 52) have been described in case series, but these do not include discussion of DWI characteristics. A single case series reports the absolute median ADC values for two hemorrhagic CVAs of 2–5 days as 2.19 and 1.10x10^{-3} mm^2/s (14). It is not clear if the hemorrhagic region was excluded from the ROI.

As in a recent case series (51), many hemorrhagic CVAs in our case series had T2-FLAIR hyperintensity surrounding the hemorrhagic region. All lesions with such hyperintensity were imaged within 2 weeks of the onset of signs, whereas no lesions older than 3 weeks had surrounding T2-FLAIR hyperintensity; in presumed hemorrhagic CVAs that were re-imaged, previously noted T2-FLAIR hyperintensity had resolved. This, as well as subjective evaluation of the pattern of the hyperintensity as following subcortical white matter, is consistent with the interpretation of the T2-FLAIR hyperintensity surrounding the hemorrhagic region as transient vasogenic edema (51, 53). We did not find evidence of decreased relative ADC values within the T2-FLAIR hyperintense regions surrounding presumed hemorrhagic CVA, which may suggest mechanisms other than hemorrhagic transformation of ischemic infarct in these cases (54).

A previous experimental study of induced intracerebral hemorrhage in dogs (26) examined T2-FLAIR, DWI, and ADC imaging characteristics up to 24 days after lesion creation. The distribution and time course for T2-FLAIR hyperintensity in the model resembles that observed in our sample population. They likewise did not identify regions of reduced ADC values consistent with restricted diffusion beyond the margins of the hemorrhagic lesion.

EPI vs. non-EPI DWI

EPI DWI uses a single excitation and multiple echoes in a train to fill all of k-space rapidly. Single-shot images are marred by marked susceptibility artifact, due to off-resonance shifts of precession during the echo train that cannot be compensated by shimming. Additionally, image spatial resolution is limited, and images are prone to geometric distortion (shrinking, scaling, shear) from uncompensated in-plane background gradients. Readout-segmented EPI (RESOLVE) is a Siemens proprietary

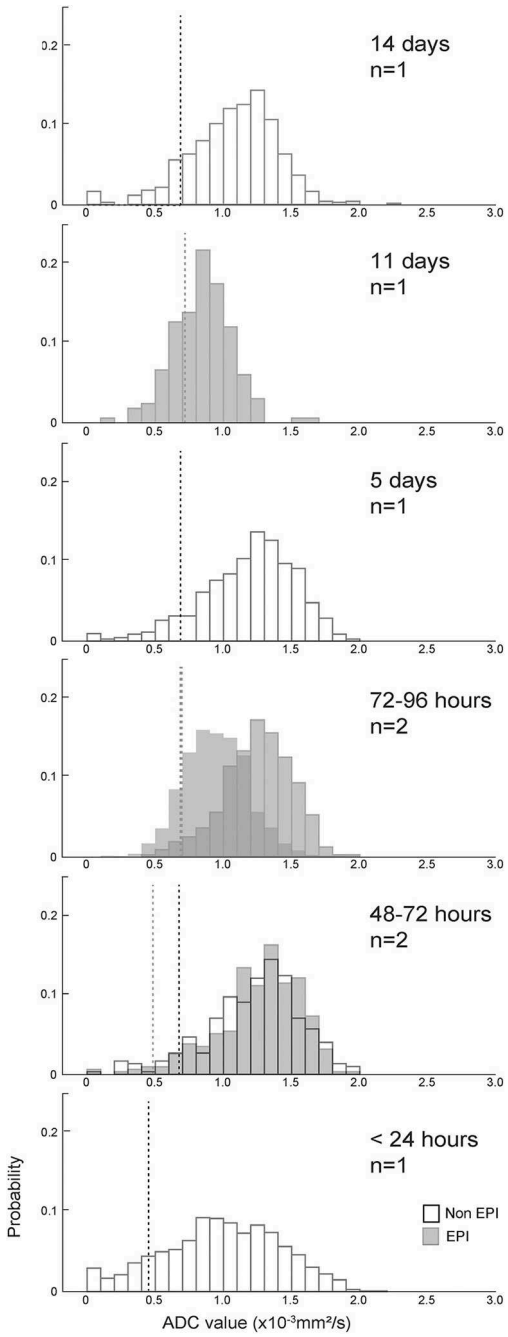

FIGURE 6
ADC value histograms for the T2-FLAIR hyperintense region adjacent to eight hemorrhagic CVAs, arranged by duration of clinical signs (more recent events below older events). Black outline bars indicate non-EPI DWI, and gray bars indicate EPI DWI. The dotted lines show median ADC values for the control regions for each histogram, with black dotted lines corresponding to non-EPI DWI, and gray dotted lines corresponding to EPI DWI. Median absolute and relative ADC values for the T2-FLAIR ROIs, median absolute ADC values for the contralateral control regions, and anatomical locations of the lesions/control selections are listed in Table 1. There was no evidence of restricted diffusion adjacent to the T2* hypointense region in any dog.

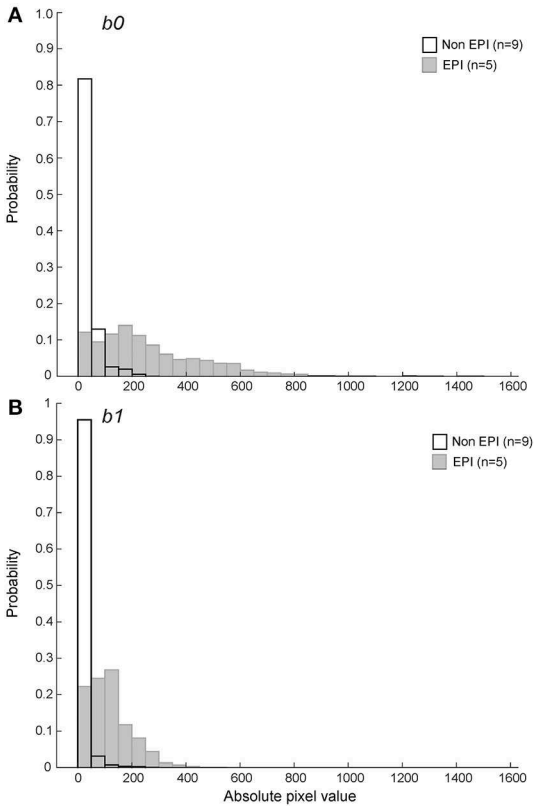

FIGURE 7
Probability histograms of pixel values within the T2* hypointense ROIs for *b0* **(A)** and *b1* **(B)** DWI series (see text for variable definitions). Non-EPI series used *b1* = 800s/mm^2 and are shown in black outline. The pixel values within ROIs defined by the T2* hypointense region were more likely to be zero or close to zero on non-EPI ADC series for both *b0* and *b1*.

multishot EPI technique that relies on parallel imaging. The multiple shots allow a single image to be formed in k-space from data acquired in two or more RF excitations, shortening the readout interval; however, the number of excitations is still lower than that in non-EPI DWI. The parallel imaging technique also infers lines of k-space during initial filling, shortening total readout duration further, which reduces the accumulation of off-resonance effects during the echo train.

Non-EPI DWI fills only a portion of k-space with data obtained from a single excitation. This allows for higher spatial resolution and less susceptibility artifact than in EPI DWI. Originally conceived as a single line of k-space per excitation, other non-EPI k-space filling schemes (e.g., radial filling as used by the Siemens proprietary non-EPI DWI sequence BLADE) have been developed to oversample the central region of k-space (representing the highest-amplitude signals), which improves signal-to-noise ratio further and allows for motion correction between excitations. Image averaging after motion correction is also employed to improve signal-to-noise ratio. However, the

large number of excitations and the repeated sampling required for image averaging both increase scan time for these sequences. Additionally, the motion correction algorithms can introduce new artifacts (55) in some circumstances.

Although several publications have reported DWI characteristics of spontaneous hemorrhagic lesions in humans (11, 13, 56, 57), the clinical interpretation of these findings is complicated by susceptibility effects of paramagnetic blood products on T2-weighted image sequences, including those used in DWI. Specifically, the problem of "T2 blackout," where susceptibility artifact causes very low pixel values in the vicinity of the paramagnetic substance, may artificially lower the pixel values on DWI within hematomas. Because EPI is considered more susceptible to paramagnetic distortion of the local magnetic field, we anticipated more evidence of T2 blackout around hemorrhagic CVAs imaged with EPI techniques than non-EPI techniques. However, we found that pixel values near zero within the T2* hypointense region were more commonly seen with non-EPI DWI, possibly as a manifestation of the lower signal-to-noise ratio in these series.

As with most retrospective clinical case series, our report is limited by the small number of cases suitable for inclusion, additional noise introduced by variability in imaging parameters used, and the presumption of diagnosis in patients with good outcomes. For hemorrhagic CVAs, there is the additional challenge of defining the hemorrhagic area, given that susceptibility artifact "blooms" from the source of the magnetic field inhomogeneity and is larger than the actual region of hemorrhage. These challenges are likely contributing factors to the overall lack of robust publications on DWI features of spontaneous canine CVAs. This report demonstrates the variability in ADC values for lesions that have the clinical behavior of CVAs, suggesting that CVA cannot necessarily be excluded as a differential solely on the absence of evidence of restricted diffusion, especially for lesions imaged beyond the acute timeframe. As with human CVAs, temporal evolution of perfusion after initial injury may influence the DWI appearance of canine CVAs, though these data are too sparse to serve as the basis for a temporally-specific reference range. Regarding canine hemorrhagic CVAs, the absence of evidence of restricted diffusion in the perilesional T2-FLAIR hyperintense regions suggests that hemorrhagic transformation of ischemic infarction is not a common etiology of solitary spontaneous intracranial hemorrhage in dogs in our sample population. Further, it may indicate that canine models of intracerebral hemorrhage (26) reflect imaging characteristics of the spontaneous clinical disease. Finally, we did not identify a clear advantage of non-EPI over EPI DWI for the characterization of presumed CVAs, with or without hemorrhage, on our 3T magnet. Specifically, EPI was not more likely to exhibit signal dropout within or immediately surrounding a region of hemorrhage (defined by the area of T2* hypointensity) than non-EPI in our case set.

To better characterize the temporal evolution of presumed spontaneous CVAs in dogs, prospectively collected serial MRI at predefined timepoints after the onset of neurological signs would be needed. To determine optimal parameters for detection of restricted diffusion in canine CVAs, a systematic exploration of the space defined by echo generation method, b-value, magnet strength, echo and repetition timing, and coil selection would be necessary. To determine the reliability of ADC calculations in this population of dogs, evaluation of agreement across and within observers would be necessary. It is likely that a combination of diffusion and perfusion-weighted imaging techniques, as is currently standard-of-care in human cerebrovascular imaging, would further improve our understanding of the evolution of parenchymal damage and recovery in canine CVA.

Data availability statement

The original contributions presented in the study are included in the article/Supplementary material, further inquiries can be directed to the corresponding author.

Author contributions

JL and JG contributed to concept and study design. SK and ED contributed to data collection. EB contributed to data analysis and initial manuscript preparation. All authors contributed to manuscript editing and refinement.

Conflict of interest

The authors declare that the research was conducted in the absence of any commercial or financial relationships that could be construed as a potential conflict of interest.

Publisher's note

Supplementary material

The Supplementary Material for this article can be found online at: https://www.frontiersin.org/articles/10.3389/fvets.2022.1008447/full#supplementary-material

References

1. Vilela P, Rowley HA. Brain ischemia: CT and MRI techniques in acute ischemic stroke. *Eur J Radiol.* (2017) 96:162–72. doi: 10.1016/j.ejrad.2017.08.014

2. Muir KW, Buchan A, von Kummer R, Rother J, Baron JC. Imaging of acute stroke. *Lancet Neurol.* (2006) 5:755–68. doi: 10.1016/S1474-4422(06)70545-2

3. Rivers CS, Wardlaw JM, Armitage PA, Bastin ME, Hand PJ, Dennis MS. Acute ischemic stroke lesion measurement on diffusion-weighted imaging–important considerations in designing acute stroke trials with magnetic resonance imaging. *J Stroke Cerebrovasc Dis.* (2007) 16:64–70. doi: 10.1016/j.jstrokecerebrovasdis.2006.11.003

4. Welch KM, Windham J, Knight RA, Nagesh V, Hugg JW, Jacobs M, et al. A model to predict the histopathology of human stroke using diffusion and T2-weighted magnetic resonance imaging. *Stroke.* (1995) 26:1983–9. doi: 10.1161/01.STR.26.11.1983

5. Braemswig TB, Usnich T, Albach FN, Brunecker P, Grittner U, Scheitz JF, et al. Early new diffusion-weighted imaging lesions appear more often in stroke patients with a multiple territory lesion pattern. *Stroke.* (2013) 44:2200–4. doi: 10.1161/STROKEAHA.111.000810

6. Pszczolkowski S, Sprigg N, Woodhouse LJ, Gallagher R, Swienton D, Law ZK, et al. Effect of tranexamic acid administration on remote cerebral ischemic lesions in acute spontaneous intracerebral hemorrhage: a substudy of a randomized clinical trial. *JAMA Neurol.* (2022) 79:468–77. doi: 10.1001/jamaneurol.2022.0217

7. Duering M, Adam R, Wollenweber FA, Bayer-Karpinska A, Baykara E, Cubillos-Pinilla LY, et al. Within-lesion heterogeneity of subcortical DWI lesion evolution, and stroke outcome: A voxel-based analysis. *J Cereb Blood Flow Metab.* (2020) 40:1482–91. doi: 10.1177/0271678X19865916

8. Kranz PG, Eastwood JD. Does diffusion-weighted imaging represent the ischemic core? An evidence-based systematic review AJNR. *Am J Neuroradiol.* (2009) 30:1206–12. doi: 10.3174/ajnr.A1547

9. Fiebach JB, Schellinger PD, Jansen O, Meyer M, Wilde P, Bender J, et al. CT and diffusion-weighted MR imaging in randomized order: diffusion-weighted imaging results in higher accuracy and lower interrater variability in the diagnosis of hyperacute ischemic stroke. *Stroke.* (2002) 33:2206–10. doi: 10.1161/01.STR.0000026864.20339.CB

10. Ni JM, Mogensen MA, Chen ZA, Shuang C, Shen TZ, Huang G. Influence of fluid-attenuated inversion-recovery on stroke apparent diffusion coefficient measurements and its clinical application. *Eur J Radiol.* (2010) 75:e76–81. doi: 10.1016/j.ejrad.2009.11.029

11. Fainardi E, Borrelli M, Saletti A, Sarubbo S, Roversi G, Bernardoni A, et al. Temporal changes in perihematomal apparent diffusion coefficient values during the transition from acute to subacute phases in patients with spontaneous intracerebral hemorrhage. *Neuroradiology.* (2013) 55:145–56. doi: 10.1007/s00234-012-1093-x

12. Schlaug G, Siewert B, Benfield A, Edelman RR, Warach S. Time course of the apparent diffusion coefficient (ADC) abnormality in human stroke. *Neurology.* (1997) 49:113–9. doi: 10.1212/WNL.49.1.113

13. Kang BK, Na DG, Ryoo JW, Byun HS, Roh HG, Pyeun YS. Diffusion-weighted MR imaging of intracerebral hemorrhage. *Korean J Radiol.* (2001) 2:183–91. doi: 10.3348/kjr.2001.2.4.183

14. Sutherland-Smith J, King R, Faissler D, Ruthazer R, Sato A. Magnetic resonance imaging apparent diffusion coefficients for histologically confirmed intracranial lesions in dogs. *Vet Radiol Ultrasound.* (2011) 52:142–8. doi: 10.1111/j.1740-8261.2010.01764.x

15. Garosi L, McConnell JF, Platt SR, Barone G, Baron JC, de Lahunta A, et al. Clinical and topographic magnetic resonance characteristics of suspected brain infarction in 40 dogs. *J Vet Intern Med.* (2006) 20:311–21. doi: 10.1111/j.1939-1676.2006.tb02862.x

16. McConnell JF, Garosi L, Platt SR. Magnetic resonance imaging findings of presumed cerebellar cerebrovascular accident in twelve dogs. *Vet Radiol Ultrasound.* (2005) 46:1–10. doi: 10.1111/j.1740-8261.2005.00001.x

17. Wada M, Hasegawa D, Hamamoto Y, Yu Y, Asada R, Fujiwara-Igarashi A, et al. Comparison of canine and feline meningiomas using the apparent diffusion coefficient and fractional anisotropy. *Front Vet Sci.* (2020) 7:614026. doi: 10.3389/fvets.2020.614026

18. Fages J, Oura TJ, Sutherland-Smith J, Jennings SH. Atypical and malignant canine intracranial meningiomas may have lower apparent diffusion coefficient values than benign tumors. *Vet Radiol Ultrasound.* (2020) 61:40–7. doi: 10.1111/vru.12814

19. Scherf G, Sutherland-Smith J, Uriarte A. Dogs and cats with presumed or confirmed intracranial abscessation have low apparent diffusion coefficient values. *Vet Radiol Ultrasound.* (2022) 63:197–200. doi: 10.1111/vru.13064

20. Maclellan MJ, Ober CP, Feeney DA, Jessen CR. Evaluation of diffusion-weighted magnetic resonance imaging at 3. 0 Tesla for differentiation between intracranial neoplastic and noninfectious inflammatory lesions in dogs. *J Am Vet Med Assoc.* (2019) 255:71–7. doi: 10.2460/javma.255.1.71

21. Bradbury A, Peterson D, Vite C, Chen S, Ellinwood NM, Provenzale J. Diffusion tensor imaging analysis of the brain in the canine model of Krabbe disease. *Neuroradiol J.* (2016) 29:417–24. doi: 10.1177/1971400916665378

22. Anaya Garcia MS, Hernandez Anaya JS, Marrufo Melendez O, Velazquez Ramirez JL, Palacios Aguiar R. *In vivo* study of cerebral white matter in the dog using diffusion tensor tractography. *Vet Radiol Ultrasound.* (2015) 56:188–95. doi: 10.1111/vru.12211

23. Leong D, Calabrese E, White LE, Wei P, Chen S, Platt SR, et al. Correlation of diffusion tensor imaging parameters in the canine brain. *Neuroradiol J.* (2015) 28:12–8. doi: 10.15274/nrj-2014-10110

24. Pierce TT, Calabrese E, White LE, Chen SD, Platt SR, Provenzale JM. Segmentation of the canine corpus callosum using diffusion-tensor imaging tractography. *AJR Am J Roentgenol.* (2014) 202:W19–25. doi: 10.2214/AJR.12.9791

25. Kang BT, Jang DP, Gu SH, Lee JH, Jung DI, Lim CY, et al. MRI features in a canine model of ischemic stroke: correlation between lesion volume and neurobehavioral status during the subacute stage. *Comp Med.* (2009) 59:459–64.

26. An D, Park J, Shin JI, Kim HJ, Jung DI, Kang JH, et al. Temporal evolution of MRI Characteristics in dogs with collagenase-induced intracerebral hemorrhage. *Comp Med.* (2015) 65:517–25.

27. Shaibani A, Khawar S, Shin W, Cashen TA, Schirf B, Rohany M, et al. First results in an MR imaging–compatible canine model of acute stroke. *AJNR Am J Neuroradiol.* (2006) 27:1788–93.

28. Harris AD, Kosior RK, Chen HS, Andersen LB, Frayne R. Evolution of hyperacute stroke over 6 hours using serial MR perfusion and diffusion maps. *J Magn Reson Imaging.* (2009) 29:1262–70. doi: 10.1002/jmri.21763

29. Xu XQ, Cheng QG, Zu QQ, Lu SS Yu J, Sheng Y, et al. Comparative study of the relative signal intensity on DWI, FLAIR, and T2 images in identifying the onset time of stroke in an embolic canine model. *Neurol Sci.* (2014) 35:1059–65. doi: 10.1007/s10072-014-1643-6

30. Xu XQ, Wu CJ, Zu QQ, Lu SS, Liu XL, Gao QQ, et al. Temporal evolution of the signal intensity of hyper-acute ischemic lesions in a canine stroke model: influence of hyperintense acute reperfusion marker. *Jpn J Radiol.* (2017) 35:161–7. doi: 10.1007/s11604-017-0615-1

31. Belayev L, Obenaus A, Zhao W, Saul I, Busto R, Wu C, et al. Experimental intracerebral hematoma in the rat: characterization by sequential magnetic resonance imaging, behavior, and histopathology. Effect of albumin therapy. *Brain Res.* (2007) 1157:146–55. doi: 10.1016/j.brainres.2007.04.077

32. Lindley RI, Wardlaw JM, Sandercock PA, Rimdusid P, Lewis SC, Signorini DF, et al. Frequency and risk factors for spontaneous hemorrhagic transformation of cerebral infarction. *J Stroke Cerebrovasc Dis.* (2004) 13:235–46. doi: 10.1016/j.jstrokecerebrovasdis.2004.03.003

33. Demirtas BS, Ocek L, Zorlu Y, Oztekin O. Factors associated with hemorrhagic transformation in infarctions involving the posterior circulation system. *J Stroke Cerebrovasc Dis.* (2019) 28:2193–200. doi: 10.1016/j.jstrokecerebrovasdis.2019.04.034

34. Wessmann A, Chandler K, Garosi L. Ischaemic and haemorrhagic stroke in the dog. *Vet J.* (2009) 180:290–303. doi: 10.1016/j.tvjl.2007.12.023

35. Swayne DE, Tyler DE, Batker J. Cerebral infarction with associated venous thrombosis in a dog. *Vet Pathol.* (1988) 25:317–20. doi: 10.1177/030098588802500413

36. Sasaki M, Yamada K, Watanabe Y, Matsui M, Ida M, Fujiwara S, et al. Variability in absolute apparent diffusion coefficient values across different platforms may be substantial: a multivendor, multi-institutional comparison study. *Radiology.* (2008) 249:624–30. doi: 10.1148/radiol.2492071681

37. Kolff-Gart AS, Pouwels PJ, Noij DP, Ljumanovic R, Vandecaveye V, de Keyzer F, et al. Diffusion-weighted imaging of the head and neck in healthy subjects: reproducibility of ADC values in different MRI systems and repeat sessions. *AJNR Am J Neuroradiol.* (2015) 36:384–90. doi: 10.3174/ajnr.A4114

38. Steens SC, Admiraal-Behloul F, Schaap JA, Hoogenraad FG, Wheeler-Kingshott CA. le Cessie S, et al. Reproducibility of brain ADC histograms. *Eur Radiol.* (2004) 14:425–30. doi: 10.1007/s00330-003-2121-3

39. Ogura A, Hayakawa K, Miyati T, Maeda F. Imaging parameter effects in apparent diffusion coefficient determination of magnetic resonance imaging. *Eur J Radiol.* (2011) 77:185–8. doi: 10.1016/j.ejrad.2009.06.031

40. Tsujita N, Kai N, Fujita Y, Hiai Y, Hirai T, Kitajima M, et al. Interimager variability in ADC measurement of the human brain. *Magn Reson Med Sci.* (2014) 13:81–7. doi: 10.2463/mrms.2012-0098

41. Moreau B, Iannessi A, Hoog C, Beaumont H. How reliable are ADC measurements? A phantom and clinical study of cervical lymph nodes. *Eur Radiol.* (2018) 28:3362–71. doi: 10.1007/s00330-017-5265-2

42. Drake-Perez M, Boto J, Fitsiori A, Lovblad K, Vargas MI. Clinical applications of diffusion weighted imaging in neuroradiology. *Insights Imaging.* (2018) 9:535–47. doi: 10.1007/s13244-018-0624-3

43. Baliyan V, Das CJ, Sharma R, Gupta AK. Diffusion weighted imaging: technique and applications. *World J Radiol.* (2016) 8:785–98. doi: 10.4329/wjr.v8.i9.785

44. Leiva-Salinas C, Wintermark M, Kidwell CS. Neuroimaging of cerebral ischemia and infarction. *Neurotherapeutics.* (2011) 8:19–27. doi: 10.1007/s13311-010-0004-2

45. Donahue MJ, Strother MK, Hendrikse J. Novel MRI approaches for assessing cerebral hemodynamics in ischemic cerebrovascular disease. *Stroke.* (2012) 43:903–15. doi: 10.1161/STROKEAHA.111.635995

46. MacLellan MJ, Ober CP, Feeney DA, Jessen CR. Diffusion-weighted magnetic resonance imaging of the brain of neurologically normal dogs. *Am J Vet Res.* (2017) 78:601–8. doi: 10.2460/ajvr.78.5.601

47. Hartmann A, Soffler C, Failing K, Schaubmar A, Kramer M, Schmidt MJ. Diffusion-weighted magnetic resonance imaging of the normal canine brain. *Vet Radiol Ultrasound.* (2014) 55:592–8. doi: 10.1111/vru.12170

48. Choi S, Noh D, Kim Y, Jeong I, Choi H, Lee Y, et al. Magnetic resonance imaging characteristics of ischemic brain infarction over time in a canine stroke model. *J Vet Sci.* (2018) 19:137–42. doi: 10.4142/jvs.2018.19.1.137

49. An H, Ford AL, Vo K, Powers WJ, Lee JM, Lin W. Signal evolution and infarction risk for apparent diffusion coefficient lesions in acute ischemic stroke are both time- and perfusion-dependent. *Stroke.* (2011) 42:1276–81. doi: 10.1161/STROKEAHA.110.610501

50. Taha A, Bobi J, Dammers R, Dijkhuizen RM, Dreyer AY, van Es A, et al. Comparison of large animal models for acute ischemic stroke: which model to use? *Stroke.* (2022) 53:1411–22. doi: 10.1161/STROKEAHA.121.036050

51. Whitlock J, Holdsworth A, Morales C, Garosi L, Carrera I. 1. 5 tesla magnetic resonance imaging features of canine intracranial intra-axial hematomas. *Front Vet Sci.* (2021) 8:778320. doi: 10.3389/fvets.2021.778320

52. Lowrie M, De Risio L, Dennis R, Llabres-Diaz F, Garosi L. Concurrent medical conditions and long-term outcome in dogs with nontraumatic intracranial hemorrhage. *Vet Radiol Ultrasound.* (2012) 53:381–8. doi: 10.1111/j.1740-8261.2012.01934.x

53. Aksoy D, Bammer R, Mlynash M, Venkatasubramanian C, Eyngorn I, Snider RW, et al. Magnetic resonance imaging profile of blood-brain barrier injury in patients with acute intracerebral hemorrhage. *J Am Heart Assoc.* (2013) 2:e000161. doi: 10.1161/JAHA.113.000161

54. Suh CH, Jung SC, Cho SJ, Woo DC, Oh WY, Lee JG, et al. MRI for prediction of hemorrhagic transformation in acute ischemic stroke: a systematic review and meta-analysis. *Acta Radiol.* (2020) 61:964–72. doi: 10.1177/0284185119887593

55. Almuqbel MM, Leeper G, Palmer DN, Mitchell NL, Russell KN, Keenan RJ, et al. Practical implications of motion correction with motion insensitive radial k-space acquisitions in MRI. *Br J Radiol.* (2018) 91:20170593. doi: 10.1259/bjr.20170593

56. Atlas SW, DuBois P, Singer MB, Lu D. Diffusion measurements in intracranial hematomas: implications for MR imaging of acute stroke. *AJNR Am J Neuroradiol.* (2000) 21:1190–4.

57. Silvera S, Oppenheim C, Touze E, Ducreux D, Page P, Domigo V, et al. Spontaneous intracerebral hematoma on diffusion-weighted images: influence of T2-shine-through and T2-blackout effects. *AJNR Am J Neuroradiol.* (2005) 26:236–41.

Frontiers in Veterinary Science

Transforms how we investigate and improve animal health

The third most-cited veterinary science journal, bridging animal and human health with a comparative approach to medical challenges. It explores innovative biotechnology and therapy for improved health outcomes.

Discover the latest Research Topics

See more →

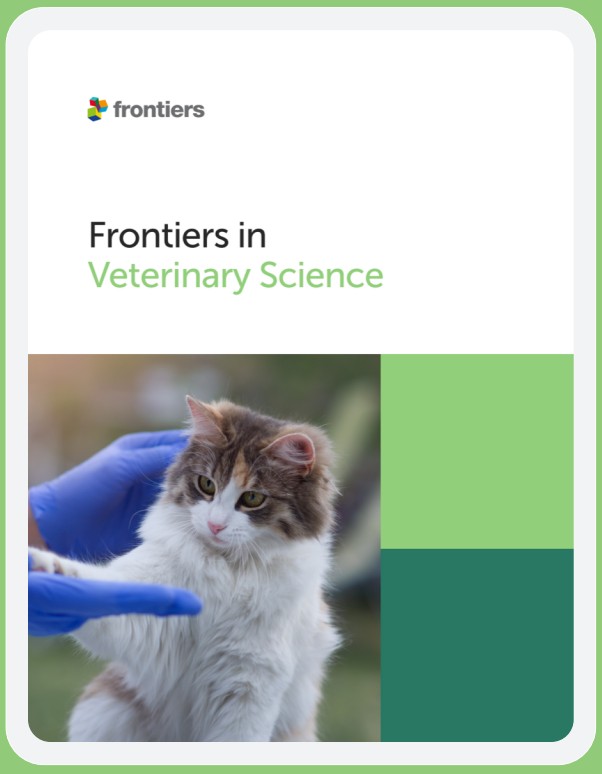

Frontiers

Avenue du Tribunal-Fédéral 34
1005 Lausanne, Switzerland
frontiersin.org

Contact us

+41 (0)21 510 17 00
frontiersin.org/about/contact